

STRUCTURE AND SPECTRA OF THE
OXALYL HALIDES

STRUCTURE AND SPECTRA OF THE OXALYL HALIDES

by

KEVIN GLEN KIDD

A Thesis

Submitted to the Faculty of Graduate Studies

in Partial Fulfillment of the Requirements

for the Degree

Doctor of Philosophy

McMaster University

March 1972

Doctor of Philosophy (1972)
(Chemistry)

McMaster University
Hamilton, Ontario

TITLE: Structure and Spectra of the Oxalyl Halides

AUTHOR: Kevin Glen Kidd

SUPERVISOR: Professor G. W. King

NUMBER OF PAGES: 210

SCOPE AND CONTENTS:

The ultraviolet absorption spectrum of oxalyl chloride-fluoride has been recorded under high resolution, and has been attributed to a superposition of the spectra of the cis isomer (which appears weakly) and the trans isomer. The ultraviolet spectra of the cis isomers of oxalyl bromide, oxalyl chloride, and oxalyl fluoride have also been identified. With the help of theoretical calculations, discrete absorption in the ultraviolet spectrum of trans oxalyl chloride-fluoride has been attributed to the superposition of four systems: (a) the singlet-singlet and singlet-triplet transitions which involve promotion of an electron from the highest energy non-bonding orbital (n_1) to the lowest energy antibonding orbital (π_1^*) and (b) the singlet-singlet and singlet-triplet transitions which involve promotion from n_1 to the second lowest energy antibonding π orbital (π_2^*). The S-S and S-T, $n_1 \rightarrow \pi_1^*$ transitions have been analyzed in detail.

Theoretical calculations have been carried out which indicate that for α, β diketones, promotion of an electron to the lowest energy antibonding skeletal orbital (σ_1^*) produces states which have a tendency toward dissociation along the C-C bond. It has been postulated that the diffuseness of the high energy absorption spectrum results from such a molecular dis-

sociation, the $A_U(\pi_1, \pi_1^*)$ state being strongly predissociated by the $A_U(n_1, \sigma_1^*)$ state while the $A_U(n_1, \pi_1^*)$ state is strongly predissociated by the $A_U(\pi_1, \sigma_1^*)$ state.

It has been postulated that the fluid phases of glyoxal and biacetyl consist of an equilibrium mixture of these molecules in various degrees of aggregation (e.g., monomeric, dimeric, trimeric,...). An ultraviolet band system previously assigned to a second $n \rightarrow \pi^*$ transition of these molecules has been reassigned to the first $n \rightarrow \pi^*$ transition of a polymeric species. Some evidence has been assembled which supports this hypothesis.

ACKNOWLEDGEMENTS

I wish to express my thanks to Dr. G. W. King for the support he has given me during the course of this research.

I would like to thank Dr. D. C. Moule for making available the facilities of his laboratory at Brock University, and for helpful suggestions; I would also like to thank Dr. D. P. Santry for help with the theoretical calculations.

I am especially grateful to my research colleagues: Dr. W. J. Balfour, E. J. Finn, E. R. Farnworth, D. Grangé, F. R. Greening, Dr. H. E. Howard-Lock, Z. R. Lemanczyk, Dr. J. O. P. McBride, P. R. McLean, R. C. Meatherall, Dr. P. Pichat, Dr. S. P. So, Dr. K. I. Srikameswaran, C. R. Subramanian, A. van Putten, and Dr. C. H. Warren; I thank them for the stimulus and the assistance they have provided in the laboratory and for the warm hospitality they have extended to myself and my family.

I am grateful to J. P. Bradford for technical assistance and to B. Spiers for assistance in carrying out Raman experiments. Thanks are also due to S. Hawley whose skillful typing of this manuscript has been a great deal of help.

Finally, this research was made possible through financial assistance from Canadian Industries Limited, The Ontario Government, and the National Research Council of Canada.

TABLE OF CONTENTS

	Page
CHAPTER 1: Introduction	1
CHAPTER 2: Experimental Techniques	7
CHAPTER 3: Molecular Orbital Calculation for trans Glyoxal and Derivatives	12
CHAPTER 4: The Near Ultraviolet Spectra of the Oxalyl Halides	95
CHAPTER 5: The Vibrational Analysis of the ${}^1, {}^3A''(n_{1a'}, \pi_{1a''}^*) \leftarrow \tilde{X}{}^1A'$ Transitions of trans Oxalyl Chloride-Fluoride	122
CHAPTER 6: Rotational Structure of the Origin Band of the ${}^1A''(n_{1a'}, \pi_{1a''}^*) \leftarrow \tilde{X}{}^1A'$ Transition of trans Oxalyl Chloride-Fluoride	157
CHAPTER 7: Conclusions	179
BIBLIOGRAPHY	182
APPENDIX I: The Vapour Phase Raman Spectrum of Oxalyl Chloride	185
APPENDIX II: The Solid State Spectrum of Oxalyl Chloride	189
APPENDIX III: The Emission Spectrum of Oxalyl Chloride	198
APPENDIX IV: Frequencies of Observed Bands in the Ultraviolet Spectrum of Oxalyl Chloride-Fluoride	201

LIST OF TABLES

Table		Page
1.1	The Character Table of the C_{2h} Point Group (for trans COXCOX)	4
1.2	The Character Table of the C_{2v} Point Group (for cis COXCOX)	4
1.3	The Character Table of the C_s Point Group (for cis and trans COXCOX)	5
1.4	Electric Dipole Allowed Transitions for the cis and trans Oxalyl Halides from the Ground State (Totally Symmetric)	5
1.5	Correlation of Symmetry Species for the Point Groups C_{2h} , C_{2v} and C_s	6
3.1	Geometries for Ground and Excited States of Glyoxal	23
3.2	Molecular Orbitals, Glyoxal $\tilde{X}(^1A_g)$ in Order of Decreasing Energy	24
3.3	Bond Order Matrix Glyoxal $\tilde{X}(^1A_g)$	25
3.4	Bond Order Matrix Glyoxal $^3A_u(n_{a_g}^-, \pi_{a_u}^*)$	26
3.5	Calculated SCF-LCAO-MO Energies For Ground and Excited States of Glyoxal with Transition Energies and Oscillator Strengths	31
3.6	One-Center Atomic Transition Moment Integrals	35
3.7	Reduction of the Spin-Orbital Mixing Integrals between Two States $^1\psi_k$ and $^3\psi_j$ which are Different in Two M.O.'s ϕ_m and ϕ_n	37

Table	Page
3.8 Values for the Spin Orbit Coupling Between the 2p Atomic Orbitals as Calculated for the Free Atom	38
3.9 Symmetries of Zeroth Order States Classified Under C_{2h} Symmetry which can Mix Through Spin-Orbit Coupling	40
3.10 Intensity for the Transition ${}^3A_u(n_{a_g}^-, \pi_{a_u}^*) \leftarrow {}^1A_g$ (G.S.) of Glyoxal Produced by Spin-Orbit Coupling	41
3.11 Intensity of the Transition ${}^3B_u(\pi_{b_g}, \pi_{a_u}^*) \leftarrow {}^1A_g$ of Glyoxal Produced by Spin-Orbit Coupling	42
3.12 Intensity of the Transition ${}^3B_u(n_{a_g}^-, \sigma_{1b_u}^*) \leftarrow {}^1A_g$ of Glyoxal Produced by Spin-Orbit Coupling	43
3.13 Force Constants of Ground and Excited States of Glyoxal	51
3.14 CNDO Geometries for Ground and Excited States of Oxalyl Fluoride	66
3.15 Molecular Orbitals for Oxalyl Fluoride $\tilde{X}({}^1A_g)$ in Order of Decreasing Energy	67
3.16 Bond Order Matrix for Oxalyl Fluoride $\tilde{X}({}^1A_g)$	70
3.17 Calculated CNDO (SCF-LCAO-MO) Energies for Ground and Excited States of Oxalyl Fluoride with Transition Energies and Oscillator Strengths	77
3.18 Intensity for the Transition ${}^3A_u(n_{oa_g}^-, \pi_{a_u}^*) \leftarrow \tilde{X}({}^1A_g)$ of Oxalyl Fluoride Produced by Spin-Orbit Coupling	79
3.19 Intensity for the Transition ${}^3B_u(\pi_{b_g}, \pi_{a_u}^*) \leftarrow \tilde{X}({}^1A_g)$ of Oxalyl Fluoride Produced by Spin-Orbit Coupling	80
3.20 Intensity for the Transition ${}^3B_u(n_{oa_g}^-, \sigma_{1b_u}^*) \leftarrow \tilde{X}({}^1A_g)$ of Oxalyl Fluoride Produced by Spin-Orbit Coupling	81

Table	Page
3.21 Force Constants for the Ground and Excited States of Oxalyl Fluoride	86
3.22 Calculated CNDO (SCF-LCAO-MO) Energies for Ground and Excited States of Oxalyl Chloride with Transition Energies	89
3.23 "Strong" Transitions of Oxalyl Chloride-Fluoride	92
3.24 "Weak" Transitions of Oxalyl Chloride-Fluoride	93
4.1 The Near Ultraviolet Systems of Glyoxal and Acrolein	97
4.2 Origins of the $n \rightarrow \pi^*(S-S)$ Transitions for cis Oxalyl Halides	110
4.3 Ground State Vibrational Frequencies for cis and trans Oxalyl Chloride	112
4.4 Ground State Vibrational Frequencies for cis and trans Oxalyl Bromide	113
4.5 Bands Observed in the ${}^1B_1(n,\pi^*) \leftarrow \tilde{X}{}^1A_1$ of cis Oxalyl Chloride	114
4.6 Bands Observed in the ${}^1B_1(n,\pi^*) \leftarrow \bar{X}{}^1A_1$ of cis Oxalyl Bromide	115
4.7 Bands Observed in the ${}^1A''(n,\pi^*) \leftarrow \bar{X}{}^1A'$ of cis Oxalyl Chloride-Fluoride	115
4.8 Principal Frequencies of the First $n \rightarrow \pi^*$ Transition of the Vibrational Structure of COFCOCl	118
5.1 Frequencies and Assignments of the $\tilde{a}({}^3A'') \leftarrow \tilde{X}({}^1A')$ Absorption Spectrum of Oxalyl Chloride-Fluoride (trans)	132
5.2 Ground and Excited State Frequencies for Oxalyl Chloride- Fluoride	136

Table	Page
5.3 Comparison of Ground and Excited State Fundamentals Observed in the S-T $n \rightarrow \pi^*$ Spectra of Oxalyl Chloride-Fluoride and a Series of Molecules	137
5.4 Comparison of Ground and Excited State Fundamentals Observed in the $n \rightarrow \pi^*$ Spectra of Oxalyl Chloride-Fluoride and Propenal	138
5.5 Fermi Resonance Involving $\nu_1-\nu_3-\nu_9$ in COFCOCl $n \rightarrow \pi^*$ (Singlet-Singlet)	143
5.6 Frequencies and Assignments of the $\tilde{A}(^1A'') \leftarrow \tilde{X}(^1A')$ Absorption Spectrum of Oxalyl Chloride-Fluoride	149
5.7 Comparison of Ground and Excited State Fundamentals Observed in the S-S $n \rightarrow \pi^*$ Spectra of Oxalyl Chloride-Fluoride and a Series of Molecules	154
5.8 Lines Observed in the $\tilde{B} \leftarrow \tilde{X}$ Transition of COFCO ³⁵ Cl	155
5.9 Lines Observed in the $\tilde{b} \leftarrow \tilde{X}$ Transition of COFCO ³⁵ Cl	156
6.1 Rotational Constants for a Series of Assumed Ground State Geometries for Oxalyl Chloride-Fluoride (trans)	163
6.2 Line Frequencies of the Observed Fine Structure in the Origin Band of COFCOCl	166
6.3 Intense Branches for the A, B and C-type Bands of an Asymmetric Top Molecule with Simple Formula for the Line Energies of the Rotor as a Near Oblate Top Where These Exist	175
A1 Ground State Vibrational Frequencies Observed by Raman Spectroscopy for Oxalyl Chloride in the Vapour Phase	188

Table		Page
A2	Bands Observed for Pure COCl_2 Solid at 77°K	192
A3	Observed Bands in the Liquid Helium Spectrum of Oxalyl Chloride in an SF_6 Matrix	195
A4	The Frequencies Observed in Emission for Oxalyl Chloride	200
A5	Frequencies of Observed Heads in the Ultraviolet Spectrum of Oxalyl Chloride-Fluoride	201

LIST OF FIGURES

Figure		Page
3.1	Co-ordinate System Used for the Calculation of the trans Glyoxal Derivatives	22
3.2	Energies of the Molecular Orbitals of Glyoxal in the Ground State	28
3.3	CNDO Energies for the "u" States of Glyoxal at the CNDO Ground State Geometry	29
3.4	CNDO Energies for the "g" States of Glyoxal at the CNDO Ground State Geometry	30
3.5	CNDO Potential Curve for Glyoxal for CC Bond Length	48
3.6	CNDO Potential Curve for Glyoxal for CO, CH Bond Lengths	49
3.7	CNDO Potential Curve for Glyoxal for COH, CCO Bond Angles	50
3.8	CNDO Spectrum of Glyoxal Compared with Experiment	52
3.9	Simple Molecular Orbital Scheme for α, β Diketones	53
3.10	Solvent Dependence of the $35,000 \text{ cm}^{-1}$ System of Glyoxal (Polymeric) and Biacetyl	56
3.11	Energies of the Molecular Orbitals of Oxalyl Fluoride in the Ground State	73
3.12	CNDO Energies for the "u" States of Oxalyl Fluoride at the CNDO Ground State Geometry	75
3.13	CNDO Energies for the "g" States of Oxalyl Fluoride at the CNDO Ground State Geometry	76
3.14	CNDO Potential Curve for (COFCOF) for CC Bond Lengths	83
3.15	CNDO Potential Curve for (COFCOF) for CO, CF Bond Lengths	84

Figure	Page	
3.16	CNDO Potential Curve for (COFCOF) for COF, CCO Bond Angles	85
4.1	Energy Level Diagram for Ground and First n, π^* Excited States of cis and trans COC ℓ COC ℓ	109
5.1	The $\tilde{a}(^3A'')$ \leftarrow $\tilde{X}(^1A')$ Transition - COFCOC ℓ (trans)	130
5.2	The Observed COFCO $^{35}C\ell$ /COFCO $^{37}C\ell$ Isotopic Splittings in the $\tilde{a}(^3A'')$ and $\tilde{X}(^1A')$ States	131
5.3	The $\tilde{A}(^1A'')$ \leftarrow $\tilde{X}(^1A')$ Transition - COFCOC ℓ (trans)	140
5.4	Fermi Resonance Pattern at $\nu_{00} + 1300 \text{ cm}^{-1}$ compared with the Normal Pattern at the Origin of the $^1A'' \leftarrow \tilde{X}^1A'$ Transition	143
6.1	The Origin Band of $\tilde{A}(^1A'')$ \leftarrow $\tilde{X}(^1A')$ Oxalyl Chloride-Fluoride	158
6.2	(a) Type C Contour Computed for the Origin of Oxalyl Chloride-Fluoride with Line Structure Produced by Head Formation in K Subbands.	159
	(b) Type C Contour Computed for the Origin of Oxalyl Chloride-Fluoride with Line Structure Produced by Multiple Coincidence of J Lines	159
6.3	(a) Type A Contour Corresponding to the Type C Contour in Figure 6.2(a).	160
	(b) Type B Contour Corresponding to the Type C Contour in Figure 6.2(a).	160
6.4	(a) Type A Contour Corresponding to the Type C Contour in Figure 6.2(b).	161
	(b) Type B Contour Corresponding to the Type C Contour in Figure 6.2(b).	161

Figure		Page
A1	The Ultraviolet Spectrum of Oxalyl Chloride at 77°K	191
A2	Microdensitometer Trace of the Absorption Spectrum of Oxalyl Chloride at Low Temperature (near 4°K)	194

CHAPTER 1

INTRODUCTION

1.1 Molecular Spectroscopy

The term molecular spectroscopy as it is used in this thesis refers to the study of the motions of the particles (nuclei and electrons) of which a molecule is composed. In the quantum mechanical description of the molecular system, a manifold of quantized energy levels is associated with the motions of the molecular particles. It is customary to separate this molecular energy into three categories according to magnitude. The electronic energy (associated with the motion of the electrons) which is an order of magnitude larger than the vibrational energy (associated with the vibrational motion of the nuclei) which is an order of magnitude larger than the rotational energy (associated with the rotational motion of the nuclei). Information about the manifold of energy levels is deduced from spectroscopic transitions which take place between the levels. The energy gained or lost by the molecule in these transitions is observed in the ultraviolet and visible (electronic) through the infra red (vibrational) to the microwave (rotational) regions of the energy spectrum. From a knowledge of the energy levels of a molecule it is possible to obtain information about the geometry of the nuclei and the nature of the electron distribution. In addition, the study of the energy manifold and the transitions observed between levels for a molecule can, potentially, lead to a better understanding of the forces which exist within and between molecules.

No attempt has been made here to review the basic theory of molecular spectroscopy since this is now textbook material. Many texts on the subject

are available, but the author has made most extensive use of the text by King⁽⁶⁾ and the text by Herzberg⁽⁷⁾. Where spectroscopic terms and formulae have been employed in the thesis, specific references have been made to these two sources. Equations have been developed only where they were necessary to detail the method used in carrying out calculations or where they have been under consideration.

1.2 The Development of the Thesis

Oxalyl chloride fluoride is a member of the group of six-atomic diketones C_2O_2XY (where X and Y may be the same or different). All the molecules of this series (i.e., X, Y = H, F, Cl, Br) show a discrete absorption system in the near ultraviolet, and a study of this system for oxalyl chloride fluoride was the starting point of this research. It was found that this discrete system of C_2O_2FCl becomes diffuse at higher energies, and is finally obscured by a series of bands representing continuous absorption. This spectral pattern is typical of the halogenated derivatives^(1,2,3), and in addition to the analysis of the discrete absorption system, an attempt was made to solve the problem of the origin of the diffuse absorption, and why it carries over into the high energy end of the discrete part of the spectrum.

Calculations were carried out to obtain the energies and wavefunctions of the ground and excited states for a number of the diketones. Estimates were also made of transition energies and intensities and these results were compared with experiment where possible. These calculations are discussed in Chapter 3.

The vibrational analysis of the discrete absorption system of oxalyl chloride fluoride (reported in Chapter 5) involved a critical examination of the studies carried out in this research group⁽¹⁾ on oxalyl chloride, oxalyl

fluoride, and oxalyl bromide. Previous studies in this research group^(1,5) have concluded that the observed features of the ultraviolet and infrared spectra of the oxalyl halides could be attributed solely to the trans isomer of these molecules. In attempting to extend the analysis of the symmetric oxalyl halides to the spectrum of COFCOCl₂, it became necessary to question the previous assignment in the symmetric oxalyl halides of a "hot band" to one of the ground state fundamentals of the trans isomer. The details of this particular aspect of the problem are reported in Chapter 4. The results of the present study indicate that the spectrum of the cis isomer of the oxalyl halides can in fact be detected in the ultraviolet.

The high resolution spectra of oxalyl chloride fluoride indicated several bands which had rotational contours showing considerable fine structure. The rotational band profile of the origin band of the strongest discrete system was studied in considerable detail, and the results are discussed in Chapter 6.

1.4 Symmetry of the Oxalyl Halides

The molecules COXCOX (trans), COXCOX (cis), and COXCOY (cis or trans) are classified under the C_{2h} , C_{2v} and C_s point groups respectively. The character tables for these point groups are given in Tables 1.1, 1.2, and 1.3.[†] The absorption spectra of the oxalyl halides arise from electric dipole transitions (see reference (6), page 58) between the electronic ground state and the different excited states. Such transitions are "allowed" only to states having the symmetries listed in Table 1.4 (see reference (6), page 280). The correlation between irreducible representations of the C_{2h} and C_s point groups is drawn in Table 1.5.

[†]For a concise discussion of group theory see reference (6), page 249.

TABLE 1.1

The Character Table of the C_{2h} Point Group
(For trans COXCOX)

C_{2h}	E	$C_2(z)$	$\sigma_h(x,y)$	i	
A_g	1	1	1	1	R_z
A_u	1	1	-1	-1	T_z
B_g	1	-1	-1	1	R_x, R_y
B_u	1	-1	1	-1	T_x, T_y

TABLE 1.2

The Character Table of the C_{2v} Point Group
(For cis COXCOX)

C_{2v}	E	$C_2(z)$	$\sigma_v(xz)$	$\sigma'_v(yz)$	
A_1	1	1	1	1	T_z
A_2	1	1	-1	-1	R_z
B_1	1	-1	1	-1	T_x, R_y
B_2	1	-1	-1	1	T_y, R_x

yz is the molecular plane.

TABLE 1.3

The Character Table of the C_s Point Group
(For cis and trans COXCOY)

C_s	E	$\sigma_h(xy)$	
A'	1	1	T_x, T_y, R_z
A''	1	-1	T_z, R_x, R_y

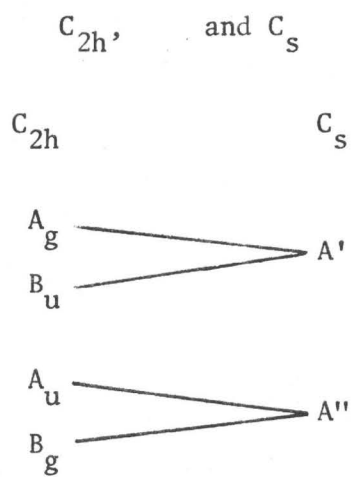
TABLE 1.4

Electric Dipole Allowed Transitions for the cis and trans
Oxalyl Halides from the Ground State (Totally Symmetric)

C_{2h}	C_{2v}	C_s
$A_u \leftarrow A_g$	$A_1 \leftarrow A_1$	$A' \leftarrow A'$
$B_u \leftarrow A_g$	$B_1 \leftarrow A_1$	$A'' \leftarrow A'$
	$B_2 \leftarrow A_1$	

TABLE 1.5

Correlation of Symmetry Species for the Point Groups

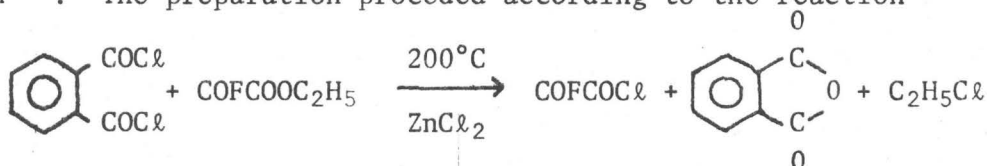


CHAPTER 2

EXPERIMENTAL TECHNIQUES

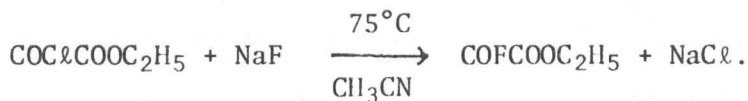
2.1 The Preparation of Oxalyl Chloride Fluoride

Oxalyl chloride fluoride was prepared by a method established by Adelhelm⁽⁸⁾. The preparation proceeded according to the reaction



The exchange reaction was carried out using a 500 ml three-necked flask fitted with dropping funnel, stirrer, and a reflux condensor. The reflux condensor was thermostated at 35°C, and was followed by a trap maintained at -80°C which was followed by a P₂O₅ drying tube to prevent moisture from entering the system. A mixture of 144 ml o-phthalyl chloride and 19.7 g anhydrous zinc chloride (ZnCl₂) were placed in the flask and heated to 200°C over a sulfuric acid temperature bath. A mixture of 56 g COFCOOC₂H₅ and 36 ml o-phthalyl chloride were placed in the dropping funnel, and was added over the course of five hours to the stirred suspension in the flask.

The ethoxalyl fluoride was obtained according to the reaction



150 g NaF and 211 g COClCOOC₂H₅ were mixed with 300 ml of CH₃CN (water free) in a 1 litre flask, and refluxed at 75° for 24 hours. The acetonitrile was removed by distillation and the COFCOOC₂H₅ purified using a spinning band distillation column. The COFCOOC₂H₅ was collected at 106-108.5°C. The anhydrous zinc chloride was prepared by reacting Zn metal with anhydrous HCl in ether which had been dried over Na metal. The ether was removed on a

vacuum line by warming the mixture at a pressure of less than 1 mm.

The volatile reaction products (including oxalyl chloride fluoride) were collected in the trap maintained at dry ice temperature. This product mixture was reported by Adelhelm to contain CO_2 , HCl , C_2H_4 , $\text{C}_2\text{H}_5\text{Cl}$, but no $\text{C}_2\text{O}_2\text{Cl}_2$ or $\text{C}_2\text{O}_2\text{F}_2$. The volatile components (CO_2 , HCl , and C_2H_2) were removed by trap-to-trap distillation at -112°C on a vacuum line. The chloroethane does not have absorption in the near ultraviolet and it was not completely removed. The ultraviolet spectrum however showed that significant quantities of both oxalyl chloride and oxalyl fluoride were present. The oxalyl chloride fluoride was separated from the oxalyl chloride and oxalyl fluoride using trap-to-trap distillation on a vacuum line with a variety of temperatures between -80°C and -23°C , achieved by the use of slush baths.[†] The separation was continued until an ultraviolet spectrum satisfactory for analysis was obtained. The amount of sample obtained which could be used for obtaining UV spectra was less than 5 ml, and even samples of the best purity achieved contained about equal quantities of $\text{C}_2\text{O}_2\text{FCl}$ and $\text{C}_2\text{H}_5\text{Cl}$ with trace amounts of $\text{C}_2\text{O}_2\text{F}_2$ and $\text{C}_2\text{O}_2\text{Cl}_2$.

2.2 The Recording and Measurement of the Ultraviolet Spectra

1. Photographic Recording

Low resolution photographs were obtained on a Bausch and Lomb, model 11, 1.5 meter grating spectrograph using a $10\ \mu$ slit width. This instrument has theoretical resolving powers of 35,000 in the first order and 70,000 in the second order where plate dispersions in the $3500\ \text{\AA}$ region are $14.8\ \text{\AA}/\text{mm}$

[†]A slush bath is a low temperature bath obtained by mixing liquid nitrogen with an organic liquid or liquid mixture.

and 7.4 \AA/mm respectively. High resolution photographs were obtained using two instruments. The majority of the high resolution photographs were recorded on a 20-foot Ebert grating spectrograph which has been described by King⁽⁹⁾. The theoretical resolving powers of this instrument are 150,000 in the first order where plate dispersion is 0.69 \AA/mm and 300,000 in the second order where plate dispersion is 0.35 \AA/mm . Slit widths ranging from 30μ ($\sim 0.2 \text{ cm}^{-1}$ at 3500 \AA in the first order) to 50μ ($\sim 0.3 \text{ cm}^{-1}$) were used.

A few bands were photographed under higher resolution using a spectrograph located in the laboratory of Dr. D. C. Moule at Brock University in St. Catharines, Ontario. This instrument which has been described by Moule et al.⁽¹⁰⁾ is a 20-foot Ebert spectrograph preceded by a Czerny-Turner quartz prism for sorting orders. Spectra were recorded in the 17th order where the theoretical resolving power is 1,300,000 and the dispersion is 0.144 \AA/mm . A slit width of 40μ ($\sim 0.05 \text{ cm}^{-1}$) was used.

The ultraviolet spectra was recorded using two types of film. Wherever possible, Kodak Spectrum Analysis 5367, No. 1, a fine-grained film, was used. It was developed in full strength Kodak D17 developer for 4 minutes and fixed in Kodak fixer. When long exposure times were required, the faster, coarser-grained Kodak I-0 film was used. It was developed in full strength Kodak K19 developer for 5-10 minutes and fixed in Kodak fixer.

The small amount of purified sample available made necessary the use of a multipass gas absorption cell. A 1.8 m cell of the type described by White⁽¹¹⁾ as modified by Bernstein and Herzberg⁽¹²⁾ was used in photographing all spectra. In the weaker absorption regions of the spectrum, the cell was used to provide up to 80 traversals, for path lengths up to 144 meters.

The light source used was a 450 watt Osram high pressure Xenon lamp.

The lamp was run at 21 amps, 120 volts (DC) and was started by means of a striking potential of about 40 kV.

Wavelength measurements of the spectra were made by direct comparison with the iron emission spectrum from a neon-filled hollow iron cathode discharge tube. Accurate wavelengths (vacuum values) for the iron arc lines were taken from tables obtained from the spectroscopy group of the Division of Physics of the National Research Council, Ottawa. The positions along the spectrogram of the absorption bands and the adjacent iron lines were measured from large scale (approximately $\times 10$) photographic enlargements of the film. The measured iron lines were fitted by the method of least squares to an equation of the form $Y = A + BX + CX^2$, and the equation was then used to calculate wavelengths for adjacent absorption bands.

Profiles of absorption bands were obtained from the film by means of a Joyce-Loebel Mk III C double-beam microdensitometer. In some instances, microdensitometer traces were used for the measurement of spectra.

2. Photoelectric Recording

Spectra in the near ultraviolet were recorded using a Cary 14 spectrometer. Spectra in the vacuum ultraviolet were recorded using a McPherson model 225, 1.5 meter spectrometer fitted with a grating ruled with 1200 lines/inch. The source used in the vacuum ultraviolet was a hydrogen high voltage discharge tube.

2.3 Additional Experiments

Experiments on the vapour phase Raman, the emission spectrum of oxalyl chloride, and the low temperature solid state absorption spectrum of oxalyl chloride have been written up in Appendices I, II, and III respectively. These appendices have been written up as self-contained units, and each contains the

pertinent experimental details.

CHAPTER 3

MOLECULAR ORBITAL CALCULATION FOR trans GLYOXAL AND DERIVATIVES

3.1 Introduction

Theoretical calculations have been carried out on molecules of the general formula $(COX)_2$, $X = H, F, Cl$ using the CNDO/2 open shell method. This semi-empirical method has proved fairly successful for calculating the energies of a variety of small molecules^(13,14,15,16,17). The CNDO/2 program was run without altering the parameterization⁽¹⁶⁾ and was applied first to the prototype dicarbonyl compound, glyoxal, with the following aims:

(a) To see how effective the method is in the identification and characterization of the electronic absorption spectral systems in the near and far ultraviolet regions.

(b) To see if CNDO calculations can be used to predict dissociative states.

(c) To check the reliability of geometries predicted by CNDO.

(d) To see if useful information about vibrational force constants can be obtained from the potential surfaces.

The calculations were extended to oxalyl fluoride and in abbreviated form to oxalyl chloride and oxalyl chloride fluoride. The latter two molecules, which contain second row elements, were not handled as well by the program.

These calculations were carried out before the spectra of the cis oxalyl halides had been identified, and only the trans isomer has been considered in these calculations. In the case of $COHCOH$, $COFCOCl$, or $COClCOCl$ the systems due to the cis isomer are not important in the ultraviolet absorption spectrum. For oxalyl fluoride, however, calculations on the cis

isomer should prove to be interesting.

3.2 An Outline of the Approximation Used

The theoretical results described in this work were obtained using the CNDO/2 open shell approximation as described by Pople and Segal⁽¹⁶⁾. The CNDO approximations are also discussed in the series of papers^(13,14,15,17). The approximations involved in this method are summarized very briefly in the following paragraphs. A more complete discussion of the material can be found in the text by Dewar⁽¹⁸⁾.

The Schrödinger equation for a system of particles is

$$\mathcal{H} \psi = E\psi \quad (3.1)$$

where E is the energy of the system, \mathcal{H} is the Hamiltonian operator which includes in principle all terms which contribute to the energy of the system, and ψ is the solution to the operator equation. For the purposes of describing the electronic energy of molecules of the size considered here, it is customary to approximate the Hamiltonian operator by the expression

$$\mathcal{H} = \sum_i \left(-\frac{\hbar^2}{2m} \nabla_i^2 - \sum_{\mu} \frac{Z_{\mu} e^2}{r_{i\mu}} \right) + \sum_{i < j} \sum \frac{e^2}{r_{ij}} \quad (3.2)$$

where \hbar is Planck's constant divided by 2π , m is the mass of the electron, ∇_i is the Laplacian operator for the "i"th electron, Z_{μ} is the mass of the " μ "th nucleus, e is the charge of the electron, $r_{i\mu}$ is the distance between electron "i" and nucleus " μ ", and r_{ij} is the distance between electron "i" and electron "j". Implicit in Equation (3.2) is the Born-Oppenheimer approximation, which assumes the separability of electronic and nuclear motions (energies).

In the Hartree-Fock method of solving Equation (3.1), the Hamiltonian operator is approximated by a sum of single electron operators and the many

electron function Ψ is approximated by a Slater determinant composed of single electron functions (molecular orbitals) $\phi_i \sigma_i$ where σ_i is a function in spin space, and ϕ_i is a function in Cartesian space. Equation (3.1) gives the energy E for a specified configuration $\phi_i \sigma_i$ as

$$E \int \Psi^2 d\tau = \sum_i \int \Psi \mathcal{H}'(i) \Psi d\tau_i \quad (3.3)$$

which after expansion of the determinants reduces to

$$E = 2 \sum_i E_i + \sum_{i < j} \sum_{\uparrow \uparrow} J_{ij} - \sum_{i < j} \sum_{\uparrow \uparrow} K_{ij} \quad (3.4)$$

$$E_i \equiv \int \phi_m(i) \left(-\frac{\hbar^2}{2m} \nabla_i^2 - \sum_{\mu} \frac{Z_{\mu} e^2}{r_{i\mu}} \right) \phi_m(i) d\tau_i \quad (3.5)$$

= K.E. of electron occupying spin orbital $\phi_m \sigma_m$
+ P.E. of electron occupying $\phi_m \sigma_n$ due to all nuclei.

$$J_{ij} \equiv \iint \phi_m(i) \phi_m(i) \frac{e^2}{r_{ij}} \phi_n(j) \phi_n(j) d\tau_i d\tau_j = \text{Coulomb repulsion} \quad (3.6)$$

$$K_{ij} \equiv \iint \phi_m(i) \phi_n(i) \frac{e^2}{r_{ij}} \phi_m(j) \phi_n(j) d\tau_i d\tau_j = \text{exchange integral} \quad (3.7)$$

where the summations over "m" and "n" are over all occupied orbitals; the terms in K_{mn} which contain different spin functions are ignored. The operator $\mathcal{H}'(i)$ is defined as the one electron operator,

$$\mathcal{H}'(i) = -\frac{\hbar^2}{2m} \nabla_i^2 - \sum_{\mu} \frac{Z_{\mu} e^2}{r_{i\mu}} + V_i \quad (3.8)$$

V_i is the inter-electron potential determined by the other electrons, and since it can only be evaluated from the J and K integrals where a set of $\phi_i \sigma_i$ are available, the Hartree-Fock method is iterative; a zeroth order set of $\phi_i \sigma_i$ is used to produce an improved set which is then recycled.

This method is called the self consistent field (SCF) method.

The next step is to approximate the single electron MO's ϕ_m by a linear combination of atomic orbitals χ_i (the LCAO-MO method).

$$\phi_m = \sum_i a_{mi} \chi_i \quad i = 1, 2, 3, \dots, m \quad (3.9)$$

Substitution of (3.9) into (3.3), (3.5), (3.6) and (3.7) with evaluation of the coefficients "a_{mi}" by the variational method produces the Roothaan equations:

$$\sum_j a_{mj} (F_{ij} - ES_{ij}) = 0 \quad (3.10)$$

$$\text{where } S_{ij} = \int \chi_i^* \chi_j d\tau \quad (3.11)$$

$$F_{ij} = \int \chi_i^* \mathcal{H} \chi_j d\tau \quad (3.12)$$

$$= \int \chi_i^* (\mathcal{H}^C) \chi_j d\tau + \sum_{k\ell} P_{k\ell} [(ij, k\ell) - \frac{1}{2}(ik, j\ell)] \quad (3.13)$$

using the abbreviations

$$\mathcal{H}^C = -\frac{\hbar^2}{2m} \nabla^2 - \sum_{\mu} \frac{Z_{\mu} e^2}{r_{\mu i}}$$

$$P_{k\ell} = 2 \sum_n a_{nk} a_{n\ell}$$

$$(ij, k\ell) = \iint \chi_i(1) \chi_j(1) \frac{e^2}{r_{12}} \chi_k(2) \chi_{\ell}(2) d\tau_1 d\tau_2 \quad (3.14)$$

$$(ik, j\ell) = \iint \chi_i(1) \chi_k(1) \frac{e^2}{r_{12}} \chi_j(2) \chi_{\ell}(2) d\tau_1 d\tau_2 \quad (3.15)$$

The solution of Equations (3.10) for polyatomic molecules is still a very complex procedure. The additional approximations introduced by the CNDO procedure are designed to reduce the calculations to manageable size. These approximations described as complete neglect of differential overlap may be summarized

$$(1) \quad S_{ij} = \delta_{ij} \quad (3.16)$$

$$(2) \quad (ij, k\ell) = 0 \quad \text{if } i \neq j, k \neq \ell \quad (3.17)$$

$$(ik, j\ell) = 0 \quad \text{if } i \neq k, j \neq \ell \quad (3.18)$$

Substitution of these approximations in Equation (3.13) produces

$$\begin{aligned} F_{ii} &= H_{ii}^c + \sum_k P_{kk} [(ii,kk) - \frac{1}{2}(ik,ik)] \\ &= H_{ii}^c + \sum_j P_{jj} (ii,jj) - \frac{1}{2} P_{ii} (ii,ii) \end{aligned} \quad (3.19)$$

$$F_{ij} = H_{ij}^c - \frac{1}{2} P_{ij} (ii,jj) \quad (3.20)$$

These expressions are commonly written in a more condensed form using the following relations.

$$H_{ii}^c = \int \chi_i^* \left(-\frac{\hbar^2}{2m} \nabla^2 - \frac{Z_A e^2}{r_{iA}} \right) \chi_j d\tau - \int \chi_i^* \sum_{B \neq A} \frac{Z_B e^2}{r_{iB}} \chi_j d\tau \quad (3.21)$$

χ_i on atom A

$$\equiv U_{ii} - \sum_{B \neq A} V_{AB} \quad (3.22)$$

$$\begin{aligned} \sum_{j \neq i} P_{jj} (ii,jj) &= \sum_{\ell}^{\text{nucleus A}} P_{\ell\ell} (ii,\ell\ell) + \sum_{B \neq A} \sum_{\ell}^{\text{nucleus B}} P_{\ell\ell} (ii,\ell\ell) \\ &\equiv P_{AA} \gamma_{AA} + \sum_{B \neq A} P_{BB} \gamma_{AB} \end{aligned} \quad (3.23)$$

$$H_{ij}^c \equiv \beta_{AB}^o S_{ij} \quad (3.24)$$

$$P_{ij} (ii,jj) = P_{ij} \gamma_{AB} \quad (3.25)$$

$$\beta_{AB}^o = \frac{1}{2} (\beta_A + \beta_B) \quad (3.26)$$

$V_{AB}, \gamma_{AA}, \gamma_{AB}, \beta_A, \beta_B$ are empirically chosen parameters.[†]

The orbital energies are given in terms of the elements of the Fock matrix by:

$$\epsilon_m = \sum_i \sum_j a_{mi} a_{mj} F_{ij} \quad (3.27)$$

[†]For the parameterization, see reference 16.

After evaluation of the Fock matrix elements, the orbital energies of a system are expressed in terms of these elements. The electronic energy of the system is obtained by summing over the energies of the occupied orbitals as in Equation 3.28.

$$E = 2 \sum_m \epsilon_m - \sum_m \sum_n (2J_{mn} - K_{mn}) \quad (3.28)$$

The CNDO method is applied here to the calculation of the energies of electronic states, of which many are open shell systems. In order to approximate the energies of these open shell states, the CNDO/2 open shell approximation was used. The philosophy behind this method is that the electron in a singly-occupied orbital can undergo exchange interaction only with electrons of the same spin. Under the SCF iterative procedure for determining the coefficients a_{mi} , the spatial part of the MO's for electrons having the same spin may be slightly different from these corresponding to the opposite spin. This effect is approximated by setting up two separate Slater determinants corresponding to α or β spin, and carrying out a complete SCF iterative calculation on each of the α and β "shells". In this approximation, the electronic energy of a system is given by

$$E = \sum_p \{ \epsilon_p - \sum_n (J_{pn} - \frac{1}{2} K_{pn}^\alpha) \} + \sum_q \{ \epsilon_q - \sum_n (J_{qn} - \frac{1}{2} K_{qn}^\beta) \} \quad (3.29)$$

p = number of electrons with α spin

q = number of electrons with β spin

$$\epsilon_m^\alpha = \sum_i \sum_j a_{mi}^\alpha a_{mj}^\alpha F_{ij}^\alpha \quad (3.30)$$

$$F_{ii}^\alpha = H_{ii}^{C\alpha} - P_{ii}^\alpha (ii,ii) + \sum_j (P_{jj}^\alpha + P_{jj}^\beta) (ii,jj) \quad (3.31)$$

$$F_{ij}^\alpha = H_{ij}^{C\alpha} - P_{ij}^\alpha (ii,jj) \quad (3.32)$$

$$P_{ij}^\alpha = \sum_n a_{ni}^\alpha a_{nj}^\alpha \quad (3.33)$$

A symmetrically equivalent set of equations exists for the shell corresponding to β electron spin. It should be noted that under this approximation, the Slater determinants employed as wavefunctions for each shell are not exact eigen functions of the total spin operator S^2 (see reference 17). In the open shell calculations carried out on glyoxal derivatives, excited states were obtained by removing an electron from the α shell and adding it to the β shell. Since the remaining occupied α molecular orbitals resemble the corresponding orbitals in the β shell very closely, this configuration is an approximate $\beta\beta$ spin configuration. The configuration employed therefore is a "near" triplet state, but does contain terms which are components of states of other multiplicities. No correction was made for this defect and the energies obtained were taken as pure triplet state energies. The energies of the corresponding singlet states were estimated by adding to the triplet state energy the value of the exchange integral between the space part of the two molecular orbitals (ϕ_m, ϕ_n) involved in the transition:

$$K_{mn} = \iint \phi_m(1) \phi_n(2) \frac{e^2}{r_{12}} \phi_n(1) \phi_m(2) dr_1 dr_2 \quad (3.34)$$

If the MO's in Equation (3.34) are expanded as LCAO's, the exchange integral becomes

$$K_{mn} = \sum_i \sum_j \sum_k \sum_l a_{mi} a_{nj} a_{nk} a_{ml} (ik, jl) \quad (3.35)$$

In the CNDO approximation, this becomes

$$\begin{aligned} K_{mn} &= \sum_i \sum_j a_{mi} a_{nj} a_{ni} a_{mj} (ii, jj) \\ &= \sum_A \sum_B \sum_i \sum_j a_{mi} a_{nj} a_{ni} a_{mj} \gamma_{AB} \end{aligned} \quad (3.36)$$

where the parameter γ_{AB} is given the CNDO/2 value (see reference 16). The

CNDO approximations are based upon the assumption that exchange terms which are due to exchange of electron 1 between the same atomic orbital χ_A in the two molecular orbitals and electron 2 between the same atomic orbital χ_B are much larger than all other types. This approximation is adequate in the case where the molecular orbitals involved in the calculation in Equation (3.36) employ the same atomic orbitals as a basic set. In the case of a pair of MO's for which the expansions as LCAO's contain no atomic orbitals in common, the exchange integral is zero. For example, an excited state which is produced by \underline{n} to π^* promotion would have zero singlet-triplet splitting. In cases where the exchange integral in the CNDO approximation was zero, the calculation was expanded to include exchange terms which are due to exchange of electron 1 between two atomic orbitals on the same atom and electron 2 between atomic orbitals on the same atom. Exchange integrals of this type were taken into account in the work by Pople, Beveridge and Dobosh⁽¹⁷⁾ on the INDO (intermediate neglect of differential overlap) method. These authors approximated the one center exchange integrals by the values of the same exchange integrals in the appropriate free atom. The same approximation has been employed here, and the values for these integrals were taken from this reference.

At this level of approximation, the exchange integral between MO's which have no projection on common atomic orbitals is given by

$$K_{mn} = \sum_A \sum_{i,j} \sum_{\text{nuclei}} a_{mi} a_{nk} a_{mi} a_{nk} (ik, ik) \quad (3.37)$$

single center

Equation (3.37) takes account of exchange of electron 1 and electron 2 between an identical pair of one center atomic orbitals.

3.3 The Electronic Structure of Glyoxal

An early molecular orbital calculation on biacetyl ($\text{COCH}_3\text{COCH}_3$) was carried out by McMurray⁽¹⁹⁾ in 1941. He applied the Hückel MO method to the π orbitals of the $\text{O}=\text{C}-\text{C}=\text{O}$ chain and assigned the near ultraviolet transitions to promotion of the non-bonding \underline{n} electrons of the oxygen atoms to the low-lying π^* orbitals. The two \underline{n} orbitals were treated as pure $p_y^{(O)}$ atomic orbitals which were perpendicular to the π system and the $\text{C}=\text{O}$ bond, without interaction with the remaining bonding orbitals. Two degenerate \underline{n} orbitals (of symmetry a_g and b_u) result from this approach, and within this framework, the two principal transitions of biacetyl at 22000 cm^{-1} and 35500 cm^{-1} were assigned as singlet-singlet $n_{a_g}^- \rightarrow \pi_{a_u}^*$ and $n_{b_u}^+ \rightarrow \pi_{b_g}^*$ respectively. This assignment of biacetyl was transferred by analogy to glyoxal (COHCOH) by Walsh⁽²⁰⁾ who assigned the transitions at 22000 cm^{-1} and 31000 cm^{-1} as singlet-singlet $n_{a_g}^- \rightarrow \pi_{a_u}^*$ and $n_{b_u}^+ \rightarrow \pi_{b_g}^*$ respectively.

Later calculations on these two molecules have refined the approximations made by McMurray, but have preserved the above assignments in the near UV. Sidman⁽²¹⁾ carried out a semi-empirical SCF-LCAO-MO virtual orbital calculation for glyoxal. This calculation was more rigorous than that carried out by McMurray, but the \underline{n} electrons were still treated as pure (non-interacting) p_y orbitals of oxygen, which are necessarily degenerate. He assigned the two near UV transitions of glyoxal as the two $n \rightarrow \pi^*$ transitions.

In the CNDO calculation carried out here on glyoxal, the \underline{n} orbitals have not been treated as being separate from the calculation of the molecular orbitals of the molecule. However, the calculation indicates that in fact there are a pair of high energy bonding molecular orbitals which can be described as \underline{n} orbitals. The coordinate system shown in Figure 3.1 was used

throughout the calculation. The orientation of the molecule was chosen to reflect the convention of labelling the p_y orbitals of the oxygen atom as the n orbitals.

The geometry of the molecule can be specified by five parameters - three bond lengths and two angles. An initial calculation was carried out on the ground state of glyoxal using a geometry which was calculated from parameter values transferred from similar molecules. The five parameters were varied systematically to minimize the calculated energy. The resulting geometry is subsequently referred to as the CNDO geometry, and the CNDO geometries of the ground and some excited states are listed in Table 3.1. The available experimental data on the ground state has been included in the table. The CNDO geometry was used throughout the calculations. (Experimental geometries were not available for the oxalyl derivatives, and it was anticipated that the CNDO geometries would have to be used in these cases.)

The basis set used in the calculations on glyoxal consisted of 18 atomic orbitals (1s on hydrogen, 2s, $2p_x$, $2p_y$, $2p_z$ on carbon and oxygen). The form of the SCF-LCAO MO's in the ground state is given in Table 3.2 with the MO's listed in order of decreasing energy. Table 3.2 lists the coefficients of the atomic orbitals for the molecular orbitals, and categorizes the MO's as n-type, σ -type or π -type, each with the corresponding symmetry under the C_{2h} point group. Molecular orbitals 8 and 10 have large projections on the p_y (oxygen) orbitals. In both cases the orbitals have at least 50% p_y (oxygen) character, and they are labelled $n_{a_g}^-$ and $n_{b_u}^+$. An energy level diagram of the ground state molecular orbitals with the electron population of the ground state is given in Fig. 3.2.

Table 3.3 gives the bond order matrix for the 1A_g (G.S.) corresponding

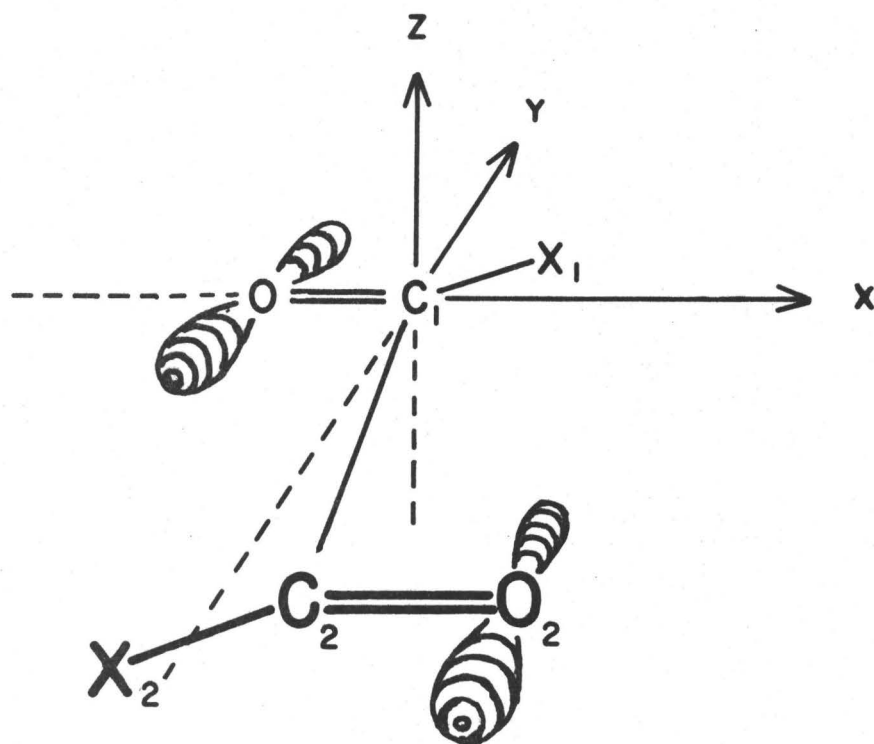


Figure 3.1. Coordinate system used for the calculation of the trans glyoxal derivatives.

TABLE 3.1

CNDO Geometries for Ground and Excited States of Glyoxal

State	r_{CC} Å	r_{CO} Å	r_{CH} Å	$\angle OCH$ deg	$\angle CCO$ deg
1A_g (G.S.)	1.44	1.26	1.12	118	123
${}^1, {}^3A_u(n_{a_g}^-, \pi_{a_u}^*)$	1.40	1.27	1.12	120	125
${}^1, {}^3B_u(\pi_{b_g}, \pi_{a_u}^*)$	1.33	1.36	1.14	118	123
${}^1, {}^3B_u(n_{a_g}^-, \sigma_{1b_u}^*)^a$		1.23	1.22		<100

^aThe energy for this state showed an unusually shallow potential curve as a function of r_{CH} and r_{CC} , and optimized at 70° for $\angle CCO$ (see Figures 3.6, 3.7, 3.8). This state may be dissociative.

Experimental Geometries for Glyoxal

State	r_{CC}	r_{CO}	r_{CH}	$\angle OCH$	$\angle CCO$
1A_g (G.S.) ^b	1.525	1.207	1.116	126.6	121.2
${}^1, {}^3A_u(n_{a_g}^-, \pi_{a_u}^*)^c$	1.362	1.325	1.090	118.3	121.9
	1.406	1.294	1.095	120.5	122.7
	1.445	1.266	1.100	122.4	123.2
	1.481	1.242	1.105	124.1	123.6
	1.514	1.219	1.100	125.8	123.9

^bElectron diffraction; results of Kuchitsu et al. (22)

^cUltraviolet spectroscopy; result of Paldus and Ramsay (23). These possible sets of values were consistent with the rotational constants obtained for the origin bonds of $C_2H_2O_2$ and $C_2D_2O_2$. A definitive geometry could not be obtained from two isotopes.

	1 * σ_{5a_g}	2 * σ_{4b_u}	3 * σ_{3b_u}	4 * σ_{2a_g}	5 * π_{b_g}	6 * σ_{1b_u}	7 * π_{a_u}	8 - n_{a_g}	9 π_{b_g}
1sH	-.130438	.061843	-.191236	.448104	0.000000	.490662	0.000000	-.330347	0.000000
2sC	-.177159	.050628	-.362384	-.338193	0.000000	-.440928	0.000000	.072157	0.000000
2s0	-.177159	.050628	.362384	-.338193	0.000000	.440928	0.000000	.072157	0.000000
2p _x ^C	.226773	.189485	.172282	.077442	0.000000	.028267	0.000000	.009269	0.000000
2p _x ⁰	.226773	-.189485	-.172282	.077442	0.000000	-.028267	0.000000	.009269	0.000000
2p _y ^C	.504174	.470516	.163360	-.028818	0.000000	-.193544	0.000000	.058251	0.000000
2p _y ⁰	-.504174	.470516	.163360	.028817	0.000000	-.193544	0.000000	-.058251	0.000000
2p _z ^C	.350921	.294556	.297753	.154842	0.000000	.076629	0.000000	.009098	0.000000
2p _z ⁰	-.350921	.294556	.297753	-.154842	0.000000	-.076629	0.000000	-.009098	0.000000
2p _x ⁰	.150106	-.381858	.422537	-.380954	0.000000	-.137599	0.000000	-.329314	0.000000
2p _y ⁰	-.150106	-.381858	.422537	.380954	0.000000	.137599	0.000000	.329314	0.000000
2p _z ^C	.017496	.061185	-.092546	-.094336	0.000000	.042067	0.000000	.523120	0.000000
2p _z ⁰	-.017496	.061185	-.092546	.094336	0.000000	-.042067	0.000000	-.523120	0.000000
2p _x ^C	0.000000	0.000000	0.000000	0.000000	-.601185	0.000000	-.447939	0.000000	.372258
2p _x ⁰	0.000000	0.000000	0.000000	0.000000	.601185	0.000000	.447939	0.000000	-.372258
2p _y ^C	0.000000	0.000000	0.000000	0.000000	.372258	0.000000	.547130	0.000000	.601185
2p _y ⁰	0.000000	0.000000	0.000000	0.000000	-.372258	0.000000	-.547130	0.000000	-.601185

	10 + n_{b_u}	11 σ_{1a_g}	12 π_{a_u}	13 σ_{2b_u}	14 σ_{3a_g}	15 σ_{4b_u}	16 σ_{5a_g}	17 σ_{6b_u}	18 σ_{7a_g}
1sH	-.241538	-.226119	0.000000	-.029285	-.281735	.396442	.135160	-.049904	.155844
2sC	.241538	-.226119	0.000000	.029285	-.281735	-.396442	.135160	.049904	.155844
2s0	-.115329	-.018805	0.000000	.161822	-.101999	.274719	.331592	-.238201	.477831
2p _x ^C	.115329	-.018805	0.000000	-.161822	-.101999	-.274719	.331592	.238201	.477831
2p _x ⁰	-.019056	-.118003	0.000000	-.307286	.151850	-.088176	-.433730	-.575372	.466247
2p _y ^C	.019056	-.118003	0.000000	.307286	.151850	.088176	-.433730	.575372	.466247
2p _y ⁰	-.135414	-.366540	0.000000	-.259296	-.063630	.182205	.315214	.309384	-.061852
2p _z ^C	.135414	.366540	0.000000	.259296	-.063630	-.182205	-.315214	-.309384	.061852
2p _x ⁰	.081104	.529430	0.000000	.541387	-.195780	.077916	-.134575	-.113838	.126727
2p _y ⁰	-.081104	-.529430	0.000000	-.541387	.195780	-.077916	.134575	.113838	-.126727
2p _z ^C	.066997	-.061798	0.000000	-.057227	-.400662	.384599	-.224025	-.032155	-.096740
2p _z ⁰	-.066997	.061798	0.000000	.057227	.400662	-.384599	.224025	.032155	.096740
2p _x ^C	.631342	-.126988	0.000000	-.122155	-.429249	.269077	-.126489	-.002402	-.027564
2p _x ⁰	-.631342	.126988	0.000000	.122155	.429249	-.269077	.126489	.002402	.027564
2p _y ^C	0.000000	0.000000	.547130	0.000000	0.000000	0.000000	0.000000	0.000000	0.000000
2p _y ⁰	0.000000	0.000000	-.547130	0.000000	0.000000	0.000000	0.000000	0.000000	0.000000
2p _z ^C	0.000000	0.000000	.447939	0.000000	0.000000	0.000000	0.000000	0.000000	0.000000
2p _z ⁰	0.000000	0.000000	-.447939	0.000000	0.000000	0.000000	0.000000	0.000000	0.000000

TABLE 3.2 Molecular Orbital Glyoxal ¹A_g (G.S.) in Order of Decreasing Energy.

	1s _{H1}	1s _{H2}	2s _{C1}	2s _{C2}	2s _{O1}	2s _{O2}	2p _x C1	2p _x C2	2p _x O1
1s _H	1.003168	.126676	.544822	-.030733	.004271	-.025047	.351252	.037228	-.044871
2s _C	.126676	1.003168	-.030733	.544822	-.025047	.004271	-.037228	-.351252	-.049463
2s _O	.544822	-.030733	1.050081	.365442	.263476	.001874	.061024	-.259061	.482051
2p _x C	-.030733	.544822	.365442	1.050081	.001874	.263476	.259061	-.061024	-.024716
2p _x O	.004271	-.025047	.263476	.001874	1.753378	.017999	-.447833	.000439	-.399743
2p _y C	.025047	.004271	.001874	.263476	.017999	1.753378	-.000439	.447833	.035478
2p _y O	.351252	-.037228	.061024	.259061	-.447833	-.000439	.915361	-.060744	-.689337
2p _z C	.037228	-.351252	-.259061	-.061024	.000439	.447833	-.060744	.915361	-.000125
2p _z O	-.044871	-.049463	.482051	-.024716	-.399743	.035478	-.689337	-.000125	1.346976
2p _x C	.049463	.044871	.024716	-.482051	-.035478	.399743	-.000125	-.689337	-.068323
2p _y C	.724752	.036540	.018573	-.428295	-.002139	-.015788	-.005555	.341311	.007091
2p _y O	.036540	-.724752	.428295	-.018573	.002139	.015788	.005555	-.341311	-.018150
2p _z C	.172262	-.004785	.021562	.093154	-.000417	-.012930	.011934	-.033740	-.004380
2p _z O	.004785	.172262	-.093154	-.021562	.000417	.012930	-.011934	.033740	.029285
2p _x O2	0.000000	0.000000	0.000000	0.000000	0.000000	0.000000	0.000000	0.000000	0.000000
2p _y C1	0.000000	0.000000	0.000000	0.000000	0.000000	0.000000	0.000000	0.000000	0.000000
2p _y C2	0.000000	0.000000	0.000000	0.000000	0.000000	0.000000	0.000000	0.000000	0.000000
2p _y O1	0.000000	0.000000	0.000000	0.000000	0.000000	0.000000	0.000000	0.000000	0.000000
2p _y O2	0.000000	0.000000	0.000000	0.000000	0.000000	0.000000	0.000000	0.000000	0.000000
2p _z C1	0.000000	0.000000	0.000000	0.000000	0.000000	0.000000	0.000000	0.000000	0.000000
2p _z C2	0.000000	0.000000	0.000000	0.000000	0.000000	0.000000	0.000000	0.000000	0.000000
2p _z O1	0.000000	0.000000	0.000000	0.000000	0.000000	0.000000	0.000000	0.000000	0.000000
2p _z O2	0.000000	0.000000	0.000000	0.000000	0.000000	0.000000	0.000000	0.000000	0.000000
1s _H	.049463	.724752	-.036540	-.172262	.004785	0.000000	0.000000	0.000000	0.000000
2s _C	.044871	.036540	-.724752	-.004785	.172262	0.000000	0.000000	0.000000	0.000000
2s _O	.024716	.018573	.428295	.021562	-.093154	0.000000	0.000000	0.000000	0.000000
2p _x C	-.482051	-.428295	-.018573	.093154	-.021562	0.000000	0.000000	0.000000	0.000000
2p _x O	-.035478	-.002139	.015788	-.000417	.012930	0.000000	0.000000	0.000000	0.000000
2p _y C	.399743	-.015788	.002139	-.012930	.000417	0.000000	0.000000	0.000000	0.000000
2p _y O	-.000125	-.005555	.341311	.011934	-.033740	0.000000	0.000000	0.000000	0.000000
2p _z C	-.689337	.341311	-.005555	-.033740	.011934	0.000000	0.000000	0.000000	0.000000
2p _z O	-.068323	.007091	-.018150	-.004380	.029285	0.000000	0.000000	0.000000	0.000000
2p _x C	1.346976	-.018150	.007091	.029285	-.004380	0.000000	0.000000	0.000000	0.000000
2p _y C	-.018150	.977003	-.351236	.212357	.058903	0.000000	0.000000	0.000000	0.000000
2p _y O	.007091	-.351236	.977003	.058903	-.212357	0.000000	0.000000	0.000000	0.000000
2p _z C	.029285	.212357	.058903	1.954033	-.09580	0.000000	0.000000	0.000000	0.000000
2p _z O	-.004380	.058903	.212357	-.09580	1.954033	0.000000	0.000000	0.000000	0.000000
2p _x C	0.000000	0.000000	0.000000	0.000000	0.000000	.867994	.320882	.936784	.045217
2p _y C	0.000000	0.000000	0.000000	0.000000	0.000000	.320882	.867994	.045217	.936784
2p _z C	0.000000	0.000000	0.000000	0.000000	0.000000	.936784	.045217	1.132006	-.320882
2p _x O	0.000000	0.000000	0.000000	0.000000	0.000000	.045217	.936784	-.320882	1.132006

TABLE 3.3 Bond Order Matrix Glyoxal ¹A_g (G.S.)

to the MO's of Table 3.2. The elements of this matrix (B.O.) ij give the sum $\sum_m c_{im} c_{jm}$ over all occupied orbitals "m" of the products of pairs of coefficients c_{im} , c_{jm} of the atomic orbitals used as a basis set. Table 3.4 gives the corresponding bond order matrix for the ${}^3A_u(n_{a_g}^-, \pi_{a_u}^*)$ excited state.

The excited states of immediate interest are those for which the electron configuration corresponds to the promotion of one electron in the molecular orbital scheme given in Fig. 3.2. A subroutine was added to the CNDO/2 Open Shell program which identified each molecular orbital by its symmetry under the C_{2h} point group. A self-consistent field calculation was then carried out for an excited state by filling the lowest energy molecular orbitals to give a specified configuration $(a_g)^i (a_u)^j (b_g)^k (b_u)^l$. In this manner, SCF calculations were carried out for those excited triplet states which lay within approximately $100,000 \text{ cm}^{-1}$ of the ground state. Singlet state energies were then obtained using the exchange energy calculated from one of Equations (3.36) or (3.37) as discussed in Section 3.2. Table 3.5 lists the singlet and triplet state energies calculated for the ground and excited states. Figures 3.3 and 3.4 give energy level diagrams of the "u" and "g" states respectively.

3.4 The Calculated Electronic Spectrum of Glyoxal

Using the CNDO data calculated for glyoxal, additional calculations were carried out to obtain the transition energies, transition intensities, and vibrational structure predicted by CNDO.

(a) Transition Energies

The transition energies were obtained by taking the differences between the excited state SCF energies and the ground state SCF energy. Both

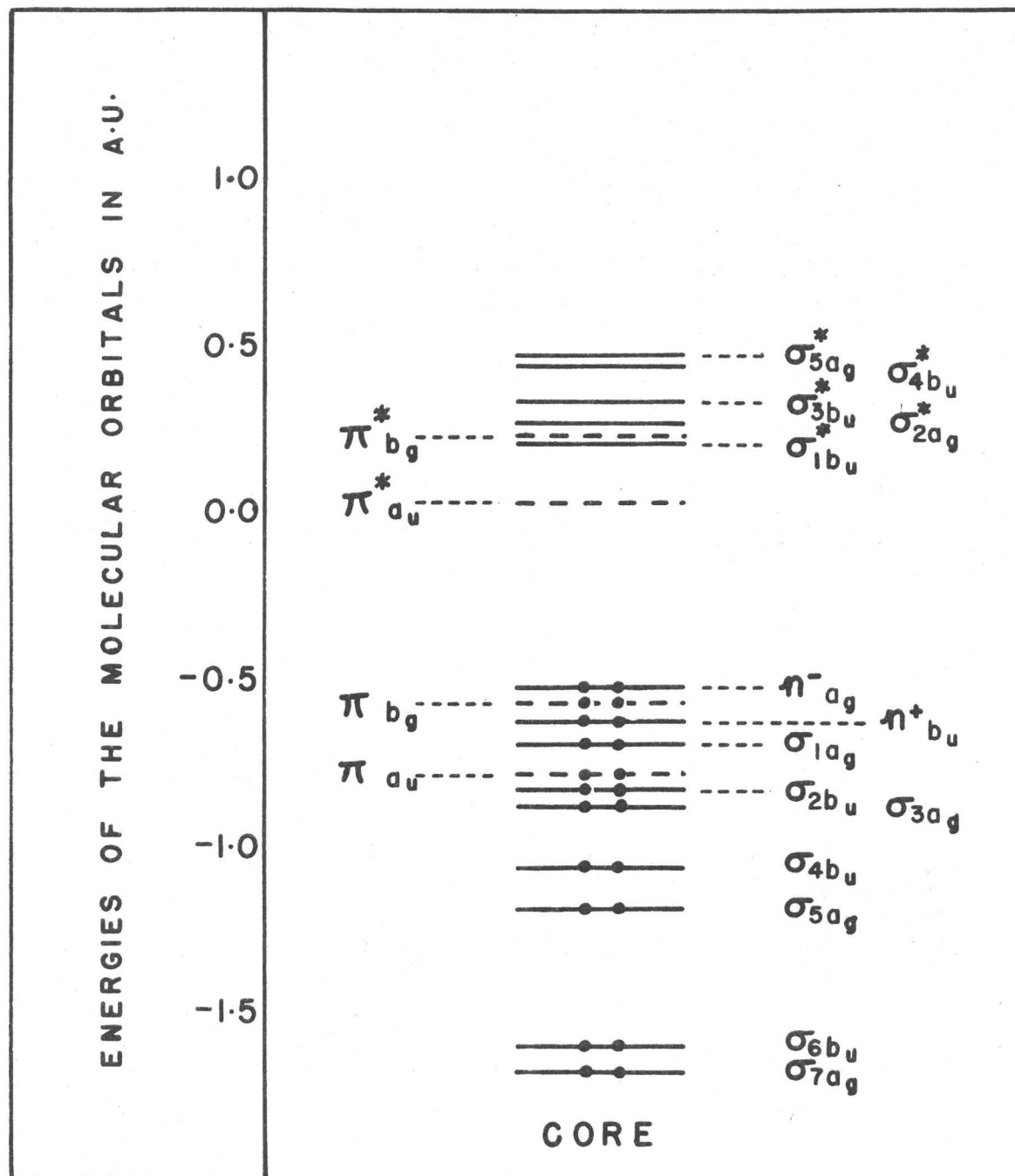


Figure 3.2 Energies (and Electron Population) of the Molecular Orbitals of Glyoxal in the Ground State. Geometry was $\text{CCO} = 123^\circ$, $\text{OCH} = 118^\circ$, $r_{\text{CC}} = 1.44$, $r_{\text{CO}} = 12.6$, $r_{\text{CH}} = 1.12$.

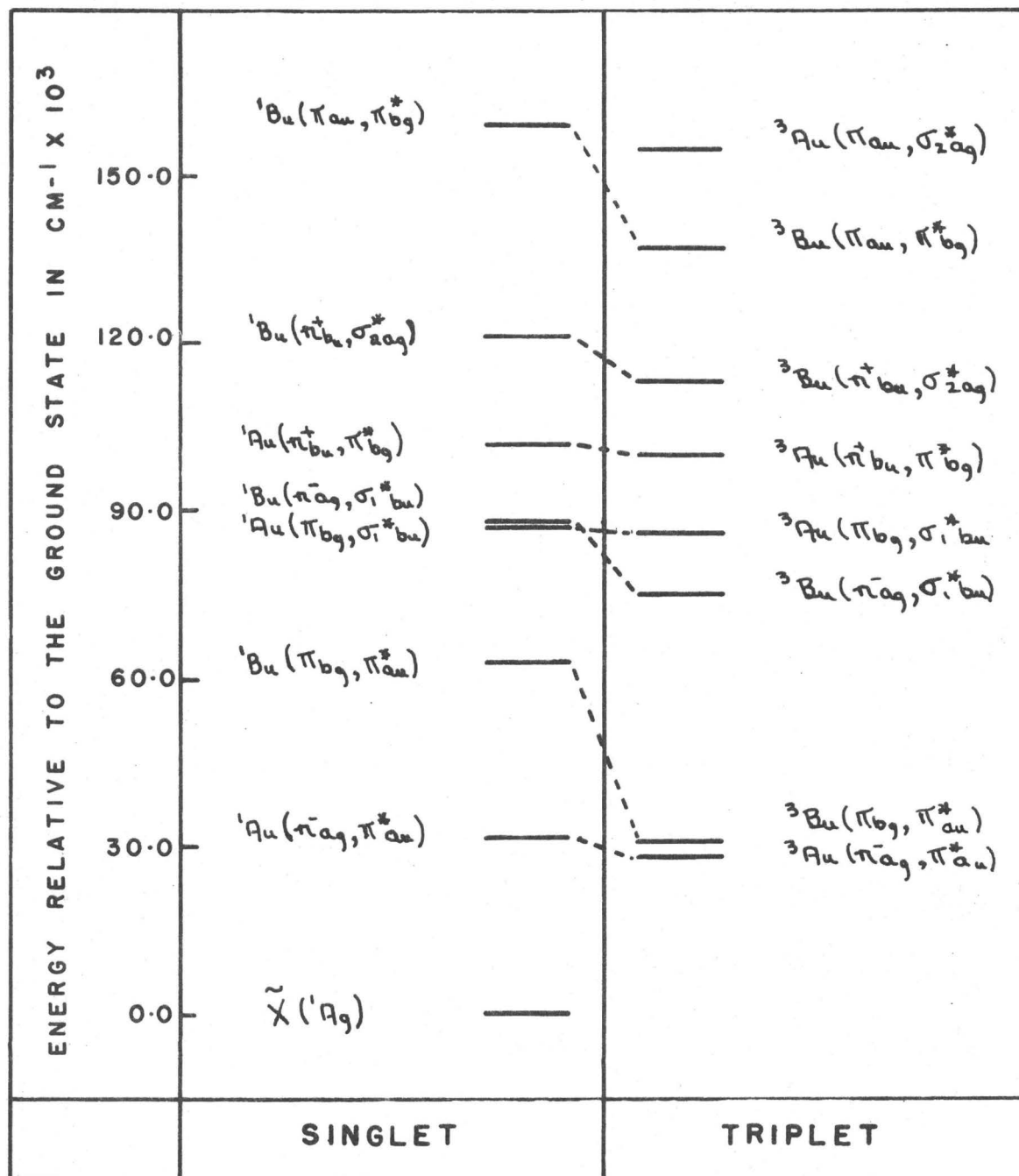


Figure 3.3 CNDO Energies for the "u" States of Glyoxal at the CNDO Ground State Geometry.

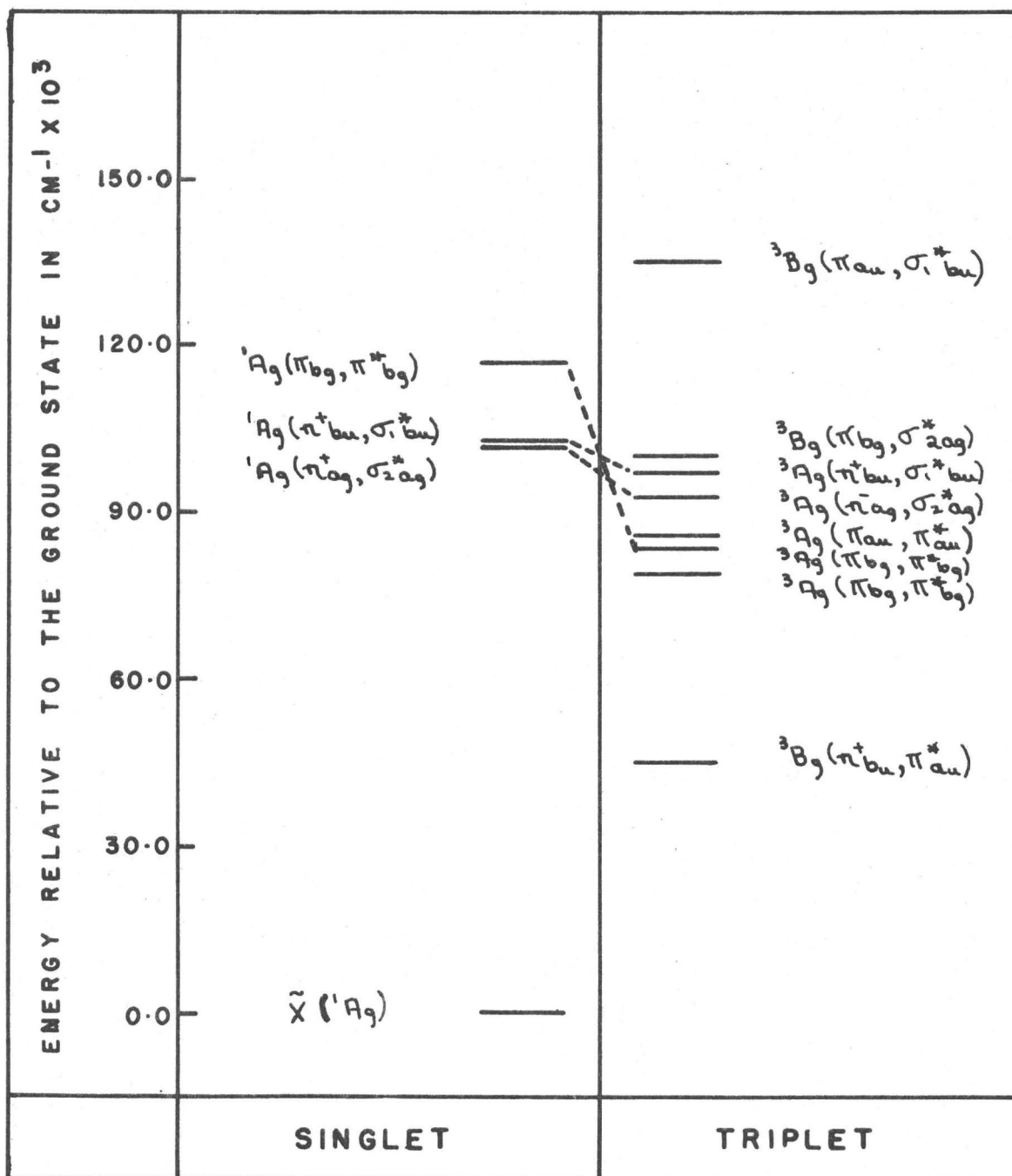


Figure 3.4 CND0 Energies for the "g" States of Glyoxal at the CND0 Ground State Geometry.

TABLE 3.5

Calculated SCF-LCAO-MO Energies for Ground and Excited States of Glyoxal with Transition Energies
and Oscillator Strengths

State	Energy ^a a.u.	Calculated		V.T.E. cm ⁻¹	Exp. ^b Origin	Exp. ^c Transition cm ⁻¹	Calc. Osc.	Exp. Strength
		Vertical a.u.	Transition Energy cm ⁻¹					
\bar{X} A _g	-52.279							
n _{a_g} ⁻ → π _{a_u} [*]	³ A _u	-52.149	0.130	28500	3500	27400	19197	0.4 × 10 ⁻⁶
	¹ A _u	-52.137	0.142	31200	3200	29600	21973	0.4 × 10 ⁻³
π _{b_g} → π _{a_u} [*]	³ B _u	-52.137	0.142	31200	3200	14700		~10 ⁻⁷
		-51.992	0.287	63000	1590	57000	50000	0.55
n _{a_g} ⁻ → σ _{1b_u} [*]	³ B _u	-51.935	0.344	75500	1300			~10 ⁻⁷
	¹ B _u	-51.879	0.400	87800	1140	50000		0.25
π _{b_g} → σ _{1b_u} [*]	³ A _u	-51.887	0.392	86000				
	¹ A _u	-51.880	0.399	87600	52500			0.2 × 10 ⁻¹
n _{b_u} ⁺ → π _{b_g} [*]	³ A _u	-51.823	0.456	100000				
	¹ A _u	-51.815	0.464	102000				0.6 × 10 ⁻²
n _{b_u} ⁺ → σ _{2a_g} [*]	³ B _u	-51.764	0.515	113000				
	¹ B _u	-51.728	0.551	121000				
π _{a_u} → π _{b_g} [*]	³ B _u	-51.657	0.622	137000				
	¹ B _u	-51.553	0.726	159000				
π _{a_u} → σ _{2a_g} [*]	³ A _u	-51.575	0.704	155000				

TABLE 3.5 (cont'd.)

State	Energy ^(a) a.u.	Calculated		Exp. V.T.E. cm ⁻¹
		Vertical a.u.	Transition Energy cm ⁻¹ Å	
n _{b_u} ⁺ → π _{a_u} [*]	³ B _g	-52.074	0.205	45000
	¹ B _g	--		
n _{a_g} ⁻ → π _{b_g} [*]	³ B _g	-51.920	0.359	78800
	¹ B _g	--		
π _{b_g} → π _{b_g} [*]	³ A _g	-51.899	0.380	83400
	¹ A _g	-51.749	0.530	116300
π _{a_u} → π _{a_u} [*]	³ A _g	-51.888	0.391	85800
	¹ A _g			
n _{a_g} ⁻ → σ _{2a_g} [*]	³ A _g	-51.857	0.422	92600
	¹ A _g	-51.814	0.465	102000
n _{b_u} ⁺ → σ _{1b_u} [*]	³ A _g	-51.835	0.444	97400
	¹ A _g	-51.812	0.467	102000
π _{b_g} → σ _{2a_g} [*]	³ B _g	-51.824	0.455	99900
	¹ B _g	--		
π _{a_u} → σ _{1b_u} [*]	³ B _g	-51.666	0.613	135000
	¹ B _g	--		

^aCalculated from the geometry CC = 1.44 Å, CO = 1.26 Å, CH = 1.12 Å, ∠OCH = 118°, ∠CCO = 123°.

^bTaken from A. D. Walsh, reference 20.

^cTaken from G. Herzberg, reference 7.

origin transition energies and vertical transition energies were calculated.[†] The vertical transition energies were obtained from the ground and excited state at the CNDO geometry. The origin transition energy was obtained using the lowest excited state energy (as obtained by optimizing parameters). The transition energies have been listed in Table 3.5. Since no attempt has been made to achieve a high degree of accuracy, the zero point energies have not been considered.

(b) Transition Intensities

(i) Singlet-Singlet Transitions

Intensities of transitions to the excited singlet states obtained in the CNDO/2 calculation were obtained using Equation (3.38) (see reference 6). Only the dipole moment transitions have been considered since we are concerned with transitions at least as intense as the electric dipole $n \rightarrow \pi^*$ transition.

$$f_{\text{OSC}} = 1.085 \times 10^{-5} \nu_{01} |\underline{M}_{01}|^2 / e^2 \quad (3.38)$$

$$\text{where } \nu_{01} = E_1 - E_0 \quad \text{in wave numbers} \quad (3.39)$$

$$\underline{M}_{01} = \int \psi_1^* \sum_i e_i \underline{r}_i \psi_0 d\tau \quad \text{in Angstrom-Coulomb} \quad (3.40)$$

$$\approx e \int \phi_m^*(i) \underline{r}_i \phi_n(i) dr_i \quad (3.41)$$

Equation (3.38) gives the oscillator strength for the transition from the ground state ψ_0 to the excited singlet state ψ_1 resulting from the promotion of an electron from MO "m" to MO "n". The reduction of Equation (3.40) when the ψ are given the form of Slater determinants to Equation (3.41) has been done in an ad hoc fashion. Pariser⁽²⁴⁾ gives the exact expression for the

[†]The distinction between 0-0 and vertical transition energies is frequently not made in comparing theoretical results with experiment.

reduced integral in the case in which ${}^1\Psi_1$ is an antisymmetrized sum of Slater determinants for a single configuration in the virtual orbital approximation. This exact expression is $\sqrt{2}$ times the expression of Equation (3.41). The approximation represented by Equation (3.41) has been used by del Bene and Jaffe⁽²⁵⁾ to calculate some very reasonable results for a number of small molecules. The results obtained for glyoxal using Expression (3.41) are in good agreement with values expected for the molecule. In the case of these calculations, the change from the virtual orbital approximation to an SCF calculation on the excited states means that integrals of the type

$$\int \phi_i^* \phi_i dr_i \quad (\phi_i \text{ not involved in the transition})$$

are now less than unity for the inner MO's. Since Expression (3.41) is multiplied by an unstated unity which is the product of all such terms, this deviation from unity could alter the value of M_{01} . In addition, the coefficients of MO's used in the CNDO method are obtained using a normalization factor which ignores overlap. This approximation produces coefficients which are on the large side, and will produce a value for the integral of Equation (3.41) which is too large. These considerations are offered as justification of the approximation made in Equation (3.41).

If ϕ_m and ϕ_n are treated as LCAO's, Equation (3.41) becomes

$$M_{01} \approx \sum_A \sum_{\text{nuclei}} \sum_k \sum_\ell a_{mk} a_{n\ell} e^{\int \chi_k^A(r_i) \chi_\ell^A dr_i} \quad (3.42)$$

$$= e \left\{ \sum_A \sum_k a_{mk} a_{n\ell} \delta_{k\ell} \frac{r_A^0}{\Lambda} + \sum_A \sum_{k < \ell} a_{mk} a_{n\ell} \int \chi_k^A(r'_A) \chi_\ell^A dr' \right\} \quad (3.43)$$

where $\underline{r}'_A = \underline{r}_i - \underline{r}_A^0$; \underline{r}_i is the position of the electron relative the origin,

\underline{r}_A is the position relative to nucleus A, and \underline{r}_A^O is the position of nucleus A. In Equation (3.43), the first term is much larger than the second. The second term was neglected except in the case of excited states for which ϕ_m and ϕ_n contained no atomic orbitals in common. For these cases, the first term is zero and the calculation was carried out using only the second term. The values used for the atomic integrals $\int \chi_k^A \underline{r}' \chi_\ell^A dr'$ are listed in Table 3.6 and were calculated using Slater orbitals for χ_k and χ_ℓ .

TABLE 3.6

One Center Atomic Transition Moment Integrals

	C	O	F
$\int 2s_{X_i} 2p_{X_i} \text{ in } \text{\AA}$	0.4710	0.3364	0.2943

The results of these oscillator strength calculations have been included in Table 3.5.

(ii) Singlet-Triplet Transitions

The approximate Hamiltonian (Equation 3.2) used for the CNDO calculations produces wavefunctions which predict zero intensity for singlet-triplet transitions. An improved description of the system is customarily obtained by including electron spin-orbit interaction as a perturbation^(26,27).

Intensities of transitions to excited triplet states were obtained using Equation (3.44)

$$\underline{M}_{01} = \int^T \sum_i^{\text{electrons}} e_i \underline{r}_i S_0 d\tau \quad (3.44)$$

$$\underline{M}_{01} = \sum_r M_{01}^r \quad (3.45)$$

$$\text{where } \underline{M}_{01}^r = \sum_m \frac{H_{m1}^r}{E_m - E_0} \underline{m}_{0m} + \sum_\mu \frac{H_{\mu 0}^r}{E_\mu - E_1} \underline{m}_{\mu 1} \quad (3.46)$$

$$H'_{m1} = \int \psi_m \mathcal{H}'_{so} \psi_1^r d\tau, H'_{\mu 0} = \int \psi_\mu^r \mathcal{H}'_{so} \psi_0 d\tau \quad (3.47)$$

$$\underline{m}_{0m} = \int \psi_0 \sum_i e_i \underline{r}_i \psi_m d\tau, \underline{m}_{\mu 1} = \int \psi_\mu^r \sum_i e_i \underline{r}_i \psi_1^r d\tau \quad (3.48)$$

In Equation (3.44) T_1 and S_0 are the new triplet and singlet wavefunctions which are corrected to the first order of the spin orbit perturbation \mathcal{H}'_{S_0} . In Equation (3.45) the superscript "r" signifies the M_S values for the triplet state (being +1, 0, or -1) and for this application it is assumed that the three levels are degenerate. In Equations (3.47) and (3.48) the wavefunctions refer to the zeroth order state wavefunctions as calculated by the CNDO method.

In Equation (3.46) the quantities \underline{m}_{0m} are the values already tabulated for the singlet-singlet transition moments; the $\underline{m}_{\mu 1}$ are also obtained from Equation (3.42). \mathcal{H}'_{S_0} takes the form

$$\mathcal{H}'_{S_0} = \frac{1}{2mc^2} \sum_i \sum_j \frac{1}{r_{i\mu}} \frac{\partial V}{\partial r_{i\mu}} \underline{S}_j \cdot \underline{L}_j + \text{two electron operator} \quad (3.49)$$

where $\underline{r}_{i\mu}$ is the distance from the "i" electron to the " μ "th nucleus, V is the electronic potential, \underline{L} and \underline{S} are the orbital and spin angular momentum operators, m is the electron mass and c the velocity of light. The two-electron term in Equation (3.49) is less important than the first term for molecular systems and is neglected. Equations (3.47) are then evaluated using the first term for \mathcal{H}'_{S_0} . When the wave functions are expressed as Slater determinants and the states are expressed in the virtual orbital approximation, the integrals in Equation (3.47) reduce, after integration over spin space, to integrals over the two MO's by which the wave functions differ (McClure⁽²⁸⁾) as summarized in Table 3.7. The spin-orbit operator (3.49) is a single electron operator and states which differ in configuration by more than two MO's from ψ_0 or ψ_1^r cannot mix with these respective states.

TABLE 3.7

Reduction of the Spin-Orbit Mixing Integrals between Two States

 ${}^1\Psi_k$ and ${}^3\Psi_j$ Which are Different in Two MO's ϕ_m and ϕ_n

Component \mathcal{H}'_{S_0}	$\int {}^1\Psi_k \mathcal{H}' {}^3\Psi_j^1 d\tau$	$\int {}^1\Psi_k \mathcal{H}' {}^3\Psi_j^0 d\tau$	$\int {}^1\Psi_k \mathcal{H}' {}^3\Psi_j^{-1} d\tau$
\mathcal{H}'_x	$\frac{1}{\sqrt{2}} \int \phi_m \mathcal{H}'_{l_x} \phi_n d\tau$	0	$-\frac{1}{\sqrt{2}} \int \phi_m \mathcal{H}'_{l_x} \phi_n d\tau$
\mathcal{H}'_y	$\frac{1}{\sqrt{2}} \int \phi_m \mathcal{H}'_{l_y} \phi_n d\tau$	0	$\frac{1}{\sqrt{2}} \int \phi_m \mathcal{H}'_{l_y} \phi_n d\tau$
\mathcal{H}'_z	0	$-\int \phi_m \mathcal{H}'_{l_z} \phi_n d\tau$	0

The results of Table 3.7 have been obtained after integration over spin-space which leaves the operators $\mathcal{H}'_{l_x}, \mathcal{H}'_{l_y}, \mathcal{H}'_{l_z}$

$$\mathcal{H}'_{l_x} = \frac{1}{2mc^2} \sum_i \text{electrons} \sum_{\mu} \text{nuclei} \frac{1}{r_{i\mu}} \frac{\partial V}{\partial r_{i\mu}} l_{xi} \quad (3.50)$$

$$\text{from } \underline{L} = l_x \underline{i} + l_y \underline{j} + l_z \underline{k} \quad (3.51)$$

Again, when the MO's ϕ_m and ϕ_n are expressed as LCAO's, the integrals in Table 3.7 become

$$\int \phi_m^* \mathcal{H}'_{l_x} \phi_n d\tau = \sum_i \sum_j c_i c_j \int \chi_i \mathcal{H}'_{l_x} \chi_j d\tau \quad (3.52)$$

Of the integrals $\int \chi_i \mathcal{H}'_{l_x} \chi_j d\tau$, only those of the form $\int p_i \mathcal{H}'_{l_x} p_j d\tau$ are non-zero and again only one center terms have been retained. For these

$$\int p_z \mathcal{H}'_{l_x} p_y d\tau = \int p_x \mathcal{H}'_{l_y} p_z d\tau = \int p_y \mathcal{H}'_{l_z} p_x d\tau = +\frac{i}{2} \xi \quad (3.53)$$

$$\int p_x \mathcal{H}'_{l_x} p_z d\tau = \int p_z \mathcal{H}'_{l_y} p_x d\tau = \int p_x \mathcal{H}'_{l_z} p_y d\tau = -\frac{i}{2} \xi \quad (3.54)$$

$$\int p_x \mathcal{A}'_{\ell_x} p_x d\tau = \int p_y \mathcal{A}'_{\ell_y} p_y d\tau = \int p_z \mathcal{A}'_{\ell_z} p_z d\tau = 0$$

$$\text{where } \xi \equiv \frac{\hbar^2 e^2}{2m^2 c^2} Z \int p_z \frac{Z^3(\text{eff})}{r^3} p_y d\tau \quad (3.55)$$

and ξ has been approximated by the value of the spin orbit coupling in the corresponding free atom with effective nuclear charge Z (eff). The values for ξ , taken from the calculations of Blume and Watson⁽²⁹⁾, are listed in Table 3.8.

TABLE 3.8

Values for the spin orbit coupling between the 2p atomic orbitals
as calculated for the free atom.

Atom	ξ^* cm ⁻¹
C	31
O	146
F	264

*The data in this table was taken from reference (29).

In summary then,

$$M_{01}^{\pm 1} = \sum_m \frac{1}{\sqrt{2}(E_m - E_1)} \left[\pm \sum_{ij} \sum a_{\gamma i} a_{\delta j} \int \chi_i \mathcal{A}'_{\ell_x} \chi_j d\tau + i \sum_{ij} \sum a_{\gamma i} a_{\delta j} \int \chi_i \mathcal{A}'_{\ell_y} \chi_j d\tau \right]_{\underline{m}_{0m}} \\ + \sum_{\mu} \frac{1}{\sqrt{2}(E - E_0)} \left[\pm \sum_{ij} \sum a_{\gamma i} a_{\delta j} \int \chi_i \mathcal{A}'_{\ell_x} \chi_j d\tau + i \sum_{ij} \sum a_{\gamma i} a_{\delta j} \int \chi_i \mathcal{A}'_{\ell_y} \chi_j d\tau \right]_{\underline{m}_{\mu 1}} \quad (3.56)$$

$$M_{01}^0 = \sum_m \left\{ \frac{1}{E_m - E_0} \sum_{ij} \sum a_{\gamma i} a_{\delta j} \int \chi_i \mathcal{A}'_{\ell_z} \chi_i d\tau \right\}_{\underline{m}_{0m}} \\ + \sum_{\mu} \left\{ \frac{1}{E - E_0} \sum_{ij} \sum a_{\gamma i} a_{\delta j} \int \chi_i \mathcal{A}'_{\ell_z} \chi_j d\tau \right\}_{\underline{m}_{\mu 1}} \quad (3.57)$$

where the subscripts γ and δ signify the two orbitals by which each perturbing state differs from Ψ_1 or Ψ_0 respectively, and the oscillator strength can be written

$$f_{\text{osc}} = 1.085 \times 10^{-5} \nu \sum_r |M_{01}^r|^2 \quad (3.58)$$

with ν given in wave numbers and M_{01}^r given in Ångstrom-Coulombs.

At the level of the Born-Oppenheimer approximation, and without spin-orbit interaction, the electronic states are identified by symmetry, multiplicity and energy. Within such a zeroth order framework, the symmetry requirements for the perturbation terms $H_{\ell m}^i$ of Equation (3.46) to be non-zero can be expressed by the rule that the direct product

$$\Gamma(1\psi) \times \begin{matrix} \Gamma(R_y) \\ \Gamma(R_x) \\ \Gamma(R_z) \end{matrix} \times \Gamma(3\Psi) \quad (3.59)$$

contain the totally symmetric representation. Use has been made of the fact that the space part of \mathcal{H}'_{S_0} transforms as a rotation. Table 3.9 gives a list of states which satisfy the symmetry requirements for mixing in the C_{2h} symmetry group.

The intensity of the transition from ground to excited triplet states was calculated for states having transition energies low enough to be of interest. The calculations for ${}^3A_u(n_{a_g}^-, \pi_{a_u}^*)$, ${}^3B_u(\pi_{b_g}^*, \pi_{a_u})$, and ${}^3B_u(n_{a_g}^-, \sigma_{b_u}^*)$ are summarized in Tables 3.10, 3.11 and 3.12. It should be noted that in these tables, the summation over all perturbing states indicated in Equations (3.56) and (3.57) have not been carried out, but instead each perturbing state has been treated as though it were the sole perturbation. The justification for this is to be found in the fact that usually there is one perturbation much larger than all the others. The observed intensity can be accounted for by

TABLE 3.9

Symmetries of Zeroth Order States Classified under C_{2h} Symmetry
which can Mix Through Spin-Orbit Coupling

Component of Ψ_{S_0} (Symmetry)	Symmetry of Zeroth Order State	Symmetries of Perturbing States
Ψ_{e_x} (B _g)	3A_u	1B_u
Ψ_{e_y} (B _g)	3A_u	1B_u
Ψ_{e_z} (A _g)	3A_u	1A_u
Ψ_{o_x} (B _g)	3B_u	1A_u
Ψ_{o_y} (B _g)	3B_u	1A_u
Ψ_{o_z} (A _g)	3B_u	1B_u
Ψ_{e_x} (B _g)	1A_g	3B_g
Ψ_{e_y} (B _g)	1A_g	3B_g
Ψ_{e_z} (A _g)	1A_g	3A_g

TABLE 3.10

Intensity for the Transition ${}^3A_u(n_{ag}^-, \pi_{au}^*) \leftarrow {}^1A_g(\text{G.S.})$

Produced by Spin-Orbit Coupling

	Perturbing Singlet State	${}^3E_1 - {}^1E_m$ a.u.	H'_{m1} a.u.	$ m_{om} /e$	$ M_{01} /e^a$	Corresponding f_{osc}	Polarization
1	${}^1B_u(\pi_{bg}, \pi_{au}^*)$	0.157	1.9×10^{-4}	0.9	1.1×10^{-3}	3.7×10^{-7}	A,B
2	${}^1B_u(n_{ag}^-, \sigma_{bu}^*)$	0.270	5×10^{-5}	0.51	9.5×10^{-5}	4.8×10^{-9}	A,B
3	${}^1B_u(n_{bu}^+, \sigma_{2ag}^*)$	0.421	*			ω^b	
4	${}^1B_u(\pi_{au}, \pi_{bg}^*)$	0.596	*			ω	
5	${}^1A_u(\pi_{bg}, \sigma_{bu}^*)$	0.269	*			ω	
6	${}^1A_u(n_{bu}^+, \pi_{bg}^*)$	0.334	*			ω	
7	${}^1A_u(\sigma_{1ag}, \pi_{au}^*)$	~ 0.3	$\sim 10^{-4}$	~ 0.1	$\sim 10^{-5}$	$\sim 10^{-9}$	C
8	${}^1A_u(\pi_{au}, \sigma_{2ag}^*)$	0.704	*			ω	
	Perturbing Triplet State	${}^1E_o - {}^3E_\mu$ a.u.	$H'_{\mu o}$ a.u.	$ m_{1\mu} /e$	$ M_{01} /e^a$	Corresponding f_{osc}	Polarization
1	${}^3B_g(n_{bu}^+, \pi_{au}^*)$	0.205	$\sim 10^{-4}$	~ 0.9	$\sim 5 \times 10^{-4}$	$\sim 10^{-7}$	A,B
2	${}^3B_g(n_{ag}^-, \pi_{bg}^*)$	0.359	$\sim 10^{-4}$	~ 0.9	$\sim 3 \times 10^{-4}$	$\sim 10^{-8}$	A,B
3	${}^3B_g(\pi_{bg}, \sigma_{2ag}^*)$	0.455		***		ω	
4	${}^3B_g(\pi_{au}, \sigma_{bu}^*)$	0.613		***		ω	
5	${}^3A_g(\pi_{bg}, \pi_{bg}^*)$	0.380	**	***		ω	
6	${}^3A_g(\pi_{au}, \pi_{au}^*)$	0.391	**			ω	
7	${}^3A_g(n_{ag}^-, \sigma_{2ag}^*)$	0.422	$\sim 10^{-4}$	~ 0.1	$\sim 10^{-5}$	$\sim 10^{-9}$	C
8	${}^3A_g(n_{bu}^+, \sigma_{bu}^*)$	0.444		***		ω	

^a Assuming only a single perturbing state.^b The symbol " ω " has been employed where mixing is negligible.* These terms are small, and under the approximation of \mathcal{H}'_{S_0} by a single electron operator become zero.** These terms are small, and under the approximation of local spherical symmetry at each atom become zero, e.g., $\langle {}^3A_g(\pi_{au}, \pi_{au}^*) | \mathcal{H}'_{S_0} | {}^1A_g(\text{G.S.}) \rangle \sim \langle \phi \pi_{au}^* | L_z | \phi \pi_{au} \rangle \sim 0$ since the operator L_z can only couple the atomic orbitals p_x and p_y .*** These terms are zero since ${}^3\psi_\mu$ differs from ${}^3\psi_1$ by four MO's.

TABLE 3.11

Intensity of the Transition ${}^3B_u(\pi_{bg}, \pi_{au}^*) \leftarrow {}^1A_g$

Produced by Spin-Orbit Coupling

	Perturbing Singlet State	${}^3E_1 - {}^1E_m$ a.u.	H'_{m1} a.u.	$ m_{om} /e$	$ M_{01} /e^a$	Corresponding f_{osc}	Polariz- ation
1	${}^1B_u(n_{ag}^-, \sigma_{1bu}^*)$	0.258	*			ω^b	
2	${}^1B_u(n_{bu}^+, \sigma_{2ag}^*)$	0.409	*			ω	
3	${}^1B_u(\pi_{au}, \pi_{bg}^*)$	0.584	*			ω	
4	${}^1A_u(n_{ag}^-, \pi_{au}^*)$	0.0 ^c	1.9×10^{-4}	0.03	5.7×10^{-4}	1.1×10^{-7}	C
5	${}^1A_u(\pi_{bg}, \sigma_{1bu}^*)$	0.257	4.3×10^{-5}	0.15	2.5×10^{-5}	2.1×10^{-10}	C
6	${}^1A_u(n_{bu}^+, \pi_{bg}^*)$	0.322	*			ω	
7	${}^1A_u(\pi_{au}, \sigma_{2ag}^*)$	0.5	*			ω	
	Perturbing Triplet State	${}^1E_o - {}^3E_e$ a.u.	$H'_{\mu 0}$ a.u.	$ m_{1\mu} /e$	$ M_{01} /e$	Corresponding f_{osc}	Polariz- ation
8	${}^3B_g(n_{bu}^+, \pi_{au}^*)$	0.205	$\sim 10^{-4}$	~ 0.03	$\sim 10^{-5}$	$\sim 10^{-9}$	A,B
9	${}^3B_g(n_{ag}^-, \pi_{bg}^*)$	0.359		***		ω	
10	${}^3B_g(\pi_{bg}, \sigma_{1ag}^*)$	0.455	$\sim 10^{-5}$	~ 0.2	$\sim 10^{-5}$	$\sim 10^{-10}$	A,B
11	${}^3B_g(\pi_{au}, \sigma_{2bu}^*)$	0.613		***		ω	
12	${}^3A_g(\pi_{bg}, \pi_{bg}^*)$	0.380	**			ω	
13	${}^3A_g(\pi_{au}, \pi_{au}^*)$	0.391	**	***		ω	
14	${}^3A_g(n_{ag}^-, \sigma_{1ag}^*)$	0.422		***		ω	
15	${}^3A_g(n_{bu}^+, \sigma_{2bu}^*)$	0.444		***		ω	

a

b

*

**

See Table 3.10 for an explanation of the code.

^cA value of 0.01 a.u. was assumed for $E({}^3B_u(\pi_{bg}, \pi_{au}^*)) - E({}^1A_u(n_{ag}^-, \pi_{au}^*))$.

It was felt that this value was representative of the error which could be expected for this number.

TABLE 3.12

Intensity of the Transition ${}^3B_u(n_{ag}^-, \sigma_{1bu}^*) \leftarrow {}^1A_g$
Produced by Spin-Orbit Coupling

	Perturbing Singlet State	${}^3E_1 - {}^1E_m$ a.u.	H'_{ml} a.u.	$ m_{om} /e$	$ M_{01} /e^a$	Corresponding f_{osc}	Polariz- ation
1	${}^1B_u(\pi_{bg}, \pi_{au}^*)$	0.057	*			ω^b	
2	${}^1B_u(n_{bu}^+, \sigma_{2ag}^*)$	0.207	*			ω	
3	${}^1B_u(\sigma_{1ag}, \sigma_{1bu}^*)$	~ 0.3	1.8×10^{-4}	~ 0.5	$\sim 10^{-4}$	$\sim 10^{-7}$	A, B
4	${}^1B_u(\pi_{au}, \pi_{bg}^*)$	0.382	*			ω	
5	${}^1B_u(n_{ag}^-, \sigma_{3bu}^*)$	~ 0.5	1.7×10^{-5}	~ 0.5	$\sim 10^{-5}$	$\sim 10^{-9}$	A, B
6	${}^1A_u(n_{ag}^-, \pi_{au}^*)$	0.214	$\sim 10^{-5}$	0.03	$\sim 10^{-6}$	$\sim 10^{-11}$	C
7	${}^1A_u(\pi_{bg}, \sigma_{1bu}^*)$	0.048	$\sim 10^{-5}$	0.15	$\sim 10^{-4}$	$\sim 10^{-7}$	C
8	${}^1A_u(n_{bu}^+, \pi_{bg}^*)$	0.112	*			ω	
9	${}^1A_u(\pi_{au}, \sigma_{2ag}^*)$	~ 0.3	*			ω	
	Perturbing Triplet State	${}^1E_o - {}^3E$ a.u.	$H'_{\mu o}$ a.u.	$ m_{1\mu} /e$	$ M_{01} /e^a$	Corresponding f_{osc}	Polariz- ation
10	${}^3B_g(n_{bu}^+, \pi_{au}^*)$	0.205		***		ω	
11	${}^3B_g(n_{ag}^-, \pi_{bg}^*)$	0.359	$\sim 10^{-4}$	~ 0.03	$\sim 10^{-5}$	$\sim 10^{-9}$	A, B
12	${}^3B_g(\pi_{bg}, \sigma_{2ag}^*)$	0.455		***		ω	
13	${}^3B_g(\pi_{au}, \sigma_{1bu}^*)$	0.613	$\sim 10^{-4}$	~ 0.2	$\sim 10^{-5}$	$\sim 10^{-9}$	A, B
14	${}^3A_g(\pi_{bg}, \pi_{bg}^*)$	0.380	**			ω	
15	${}^3A_g(\pi_{au}, \pi_{au}^*)$	0.391	**			ω	
16	${}^3A_g(n_{ag}^-, \sigma_{2ag}^*)$	0.422	$\sim 10^{-5}$	~ 0.5	$\sim 10^{-5}$	$\sim 10^{-9}$	C
17	${}^3A_g(n_{bu}^+, \sigma_{1bu}^*)$	0.444	$\sim 10^{-4}$	~ 0.5	$\sim 10^{-4}$	$\sim 10^{-7}$	C

a

b

*

**

See Table 3.10 for an explanation of the code.

this one term, and the system used in the tables emphasizes the relative importance of different perturbing states. The polarization of the transition as allowed by each perturbing state is the same as that of $\underline{m_{om}}$ or $\underline{m_{\mu 1}}$.

The estimated intensities for transitions to excited triplet states have been included in Table 3.5.

(c) Vibrational Structure

The CNDO energy of a system is the energy of the system of particles relative to the energy of the isolated electrons and cores (nuclei plus non-valence electrons). This energy (E_T) is the sum of the electronic energy (E_e given by Equation 3.2) and the nuclear energy (E_n given by the repulsion between the cores as point charges). In the Born-Oppenheimer approximation this energy provides the potential field in which the nuclei move. The most prominent structure of an electronic system arises from vibrational motion of the nuclei, and the vibrational structure predicted by the CNDO/2 force field has been calculated for comparison with experiment.

The vibrational motion of the nuclei is most compactly described in matrix notation. There are $3N-6$ mutually orthogonal modes of vibration (called normal modes) for a non-linear polyatomic molecule. Since the form of these modes is not intuitively obvious, the vibrations are customarily described on a first order basis as a combination of bond stretches and angle changes which are not necessarily orthogonal. The true normal modes, and vibrational energies are then obtained as eigenvectors and eigenvalues in the solution of the equation

$$[(F)(G) - \lambda(E)]\underline{S}^0 = 0 \quad (3.60)$$

obtained in the Lagrangian formalism where (E) is the unit matrix and

$$2V \equiv \underline{S}^t (F) \underline{S} \quad (V = \text{potential energy}) \quad (3.61)$$

$$2T \equiv \underline{\dot{S}}^t (G^{-1}) \underline{\dot{S}} \quad (T = \text{kinetic energy}) \quad (3.62)$$

\underline{S} is a column vector called a symmetry coordinate, which describes the internal motion of the molecule as the projections on a basis set composed of changes in bond lengths and bond angles. The components S_i of the vector \underline{S} have the form

$$S_i = S_i^0 \sin (t\sqrt{\lambda} + \delta) \quad (3.63)$$

where S_i^0 , λ , and δ are constants and t is the time.

The matrix (F) in Equation (3.61) is called the force constant matrix. For glyoxal, nine of the vibrations lie in the plane, and three lie out of the plane of the molecule. The in plane and out of plane motions are mechanically separable, and the in plane vibrations are considered as a separate problem. For the in plane vibrations, the \underline{S} vector takes the form (see Figure 3.1)

$$\begin{aligned} \underline{S} &= \Delta r_{CC} \underline{e}_1 + \Delta r_{CO1} \underline{e}_2 + \Delta r_{CO2} \underline{e}_3 + \Delta r_{CH1} \underline{e}_4 + \Delta r_{CH2} \underline{e}_5 \\ &\quad + f_1(r_{CH}, r_{CO}) \Delta(\angle OCH)_1 \underline{e}_6 + f_1 \Delta(\angle OCH)_2 \underline{e}_7 \\ &\quad + f_2(r_{CO}, r_{CC}) \Delta(\angle CCO) \underline{e}_8 + f_2 \Delta(\angle CCO) \underline{e}_9 \\ &\equiv \sum_i S_i \underline{e}_i \\ &\equiv \begin{pmatrix} S_1 \\ S_2 \\ \vdots \\ S_9 \end{pmatrix} \end{aligned} \quad (3.64)$$

In this basis set, the elements of the (F) matrix define what is called the general valence force field. If the energy obtained in the CNDO/2 calculation is expressed as a Taylor's series, the correspondence between the matrix elements F_{ij} and the Taylor's series coefficients is obvious.

$$2E_T = \sum_{i=1}^9 A_i S_i^2 + \sum_{i=1}^9 \sum_{j=1}^9 B_{ij} S_i S_j \quad (3.65)$$

$$F_{ii} = A_i, \quad F_{ij} = B_{ij} \quad (3.66)$$

The general valence force field is not commonly used. In particular, a very thorough study of glyoxal and its derivatives has been carried out by Fleury⁽³⁰⁾ using a Urey-Bradley force field. For comparison with the theoretical results, the Urey-Bradley force field must be converted into the form of the general valence force field. The potential energy in Urey-Bradley space is given by

$$\begin{aligned} 2V = & \sum_{i=1}^5 [2K'_i r_i \Delta r_i + K_i (\Delta r_i)^2] \\ & + \sum_{i=1}^4 [2H'_i f_i^2 \Delta(\mathcal{L})_i + H_i (f_i \Delta(\mathcal{L})_i)^2] \\ & + \sum_{i < j} [2F'_{ij} q_{ij} \Delta q_{ij} + F_{ij} \Delta q_{ij}^2] \\ & + f_{\text{CO},\text{CO}} \Delta r_{\text{CO1}} \Delta r_{\text{CO2}} \end{aligned} \quad (3.67)$$

where the Δr_i and $\Delta(\mathcal{L})_i$ have the form as given in Equation (3.64) and the q_{ij} are the separations between the non-bonded pairs of atoms and the summations over i and j are over all non-bonded pairs to be considered.

Equation (3.67) has more than nine variables, and contains redundancies and linear terms which disappear when the q_{ij} are substituted by the analytic forms in terms of the nine S_i . The resulting expression for the Urey-Bradley potential is then directly comparable with Equations (3.61) and (3.65). It is possible to express the A_i and B_{ij} of Equation (3.61) as functions of the K , K' , H , H' , F , and F' . The terms in the A_i constitute the major part of the Urey-Bradley potential, and only these terms were determined from the

theoretical calculations. The expansions for the A_i in Urey-Bradley space are summarized in Table 3.13. The A_i were then evaluated using the Urey-Bradley constants and the geometry given by Fleury.

The CNDO energy for the ground and excited states was calculated over a range of values for each parameter. The one-dimensional potential energy surfaces are given in Figures 3.5, 3.6, and 3.7. It is seen that the predicted geometries for singlet and triplet states are the same, and only a common geometry is considered. The optimum geometry was determined for the $A_u(na_g^-, \pi a_u^*)$, $B_u(\pi b_g, \pi a_u^*)$, and $B_u(na_g^-, \sigma b_u^*)$ excited states. These geometries are compared with the CNDO ground state geometry in Table 3.1. The available experimental results have been included.

At the point of equilibrium, the potential energy curves can be expressed by the Taylor's series

$$2E = \frac{\partial^2 E}{\partial p_i^2} (p_i - p_{i \text{ eqm}})^2 = A_i' \Delta p_i^2 \quad (3.68)$$

The values of the A_i' for the five parameters p_i were determined by least squares fit. In the case of all but the r_{CC} , these A_i' are not identical to the A_i of Equation (3.65). This difference arises because a variation in the parameter p_{CO} results in the simultaneous displacements of the bonds r_{CO1} and r_{CO2} . It can be shown that

$$\begin{aligned} \frac{\partial^2 E}{\partial p_{CO}^2} \Delta p_{CO}^2 &= \frac{\partial^2 E}{\partial r_{CO1}^2} \Delta r_{CO1}^2 + \frac{\partial^2 E}{\partial r_{CO2}^2} \Delta r_{CO2}^2 + 2 \frac{\partial^2 E}{\partial r_{CO1} \partial r_{CO2}} \Delta r_{CO1} \Delta r_{CO2} \\ &= \left(\frac{\partial^2 E}{\partial r_{CO1}^2} + 2 \frac{\partial^2 E}{\partial r_{CO1} \partial r_{CO2}} + \frac{\partial^2 E}{\partial r_{CO2}^2} \right) \Delta p_{CO}^2 \end{aligned} \quad (3.69)$$

This result enables us to summarize

$$A_i' = 2A_i + 2B_{i1, i2} \quad i = CO, CH, \angle OCH, \angle CCO \quad (3.70)$$

$$A_i' = A_i \quad i = CC \quad (3.71)$$

Figure 3.5

- VII $1,^3A_u(n_{b_u}^+, \pi_{b_g}^*)$
- VI $1B_u(n_{a_g}^-, \sigma_{b_u}^*)$
- V $1,^3A_u(\pi_{b_g}, \sigma_{b_u}^*)$
- IV $3B_u(n_{a_g}^-, \sigma_{b_u}^*)$
- III $1B_u(\pi_{b_g}, \pi_{a_u}^*)$
- II $3B_u(\pi_{b_g}, \pi_{a_u}^*)$
- I $1,^3A_u(n_{a_g}^-, \pi_{a_u}^*)$

CC Bond Length

CC = 1.22 Å, CH = 1.09 Å

CCO = 120°, OCH = 118°

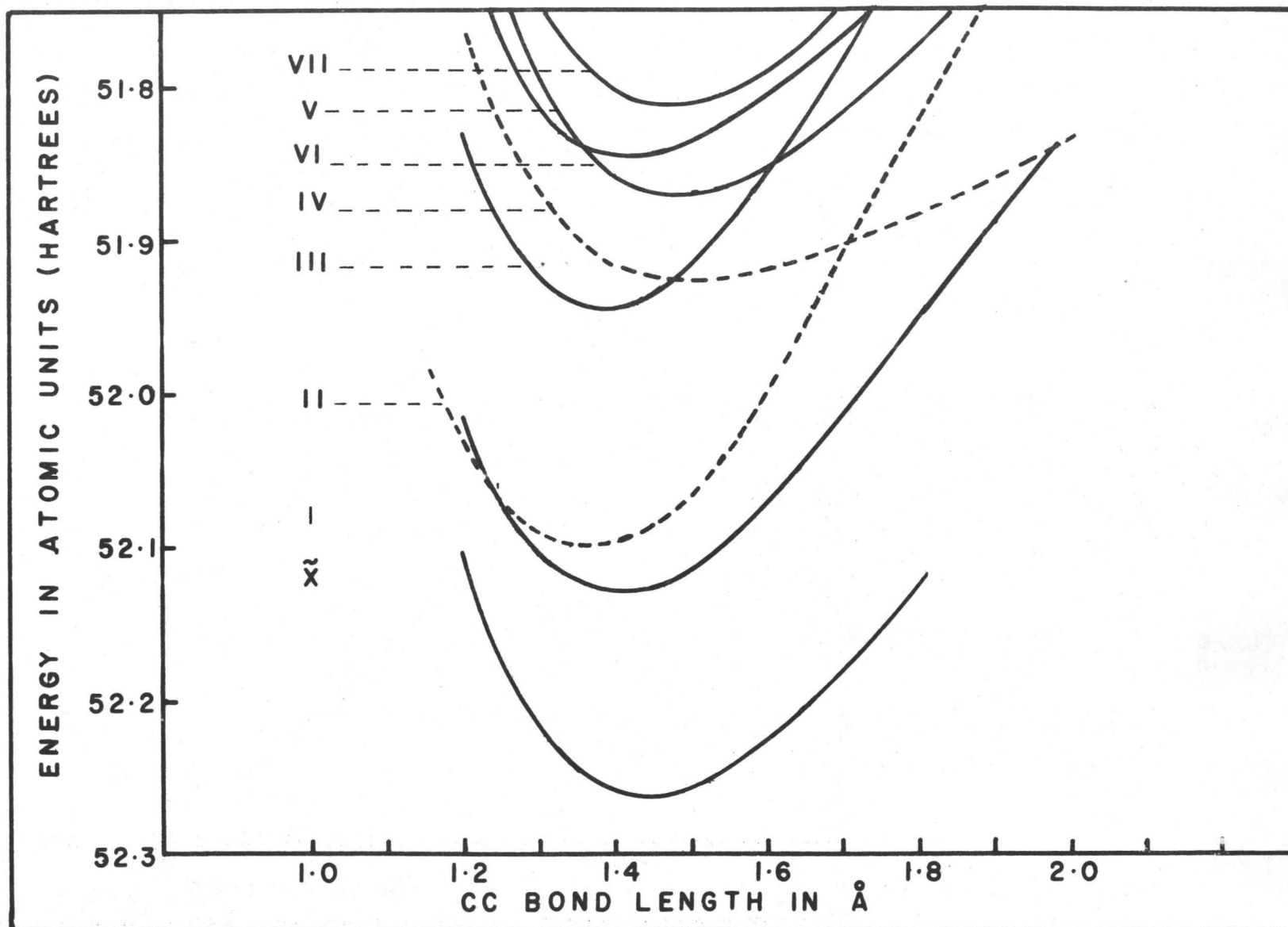


Fig. 3.5. CND0 Potential Curve for Glyoxal for CC Bond Length.

Figure 3.6

VII	$1, {}^3A_u(n_{b_u}^+, \pi_{b_g}^*)$
VI	$1B_u(n_{a_g}^-, \sigma_{b_u}^*)$
V	$1, {}^3A_u(\pi_{b_g}, \sigma_{b_u}^*)$
IV	${}^3B_u(n_{a_g}^-, \sigma_{b_u}^*)$
III	$1B_u(\pi_{b_g}, \pi_{a_u}^*)$
II	${}^3B_u(\pi_{b_g}, \pi_{a_u}^*)$
I	$1, {}^3A_u(n_{a_g}^-, \pi_{a_u}^*)$

CO Bond Length

$$CC = 1.43 \text{ \AA}, CH = 1.09 \text{ \AA}$$

$$CCO = 120^\circ, OCH = 118^\circ$$

CH Bond Length

$$CO = 1.25 \text{ \AA}, CC = 1.43 \text{ \AA}$$

$$CCO = 120^\circ, OCH = 118^\circ$$

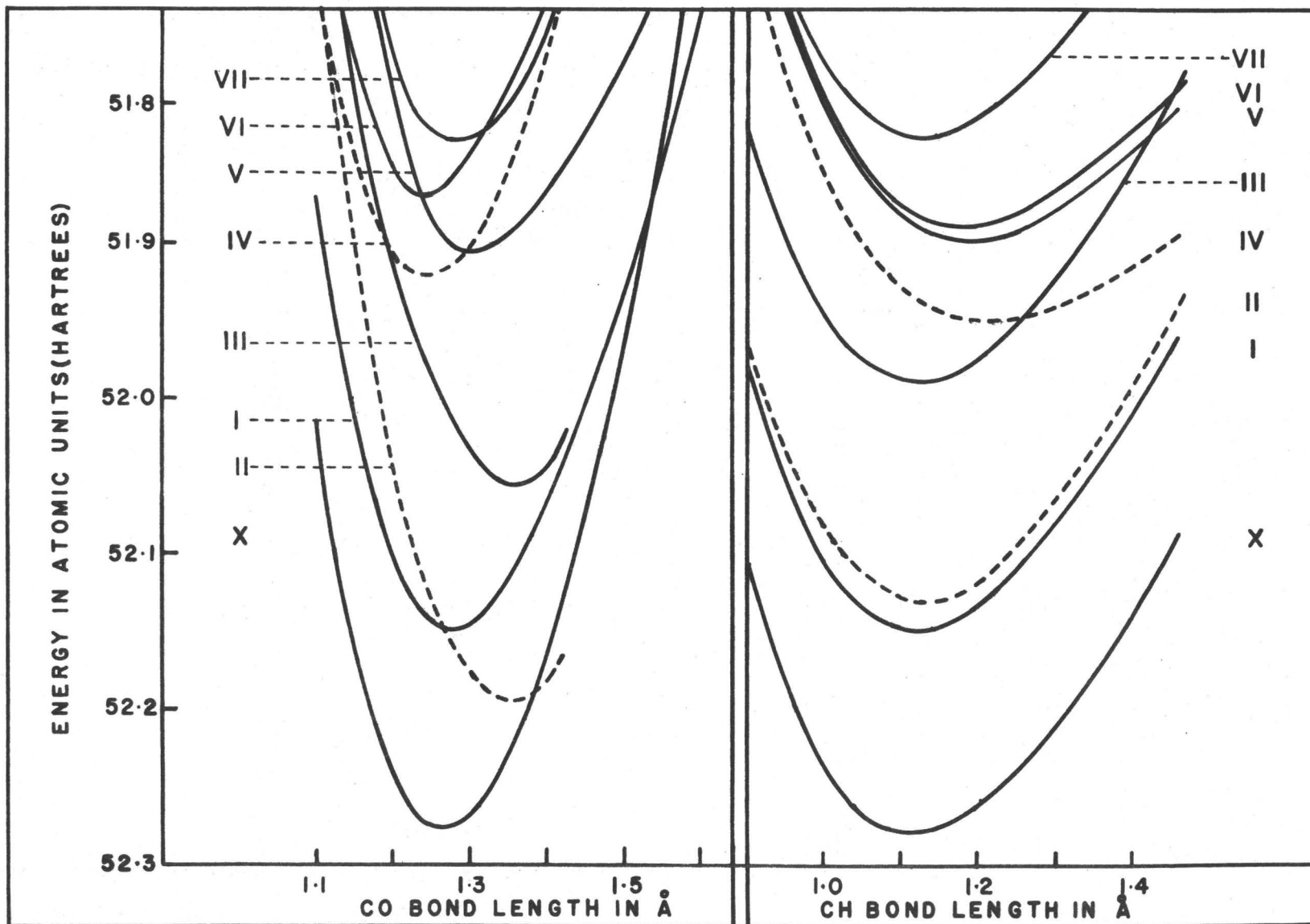


Figure 3.6 CND0 Potential Curve for Glyoxal for CO, CH Bond Lengths.

Figure 3.7

- VII $1,^3A_u(n_{b_u}^+, \pi_{b_g}^*)$
- VI $1B_u(n_{a_g}^-, \sigma_{b_u}^*)$
- V $1,^3A_u(\pi_{b_g}, \sigma_{b_u}^*)$
- IV $3B_u(n_{a_g}^-, \sigma_{b_u}^*)$
- III $1B_u(\pi_{b_g}, \pi_{a_u}^*)$
- II $3B_u(\pi_{b_g}, \pi_{a_u}^*)$
- I $1,^3A_u(n_{a_g}^-, \pi_{a_u}^*)$

OCH Angle

CC = 1.43 Å, CO = 1.25 Å, CH = 1.12 Å

CCO = 121°

CCO Angle

CC = 1.43 Å, CO = 1.25 Å, CH = 1.12 Å

OCH = 121°

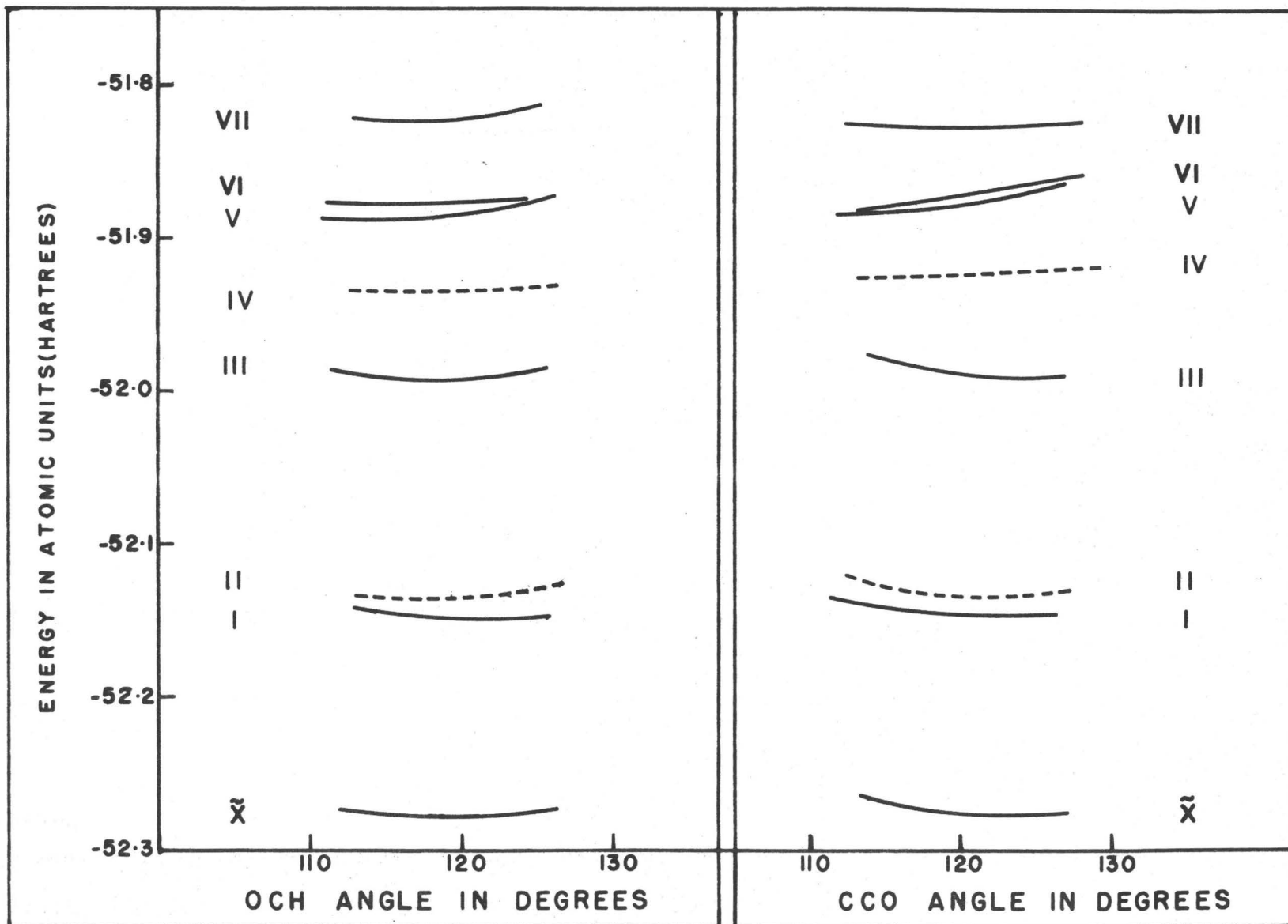


Figure 3.7 CNDO Potential Curve for Glyoxal for COH, CCO Bond Angles.

TABLE 3.13

The Expansion of the Diagonal Quadratic Taylor's Series Coefficients
for the Potential Energy in Urey-Bradley Space (Glyoxal)

Coefficient	Parameter	Expansion ^a
A ₁	Δr_{CC}	$K_{CC} + 1.70 F_{CCO} + 1.49 F_{CCH} + 2.0 F_{O\dots H}$
A ₂ , A ₃	$(\Delta r_{CO})_{1,2}$	$K_{CO} + 0.7 F_{CCO} + 0.83 F_{OCH} + 0.30 F_{O\dots H}$
A ₄ , A ₅	$(\Delta r_{CH})_{1,2}$	$K_{CH} + 0.80 F_{OCH} + 0.63 F_{CCH} + 0.42 F_{O\dots H}$
A ₆ , A ₇	$\Delta(\angle OCH)_{1,2}$	$1.35H_{OCH} + 1.77H_{CCH} + 0.16F_{OCH} + 0.40F_{CCH} + 1.02F_{O\dots H}$
A ₈ , A ₉	$\Delta(\angle CCO)_{1,2}$	$1.84H_{CCO} + 1.77H_{CCH} + 0.40F_{CCH} + 0.26F_{CCO} + 2.02F_{O\dots H}$

^aThe geometry used for this expansion was that used by Fleury⁽³⁰⁾ as taken from the electron diffraction results of Kuchitsu et al.⁽²²⁾

CNDO^b and Experimental^c General Valence Force Field Force Constants
for Ground and Excited States of Glyoxal

State	Δp_{CC}	Δp_{CO}	Δp_{CH}	Δp_{OCH}	Δp_{CCO}
	millidyne/Å			millidyne-Å/rad ²	
$\tilde{X} \ ^1A_g$	16.4	66.6	23.6	2.0	3.4
1A_g (G.S.) ^c exp.	4.28	21.07	8.50	1.7	2.7
$^1A_u(n\bar{a}_g, \pi^*_{a_u})$	18.6	59.0	22.6	2.6	1.3
$^3A_u(n\bar{a}_g, \pi^*_{a_u})$	18.0	59.0	22.3	2.4	1.0

^bLeast squares fit to eight CNDO energies within 0.04 Å or 4° of equilibrium.

^cExperimental values are obtained from the force constants of Fleury⁽³⁰⁾.

Table 3.13 compares the A_1' from the CNDO data with the corresponding quantities of Equations (3.70) and (3.71) determined from the normal coordinate analysis of Fleury.

3.5 CNDO and Experiment for Glyoxal

(a) The Electronic Systems

Figure 3.8 shows a reconstruction of the spectrum predicted for glyoxal by the results discussed in Section 3.4. No spectrophotometer trace of glyoxal was available, and a spectrophotometer trace of biacetyl (COCH COCH) is included in Figure 3.8 since the biacetyl spectrum is very similar to the spectrum reported for glyoxal^(20,31,32). Inspection of Figure 3.8 indicates that the CNDO calculations predict that there is only one system of the intensity of the S-S $n \rightarrow \pi^*$ transition in the near ultraviolet whereas two systems are observed experimentally (as in biacetyl). These two systems have been assigned to two $\underline{n} \rightarrow \pi^*$ transitions since the assignment was suggested by McMurray⁽¹⁹⁾. On the basis of the Huckel MO method this assignment appears reasonable (see Figure 3.9).

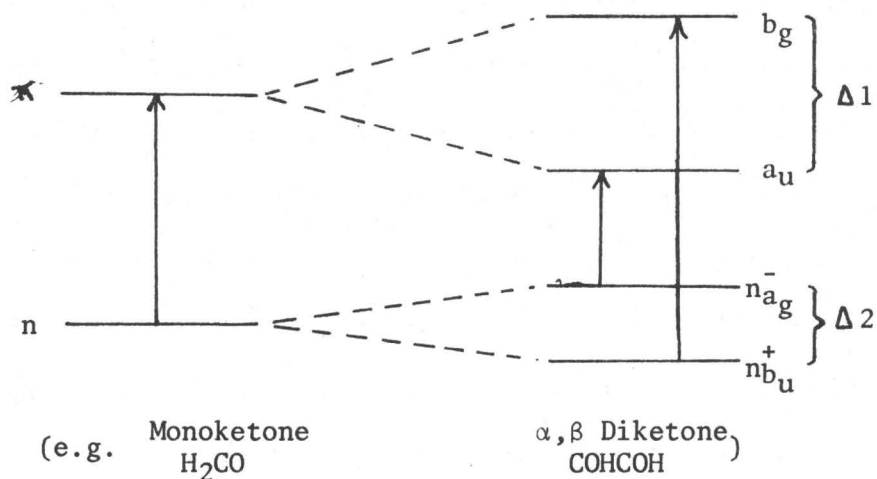


Figure 3.9. Simple Molecular Orbital Scheme for α, β Diketones

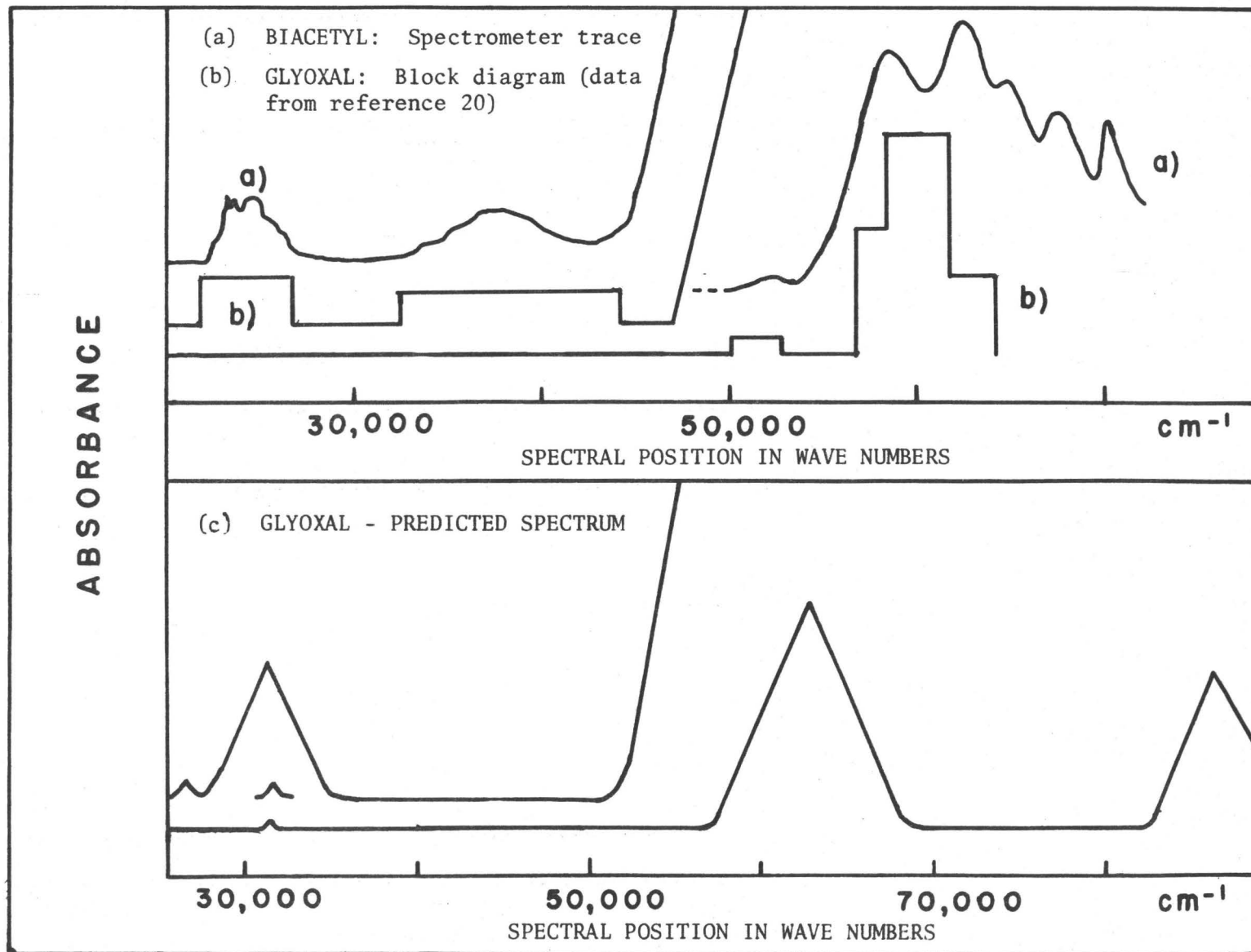


Figure 3.8 CNDO Spectrum of Glyoxal Compared with Experiment.

The $\underline{n} \rightarrow \pi^*$ transition which has a frequency $\sim 29,000 \text{ cm}^{-1}$ for a monoketone is split into two transitions at $29,000 \pm (\Delta 1 + \Delta 2) \text{ cm}^{-1}$. Thus transitions at $\sim 22,000 \text{ cm}^{-1}$ and 31000 cm^{-1} for glyoxal and $\sim 23,000 \text{ cm}^{-1}$ and 36000 cm^{-1} for biacetyl are conveniently assigned to two $\underline{n} \rightarrow \pi^*$ transitions: $\underline{n}_{a_g}^- \rightarrow \pi_{a_u}^*$, and $\underline{n}_{b_u}^+ \rightarrow \pi_{b_g}^*$. There have, in addition, been suggestions (see the text by Murrell⁽³³⁾) that there should be four electron absorption transitions for α - β diketones. It is apparent, however, that in the C_{2h} point group, two of these are symmetry-forbidden. The 21973 cm^{-1} system (I in Figure 3.8a) of glyoxal has been studied in detail by Brand⁽³²⁾, King⁽³⁴⁾, Paldus and Ramsay⁽²³⁾, Birss et al.⁽³⁵⁾, and Agar et al.⁽³⁶⁾ It has been established that the excited state is 1A_u and the assignment as the first $\underline{n} \rightarrow \pi^*$ transition seems unequivocal. The corresponding (22896 cm^{-1}) system (I) of biacetyl observed by Sidman and McClure⁽³⁷⁾ in the crystalline phase has very similar vibrational structure, and again is assigned as the first $\underline{n} \rightarrow \pi^*$ system. The transitions (II) observed at 31000 cm^{-1} (glyoxal) and 35000 cm^{-1} (biacetyl) consist of diffuse bands and thus cannot be analyzed in detail. That these systems might not be the second $\underline{n} \rightarrow \pi^*$ transitions is suggested by the CNDO calculation which predicted that this transition lies to much higher energy ($\sim 100,000 \text{ cm}^{-1}$). The departure from the predictions of simple MO theory with respect to the second $\underline{n} \rightarrow \pi^*$ transition is found to arise from the fact that in the SCF calculation removal of an electron from the $\underline{n}_{a_g}^-$ molecular orbital produces much greater stabilization of the remaining MO's than does removal from the $\underline{n}_{b_u}^+$ orbital. The discrepancy for this transition is much larger than has been found for other parts of this CNDO calculation of glyoxal. It appears unlikely that the second band system is the $\underline{n}_{b_u}^+ \rightarrow \pi_{b_g}^*$ transition. The possibility that this band system might be

due to the $^3(\pi \rightarrow \pi^*)$ or $^3(n \rightarrow \sigma^*)$ transitions was considered, but neither of the oscillator strengths for these transitions (see Table 3.5 or the calculations summarized in Tables 3.11 and 3.12) are large enough to account for the transition intensity.

After the previous assignment of this band system had been questioned, it was found that some of the experimental observations on these molecules were not in agreement with the assignment to the $\underline{n}_{bu}^+ \rightarrow \pi_{bg}^*$ transition. In a number of spectra recorded under different conditions, the intensity of the 33000 cm^{-1} band is found to vary relative to the 22000 cm^{-1} band. For example, the room temperature vapour phase spectrum of biacetyl (see Figure 3.10) indicates an intensity for the 35000 cm^{-1} band which is about half that of the 23000 cm^{-1} band, while in the crystalline phase it has been observed under conditions which indicate an intensity equivalent to the first $\underline{n} \rightarrow \pi^*$ triplet (approximately $1/1000$ that of the 23000 cm^{-1} band). Unusual intensity changes have been noted for the solution spectra of biacetyl and glyoxal by Carpenter and Forster⁽³⁸⁾, and by Forster^(39,40). They found that the intensity in solution spectra of the 23000 cm^{-1} (biacetyl) or 23000 cm^{-1} (glyoxal) band was much lower when the solvent molecule contained an oxygen atom (e.g., in ethers or alcohols) than it was in non-oxygen containing solvents. These workers did not consider the second band in the near ultraviolet. Figure 3.10 gives Cary traces of biacetyl in the vapour and liquid phases, and in solution in water. It is seen that in water solution the intensity of the second band increases at the expense of the first. In view of the well-known ability of simple ketones and diketones to form reversible polymeric linkages it is proposed here that the second band in the near ultraviolet spectra of α,β -diketones be assigned to a species which has undergone molecular association.

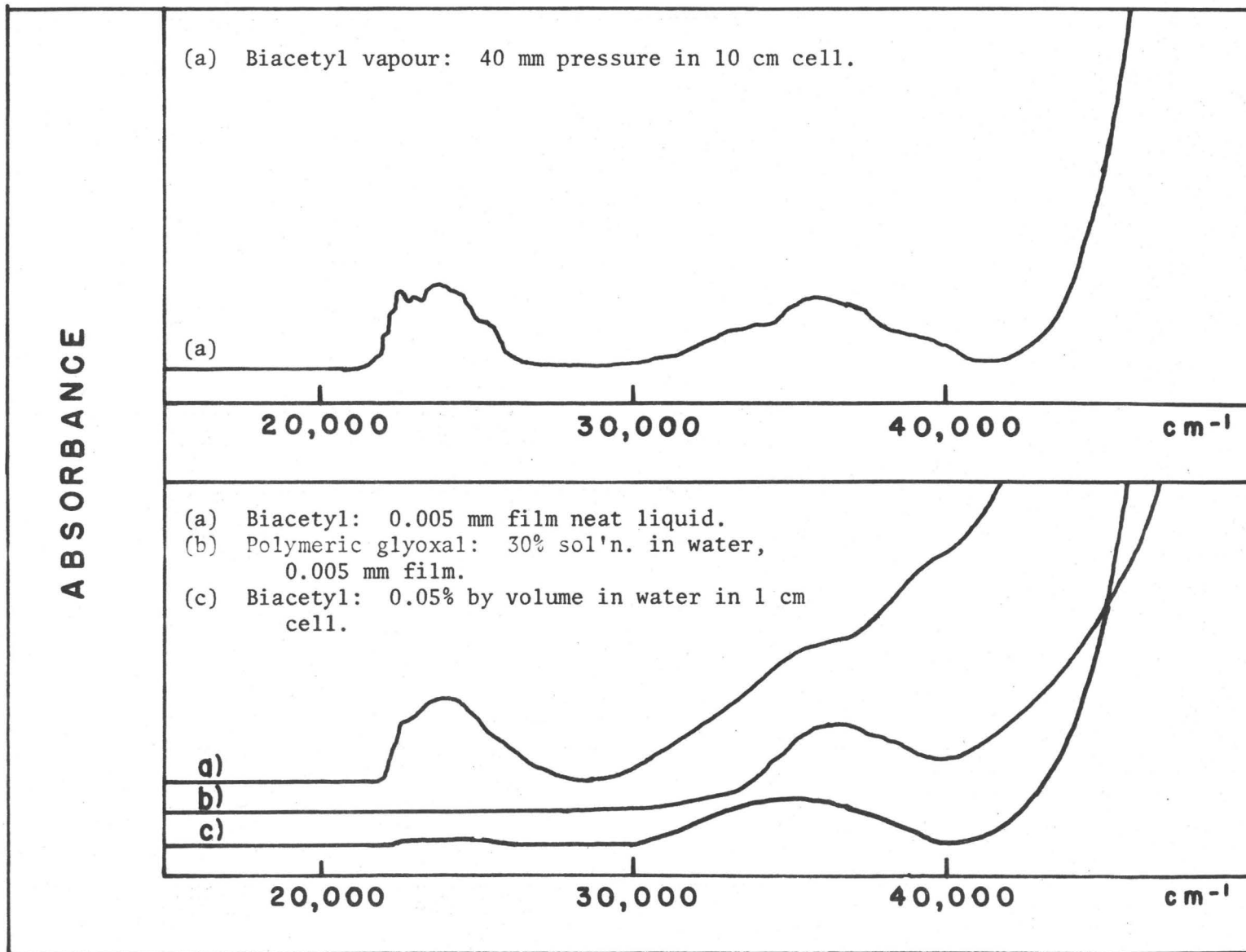


Figure 3.10 $35,000 \text{ cm}^{-1}$ System of Glyoxal (Polymeric) and Biacetyl.

The form of the condensed species has not been considered in detail. It is likely to be a dimeric form interconverting with a monomeric form to account for the significant quantity present in the vapour phase. The results of Carpenter and Forster suggested that association results from the attack by the oxygen atom of a solvent molecule. The mode of polymerization for formaldehyde would suggest a linkage between an oxygen and a carbonyl carbon. This picture is supported by the charge distribution calculated from the CNDO data. In the ground state, the charge distribution shows carbon as positive (0.19 a.u.) and oxygen negative (0.19 a.u.) with considerable polarity of the carbonyl bond (although molecular dipole moment is zero through symmetry). An intramolecular C...O linkage would destroy the conjugation of the two carbonyl groups and the dimer should have an $\underline{n} \rightarrow \pi^*$ transition in the same region as monoketones (see the spectrum of polymeric glyoxal, Figure 3.10). The 2800 Å band for α, β diketones is assigned as the $\underline{n} \rightarrow \pi^*$ transition of the dimeric species of this molecule. If the oscillator strength for the dimer $n \rightarrow \pi^*$ transition is the same as for the monomer the band intensity suggests a dimer concentration of approximately 25% in the vapour phase (peak area is half and transition energy double that of the monomer transition - see Equation (3.38)). This estimate would be low if the oscillator strength increased in the dimer or if considerable amounts of the dimer occurred on the window surfaces. No residual spectrum was found after sample removal.

In addition to the ${}^1, {}^3A_u(n_{a_g}^-, \pi_{a_u}^*) \leftarrow \tilde{X}{}^1A_g$ systems of glyoxal, these calculations indicate the possible appearance in the near ultraviolet of a transition to the ${}^3B_u(\pi_{b_g}^-, \pi_{a_u}^*)$ upper state. The calculations suggest that this transition has an energy comparable to that of the first $n \rightarrow \pi^*$ (S-S)

(see Table 3.5) and an intensity comparable to that for the $n \rightarrow \pi^*$ (S-T) (see Table 3.11). In this context it is noted that Goetz, McHugh and Ramsay⁽⁴¹⁾ have recently observed a series of weak S-T bands at 4350 Å in the magnetic rotation spectrum of glyoxal. These bands did not appear to belong to the ${}^3A_u(na_g^-, \pi a_u^*)$ system, and were left unassigned.

The vacuum ultraviolet spectrum of glyoxal has been examined by Walsh⁽²⁰⁾ and consists of a number of diffuse bands. He reports wavelengths of 2050-1850 Å (weak), 1750 Å (strong), 1667 Å (very strong), 1601 Å (strong), 1355 Å, 1324 Å. The corresponding spectrum of biacetyl has been reported by Ells⁽⁴²⁾. He lists a large number of bands which he describes as sharp. A spectrophotometer trace of biacetyl vapour was recorded in the vacuum UV for the present use (see Figure 3.5). In this spectrum, no sharp peaks are observed. The spectrum resembles closely that reported for glyoxal, with band maxima at the following wave lengths: 1900 Å (III in Figure 3.8, weak), 1720 Å (IV, very strong), 1610 Å (V, very strong), 1550 Å (medium), 1480 Å (medium), 1430 Å (weak). All bands are broad and contain no indication of vibrational structure. In addition, a photograph of biacetyl at 0.01 meter-atm. on a 20' Eagle Spectrograph showed no trace of sharp bands. It is concluded that the lines reported by Ells must be due to the presence of an impurity, perhaps a photodecomposition product. Several obvious possibilities such as O₂, CO₂, CO, and H₂O do not explain the reported peaks.

Walsh assigns two valence shell transitions in the spectrum of glyoxal below 2000 Å. He assigns the 2050-1850 Å band to an $\underline{n} \rightarrow \sigma^*$ transition and the 1667 Å band to a $\pi \rightarrow \pi^*$ transition. He notes that these transitions probably have considerable Rydberg character. Lucazeau and Sandorfy⁽⁴³⁾ have analyzed the vacuum ultraviolet spectra of a series of simple aldehydes on

the basis of two $n \rightarrow \sigma^*$, the first $\pi \rightarrow \pi^*$, and (possibly) the first $\sigma \rightarrow \sigma^*$ transitions. These transitions are superimposed on a large number of sharp features starting at about 1800 \AA , which are assigned to the three Rydberg transitions $n \rightarrow R_s$, $n \rightarrow R_p$, and $n \rightarrow R_d$. In the vacuum UV spectra of glyoxal and biacetyl, the most striking feature is the complete absence of Rydberg-like features. This fact would suggest two possibilities. Either the first members of the Rydberg transitions have shifted to the blue and lie under the intense continuous absorption, or the σ^* orbitals involve $n = 3$ orbitals heavily with the $\underline{n} \rightarrow \sigma^*$ diffuse and the $\underline{n} \rightarrow R_{3s,3p,3d}$ not isolated as discrete Rydberg transitions. The existing data on the ionization potentials of these compounds lists formaldehyde 10.88 eV, acetaldehyde 10.23 eV, ketene 9.60 eV, glyoxal 9.48 eV (taken from reference 7) and discredits the first idea.

The spectrum of glyoxal in the vacuum ultraviolet then suggests valence shell transitions with considerable Rydberg involvement. The calculated data of Table 3.5 suggests three transitions which may be discernable, the ${}^1B_u(\pi_{bg}, \pi_{au}^*)$, ${}^1B_u(n_{ag}^-, \sigma_{bu}^*)$, and the ${}^1A_u(\pi_{bg}, \sigma_{bu}^*)$. The CNDO energies of the two latter states which involve the σ_{bu}^* orbital are much too high to be acceptable. Sandorfy suggests that transitions in this region have some character due to atomic orbitals with quantum number three, and it is possible that the discrepancy in predicted transition energies arises from the neglect of $n = 3$ atomic orbitals in the CNDO calculation.

Sandorfy assigns the $\pi \rightarrow \pi^*$ transition in the aldehydes to the 1500 \AA ($67,000 \text{ cm}^{-1}$) region. It has little vibrational structure. In glyoxal and biacetyl a red shift is expected for this band (see Figure 3.9), and a red shift of $20,000 \text{ cm}^{-1}$ would place it at 1750 \AA . Thus the band at 1750 \AA

(glyoxal) or 1720 Å (biacetyl) is assigned as ${}^3B_u(\pi_{bg}, \pi_{au}^*)$. There is good agreement with the energy predicted by CNDO.

In the series formaldehyde⁽⁴⁴⁾, to acetaldehyde⁽⁴³⁾ and acetone⁽⁴⁵⁾ systems appear in the region from 2000 Å to 1600 Å which have well-defined vibrational structure and which appear to have no analogue in formaldehyde. These systems are assigned to $\underline{n} \rightarrow \sigma^*$ transitions and arise because of the availability of a 2p orbital on the CH₃ carbon which can form a lower energy antibonding σ^* orbital (and higher energy bonding orbital) than is available in formaldehyde. These transitions are expected for biacetyl and glyoxal, but the vacuum ultraviolet absorption appears diffuse for these two molecules. Two possible explanations are: 1) the molecules which are rigid and planar in the ground states can undergo internal rotation in the high energy excited states, or 2) the molecule dissociates in the appropriate excited states.

Since internal rotation exists in acetone, which has structured absorption in the vacuum ultraviolet, molecular dissociation is the more likely cause of diffuseness in the high energy spectra of glyoxal and biacetyl. It can be seen from Table 3.2 that the σ_{1bu}^* orbital is strongly antibonding along the C-C bond and along the two C-H bonds. In addition, the CNDO calculations (see Figures 3.5, 3.6) show that the potential energy curves with respect to the C-C and C-H bond lengths are noticeably shallower for the states which involve promotion to the σ_{1bu}^* orbital (i.e., $B_u(n_{ag}^-, \sigma_{1bu}^*), A_u(\pi_{bg}, \sigma_{bu}^*)$) than they are for the other excited states. Although a completely dissociative path could not be obtained from the CNDO calculations, it is felt that the evidence indicates molecular dissociation as the cause of the diffuseness of vacuum ultraviolet transitions.

Table 3.5 predicts an intensity for the $n \rightarrow \sigma^*$ transition comparable

to that for the $\pi - \pi^*$ at 1750 Å. The strong absorption at 1667 Å (glyoxal) and 1610 Å (biacetyl) is assigned to a transition to ${}^1B_u(n_a^-, \sigma_{1b_u}^*)$. The bands and continuous absorption to the blue of this arises from the additional $\sigma \rightarrow \sigma^*$, $n \rightarrow \sigma^*$ and $\pi \rightarrow \pi^*$ transitions. The absorption in the region of 2000 Å - 1850 Å (glyoxal and biacetyl) is weak relative to the $\pi \rightarrow \pi^*$ transition and strong relative to the $n \rightarrow \sigma^*$. This fits the intensity predicted for the $\pi \rightarrow \sigma^*$ transition (see Table 3.5) and is assigned as ${}^1A_u(\pi_{b_g}, \sigma_{b_u}^*)$.

(b) The CNDO Geometry

The geometry which minimizes the CNDO energy (referred to as the CNDO geometry) has been compared in Table 3.1 with the available experimental data. Experimentally, King⁽³⁴⁾ and Paldus and Ramsay⁽²³⁾ have determined the rotational constants for glyoxal and a series of deuterated derivatives in the ground and first excited singlet state from the UV spectra, and Kuchitsu et al.⁽²²⁾ have carried out an electron diffraction study on the ground state. The spectroscopic work was carried out on a limited number of isotopically substituted molecules, and it was only possible to specify a series of geometries which would reproduce all the available rotational constants. Kuchitsu et al. combined the spectroscopic results with electron diffraction results and determined a single geometry for the ground state which has been listed in Table 3.1.

In considering the CNDO geometry, it might be noted that the CNDO value for the C-C bond of 1.44 Å is more in agreement with the partial double bond character expected for this molecule (compare C-C single bond ~ 1.54 Å and C=C double bond ~ 1.34 Å). In fact electron diffraction results by the same authors⁽²²⁾ find a C-C bond length of 1.463 Å for butadiene ($\text{CH}_2\text{CH}=\text{CHCH}_2$) and 1.478 Å for acrolein ($\text{CH}_2\text{CH}=\text{CHO}$), and the value of 1.525

\AA quoted for glyoxal appears to be high. In addition, since the calculated electron diffraction geometry was based on the sets of results from the rotational analysis, an error in either $r(\text{C-C})$ or $r(\text{C=O})$ would result in an approximately equal and opposite error in the other (see references 23 or 24).

The CNDO geometry for the ${}^1A_u(n\bar{a}_g, \pi^*a_u)$ excited state predicts a small change from the ground state in the bond angles, and in the C=O and C-H bond lengths and a larger change in the C-C bond length. These changes are not in agreement with the vibrational analysis of the UV spectrum (see reference 32). The appearance of the progressions in vibrational modes involving C=O stretch, C-C stretch and $\angle\text{CCO}$ bend predict the largest changes to be in $r(\text{C=O})$ with significant changes in $r(\text{C-C})$ and $\angle\text{CCO}$ and small changes in the other parameters.

The CNDO calculation on the ${}^1B_u(n\bar{a}_g, \sigma^*b_u)$ excited state produced a very anomalous decrease in energy with decrease in the CCO bond angle below 100° . The CNDO energy was minimized at $\angle\text{CCO} = \sim 55^\circ$ and $r(\text{C-C}) \sim 1.7 \text{\AA}$. The unusual values of these parameters and the shallow potential well found for the variation of the energy with $r(\text{C-C})$ (see Figure 3.5) suggest that this state may be dissociative.

The evidence obtained from the calculations on glyoxal indicate that CNDO cannot be used in the manner outlined to predict accurate geometries. It is felt, however, that the results are close enough to the true geometry to warrant using this method of selecting a geometry for calculation of energy levels.

(c) The Vibrational Structure

The ground state vibrational spectrum of glyoxal has been investigated

in the infra-red by Harris⁽⁴⁴⁾, and a normal coordinate analysis has been carried out by Fleury⁽³⁰⁾.

The infra-red work contains some information pertinent to the problem of intermolecular association. Harris observes that on removal of the sample from the cell, a residual infra-red spectrum attributed to polymer on the windows remained. The principal features of this spectrum were two weak bands lying directly under the C=O and C-H stretching modes of glyoxal, and a very broad band at $\sim 700\text{ cm}^{-1}$ which appeared almost as strongly as it did in the vapour phase spectrum. It can be concluded that apart from the broad band at 700 cm^{-1} (which could originate in a weak O...C linkage), a dimeric species would not be detectable as a separate spectrum. It is interesting to note that for the oxalyl halides there is a similar broad band which appears in the region of $700\text{-}1200\text{ cm}^{-1}$. This band, particularly for the bromide, shows a marked decrease in width and intensity in the crystalline spectrum at liquid nitrogen temperature. It is possible that this absorption originates in a weak intermolecular associative linkage which does not form in the solid phase.

The CNDO force constants shown in Table 3.13 are different from the force constants obtained from the normal coordinate analysis of Fleury⁽³⁰⁾. Inspection of Table 3.13 indicates that stretching force constants differ by a factor of approximately 3 while bending force constants differ by a factor of approximately 1.5. An analogous treatment of oxalyl fluoride (see Section 3.7) shows a similar pattern in the discrepancies between CNDO force constants and those obtained from a normal coordinate analysis.

(d) Perturbations

The calculations carried out here have provided estimates of the energies of the ground and low-lying excited states of glyoxal (see Table 3.5

and Figures 3.2 and 3.3). It is thus possible to comment upon the observation, spectroscopically, of electronic perturbations.

The ${}^3A_u(n_{ag}^-, \pi_{au}^*) \leftarrow \tilde{X}{}^1A_g$ transition is observable through perturbation by other excited states as indicated in Table 3.10. The calculations summarized in Table 3.10 suggest perturbation of ${}^3A_u(n_{ag}^-, \pi_{au}^*)$ by ${}^1B_u(\pi_{bg}, \pi_{au}^*)$ as the most likely cause of the observed intensity with perturbation by ${}^1B_u(n_{ag}^-, \sigma_{bu}^*)$ or perturbation of $\tilde{X}{}^1A_g$ by ${}^3B_g(n_{bu}^+, \pi_{au}^*)$ or ${}^3B_g(n_{ag}^-, \pi_{bg}^*)$ as other possibilities. In all these cases the transition moment would be in the plane and the bands observed should have the rotational structure of type A-B hybrid bands. In a study of the magnetic rotation spectrum of glyoxal, Goetz et al. (41) refer to unpublished work by Ramsay and Tyrrell which indicates that the 0-0 band of the singlet-triplet transition is an A-B hybrid.

In the ${}^1A_u(n_{ag}^-, \pi_{au}^*) \leftarrow \tilde{X}{}^1A_g$ spectrum the appearance of type A-B hybrid bands (see reference 32) indicates the appearance of a forbidden component through vibronic perturbation. The hybrid bands are assigned to transitions in which one quantum in the out of plane wagging mode (b_g symmetry) is active. These bands with b_g vibrational symmetry must gain intensity through vibronic perturbation by a 1B_u state. Brand (32) has proposed ${}^1B_u(\pi_{bg}, \pi_{au}^*)$ as the perturbing state. The calculated and experimental state energies of Table 3.5 support his suggestion, and indicate that ${}^1B_u(n_{ag}^-, \sigma_{bu}^*)$ is also a potential perturbing state.

The $B_u(n_{ag}^-, \sigma_{bu}^*)$ and $A_u(\pi_{bg}, \sigma_{bu}^*)$ have been proposed here to be dissociative states. Participation (through perturbation) in a transition by either of these states should result in predissociation of the excited state levels. In view of the diffuseness of the ${}^1B_u(\pi_{bg}, \pi_{au}^*) \leftarrow \tilde{X}{}^1A_g$ transition it is presumed that there is significant mixing between this excited state and

the ${}^1B_u(n_{ag}^-, \sigma_{1b_u}^*)$ state. Thus, any mixing between $A_u(n_{ag}^-, \pi_{au}^*)$ and the states of immediately higher energy is likely to result in predissociation of the $n \rightarrow \pi^*$ transition to higher energy. Such an effect is observed particularly strongly for the halogenated derivatives of glyoxal.

3.8 Oxalyl Fluoride

The calculations that were carried out for glyoxal (see Sections 3.3 and 3.4) were repeated for oxalyl fluoride. The ultraviolet spectrum of this molecule is not as well understood as the spectrum of glyoxal, and it was hoped that with the CNDO calculations on glyoxal as a guide to reliability such calculations would be of use in the assignment of the oxalyl fluoride spectrum.

The ground state geometry of oxalyl fluoride was not known, and initial calculations were carried out using molecular parameters transferred from similar compounds. As previously these were refined to give a CNDO geometry, obtained by minimizing energy with respect to the five molecular parameters, and the CNDO geometry was used for the energy calculations. The CNDO geometry (ground and excited states) is summarized in Table 3.14. The coordinate system was fixed in the molecule as for glyoxal (see Figure 3.1). The basis set used in the calculations consisted of 24 atomic orbitals, the $2s$, $2p_x$, $2p_y$, and $2p_z$ orbitals on each atom. The set of SCF-LCAO molecular orbitals for the ground state of oxalyl fluoride are given in Table 3.15. The corresponding bond order matrix is listed in Table 3.16. Inspection of Table 3.15 indicates that here, as with glyoxal, two of the highest energy bonding orbitals have greater than 50% p_y (oxygen) character, and these orbitals are designated n_0^- and n_0^+ . In addition, it can be seen that for oxalyl fluoride a hybrid combination of the p_x and p_y atomic orbitals on

TABLE 3.14

CNDO Geometries for Ground and Excited States
of Oxalyl Fluoride

State	r_{CC} Å	r_{CO} Å	r_{CF} Å	$\angle \text{OCF}$ deg.	$\angle \text{CCO}$ deg.
\tilde{X}^1A_g	1.46	1.26	1.34	118	123
$1,^3A_u(n_{ag}^-, \pi_{au}^*)$	1.40	1.28	1.34	122	117
$1,^3B_u(\pi_{bg}, \pi_{au}^*)$	1.35	1.35	1.34	113	127
$1,^3B_u(n_{ag}^-, \sigma_{bu}^*)$	1.7	1.27	1.32	121	55

	1	2	3	4	5	6	7	8	9
	$\sigma_{5a_g}^*$	$\sigma_{4b_u}^*$	$\sigma_{3b_u}^*$	$\sigma_{2a_g}^*$	$\pi_{b_g}^*$	$\sigma_{1b_u}^*$	$\pi_{a_u}^*$	$n_{o a_g}^-$	π_{1b_g}
2sO	-207274	-201108	.147098	-125271	0.000000	-060351	0.000000	.006325	0.000000
	-207274	-201108	-.147098	-.125271	0.000000	.060351	0.000000	.006325	0.000000
2sF	.095505	.039016	-.137795	-.169450	0.000000	-.156175	0.000000	-.029908	0.000000
	.095505	-.039016	.137795	-.169450	0.000000	.156175	0.000000	-.029908	0.000000
2sC	.113569	-.009426	-.210840	.359283	0.000000	.544403	0.000000	.114002	0.000000
	.113569	.009426	.210840	.359283	0.000000	-.544403	0.000000	.114002	0.000000
2p _x ^O	-.326151	.322193	.255678	-.231766	0.000000	-.145757	0.000000	-.168250	0.000000
	.326151	.322193	.255678	.231766	0.000000	-.145757	0.000000	.168250	0.000000
2p _x ^F	-.044286	-.093741	.107320	.179667	0.000000	.123231	0.000000	-.030420	0.000000
	.044286	-.093741	.107320	-.179667	0.000000	.123231	0.000000	.030420	0.000000
2p _x ^C	-.500681	.453512	.203646	-.031918	0.000000	.221245	0.000000	.176378	0.000000
	.500681	.453512	.203646	.031918	0.000000	.221245	0.000000	-.176378	0.000000
2p _y ^O	.033170	.065940	-.118491	-.104338	0.000000	-.034931	0.000000	.542892	0.000000
	-.033170	.065940	-.118491	.104338	0.000000	-.034931	0.000000	-.542892	0.000000
2p _y ^F	-.158155	-.023328	.218020	.259714	0.000000	.297254	0.000000	.283766	0.000000
	.158155	-.023328	.218020	-.259714	0.000000	.297254	0.000000	-.283766	0.000000
2p _y ^C	-.223355	-.367129	.484755	.401444	0.000000	.025124	0.000000	-.224658	0.000000
	.223355	-.367129	.484755	-.401444	0.000000	.025124	0.000000	.224658	0.000000
2p _z ^O	0.000000	0.000000	0.000000	0.000000	.360689	0.000000	-.517942	0.000000	-.591090
	0.000000	0.000000	0.000000	0.000000	-.360689	0.000000	-.517942	0.000000	.591090
2p _z ^F	0.000000	0.000000	0.000000	0.000000	.121347	0.000000	-.137163	0.000000	.233121
	0.000000	0.000000	0.000000	0.000000	-.121347	0.000000	-.137163	0.000000	-.233121
2p _z ^C	0.000000	0.000000	0.000000	0.000000	-.595968	0.000000	.461435	0.000000	-.310270
	0.000000	0.000000	0.000000	0.000000	.595968	0.000000	.461435	0.000000	.310270

Table 3.15 Molecular Orbitals for Oxalyl Fluoride $\tilde{X}(^1A_g)$ in Order of Decreasing Energy.

	10	11	12	13	14	15	16	17	18
	n_{ob}^+	π_{2a_u}	n_{Fa}^-	n_{Fb}^+	σ_{1a_g}	π_{3b_g}	σ_{2b_u}	σ_{3a_g}	π_{4a_u}
2sO	-.027982	0.000000	.102097	-.142218	.136013	0.000000	-.299257	-.197386	0.000000
	.027982	0.000000	.102097	.142218	.136013	0.000000	.299257	-.197386	0.000000
2sF	-.013652	0.000000	-.000980	.008050	-.052466	0.000000	.029643	-.148896	0.000000
	.013652	0.000000	-.000980	-.008050	-.052466	0.000000	-.029643	-.148896	0.000000
2sC	-.038624	0.000000	-.020487	.157282	-.051050	0.000000	.091070	.160835	0.000000
	.038624	0.000000	-.020487	-.157282	-.051050	0.000000	-.091070	.160835	0.000000
2p _x ^O	-.109016	0.000000	-.417011	.362002	-.262383	0.000000	.380058	.215753	0.000000
	.109016	0.000000	.417011	.362002	.262383	0.000000	.380058	-.215753	0.000000
2p _x ^F	.231554	0.000000	-.427943	.457695	.259849	0.000000	-.359389	-.441371	0.000000
	.231554	0.000000	.427943	.457695	-.259849	0.000000	-.359389	.441371	0.000000
2p _x ^C	-.098960	0.000000	.265235	-.130245	.156945	0.000000	-.214740	-.039979	0.000000
	-.098960	0.000000	-.265235	-.130245	-.156945	0.000000	-.214740	.039979	0.000000
2p _y ^O	.629071	0.000000	-.245760	-.184735	.216941	0.000000	-.046898	.236658	0.000000
	.629071	0.000000	.245760	-.184735	-.216941	0.000000	-.046898	-.236658	0.000000
2p _y ^F	.162826	0.000000	-.010178	-.244737	-.485126	0.000000	.280172	-.221213	0.000000
	.162826	0.000000	.010178	-.244736	.485126	0.000000	.280172	.221213	0.000000
2p _y ^C	.001158	0.000000	-.035647	-.058779	.180922	0.000000	-.029306	.255153	0.000000
	.001158	0.000000	.035647	-.058779	-.180922	0.000000	-.029306	-.255153	0.000000
2p _z ^O	0.000000	.406991	0.000000	0.000000	0.000000	-.143235	0.000000	0.000000	.257089
	0.000000	.406991	0.000000	0.000000	0.000000	.143235	0.000000	0.000000	.257089
2p _z ^F	0.000000	-.486750	0.000000	0.000000	0.000000	-.656452	0.000000	0.000000	.494228
	0.000000	-.486750	0.000000	0.000000	0.000000	.656452	0.000000	0.000000	.494228
2p _z ^C	0.000000	.312143	0.000000	0.000000	0.000000	-.220351	0.000000	0.000000	.435482
	0.000000	.312143	0.000000	0.000000	0.000000	.220351	0.000000	0.000000	.435482

Table 3.15 (Cont'd.)

	19	20	21	22	23	24
	σ_{4b_u}	σ_{5a_g}	σ_{6a_g}	σ_{7b_u}	σ_{8b_u}	σ_{9a_g}
2s ₀	-.080256	-.326616	.462450	-.559313	-.066627	.229961
	.080256	-.326616	.462450	.559313	.066627	.229961
2s _F	-.248938	-.124211	-.394457	.086996	-.620025	.515095
	.248938	-.124211	-.394457	-.086996	.620025	.515095
2s _C	.205032	.301429	.245866	-.210503	-.195472	.405978
	-.205032	.301429	.245866	.210504	.195472	.405978
2p _{x0}	.093294	.092546	.075576	-.111548	-.032472	.089524
	.093294	-.092546	-.075576	-.111548	-.032472	-.089524
2p _{xF}	-.254740	.131813	-.033109	.077804	.036066	-.029952
	-.254740	-.131813	.033109	.077804	.036066	.029952
2p _{xC}	.098421	.302177	-.165521	.340406	-.073981	.043621
	.098421	-.302177	.165520	.340406	-.073981	-.043621
2p _{y0}	.210529	-.165691	-.048402	.014058	-.061764	.004066
	.210529	.165691	.048402	.014058	-.061764	-.004066
2p _{yF}	-.441616	-.187730	-.052769	-.022250	.056023	-.067820
	-.441616	.187730	.052769	-.022250	.056023	.067820
2p _{yC}	.258690	-.327215	-.175388	.014944	-.241119	.039331
	.258691	.327215	.175388	.014944	-.241119	-.039331
2p _{z0}	0.000000	0.000000	0.000000	0.000000	0.000000	0.000000
	0.000000	0.000000	0.000000	0.000000	0.000000	0.000000
2p _{zF}	0.000000	0.000000	0.000000	0.000000	0.000000	0.000000
	0.000000	0.000000	0.000000	0.000000	0.000000	0.000000
2p _{zC}	0.000000	0.000000	0.000000	0.000000	0.000000	0.000000
	0.000000	0.000000	0.000000	0.000000	0.000000	0.000000

Table 3.15 (Cont'd.)

	$2s0_1$	$2s0_2$	$2sF_1$	$2sF_2$	$2sC_1$	$2sC_2$	$2p_x0_1$	$2p_x0_2$	$2p_xF_1$
$2s0$	1.753386	.014302	.002952	-.008904	.269131	.004947	-.411267	-.029313	.047941
	.014302	1.753386	-.008904	.002952	.004947	.269131	.029313	.411267	.005644
$2sF$.002952	-.008904	1.834674	.014203	.213029	-.012491	-.016426	.016034	.144359
	-.008904	.002952	.014203	1.834674	-.012491	.213029	-.016034	.016426	-.006027
$2sC$.269131	.004947	.213029	-.012491	1.029716	.398880	.512074	.032385	-.210403
	.004947	.269131	-.012491	.213029	.398880	1.029716	-.032385	-.512074	-.028372
$2p_x^0$	-.411267	.029313	-.016426	-.016034	.512074	-.032385	1.307931	-.060676	-.095882
	-.029313	.411267	.016034	.016426	.032385	-.512074	-.060676	1.307931	-.012790
$2p_x^F$.047941	.005644	.144359	-.006027	-.210403	-.028372	.095882	-.012790	1.860950
	-.005644	-.047941	.006027	-.144359	.028372	.210403	-.012790	.095882	-.002442
$2p_x^C$	-.431306	.000198	.174566	-.005334	-.005566	.283102	-.672801	.008926	-.044762
	-.000198	.431306	.005334	-.174566	-.283102	.005566	.008926	-.672801	.019344
$2p_y^0$	-.001378	-.016315	-.089228	.006930	-.056834	.076979	-.018885	.033979	-.085575
	.016315	.008378	-.006930	.089228	-.076979	-.056834	.033979	-.018885	.005793
$2p_y^F$	-.019146	.018432	.272253	-.036579	-.382229	.080959	.007144	-.027082	-.230704
	-.018432	.019146	.036579	-.272253	-.080959	.382229	-.027082	.007144	-.017051
$2p_y^C$.016211	.000393	.349353	.008437	-.069114	-.408548	.036673	-.044299	-.342999
	-.000393	-.016211	-.008437	-.349353	.408548	.069114	-.044299	.036673	-.014972
$2p_z^0$	0.000000								
	0.000000	0.000000	0.000000	0.000000	0.000000	0.000000	0.000000	0.000000	0.000000
$2p_z^F$	0.000000	0.000000	0.000000	0.000000	0.000000	0.000000	0.000000	0.000000	0.000000
	0.000000	0.000000	0.000000	0.000000	0.000000	0.000000	0.000000	0.000000	0.000000
$2p_z^C$	0.000000	0.000000	0.000000	0.000000	0.000000	0.000000	0.000000	0.000000	0.000000
	0.000000	0.000000	0.000000	0.000000	0.000000	0.000000	0.000000	0.000000	0.000000

Table 3.16 Bond Order Matrix for Oxalyl Fluoride $\tilde{X}(^1A_g)$.

	$2p_x^F$	$2p_x^C$	$2p_x^C$	$2p_y^0$	$2p_y^0$	$2p_y^F$	$2p_y^F$	$2p_y^C$	$2p_y^C$
2s0	-.005644	.431306	-.000198	-.008378	.016315	-.019146	-.018432	.016211	-.000393
	-.047941	.000198	.431306	-.016315	.008378	.018432	.019146	.000393	-.016211
2sF	.006027	.174566	.005334	-.089228	-.006930	.272253	.036579	.349353	-.008437
	-.144359	-.005334	-.174566	.006930	.089228	-.036579	-.272253	.008437	-.349353
2sC	.028372	-.005566	-.283102	.056834	-.076979	-.382229	-.080959	-.069114	.408548
	.210403	.283102	.005566	.076979	-.056834	.080959	.382229	-.408548	.069114
$2p_x^0$	-.012790	.672801	-.008926	-.018885	.033979	.007144	-.027082	.036673	-.044299
	.095882	.008926	-.672801	.033979	-.018885	-.027082	.007144	-.044299	.036673
$2p_x^F$	-.002442	-.044762	.019344	.085575	-.005793	-.230704	-.017051	-.342999	-.014972
	1.860950	.019344	-.044762	.005793	.085575	-.017051	-.230704	-.014972	-.342999
$2p_x^C$.019344	.896546	-.088164	.029906	-.021788	-.340521	-.057752	-.074137	.321785
	-.044762	-.088164	.896546	-.021788	.029906	-.057752	-.340521	.321785	-.074137
$2p_y^0$	-.005793	-.029906	-.021788	1.938518	-.014682	.138177	.010759	.260316	.065241
	.085575	-.021788	.029906	-.014682	1.938518	.010759	.138177	.065241	.260316
$2p_y^F$	-.017051	-.340521	-.057752	.138177	-.010759	1.544242	-.087797	-.522724	.035135
	-.230704	-.057752	-.340521	.010759	.138177	-.087797	1.544242	.035135	-.522724
$2p_y^C$	-.014972	-.074137	.321785	.260316	.065241	-.522724	.035135	.834038	-.318855
	-.342999	.321785	-.074137	.065241	.260316	.035135	-.522724	-.318855	.834038
$2p_z^0$	0.000000	0.000000	0.000000	0.000000	0.000000	0.000000	0.000000	0.000000	0.000000
	0.000000	0.000000	0.000000	0.000000	0.000000	0.000000	0.000000	0.000000	0.000000
$2p_z^F$	0.000000	0.000000	0.000000	0.000000	0.000000	0.000000	0.000000	0.000000	0.000000
	0.000000	0.000000	0.000000	0.000000	0.000000	0.000000	0.000000	0.000000	0.000000
$2p_z^C$	0.000000	0.000000	0.000000	0.000000	0.000000	0.000000	0.000000	0.000000	0.000000
	0.000000	0.000000	0.000000	0.000000	0.000000	0.000000	0.000000	0.000000	0.000000

Table 3.16 (Cont'd.)

	$2p_z^0_1$	$2p_z^0_2$	$2p_z^F_1$	$2p_z^F_2$	$2p_z^C_1$	$2p_z^C_2$
2s ₀	0.000000	0.000000	0.000000	0.000000	0.000000	0.000000
2s _F	0.000000	0.000000	0.000000	0.000000	0.000000	0.000000
2s _C	0.000000	0.000000	0.000000	0.000000	0.000000	0.000000
2p _x ⁰	0.000000	0.000000	0.000000	0.000000	0.000000	0.000000
2p _x ^F	0.000000	0.000000	0.000000	0.000000	0.000000	0.000000
2p _x ^C	0.000000	0.000000	0.000000	0.000000	0.000000	0.000000
2p _y ⁰	0.000000	0.000000	0.000000	0.000000	0.000000	0.000000
2p _y ^F	0.000000	0.000000	0.000000	0.000000	0.000000	0.000000
2p _y ^C	0.000000	0.000000	0.000000	0.000000	0.000000	0.000000
2p _z ⁰	1.221353	-.273364	-.229746	-.056221	.904191	.052636
2p _z ^F	-.273364	1.221353	-.056221	-.229746	.052636	.904191
2p _z ^C	-.229746	-.056221	1.931337	-.009071	.276268	-.016174
	-.056221	-.229746	-.009071	1.931337	-.016174	.276268
	.904191	.052636	.276268	-.016174	.847310	.282435
	.052636	.904191	-.016174	.276268	.282435	.847310

Table 3.16 (Cont'd.)

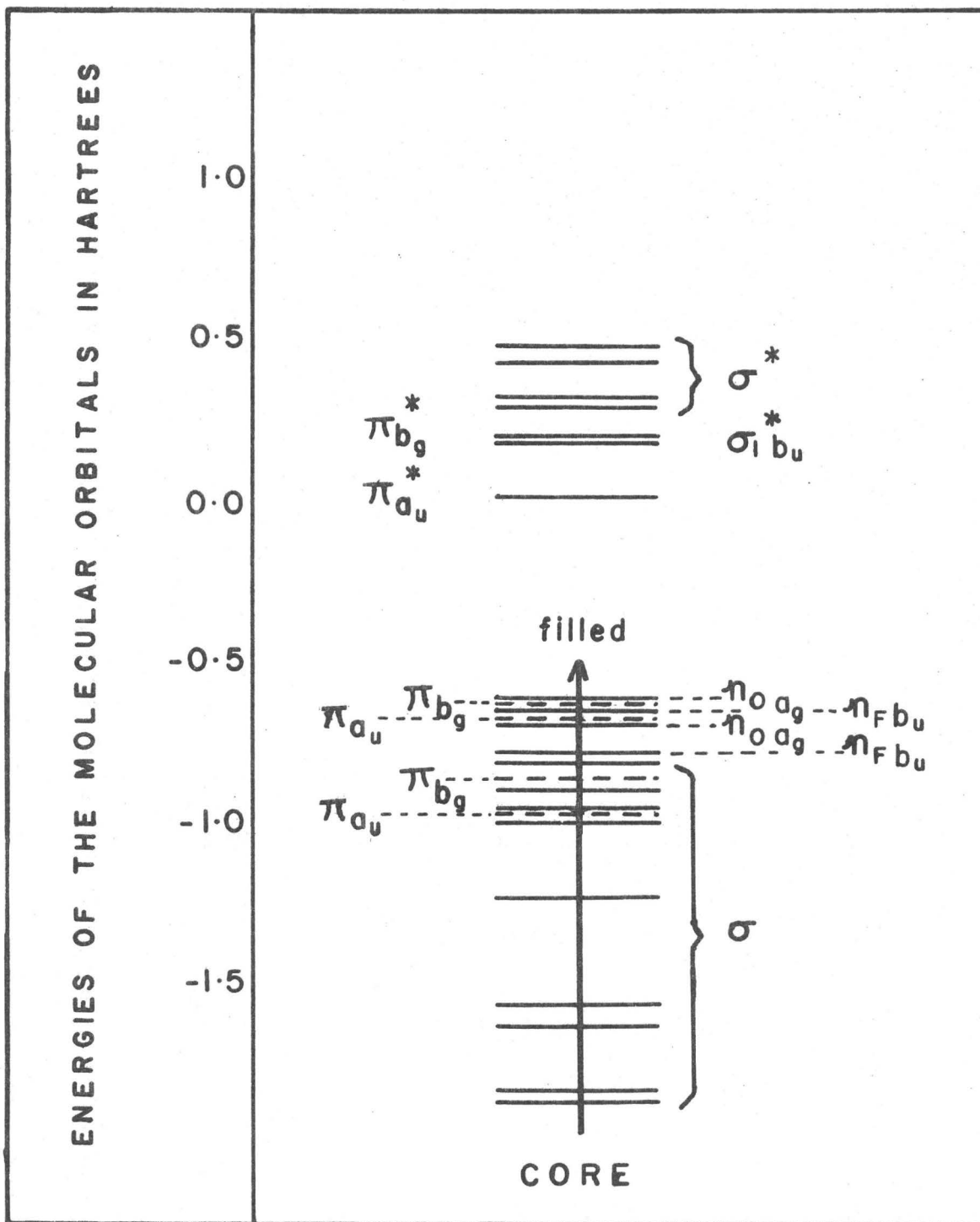


Figure 3.11 Energies of the Molecular Orbitals of Oxalyl Fluoride in the Ground State

fluorine can act as non-bonding orbitals, and two of the MO's have been designated n_F^- and n_F^+ . In both these orbitals the p_x , p_y (fluorine) character is approximately 50%. The remaining orbitals have been labelled σ -, π -type. An energy level diagram of the ground state molecular orbitals with the electron population of the ground state is given in Figure 3.11. It might be noted that four of the six π MO's are filled (bonding) and two are unfilled (anti-bonding). This differs from the results expected from a simple Hückel treatment of the π system.

(a) Energies

SCF calculations were carried out on the ground state and a series of excited states produced by promotion of a single electron. Triplet state energies were obtained from the CNDO open shell calculation, and singlet state energies were obtained by the methods outlined in Section 3.2. The state energies are summarized in Table 3.17 and an energy level diagram is given for the u states in Figure 3.12 and for the g states in Figure 3.13. The ground state of oxalyl fluoride has 1A_g symmetry (in the C_{2h} point group) and transitions to all the u states are electric dipole allowed. The transition energies for the u states have been included in Table 3.17.

(b) Transition Intensities

Transition intensities were calculated by the methods outlined in Section 3.4. These intensities have been included in Table 3.17. The calculations involved in determining singlet-triplet intensities through spin-orbit interaction have been summarized for transitions to the three excited states $^3A_u(n_{a_g}^-, \pi_{a_u}^*)$, $^3B_u(\pi_{b_g}, \pi_{a_u}^*)$, $^3B_u(n_{a_g}^-, \sigma_{1b_u}^*)$ in Tables 3.18, 3.19 and 3.20.

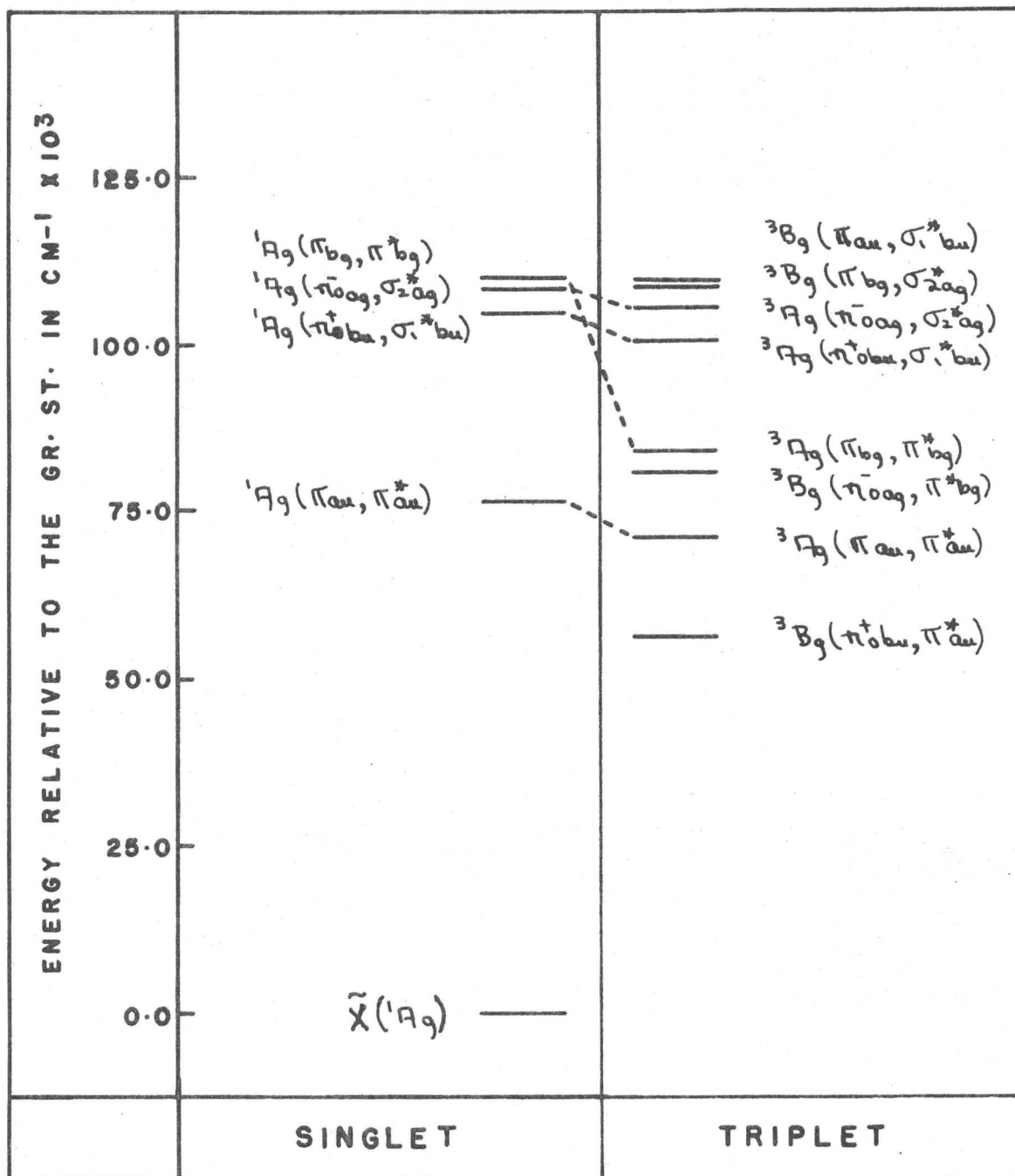


Figure 3.13 CNDO Energies for the "g" States of Oxalyl Fluoride at the CNDO Ground State Geometry.

TABLE 3.17

Calculated CNDO (SCF-LCAO-MO) Energies for Ground and Excited States of Oxalyl Fluoride

with Transition Energies and Oscillator Strengths

State	Energy a.u.	Calculated Vertical Transition Energy a.u.	cm ⁻¹	Å	Exp. V.T.E. cm ⁻¹	Calc. Origin Transition cm ⁻¹	Exp. ^a	Calculated Oscillator Strength
$1\tilde{X}$	$1A_g$	-106.281						
$n_{oag}^- \rightarrow \pi_{au}^*$	$3A_u$	-106.120	0.161	35336	2829	32290	29941	$\sim 10^{-7}$
	$1A_u$	-106.108	0.173	37891	2640	36020	32815	1.5×10^{-3}
$\pi_{bg} \rightarrow \pi_{au}^*$	$3B_u$	-106.124	0.157	34458	2902	16680		$\sim 10^{-8}$
	$1B_u$	-106.001	0.280	61454	1627	44115		0.40
$n_{fag}^- \rightarrow \pi_{au}^*$	$3A_u$	-105.971	0.310	68038	1470			$\sim 10^{-7}$
	$1A_u$	-105.958	0.323	70892	1411			6.1×10^{-3}
$n_{oag}^- \rightarrow \sigma_{1bu}^*$	$3B_u$	-105.905	0.376	82524	1211			
	$1B_u$	-105.862	0.419	91962	1087			0.19
$\pi_{bg} \rightarrow \sigma_{1bu}^*$	$3A_u$	-105.882	0.399	87572	1141			
	$1A_u$	-105.873	0.408	89547	1116			2.3×10^{-2}
$n_{obu}^+ \rightarrow \pi_{bg}^*$	$3A_u$	-105.817	0.464	101838	981			
	$1A_u$	-105.810	0.471	103375	967			2.2×10^{-4}
$\pi_{au} \rightarrow \pi_{bg}^*$	$3B_u$	-105.757	0.524	115007	869			
	$1B_u$	-105.675	0.606	133004	751			0.32
$n_{obu}^+ \rightarrow \sigma_{2ag}^*$	$3B_u$	-105.702	0.579	127078				
	$1B_u$	-105.663	0.618	135638				0.18

^aFrom Balfour, reference (1).

TABLE 3.17 (cont'd.)

State	Calculated			
	Energy a.u.	Vertical a.u.	Transition cm ⁻¹	Energy Å
$n_{obu}^+ \rightarrow \pi_{au}^*$	${}^3B_{1g}^g$ -106.031	0.257	56406	1773
$\pi_{au} \rightarrow \pi_{au}^*$	${}^3A_{1g}^g$ -105.957	0.324	71111	1406
	${}^1A_{1g}^g$ -105.832	0.349	76598	1306
$n_{oag}^- \rightarrow \pi_{bg}^*$	${}^3B_{1g}^g$ -105.910	0.371	81428	1228
$\pi_{bg} \rightarrow \pi_{bg}^*$	${}^3A_{1g}^g$ -105.896	0.385	84499	1183
	${}^1A_{1g}^g$ -105.757	0.524	115007	
$n_{obu}^+ \rightarrow \sigma_{1bu}^*$	${}^3A_{1g}^g$ -105.823	0.458	100521	
	${}^1A_{1g}^g$ -105.804	0.477	104680	
$n_{oag}^- \rightarrow \sigma_{2ag}^*$	${}^3A_{1g}^g$ -105.800	0.481	105569	
	${}^1A_{1g}^g$ -105.788	0.493	108203	
$\pi_{bg} \rightarrow \sigma_{2ag}^*$	${}^3B_{1g}^g$ -105.786	0.495	108642	
$\pi_{au} \rightarrow \sigma_{1bu}^*$	${}^3B_{1g}^g$ -105.785	0.496	108861	

TABLE 3.18

Intensity for the Transition ${}^3A_u(n_{\text{Oag}}^-, \pi_{\text{Au}}^*) \leftarrow \tilde{X}{}^1A_g$ of Oxalyl Fluoride

Produced by Spin Orbit Coupling

Perturbing Singlet State m	${}^3E_1 - {}^1E_m$ a.u.	$ H'_{m1} $ a.u.	$ m_{\text{om}} /e$	$ M_{01} /e^a$	Corresponding f_{osc}	Polarization
1 ${}^1B_u(\pi_{\text{bg}}, \pi_{\text{Au}}^*)$	0.119	9.5×10^{-5}	0.77	6.2×10^{-4}	1.4×10^{-7}	A,B
2 ${}^1B_u(n_{\text{Oag}}^-, \sigma_{\text{1bu}}^*)$	0.258	7.0×10^{-5}	0.45	1.2×10^{-4}	5.6×10^{-9}	A,B
3 ${}^1B_u(\pi_{\text{Au}}, \pi_{\text{bg}}^*)$		*			ω^b	
4 ${}^1B_u(n_{\text{Obu}}^+, \sigma_{\text{2ag}}^*)$		*			ω	
5 ${}^1A_u(n_{\text{Fag}}^-, \pi_{\text{Au}}^*)$	0.162	2.7×10^{-4}	0.09	1.5×10^{-4}	8.6×10^{-9}	C
6 ${}^1A_u(\pi_{\text{bg}}, \sigma_{\text{1bu}}^*)$		*			ω	
7 ${}^1A_u(n_{\text{Obu}}^+, \pi_{\text{bg}}^*)$		*			ω	
8 ${}^1A_u(\pi_{\text{Au}}, \sigma_{\text{2ag}}^*)$		*			ω	

Perturbing Triplet State μ	${}^1E_0 - {}^3E_\mu$ a.u.	$ H'_{\mu 0} $ a.u.	$ m_{1\mu} /e$	$ M_{01} /e$	Corresponding f_{osc}	Polarization
1 ${}^3B_g(n_{\text{Obu}}^+, \pi_{\text{Au}}^*)$	0.257	1.6×10^{-4}	~ 0.5	$\sim 10^{-4}$	$\sim 10^{-9}$	A,B
2 ${}^3B_g(n_{\text{Oag}}^-, \pi_{\text{bg}}^*)$	0.371	1.2×10^{-4}	~ 0.7	$\sim 10^{-4}$	$\sim 10^{-9}$	A,B
3 ${}^3B_g(\pi_{\text{bg}}, \sigma_{\text{2ag}}^*)$			***		ω	
4 ${}^3B_g(\pi_{\text{Au}}, \sigma_{\text{1bu}}^*)$			***		ω	
5 ${}^3A_g(\pi_{\text{Au}}, \pi_{\text{Au}}^*)$		**			ω	
6 ${}^3A_g(\pi_{\text{bg}}, \pi_{\text{bg}}^*)$		**	***		ω	
7 ${}^3A_g(n_{\text{Obu}}^+, \sigma_{\text{1bu}}^*)$			***		ω	
8 ${}^3A_g(n_{\text{Oag}}^-, \sigma_{\text{2ag}}^*)$	0.481	2.2×10^{-5}	~ 0.2	$\sim 10^{-5}$	$\sim 10^{-10}$	C

^a Assuming only a single perturbing state.^b The symbol " ω " has been employed where mixing is negligible.* These terms are small, and under the approximation of \mathcal{H}'_{SO} by a single electron operator become zero.** These terms are small, and under the approximation of local spherical symmetry at each atom become zero, e.g., $\langle {}^3A_g(\pi_{\text{Au}}, \pi_{\text{Au}}^*) | \mathcal{H}'_{\text{SO}} | {}^1A_g(\text{G.S.}) \rangle \sim \langle \phi_{\text{Au}} | L_z | \phi_{\text{Au}} \rangle \sim 0$ since the operator L_z can only couple the atomic orbitals p_x and p_y .*** These terms are zero since ${}^3\psi_\mu$ differs from ${}^3\psi_1$ by four MO's.

TABLE 3.19

Intensity for the Transition ${}^3B_u(\pi_b, \pi_{a_u}^*) \leftarrow \tilde{X}{}^1A_g$ of Oxalyl Fluoride
Produced by Spin Orbit Coupling

Perturbing Singlet State	${}^3E_1 - {}^1E_m$ a.u.	$ H'_{ml} $ a.u.	$ m_{om} /e$	$ M_{01} /e$	Corresponding f_{osc}	Polarization
1 ${}^1B_u(n_{oa_g}, \sigma_{1b_u}^*)$		*			ω	
2 ${}^1B_u(\pi_{a_u}, \pi_{b_g}^*)$		*			ω	
3 ${}^1B_u(n_{ob_u}, \sigma_{2a_g}^*)$		*			ω	
4 ${}^1A_u(n_{oa_g}, \pi_{a_u}^*)$	0.024	9.5×10^{-5}	0.06	2.4×10^{-4}	2.2×10^{-8}	C
5 ${}^1A_u(\pi_{b_g}, \sigma_{1b_u}^*)$	0.251	7.0×10^{-5}	0.15	4.2×10^{-5}	6.6×10^{-10}	C
6 ${}^1A_u(n_{ob_u}, \pi_{b_g}^*)$		*			ω	
7 ${}^1A_u(\pi_{a_u}, \sigma_{2a_g}^*)$		*			ω	

Perturbing Singlet State	${}^1E_o - {}^3E_\mu$ a.u.	$ H'_{\mu o} $ a.u.	$ m_{1\mu} /e$	$ M_{01} /e$	Corresponding f_{osc}	Polarization
1 ${}^3B_g(n_{ob_u}, \pi_{a_u}^*)$	0.257	1.6×10^{-4}	~ 0.05	$\sim 10^{-5}$	$\sim 10^{-10}$	A,B
2 ${}^3B_g(n_{oa_g}, \pi_{b_g}^*)$			***			
3 ${}^3B_g(\pi_{b_g}, \sigma_{2a_g}^*)$	0.495	1.8×10^{-4}	~ 0.1	$\sim 10^{-5}$	$\sim 10^{-10}$	A,B
4 ${}^3B_g(\pi_{a_u}, \sigma_{1b_u}^*)$			***			
5 ${}^3A_g(\pi_{a_u}, \pi_{a_u}^*)$		**				
6 ${}^3A_g(\pi_{b_g}, \pi_{b_g}^*)$		**				
7 ${}^3A_g(n_{ob_u}, \sigma_{1b_u}^*)$			***			
8 ${}^3A_g(n_{oa_g}, \sigma_{2a_g}^*)$			***			

a

b

*

**

See Table 3.18 for an explanation of the code.

TABLE 3.20

Intensity for the Transition ${}^3B_u(n\bar{o}a_g, \sigma^*1b_u) \leftarrow \tilde{X}{}^1A_g$ of Oxalyl Fluoride
Produced by Spin Orbit Coupling

Perturbing Singlet State	${}^3E_1 - {}^1E_m$ a.u.	$ H'_{m1} $ a.u.	$ m_{om} /e$	$ M_{01} /e$	Corresponding f_{osc}	Polarization
1 ${}^1B_u(\pi_{bg}, \pi_{au}^*)$		*			ω	
2 ${}^1B_u(\pi_{au}, \pi_{bg}^*)$		*			ω	
3 ${}^1B_u(n\bar{o}b_u, \sigma^*2a_g)$		*			ω	
4 ${}^1A_u(n\bar{o}a_g, \pi_{au}^*)$	0.203	7.0×10^{-5}	0.06	2.1×10^{-5}	4.0×10^{-10}	C
5 ${}^1A_u(\pi_{bg}, \sigma^*1b_u)$	0.032	1.2×10^{-4}	0.15	5.6×10^{-4}	2.8×10^{-7}	C
6 ${}^1A_u(n\bar{o}b_u, \pi_{bg}^*)$		*			ω	
7 ${}^1A_u(\pi_{au}, \sigma^*2a_g)$		*			ω	
Perturbing Triplet State	${}^1E_0 - {}^3E_\mu$ a.u.	$ H'_{\mu 0} $ a.u.	$ m_{1\mu} /e$	$ M_{01} /e$	Corresponding f_{osc}	Polarization
1 ${}^3B_g(n\bar{o}b_u, \pi_{au}^*)$			***		ω	
2 ${}^3B_g(n\bar{o}a_g, \pi_{bg}^*)$	0.371	1.2×10^{-4}	~ 0.1	$\sim 10^{-5}$	$\sim 10^{-10}$	A,B
3 ${}^3B_g(\pi_{bg}, \sigma^*2a_g)$			***		ω	
4 ${}^3B_g(\pi_{au}, \sigma^*1b_u)$	0.496	2.2×10^{-4}	~ 0.05	$\sim 10^{-5}$	$\sim 10^{-10}$	A,B
5 ${}^3A_g(\pi_{au}, \pi_{au}^*)$		**	***		ω	
6 ${}^3A_g(\pi_{bg}, \pi_{bg}^*)$		**	***		ω	
7 ${}^3A_g(n\bar{o}b_u, \sigma^*1b_u)$	0.458	9.7×10^{-5}	0.5	$\sim 10^{-4}$	$\sim 10^{-8}$	C
8 ${}^3A_g(n\bar{o}a_g, \sigma^*2a_g)$	0.481	2.2×10^{-5}	0.5	$\sim 10^{-5}$	$\sim 10^{-10}$	C

a

b

* See Table 3.18 for an explanation of the code.

**

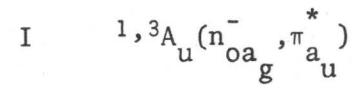
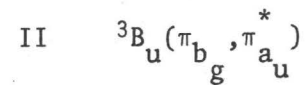
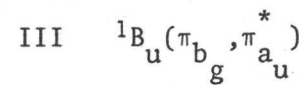
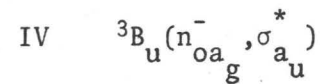
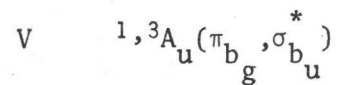
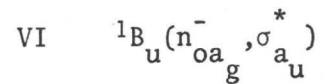
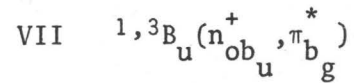
(c) The Vibrational Structure

Figures 3.14, 3.15, and 3.16 show the CNDO potential energy curves for the five parameters which determine the geometry of oxalyl fluoride. Again the force constants were obtained from these curves. Fleury⁽³⁰⁾ has obtained the force constants in a Urey-Bradley force field from a normal coordinate analysis of the ground state. The Urey-Bradley force field has been converted to give general valence force constants according to the formulae given in Table 3.21, and the CNDO force constants have been included in this table.

(d) Theory and Experiment for Oxalyl Fluoride

The UV spectrum of oxalyl fluoride is quite complex; Balfour⁽¹⁾ has discussed it in considerable detail, but has left some aspects of the analysis unsolved. It was hoped that the CNDO calculation might indicate the presence of overlapping electronic transitions. In particular, it was anticipated that with fluorine atoms present additional nonbonding orbitals might arise which could result in new low-lying electronic transitions. By inspection of Figure 3.11 and Table 3.17 it can be seen that this result is not found in the CNDO results. The only low energy transitions for trans oxalyl fluoride are those to ${}^3A_u(n_{Oag}^-, \pi_{au}^*)$, ${}^3B_u(\pi_{bg}, \pi_{bu}^*)$ and ${}^1A_u(n_{Oag}^-, \pi_{au}^*)$ with the first two very weak in intensity. In terms of CNDO theory the pattern of electronic transitions is little different from the pattern of the spectrum calculated for glyoxal. No new electronic transition is obtained from the CNDO results which could account for the complexity of the near ultraviolet spectrum. These calculations, therefore, resulted in the proposal (discussed in Chapter 4) that a large part of the discrete absorption is attributable to the cis isomer.

Figure 3.14



CC Bond Length

CO = 1.25 Å, CF = 1.34 Å

CCO = 128, OCF = 118

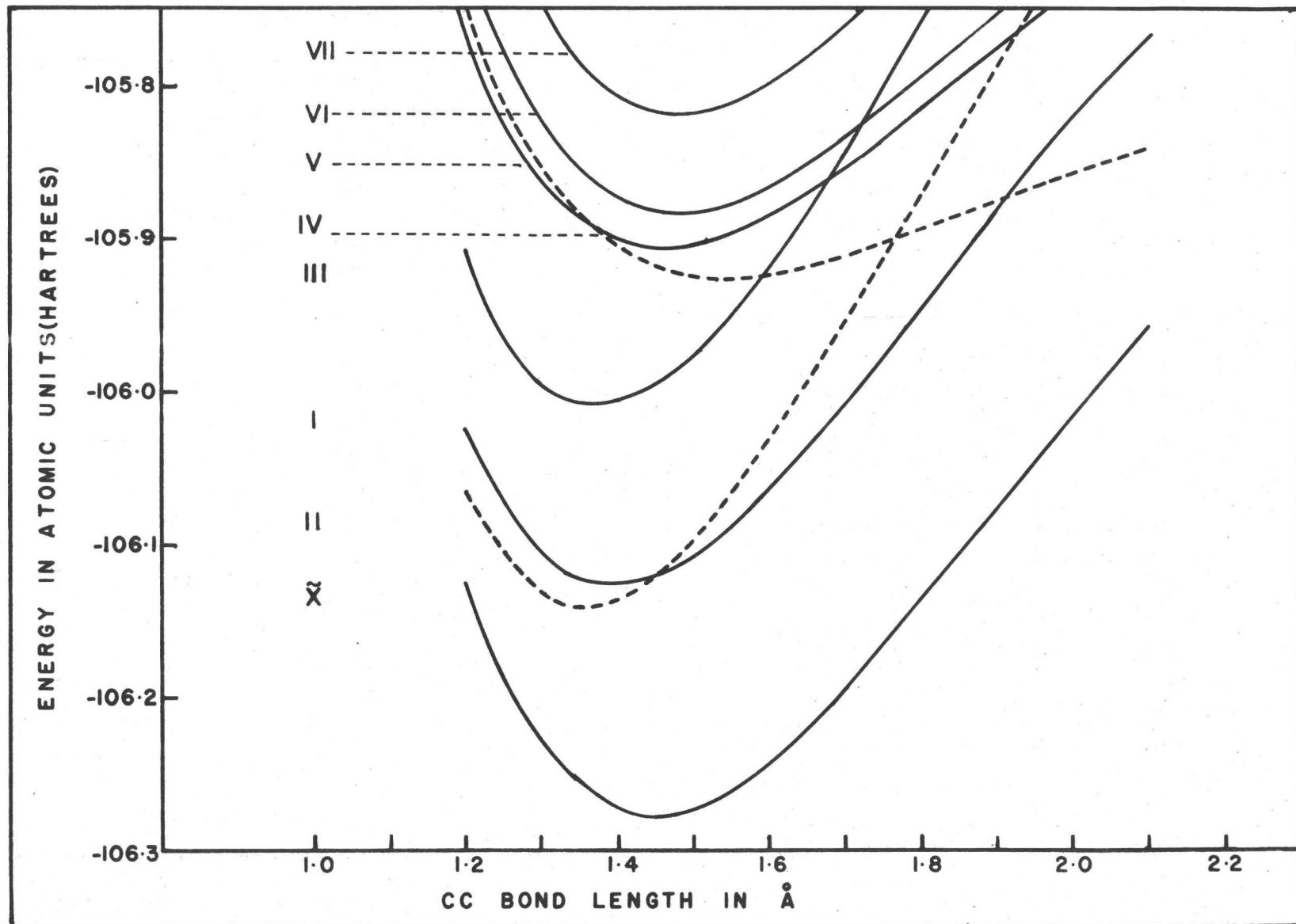


Figure 3.14 CND0 Potential Curve for (COFCOF) for CC Bond Lengths.

Figure 3.15

VII	$1, {}^3B_u^+(n_{ob_u}^+, \pi_{bg}^*)$
VI	${}^1B_u^-(n_{oa_g}^-, \sigma_{au}^*)$
V	$1, {}^3A_u^-(\pi_{bg}, \sigma_{bu}^*)$
IV	${}^3B_u^-(n_{oa_g}^-, \sigma_{au}^*)$
III	${}^1B_u^-(\pi_{bg}, \pi_{au}^*)$
II	${}^3B_u^-(\pi_{bg}, \pi_{au}^*)$
I	$1, {}^3A_u^-(n_{oa_g}^-, \pi_{au}^*)$

CO Bond Length

$$CC = 1.45 \text{ \AA}, \quad CF = 1.35 \text{ \AA}$$

$$CCO = 120^\circ, \quad OCF = 118^\circ$$

CF Bond Length

$$CC = 1.45 \text{ \AA}, \quad CO = 1.25 \text{ \AA}$$

$$CCO = 120^\circ, \quad OCF = 118^\circ$$

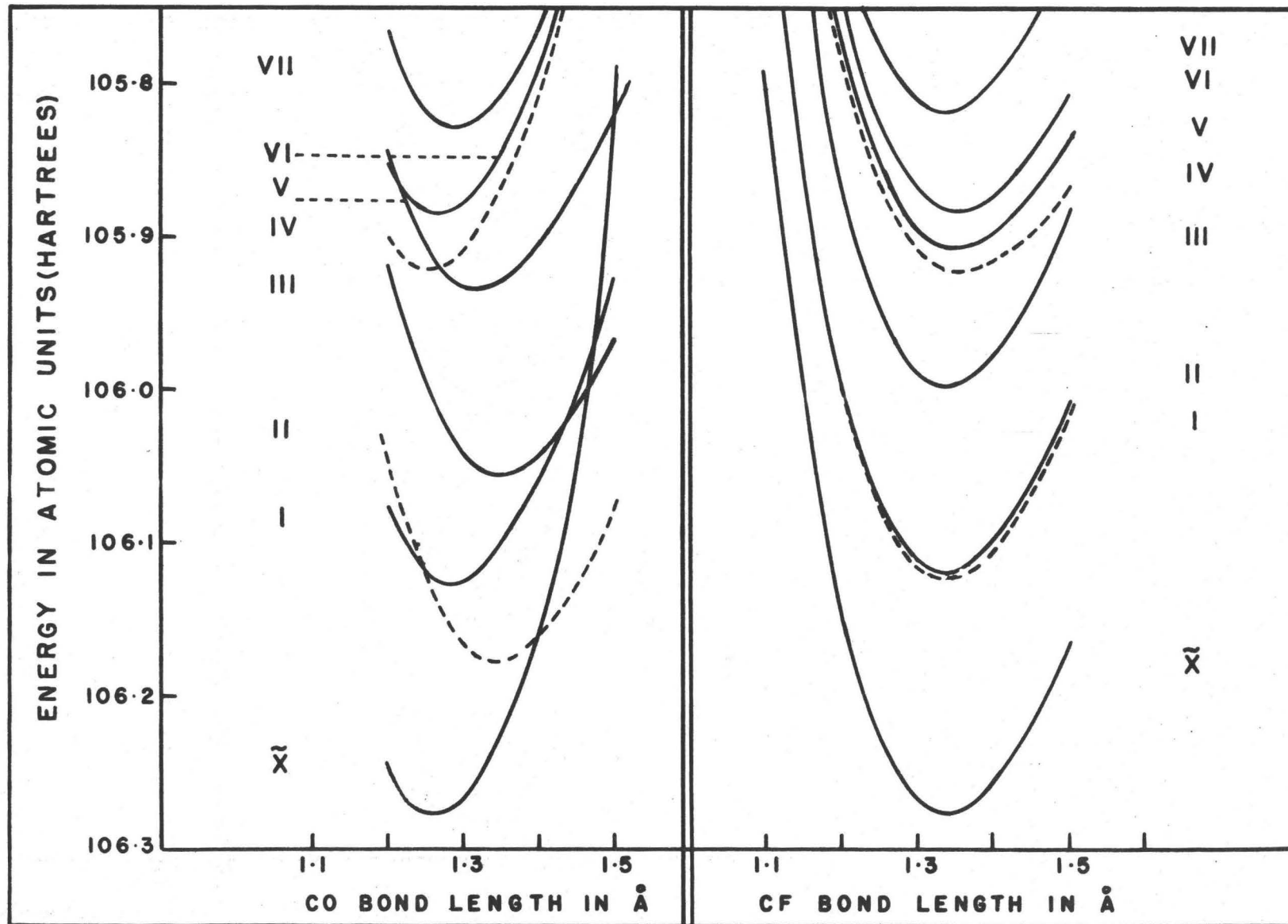


Figure 3.15 CNDO Potential Curve for (COFCOF) for CO, CF Bond Lengths.

Figure 3.16

- VII $1,^3B_u(n_{ob_u}^+, \pi_{bg}^*)$
 VI $1B_u(n_{oa_g}^-, \sigma_{au}^*)$
 V $1,^3A_u(\pi_{bg}, \sigma_{bu}^*)$
 IV $3B_u(n_{oa_g}^-, \sigma_{au}^*)$
 III $1B_u(\pi_{bg}, \pi_{au}^*)$
 II $3B_u(\pi_{bg}, \pi_{au}^*)$
 I $1,^3A_u(n_{oa_g}^-, \pi_{au}^*)$

COF Bond Angle

CC = 1.45 Å, CO = 1.25 Å, CF = 1.33 Å

CCO = 120°

CCO Bond Angle

CC = 1.45 Å, CO = 1.25 Å, CF = 1.33 Å

OCF = 120°

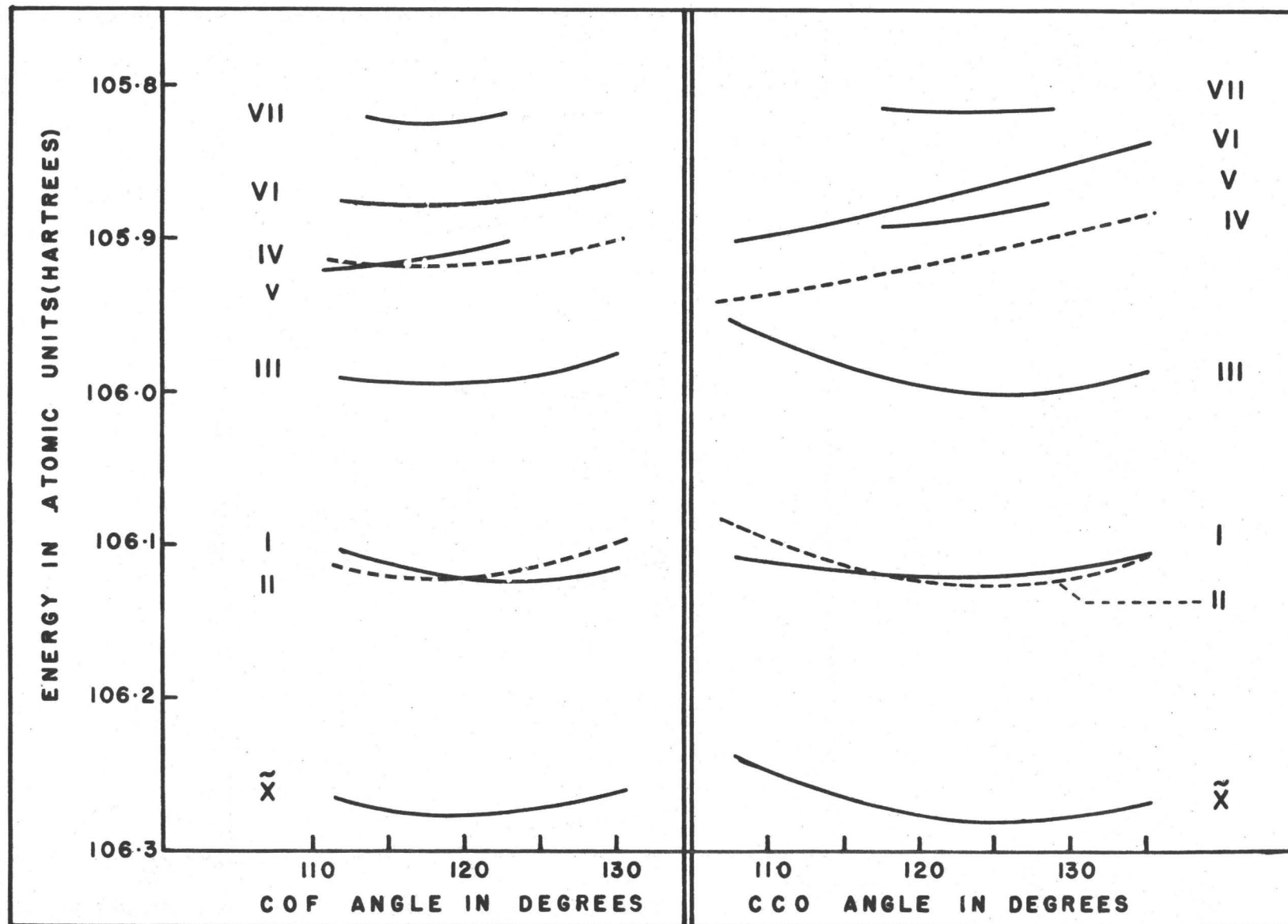


Figure 3.16 CNDO Potential Curve for (COFCOF) for COF, CCO Bond Angles.

TABLE 3.21

The Expansion of the Diagonal Quadratic Taylor's Series Coefficients
for the Potential Energy in Urey-Bradley Space for Oxalyl Fluoride

Coefficient	Parameter	Expansion ^a
A ₁	r _{CC}	K _{CC} + 1.70 F _{CCO} + 1.49 F _{CCF} + 1.94 F _{O...F}
A ₂ , A ₃	(Δr _{CO}) _{1,2}	K _{CO} + 0.75 F _{CCO} + 0.78 F _{OCF} + 0.27 F _{O...F}
A ₄ , A ₅	(Δr _{CF}) _{1,2}	K _{CF} + 0.83 F _{OCF} + 0.67 F _{CCF} + 0.25 F _{O...F}
A ₆ , A ₇	Δ(∠OCF) _{1,2}	1.59H _{OCF} +2.06H _{CCF} +0.21F _{OCF} +0.52F _{CCF} +1.39F _{O...F}
A ₈ , A ₉	Δ(∠CCO) _{1,2}	1.81H _{CCO} +2.06H _{CCF} +0.52F _{CCF} +0.29F _{CCO} +2.41F _{O...F}

^aThe geometry used in the expansion was that used by Fleury⁽³⁰⁾.

CNDO^b and Experimental GVFF Force Constants

State	Δp _{CC}	Δp _{CO}	Δp _{CF}	Δp _{OCF}	Δp _{CCO}
	millidyne/Å			millidyne-Å/rad ²	
\tilde{X}^1A_g	13.8	60.9	44.5	4.4	3.9
1A_g (G.S.) exp. ^c	3.6	24.1	6.4	2.32	2.26
$^1,^3A_u(n_{a_g}^-, \pi_{a_u}^*)$	17.1	54.8	47.1	3.86	1.86
$^3A_u(\pi_{b_g}, \pi_{a_u}^*)$	20.6	45.4	49.2	3.58	4.36
$^1A_u(\pi_{b_g}, \pi_{a_u}^*)$	24.1	50.3	45.8	4.20	4.23

^bLeast squares fit to eight CNDO energies within 0.04 Å or 4° of the equilibrium geometry.

^cExperimental values are obtained from the force constants of Fleury⁽³⁰⁾.

A second feature which was under consideration in the near UV spectrum of oxalyl fluoride (and the other oxalyl halides) was the observation of a strong underlying continuous absorption. Inspection of Table 3.4 indicates that the potential energy curve for the C-C bond length is quite shallow for the $1,3B_u(n_{Oa_g}^-, \sigma_{1b_u}^*)$ and also for the $1,3A_u(\pi_{b_g}, \sigma_{1b_u}^*)$ states. By optimizing the remaining four geometric parameters it was found that the energy of the $1,3B_u(n_{Oa_g}^-, \sigma_{1b_u}^*)$ state decreased as $r(C-C)$ was extended to 1.6 \AA . These results suggest that promotion to the $\sigma_{1b_u}^*$ MO may produce a state which is dissociative along the C-C bond, thus giving rise to continuous absorption in the vacuum UV. Again, as for glyoxal, perturbation by the higher energy states of the $A_u(n_{Oa_g}^-, \pi_{a_u}^*)$ state will lead to predissociation of this state to higher energies, as is observed experimentally.

The results in Table 3.20 indicate that, as in glyoxal, the calculated force constants are too large, but there is not the same internal consistency. At this time, the reliability of the calculated force constants is not known, and a discussion of the discrepancies does not seem to be justified.

3.9 Oxalyl Chloride

An attempt was made to repeat the calculations made on glyoxal and oxalyl fluoride for oxalyl chloride. In the calculation of the potential energy curves and the CNDO geometry it was found that the calculated energy dropped with increasing $\angle CCO$ to the point where large $\angle CCO$ created near superposition of the chlorine atom on the carbon atom. This result is unacceptable and it was concluded that the CNDO/2⁽¹⁶⁾ program does not work as well for molecules containing the second row element chlorine. A reduced number of calculations were carried out for oxalyl chloride and oxalyl chloride fluoride. Since it was not possible to obtain a CNDO geometry, a geometry was

estimated. Bond lengths and angles were transferred from the previous calculations on COHCOH and COFCOF, and a value of 1.75 Å was chosen for $r(\text{C}-\text{Cl})$ by comparison with similar molecules. Energies for the ground and several excited states were calculated for the one geometry only. These state energies together with vertical transition energies are listed in Table 3.22; the geometry used for the calculation is included in the table.

The molecular orbitals calculated for oxalyl chloride are not easily labelled as were the MO's of glyoxal and oxalyl fluoride. In this case, the highest non-bonding orbital can still be labelled as an n orbital, but it is no longer localized on the oxygen atom. For oxalyl chloride the n orbitals are composed principally of projections on the planar p atomic orbitals on both oxygen and chlorine, with the result that there is an increased number of non-bonding orbitals. It can be seen in Table 3.22 that the CNDO calculations predict two low energy $n \rightarrow \pi^*$ (S-S) transitions.

A spectrophotometer trace of oxalyl chloride vapour shows that the strongest absorption is a broad featureless band at 1550 Å (64500 cm^{-1}). This peak is followed to higher energy by a series of weaker bands, also without structure. At 1975 Å ($50,600 \text{ cm}^{-1}$) there is a structureless band which is weak relative to the 1550 Å absorption, and at 3678 Å (27188.9 cm^{-1}) there is the origin of the discrete ${}^1\text{A}_u(n_{1ag}, \pi_{1au}^*) \leftarrow \tilde{\text{X}}^1\text{A}_g$ transition which is weak relative to the 1975 Å absorption. There is no sign in the vapour phase spectrum of the second predicted $n \rightarrow \pi^*$ spectrum, but the extensive predissociation of the first $n \rightarrow \pi^*$ transition and the rapidly increasing intensity of the absorption background combine to make its identification

TABLE 3.22

Calculated CNDO (SCF-LACO-MO) Energies for Ground and Excited States
of Oxalyl Chloride with Transition Energies

State	Energy ^a a.u.	Vertical a.u.	Calculated Transition cm ⁻¹	Energy Å	Exp. V.T.E. cm ⁻¹
\tilde{X} $1A_g$	-81.681				
$n1a_g \rightarrow \pi^*1a_u$ $1,3A_u$	-81.546	0.135	29600	3380	27188.9
$\pi1b_g \rightarrow \pi^*1a_u$ $3B_u$	-81.537	0.154	33600	2980	
$1B_u$	-81.428	0.253	55500	1800	64500
$n2a_g \rightarrow \pi^*1a_u$ $1,3A_u$	-81.513	0.168	36900	2710	33800 ^b
$n1a_g \rightarrow \sigma^*1b_u$ $3B_u$	-81.419	0.262	57500	1740	
$1B_u$	-81.354	0.327	71800	1390	64500
$\pi1b_g \rightarrow \sigma^*1b_u$ $1,3A_u$	-81.378	0.303	66500	1500	50600
$\pi2a_u \rightarrow \sigma^*2a_g$ $1,3A_u$	-81.293	0.388	85200	1180	

^aThe geometry used was: $r(CC) = 1.46 \text{ \AA}$, $r(CO) = 1.26 \text{ \AA}$, $r(CCl) = 1.75 \text{ \AA}$,
 $\angle CCO = 123^\circ$, $\angle OCCl = 118^\circ$.

^bTentative assignment from the solid phase spectrum.

unlikely. It is noted, however, that there is evidence in the solid phase of a second discrete absorption system just to the blue of the 3678 Å system. A sharp peak at 2960 Å (33800 cm⁻¹) in the solid is tentatively assigned to ${}^1A_u(n2a_g, \pi^*1a_u) \leftarrow \tilde{X}^1A_g$. The absorption at 1975 Å is assigned to ${}^1A_u(\pi 1b_g, \sigma^*1b_u) \leftarrow \tilde{X}^1A_g$ and the absorption of 1550 Å because of its intensity is assigned to the overlap of the first $n \rightarrow \sigma^*$ and $\pi \rightarrow \pi^*$ transitions.

3.10 Oxalyl Chloride-Fluoride

The results of the CNDO/2 calculations on oxalyl chloride indicated that the program used was not reliable for molecules containing second row elements. As with oxalyl chloride, a small set of calculations were carried out on COFCOCl₂ to obtain some information about the number and nature of the low-lying electronic transition which can be expected for this molecule.

The calculations were carried out using a basis set of 29 atomic orbitals which included the 2s and 2p orbitals on the first row atoms and the 3s, 3p and 3d orbitals on the second row atoms. The oxalylchloride fluoride molecule belongs to the C_s point group, and it can be seen from Table 1.4 that transitions are possible to excited states of symmetry A' and A". Electric dipole transitions are allowed to all excited states. It is found by inspection of the molecular orbitals calculated for COFCOCl₂ that they can be given approximate designations with respect to the irreducible representations of the C_{2h} point group. Although oscillator strengths were not calculated for this molecule, it is anticipated that transitions to excited states which have approximate A_u or B_u symmetry will be strong while transitions to excited states which have approximate A_g or B_g symmetry (which are electric dipole forbidden under the C_{2h} point group) will be weak.

The energies of the ground and low-lying excited states of oxalyl

chloride-fluoride were calculated. A CNDO geometry was not determined, so a geometry was estimated using parameter values transferred from previous calculations and assuming a value of 1.75 Å for $r(\text{C-Cl})$ (by analogy to similar compounds). The calculated energies are given in Tables 3.23 and 3.24. The excited states listed in Table 3.23 have approximate A_u or B_u symmetry and should give rise to strong transitions in the ultraviolet. The excited states listed in Table 3.23 correspond to approximate A_g or B_g symmetry and should give rise to weak transitions.

It can be seen in Tables 3.23 and 3.24 that the calculated energies are much lower than the experimental values. Because the results are not too useful, the singlet-triplet splittings for the $n \rightarrow \pi^*$ states were not calculated. Although the agreement with experiment is not good for this molecule, it is possible to draw some conclusions which are useful in the later assignment of the discrete spectrum of COFCOCl.

The calculations indicate that the lowest energy transition for COFCOCl should be the $n \rightarrow \pi^*$ transition which correlates with ${}^1, {}^3A_u(n_{ag}^-, \pi_{au}^*) \leftarrow \tilde{X}^1A_g$ of the C_{2h} oxalyl halides. The assignment of the discrete absorption (discussed in detail in Chapter 5) is based on an $n \rightarrow \pi^*$ (S-S) origin at 28725 cm^{-1} and an $n \rightarrow \pi^*$ (S-T) origin at 25828 cm^{-1} . These systems are identified in these calculations as the ${}^1, {}^3A''(n_{1a'}, \pi_{1a'}^*) \leftarrow \tilde{X}^1A_g$ transitions. In addition, the calculation indicates that there should be a weaker $n \rightarrow \pi^*$ transition of comparable energy slightly to the blue of the first system. This is in agreement with experimental evidence since a short series of bands can be identified in both the 28725 cm^{-1} and 25828 cm^{-1} systems as independent systems. Thus band systems in the region of 30815 cm^{-1} and 28098 cm^{-1} have been labelled $\tilde{B}^1 \leftarrow \tilde{X}^1$ and $\tilde{b}^3 \leftarrow \tilde{X}^1$ and are tentatively assigned as ${}^1, {}^3A''(n_{1a'}, \pi_{2a'}^*) \leftarrow \tilde{X}^1A_g$.

TABLE 3.23

"Strong" Transitions of Oxalyl Chloride Fluoride

(Correlate with Allowed Transitions of C_{2h} Oxalyl Derivatives)

State	Energy ^a a.u.	Vertical Transition a.u.	Calculated Transition Energy cm ⁻¹	Energy Å	Exp. V.T.E. cm ⁻¹
\tilde{X} $1A'$	-93.974				
$n_1 \rightarrow \pi_1^*$ $1, 3A''$	-93.899	0.075	16460	6075	25828 28725
$\pi_1 \rightarrow \pi_1^*$ $3A'$	-93.824	0.150	32921	3038	
$1A'$	-93.644	0.330	72428	1381	
$\pi_1 \rightarrow \sigma_1^*$ $1, 3A''$	-93.761	0.213	46749	2139	
$n_1 \rightarrow \sigma_1^*$ $3A'$	-93.749	0.225	49382	2025	
$1A'$	-93.661	0.313	68697	1456	
$n_2 \rightarrow \pi_2^*$ $1, 3A'$	-93.725	0.249	54650	1830	

TABLE 3.24

"Weak" Transitions of Oxalyl Chloride Fluoride

(Correlate with Forbidden Transitions of C_{2h} Oxalyl Derivatives)

State	Energy ^a a.u.	Vertical Transition a.u.	Calculated Transition Energy cm ⁻¹	Energy Å	Exp. V.T.E. cm ⁻¹
$n_1 \rightarrow \pi_2^*$ $1, 3A''$	-93.895	0.079	17339	5767	28098 30815
$n_2 \rightarrow \pi_1^*$ $1, 3A''$	-93.813	0.161	35336	2830	
$n_2 \rightarrow \sigma_1^*$ $3A'$	-93.759	0.215	47188	2119	
$1A'$	-93.756	0.218	47846	2090	
$\pi_1 \rightarrow \pi_2^*$ $3A'$	-93.752	0.222	48724	2052	
	-93.698	0.276	60576	1651	

^aCalculated for the geometry $\angle CCO_1 = \angle CCO_2 = 123^\circ$, $\angle OCCl = \angle OCF = 118^\circ$,
 $CC = 1.46 \text{ \AA}$, $CO = 1.26 \text{ \AA}$, $CCl = 1.75 \text{ \AA}$, $CF = 1.34 \text{ \AA}$.

3.11 General Discussion of the Theoretical Results

An intensive comparison has been made in this Chapter between the experimental electronic spectra of some simple α,β diketones and the transitions predicted by a CNDO/2 program. Agreement between calculated and experimental transition energies is close enough (particularly for the low energy transitions) to indicate the usefulness of applying CNDO calculations to spectroscopic problems. The results obtained confirm the conclusions of intuitive molecular orbital considerations on some points, but also suggest new interpretations of other points. Good agreement between calculated and experimental transition energies was obtained for oxalyl fluoride and oxalyl chloride. Agreement for glyoxal was not as good but still close enough to be useful, while agreement for the asymmetrically substituted oxalyl chloride-fluoride was quite poor.

Potential energy curves for the bond lengths and bond angles were calculated for glyoxal and oxalyl fluoride. These potential energy curves suggest that diffuseness in the high energy spectra of the α,β diketones occurs for the following reasons:

(1) Excited electronic states which involve promotion of an electron to the σ_1^* orbital have much shallower potential energy curves along the C-C and C-H bonds for glyoxal and along the C-C bond for oxalyl fluoride. It was not possible to obtain a dissociative path for an isolated state produced by single excitation, but the observed potential energy curves indicate a tendency toward molecular dissociation in the $B_u(n_1, \sigma_1^*)$ and $A_u(\pi_1, \sigma_1^*)$ excited states.

(2) From Figures 3.5, 3.6 and 3.7, it can be seen that the shallow potential energy curves of the $B_u(n_1, \sigma_1^*)$ and $A_u(\pi_1, \sigma_1^*)$ states can intersect the

steeper potential energy curves of the $B_u(\pi_1, \pi_1^*)$ and $A_u(n_1, \pi_1^*)$ excited states. Thus the calculations indicate no reason to expect transitions to the latter two states to be diffuse, when the isolated states are considered separately from the excited state manifold. However, the $B_u(\pi_1, \pi_1^*)$ state can be predissociated by the $B_u(n_1, \sigma_1^*)$ state while the $A_u(n_1, \pi_1^*)$ state can be predissociated by the $A_u(\pi_1, \sigma_1^*)$ state. The energies calculated for the $B_u(n_1, \sigma_1^*)$ and $A_u(\pi_1, \sigma_1^*)$ were much too high to agree with spectroscopic observations. This fact has been attributed to the restricted nature of the set of atomic orbitals employed as a basis set (e.g., 3s orbitals which were not included should make a significant contribution to the σ_1^* molecular orbital). The energies calculated for the $B_u(\pi_1, \pi_1^*)$ and $A_u(n_1, \pi_1^*)$ orbital are in fairly good agreement. The perturbing states are thus much nearer in energy than appears to be the case in the CNDO/2 potential energy curves.

CHAPTER 4

THE NEAR ULTRAVIOLET SPECTRA OF THE OXALYL HALIDES

4.1 Introduction

The vapour phase ultraviolet spectrum of oxalyl chloride-fluoride has been recorded under high resolution and studied extensively in this work. This study has involved a critical consideration of similar studies carried out on oxalyl fluoride, oxalyl chloride and oxalyl bromide^(1,2,3,4). In this re-examination of the spectra of these compounds, minor features of the spectrum were studied in greater detail than in previous work. Recent infra red and Raman work^(54,55,56) on these compounds has suggested the possibility of the presence in the vapour phase of an equilibrium mixture of the cis and trans planar configurations of these molecules, and a careful consideration of the ultraviolet spectra has led to the conclusion that the spectrum of the cis isomer does appear in the vapour phase as a weak system of bands. In addition, examination of the discrete spectra of all the oxalyl halides indicates an increasing complexity in the series oxalyl chloride, oxalyl chloride-fluoride, oxalyl fluoride. These two points are discussed in this chapter with a view to establishing a better understanding of the near ultraviolet spectra of the oxalyl halides.

4.2 Description of the Discrete Spectra of Oxalyl Halides

The electronic systems of oxalyl chloride-fluoride originating at 3872 Å and 3480 Å have been assigned to transitions to the lowest-lying $^3A''(n \rightarrow \pi^*)$ and $^1A''(n \rightarrow \pi^*)$ states of the trans form respectively. The corresponding transitions have been analyzed in detail for a number of similar compounds - oxalyl chloride^(2,3), oxalyl bromide⁽⁴⁾, glyoxal^{(32,35,}

36,41,45,46) and propenal (acrolein) (47,48,49,50), and an extensive study has been made of oxalyl fluoride⁽¹⁾. The vibrational patterns established for the $n \rightarrow \pi^*$ transitions in these molecules have been used as a guide to the vibrational analysis of oxalyl chloride-fluoride. Fortunately, high resolution photographs of the spectra of all six compounds were available for purposes of comparison.

In this series of compounds, glyoxal and acrolein have the simplest $n \rightarrow \pi^*$ spectra. Both molecules exhibit discrete absorption in the near UV. This absorption is apparently produced by the superposition of four different electronic transitions, $\text{trans}^1,^3A_u(n,\pi^*) \leftarrow ^1A_g(\text{G.S.})$ and $\text{cis}^1,^3B_1(n,\pi^*) \leftarrow ^1A_g$, which are summarized in Table 4.1. Of these systems, the highest energy $\text{trans}^1A_u(n,\pi^*) \leftarrow ^1A_g$ transition is the most intense. The $^1B_1 \leftarrow ^1A_1(\text{cis})$ and $^3A_u \leftarrow ^1A_g(\text{trans})$ are weaker by a factor of approximately 1000 and the $^3B_1 \leftarrow ^1A_1(\text{cis})$ much weaker still. Because the transitions of the cis (or gauche) isomer are weak and because they lie in the regions where hot bands of the trans isomer are found, the identification of the cis spectra of glyoxal and acrolein was quite difficult.

For the $n \rightarrow \pi^*$ systems of glyoxal and acrolein, the intensity (absorption) distribution among the bands of the system is very distinctive. The origin band is characterized by a sudden increase in intensity with increasing frequency, followed by a band system of decreasing intensity, composed of short progressions (one or two members), with a renewed increase of intensity at each member of the progression in the excited state ν_{CO} , which acts as a new sub-origin. The band systems which accompany the sub-origins repeat the pattern of the vibrational structure based on the origin. For both glyoxal and acrolein the major part of the absorption spectrum

TABLE 4.1

The Near Ultraviolet Systems of Glyoxal and Acrolein

	${}^1A_u(n,\pi^*) \leftarrow {}^1A_g$	${}^1B_1(n,\pi^*) \leftarrow {}^1A_1$	${}^3A_u(n,\pi^*) \leftarrow {}^1A_g$	${}^3B_1(n,\pi^*) \leftarrow {}^1A_1$
	trans	cis*	trans	cis*
Glyoxal	4550 Å ^a	4875 Å ^b	5207 Å ^c	-
Acrolein	3865 Å ^d	4060 Å ^e	4122 Å ^e	4322 Å ^f

* For acrolein it is stated only that this configuration could be cis or gauche.

^aBrand⁽³²⁾

^bCurrie and Ramsay⁽⁴⁶⁾, Holzer and Ramsay⁽⁴⁵⁾

^cGoetz, McHugh and Ramsay⁽⁴¹⁾

^dBrand and Williamson⁽⁴⁷⁾, Hollas⁽⁴⁸⁾

^eAlves, Christoffersen, and Hollas⁽⁴⁹⁾

^fBair, Goetz and Ramsay⁽⁵⁰⁾

(near UV) could be accounted for by the $n \rightarrow \pi^*$ (S-S and S-T) transitions of the trans configuration only.

The oxalyl halides also absorb in the near UV. In these cases the absorption appears to consist of the superposition of discrete absorption on continuous absorption with predissociation of the discrete absorption to higher energy. This predissociation becomes more pronounced through the series oxalyl fluoride, chloride-fluoride, chloride, and bromide. Predissociation is less pronounced in the spectrum of glyoxal. In addition, the discrete spectrum of the oxalyl halides appears to be more complex than its counterpart in glyoxal. This complexity results from an increased number of bands in the system, plus a deviation from the intensity pattern observed in glyoxal and acrolein; the complexity increases in the series oxalyl chloride, chloride-fluoride, and fluoride. Consider, then, the general features of the ultraviolet spectra of the oxalyl halides:

(a) Oxalyl Chloride

For oxalyl chloride, a discrete system appears in the region 3000-4000 Å with origin at 3678 Å ($27,188.9 \text{ cm}^{-1}$) under pressure-path conditions of approximately 0.05 m-atm. This system has been analyzed as a single system by Balfour and King⁽²⁾ and assigned to an $n \rightarrow \pi^*$ (S-S) transition. It resembles the corresponding spectrum of glyoxal; the origin is characterized by a sudden increase of intensity with increasing frequency followed by a band system of decreasing intensity with a renewed increase of intensity 1460 cm^{-1} to the blue of the origin (corresponding to one quantum of carbonyl stretch in the excited state). The origin band shows rotational fine structure and is accompanied by progressions and sequences, each consisting of one or two members, which become rotationally diffuse several hundred

wave-numbers from the origin, and vibrationally diffuse after about 500 cm^{-1} . In the spectrum just to the blue of the origin, a few fundamental bands stand out prominently and weaker bands can be assigned in terms of the frequencies of these fundamentals. The first member of the progression in the excited state carbonyl stretching mode appears to be diffuse, as is the subsidiary band system which accompanies it. The assignment of this system appears to be quite acceptable, but there is one group of weak bands approximately 1000 cm^{-1} to the red of 3678 Å which it was difficult to fit into the $n \rightarrow \pi^*$ (S-S) system. These bands have been reassigned to the cis molecule in this work (see Section 4.3).

At pressure-path conditions between 0.25 and 0.5 m atm. a second system of oxalyl chloride appears with origin at 4103 Å (24370.2 cm^{-1}). This system has been analyzed as a single system by Balfour and King⁽³⁾ and assigned as $n \rightarrow \pi^*$ (S-T). The vibrational structure of this transition parallels that of the $n \rightarrow \pi^*$ (S-S) system with minor changes in the frequencies of the active fundamentals. The assignment to a single system appears to be acceptable in this case.

(b) Oxalyl Fluoride

For oxalyl fluoride, a discrete absorption system appears in the region near 3000 Å under pressure-path conditions of approximately 0.05 m-atm. An attempt has been made to analyze this as a single electronic transition analogous to the 3678 Å system of oxalyl chloride⁽¹⁾; however a consideration of the general appearance of this spectrum indicates that this interpretation is too simple. As with oxalyl chloride, this absorption results from the superposition of a discrete system on a continuum; however for oxalyl fluoride, the effect of predissociation is much less noticeable

(the system remains vibrationally discrete over the interval of several thousand cm^{-1} to the blue of the origin). The discrete part of the COFCOF system is more complex than the corresponding system of COClCOCl in terms of both the number of bands present and the intensity distribution in the band system. The system is characterized by a sudden increase of intensity at 3082 Å (32445.0 cm^{-1}) followed by a band system of decreasing intensity. Instead of a decrease of intensity to the first member of the progression in excited state C=O stretch, a renewed increase of intensity is observed only 370 cm^{-1} to the blue at 3047 Å (32815.3 cm^{-1}) followed again by a renewed increase of intensity at 3032 Å (32976.4 cm^{-1}). The intensities in this series of bands is such that 3032 Å > 3047 Å > 3082 Å. The band at 3032 Å is then followed by a band sub-system of decreasing intensity. Approximately 1000 cm^{-1} to the blue of the first strong band, the spectrum becomes a very complex series of closely spaced bands; no prominent feature appears which can be identified as the first member of the progression in ν_{CO}^1 from the 3082 Å band as an origin. However if the 3050 Å band is taken to be an origin, it is possible to assign $(\nu_{\text{CO}}^1)_0$. These features suggest the presence of at least two electronic transitions.

At pressure-path conditions of approximately 2 m-atm., a weaker spectrum appears with origin (marked by the normal intensity pattern) at 3340 Å (29941.9 cm^{-1}). The anomalies of the stronger part of the spectrum do not appear to be present here. The assignment of this system⁽¹⁾ to the $n \rightarrow \pi^*$ (S-T) transition accounts for most of the bands in this weaker system.

(c) Oxalyl Chloride-Fluoride

For oxalyl chloride-fluoride, a discrete absorption system appears

in the region near 3500 Å under pressure-path conditions of approximately 0.05 m-atm. The pattern of the band system is more complex than the corresponding system of oxalyl chloride, but less complex than that of oxalyl fluoride. The origin is assigned to a band at 3481 Å (28724.1 cm⁻¹), and the system is assigned as ${}^1A''(n_{1a'}, \pi_{1a}^*) \leftarrow \tilde{X}{}^1A'$ on the basis of the calculations of Section 3.10. The 3481 Å band is characterized by a sudden increase in absorption intensity with increasing frequency followed by a complex band system for which the intensity decreases through a renewed increase of intensity at +1285 cm⁻¹ and again at +2535 cm⁻¹. The origin band shows rotational fine structure and is accompanied by progressions and sequences, each consisting of one or two members, which become rotationally diffuse several hundred wave numbers from the origin, but which do not become vibrationally diffuse until the third member of the progression in the excited state carbonyl stretching mode. Again the discrete absorption is superimposed upon continuous absorption, but the predissociation does not set in as soon as it does for oxalyl chloride. Under low resolution, then, this system appears to be a single electronic system in which a larger number of fundamentals are active in forming progressions that is the case with the more symmetric molecules of the series. The complexities of this system show up in the high resolution spectrum, where it is found that the band at +1285 cm⁻¹ which is assigned as $(\nu_{CO})_0^1$ is a doublet with the strongest component at +1279 cm⁻¹ plus a band about half as intense at 1294 cm⁻¹. In addition, neither of these bands appears to act as a new sub-origin for a band system similar to the one which is associated with the 3481 Å band. By analogy with the other oxalyl compounds, the existence of a second electronic transition must be considered in analyzing the strong discrete system. This

point is discussed in Section 4.3. Approximately 1000 cm^{-1} to the red of the band at 3481 \AA there are a number of weak bands which cannot be fitted into an analysis of the 3841 \AA system as hot bands. As with oxalyl chloride these bands are assigned to the cis molecule (see Section 4.3).

At pressure-path conditions of approximately 1 m-atm., a weaker spectrum appears, originating at 3872 \AA (25828.7 cm^{-1}). This spectrum is assigned to the ${}^3A''(n_{1a'}, \pi_{2a'}^*) \leftarrow \tilde{X}^1A'$ transition. The vibrational pattern associated with this system is very similar to the vibrational pattern associated with the 3481 \AA system, but the complexities which occur at $+1285\text{ cm}^{-1}$ in the strong system do not occur here. A number of weak bands occur about 3000 cm^{-1} to the blue of 3872 \AA . They have sufficient intensity that they cannot be ignored. They are considered to arise from a different electronic transition. Such a transition is not apparent in the spectrum of oxalyl chloride but could exist for oxalyl fluoride.

4.3 The $n \rightarrow \pi^*$ Spectra of cis Oxalyl Halides

The general appearance of the spectra of the oxalyl halides strongly suggest the presence of several over-lapping electronic transitions. The observation of the $n \rightarrow \pi^*$ transition for cis glyoxal⁽⁴¹⁾ and cis acrolein^(49,50) just to the red of the corresponding transition for the trans molecule suggested searching the spectra of the oxalyl halides for the cis $n \rightarrow \pi^*$ transition.

The question of the existence of the cis isomer of the oxalyl halides in the vapour phase has been the source of a certain amount of controversy. There is general agreement that the main features of the spectra (with the exception of the unpublished UV spectra of oxalyl fluoride) are due to the planar trans conformation, but the presence or absence of a spectrum due to the cis conformation is more difficult to establish, largely because the

spectral features should resemble those of the trans isomer very closely.

The vibrational infra-red and Raman spectra of oxalyl chloride, oxalyl chloride-fluoride, and oxalyl fluoride were studied in the vapour and liquid phases by Hencher and King^(51,52) and oxalyl bromide was studied in the fluid phases by Kidd and King⁽⁵³⁾. In these analyses, the observed bands were attributed solely to the trans isomer. More recently, Durig et al. have carried out a series of studies on oxalyl bromide⁽⁵⁴⁾, chloride⁽⁵⁵⁾, and fluoride⁽⁵⁶⁾ in which the low temperature spectra of these compounds in the solid phase has been examined. The solid state infra-red and Raman spectra have been interpreted by these authors as indicating the presence of a cis isomer in the fluid phases. The cis isomer decreases in concentration[†] with a decrease of temperature and disappears on crystallization. Although the assignment of the cis spectrum in the fluid phase requires that many fundamental modes are not separately distinguishable because of coincidences with the corresponding fundamentals of the trans isomer, the cis C-C stretch fundamental stands out strongly in the infra-red, while the corresponding transition of the trans isomer is symmetry forbidden. The coincidence between modes of cis and trans isomers is reasonable, and the argument in favour of observable quantities of cis isomer is plausible.

Several points of view have also been established with respect to the near ultraviolet spectra of the oxalyl halides. Saksena and Jauhri⁽⁵⁷⁾ have described the discrete absorption of oxalyl chloride on the basis of two

[†]The bands in the infra-red spectrum of oxalyl fluoride did not exhibit a noticeable temperature affect in the fluid phase but the cis isomer did disappear on crystallization.

origins - one at 3678 \AA (27188.9 cm^{-1}) assigned to the cis isomer and one at 3550 \AA (28144 cm^{-1}) assigned to the trans isomer. Sidman⁽⁵⁸⁾ from the high temperature studies on oxalyl chloride that the discrete absorption was due solely to the trans isomer and he attributed the underlying continuum to the cis isomer. Balfour and King^(2,3,4) and Balfour⁽¹⁾ in the study of the bromide, chloride and fluoride have accepted the conclusion of Hencher and King that only the trans isomer is present in observable quantities and have assigned the discrete bands to a single trans isomer.

The UV spectra of the oxalyl halides were reviewed in a search for the spectrum of the cis compound, and in addition a series of new experiments was carried out:

- (1) Attempts were made to obtain the Raman spectra of these compounds in the vapour phase. This experiment is discussed in Appendix I.
- (2) Attempts were made to obtain emission spectra. This experiment is discussed in Appendix III.
- (3) Attempts were made to obtain low temperature solid state ultraviolet absorption spectra. The experiment is discussed in Appendix II.

In glyoxal, the origin of the cis $n \rightarrow \pi^*$ transition occurs 1500 cm^{-1} to the red of the origin of the trans compound. A similar separation might be expected for the oxalyl compounds, and in all cases there is a band at about 1000 cm^{-1} to the red of the strong singlet-singlet origin which does not fit into the analysis of the weaker S-T spectrum and has intensity appropriate for a hot band of the singlet-singlet spectrum. In the analysis of the spectra of the chloride and bromide, BK identified this band as due to excitation of one quantum of the ground state mode designated C-C stretch. This assignment required a vapour-liquid frequency shift of 139 cm^{-1} for this

mode in the chloride and 106 cm^{-1} in the bromide. Although these shifts appeared abnormally large, agreement between the frequencies observed in the sub-spectrum originating on this band and the frequencies observed in the $n \rightarrow \pi^*$ (S-S) system supported its assignment to the $n \rightarrow \pi^*$ (S-S) system.

The Raman results obtained for oxalyl chloride in the vapour phase do not support the postulate of a large vapour-liquid shift in the C-C stretching mode. The vapour phase value of 1066 cm^{-1} agrees with the liquid phase value of 1060 cm^{-1} within experimental error. In addition, no band is found at or near the value of 1217 cm^{-1} required by the ultra-violet assignment by BK of the hot band.[†] The emission spectrum of oxalyl chloride gave no indication of a ground state fundamental at 1217 cm^{-1} ; however it is postulated that the emission arises from the cis isomer (see Appendix III). This spectrum could not then give the trans ground state frequencies.

The solid state UV absorption spectrum of oxalyl chloride shows a strong origin band at 3685 \AA and a weak origin band near 4010 \AA . This confirms 3678 \AA and 4103 \AA in the vapour phase as origins of the singlet-singlet and singlet-triplet transition, and refutes the postulate by Saksena and Jauhri of the 3678 \AA band as the origin of the cis isomer (which is not present in the solid).

On the basis of the evidence available, an assignment of a weak cis $n \rightarrow \pi^*$ transition can be made for all the oxalyl halides studied. The origin of the singlet-singlet transition in cis oxalyl bromide, chloride, and

[†]The vapour phase ^{Raman}spectra were run under conditions of large slit width and high sensitivity. The poor quality of the spectrum obtained makes it impossible to be certain that there is no band at 1217 cm^{-1} .

chloride-fluoride is taken to be the band formerly assigned to $(\nu_{CC})_1^0$ of the molecule in the trans configuration. It occurs approximately 1000 cm^{-1} to the red of the trans origin and has an intensity similar to that of the trans singlet-triplet bands. The case of oxalyl fluoride is more difficult. In the assignment by Balfour, the first cold band at 3082 \AA was considered to be the trans origin and a band at 802 cm^{-1} to the red was assigned to $(\nu_{C-C})_1^0$. In this case, the frequency of the C-C stretching mode from the UV agrees very well with the liquid phase Raman value of 804 cm^{-1} for the CC stretch in the trans isomer, but also equally well with the vapour phase infrared value of 799 cm^{-1} for the cis isomer. Therefore, the complexity of the cold spectra suggests the assignment of 3082 \AA as the origin of the $n \rightarrow \pi^*$ (S-S) transition of the cis isomer with the trans origin being either of the strong bands at 3047 \AA or 3032 \AA .

This reassignment of the spectra of the oxalyl halides requires that the ground state C-C stretching mode does not appear in the $n \rightarrow \pi^*$ transition of the trans compound. This resolves an apparent difficulty with the previous analysis. The cold spectral bands indicate that there is a small Franck-Condon factor associated with this mode in the excited state. A correspondingly small Franck-Condon factor is expected for the ground state and this, combined with the small Boltzmann ($\sim 10^{-3}$) population for such a high energy mode would predict that it should not appear in the spectra. The appearance of $\nu''(CC)$ to give a hot band on the 3082 \AA origin of oxalyl fluoride suggests that a different Franck-Condon distribution (i.e., different change of geometry) is associated with this system; 3082 \AA is therefore assigned as the origin of the cis $n \rightarrow \pi^*$ (S-S) transition. In the cold part of the cis spectrum, it is possible to assign a strong band at $+1146\text{ cm}^{-1}$ from 3082 \AA

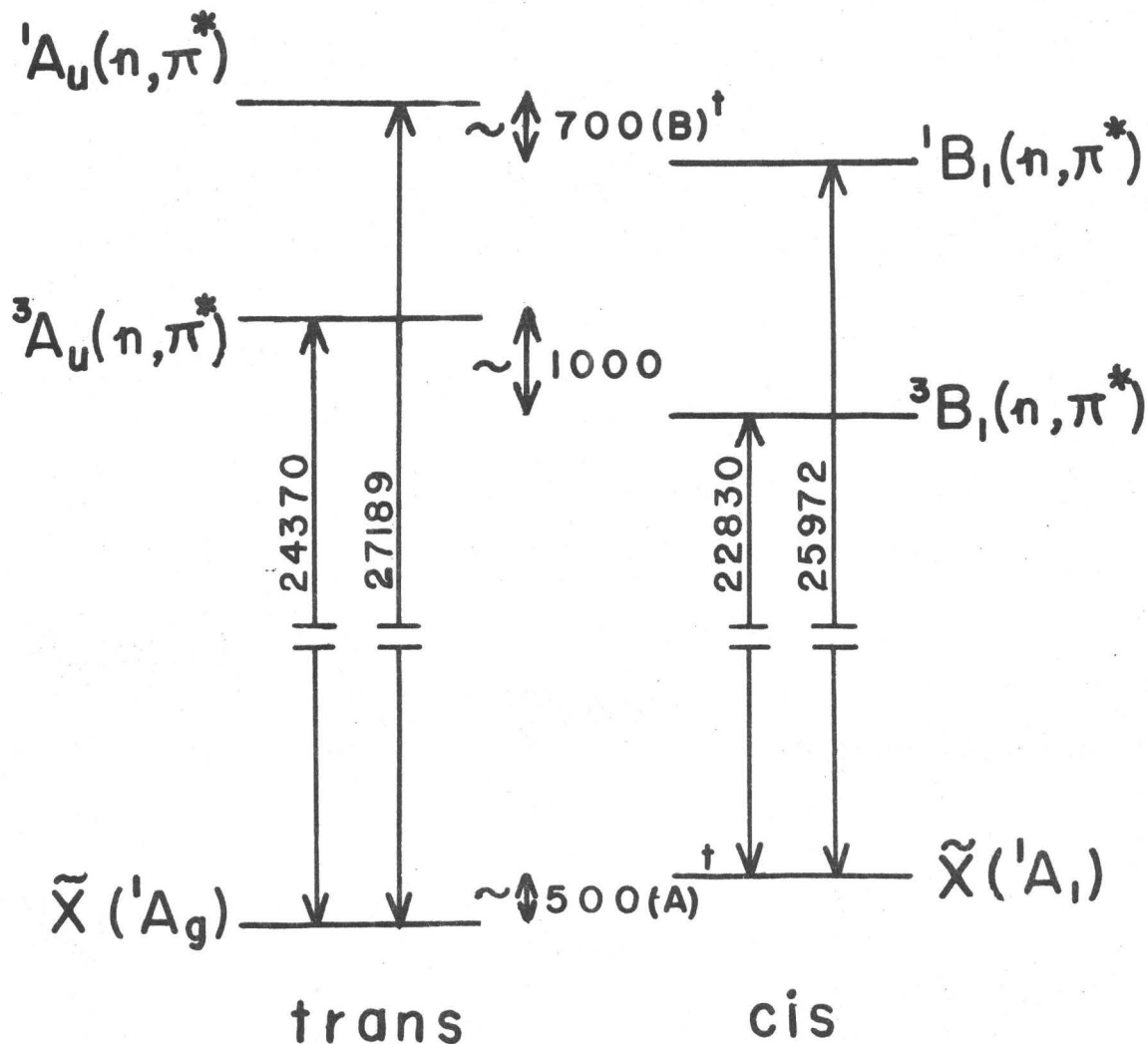
as $(\nu_{C-C})_0^1$ but no strong progression in $\nu_{C=O}^1$ appears for this origin. On the other hand, it is possible to assign a progression in $\nu_{C=O}^1$ in the excited state from 3047 Å as an origin but none in ν_{CC}^1 . The band at 3047 Å is therefore considered a possible origin of the trans $n \rightarrow \pi^*$ (S-S) transition.

The observed origins of the $n \rightarrow \pi^*$ (S-S) transitions in the cis oxalyl halides are listed in Table 4.2. With the exception of the fluoride, these transitions have an intensity which is approximately the same as that of the S-T system of the trans isomer. This indicates a very low concentration for the cis isomer. In the case of the fluoride, the cis spectrum has approximately half the intensity of the corresponding trans spectrum and indicates a fairly high cis concentration relative to that of the trans molecule. Table 4.2 includes an estimate of the cis/trans ratio and the corresponding Boltzmann ΔE for the compounds studied. These estimates assume equal oscillator strengths for the $n \rightarrow \pi^*$ transitions of the two isomers, and can only be considered correct as an order of magnitude.

The origins of the $n \rightarrow \pi^*$ (S-T) transition of the cis isomers have not been assigned. In the case of the fluoride, a sufficiently high cis concentration is present that this transition might be observed. A cursory examination of the $n \rightarrow \pi^*$ (S-T) assignment of the 3340 Å system of oxalyl fluoride⁽¹⁾ indicates no obvious discrepancies, and no conclusion has been reached on this point. The only firm information about the singlet-triplet spectra of the cis compound was obtained for oxalyl chloride in emission (see Appendix III). The emission spectrum suggests an origin at 4380 Å (22830 cm^{-1}) for the cis $n \rightarrow \pi^*$ (S-T), approximately 1540 cm^{-1} to the red of the origin of the trans $n \rightarrow \pi^*$ (S-T).

From the data of Table 4.1 it is possible to construct an energy level diagram for the ground and first excited state of the cis and trans isomers. This has been done for oxalyl chloride in Figure 4.1. It can be seen from Table 4.1 that the cis isomer is approximately 500 cm^{-1} higher in energy than the trans for oxalyl bromide, chloride, and chloride-fluoride. This compares with approximately 700 cm^{-1} in acrolein⁽⁴⁹⁾ and approximately 1125 cm^{-1} in glyoxal⁽⁴⁶⁾. For oxalyl fluoride, however, the cis isomer is only about 100 cm^{-1} higher in energy than the trans. This small energy separation accounts for the failure to discover the 3082 \AA (COFCOF) band as a "hot" band in temperature-intensity studies. A similar behaviour was observed in the infra-red, where Durig et al.⁽⁵⁶⁾ report that cooling to -61°C produced only slight changes in the relative intensities of the cis/trans infra-red bands.

The bands of the cis $n \rightarrow \pi^*$ (S-S) O-O bands of the oxalyl halides are found to have rotational contours which are very similar to those observed for the trans isomer. This was initially a puzzling feature of the assignment of the UV spectrum of the cis isomer; however, a study of the rotational structure of the 3482 \AA band of COFCOCl (discussed in Chapter 6) provides an explanation. For the oxalyl halides, the molecules are rendered very massive by the halogen substituents and the rotational constants are correspondingly small. The bands have the appearance of infra-red bands in which P, Q, and R branches are present. By means of computer reconstruction of band contours it is found that the Q branch is shaded to the blue, or to the red, or forms a spike according to whether ΔC (the change of the greatest moment of inertia) is positive, negative or zero. The Q branch forms the most prominent feature of the contour which otherwise is quite regular and devoid



†) These designations refer to the quantities indicated in Table 4.2.

Figure 4.1 Energy Level Diagram for the Ground and First $n \rightarrow \pi^*$ Excited States of cis and trans Oxalyl Chloride (energies are indicated in cm^{-1}).

TABLE 4.2

Origins of the $n \rightarrow \pi^*(S-S)$ Transition for cis Oxalyl Halides

Compound	Origin cis	Origin trans	Separation cm^{-1} A + B ^c	Estimate ^a cis/trans ratio	Estimate ^b ΔE A ^c
(COF) ₂	3082 Å 32445.0 cm^{-1}	3047 Å 32815.3 cm^{-1}	370.3	0.7	100
COFCOCl	3658 Å 27335.1 cm^{-1}	3481 Å 28724.5 cm^{-1}	1389.4	0.05	650
(COCl) ₂	3850 Å 25971.8 cm^{-1}	3678 Å 27188.9 cm^{-1}	1271.1	0.1	500
(COBr) ₂	4123 Å 24255 cm^{-1}	3942 Å 25371 cm^{-1}	1116	0.1	500

^aObtained from the relative intensities on photographic film assuming the $n \rightarrow \pi^*$ oscillator strength is the same for both isomers.

^bObtained from estimated cis/trans ratio using Boltzmann statistics.

^cThese quantities are illustrated in Figure 4.1.

of minor features. The $n \rightarrow \pi^*$ (S-S) 0-0 band is C-type (polarized perpendicular to the plane of the molecule) for both isomers. The band contour is determined not so much by the rotational constants (which will be slightly different for cis or trans) but by the respective values of ΔC . ΔC depends on the overall contraction or expansion of the molecule in the molecular plane and is less likely to be different for the two isomers.

In addition to the similarity of the band contours for the cis and trans spectra it is anticipated that the frequencies of the vibrational modes for the excited state of the two isomers will be very similar, as was found for the ground states of oxalyl chloride and bromide by Durig et al. (see Tables 4.3, 4.4). Because of the proximity of the cis $n \rightarrow \pi^*$ (S-S) system to the stronger trans $n \rightarrow \pi^*$ (S-S) system, the isolation of the cis spectrum is quite difficult. Table 4.5 lists the bands of the oxalyl chloride spectrum which can be assigned most satisfactorily to the spectrum of the cis isomer. In the case of oxalyl chloride, the observed isotopic shifts were of great help in separating the two spectra. (Chlorine has two isotopes, Cl^{37} and Cl^{35} , which occur naturally in the ratio 1:3. These different isotopic molecular species have slightly different frequencies for the vibrational modes of the molecule. As described in reference 2 this results in isotopic shifts for bands of the ultraviolet spectrum.) The band at 3847 \AA has no apparent isotopic shift which supports its assignment as an origin band. The isotopic shift, where observed, has been included in the table.

For oxalyl bromide, the quality of the ultraviolet spectrum makes it difficult to isolate much of the cis band system. A few bands of the cis ${}^1\text{B}_1(n, \pi^*) \leftarrow {}^1\text{A}_1(\text{G.S.})$ system are listed in Table 4.6. For oxalyl chloride-fluoride, also, the poor quality of the spectrum obtained in this region makes

TABLE 4.3

Ground State Vibrational Frequencies (in cm^{-1}) for cis and trans
Oxalyl Chloride^a

Description	Mode	Trans		Cis		
		Symmetry	Frequency ^b	Frequency ^c	Symmetry	Mode
C=O stretch	ν_1	a_g	1762	1774	a_1	ν_1
C-C stretch	ν_2		1093	1059 ^d		ν_2
C-Cl stretch	ν_3		620	533		ν_3
ClCO bend	ν_4		427	400		ν_4
(ClCO) rock	ν_5		287	183		ν_5
(ClCO) wag	ν_6	a_u	391	519	a_2	ν_6
(ClCO) torsion	ν_7		55	-		ν_7
(ClCO) wag	ν_8	b_g	442	205	b_2	ν_{12}
C=O stretch	ν_9	b_u	1769	1769 ^b	b_1	ν_8
C-Cl stretch	ν_{10}		756	800		ν_9
ClCO bend	ν_{11}		498	350		ν_{10}
(ClCO) rock	ν_{12}		220	194		ν_{11}

^aFrom the results of Durig and Hannum⁽⁵⁵⁾.

^bSolid state values.

^cLiquid state values.

^dVapour phase values.

TABLE 4.4

Ground State Vibrational Frequencies (in cm^{-1}) for cis and trans
Oxalyl Bromide^a

Description	Mode	trans		cis		
		Symmetry	Frequency ^b	Frequency ^c	Symmetry	Mode
C=O stretch	ν_1	a_g	1752	1807	a_1	ν_1
C-C stretch	ν_2		1052	1003		ν_2
C-Br stretch	ν_3		582	520		ν_3
COBr bend	ν_4		345	-		ν_4
(COBr) rock	ν_5		191	167		ν_5
(COBr) wag	ν_6	a_u	362	362 ^d	a_2	ν_6
(COBr) torsion	ν_7		40			ν_7
(COBr) wag	ν_8	b_g	358	113	b_2	ν_{12}
C=O stretch	ν_9	b_u	1792	1810	b_1	ν_8
C-Br stretch	ν_{10}		664	770		ν_9
COBr bend	ν_{11}		405	325		ν_{10}
(COBr) rock	ν_{12}		176	123		ν_{11}

^aFrom the results of Durig and Hannon⁽⁵⁴⁾.

^bSolid state values.

^cLiquid phase values.

^dVapour phase values.

TABLE 4.5

Bands Observed in the ${}^1B_1(n,\pi^*) \leftarrow \tilde{X}{}^1A_1$ of cis Oxalyl Chloride

ν_{vac} (cm^{-1})	Intensity	Assignment ^b	Separation From 0-0 Band	Isotope Shift	
				$\nu_{(35,35)} - \nu_{(35,37)}$	$\nu_{(35,35)} - \nu_{(37,37)}$
25890.2	vvw	10_1^1	-81.6		
25940.5	vvw	11_3^3	-31.3		
25950.6	vw	11_2^2	-21.2	-1.7	
25961.0	w	11_1^1	-10.8	-1.0	-1.9
25971.8	mw	0_0^0			
26007.2	vw	6_1^1	+35.4		
26052.3	w	7_1^1	+80.5	+1.0	
26087.5	vvw	$6_1^1 7_1^1$	+35.4+80.3		
26136.7	vw	7_2^2	+80.5+84.4		
26178.6	vw	12_0^1	+206.8		
26256.0	vvw	$12_0^1 7_1^1$	+206.8+77.4		
26257.3	vw	5_0^1	+285.5	1.3	
26287.0	vvw	$4_0^1 10_1^1$	+398.6-83.4		
26331.9	vvw	$5_0^1 7_1^1$	+285.5+74.6		
26370.4	mw	4_0^1	+398.6	1.6	4.7
26406.8	vvw	$4_0^1 6_1^1$	+398.6+36.4		
26447.6	vvw	$4_0^1 7_1^1$	+398.6+77.2	2.9	
26543.8	vvw	5_0^2	+285.5+286.5	3.2	
26590.2	mw	3_0^1	+618.4		
26643.0	mw	$4_0^1 5_0^1$	+398.6+272.5		

^aTaken from Balfour and King⁽²⁾.^bObtained by adapting the assignment by Balfour and King⁽²⁾.

TABLE 4.6

Bands Observed in the ${}^1B_1(n,\pi^*) \leftarrow \tilde{X}{}^1A_1$ of cis Oxalyl Bromide

ν_{vac}^a (cm ⁻¹)	Intensity	Assignment	Separation From O-O Band
24255	w	0 ₀ ⁰	
24286	vw	6 ₁ ¹	+31
24316	vw	7 ₁ ¹	+61
24436	vw	5 ₀ ¹	+181
24552	vvw	4 ₀ ¹	+297

^aTaken from Balfour and King⁽⁴⁾.

TABLE 4.7

Bands Observed in the ${}^1A''(n,\pi^*) \leftarrow \tilde{X}{}^1A'$ of cis

Oxalyl Chloride-Fluoride

ν_{vac}^a (cm ⁻¹)	Intensity	Assignment	Separation From O-O Band
27335.1	w	0 ₀ ⁰	
27417.3	vw	12 ₁ ¹	+82.2
27469.3	vw	11 ₀ ¹	+134.2
27515	vvw	9 ₀ ¹	+180
27614.5	vw	8 ₀ ¹	+279.4
27750.2	vw	7 ₀ ¹	+415.1
27889.8	vvw	8 ₀ ²	+554.7
27939.8	vvw		+604.8

it difficult to isolate much of the ${}^1A''(n,\pi^*) \leftarrow \tilde{X}{}^1A'$ system. A few bands of the system have been listed in Table 4.7.

Oxalyl fluoride has the most intense (cis relative to trans) ultra-violet spectrum of the oxalyl halides studied. This makes it, potentially, the best source of information about the spectral properties of the cis isomer.

4.4 Complexities in the "Cold" Spectral Bands of Oxalyl Chloride-Fluoride

In the series of molecules, glyoxal, oxalyl fluoride, and oxalyl chloride, it was originally anticipated that the substitution for hydrogen by a halogen atom with its increased number of electrons might produce additional low energy transitions for the oxalyl halides. The calculations discussed in Chapter 3 have contradicted this hypothesis, and the analysis of oxalyl fluoride has not progressed sufficiently to permit comparison of the calculation with experiment on this point. Oxalyl chloride-fluoride, however, has lower symmetry than these molecules, and for COFCOCl there is found to be an additional low energy $n \rightarrow \pi^*$ transition which is allowed.

It was noted in Section 4.2 that the "cold" spectrum accompanying the trans ${}^1A_u(n,\pi^*) \leftarrow {}^1A_g$ origin of oxalyl fluoride and the trans ${}^1A''(n_1,\pi_1^*) \leftarrow {}^1A'$ origin of oxalyl chloride-fluoride appeared to be more complex than the corresponding spectrum of glyoxal. For oxalyl chloride-fluoride then the cold spectrum may be complicated in a manner similar to the spectrum of oxalyl fluoride and which is not predicted by the theoretical calculations. In addition, however, the appearance of a second $n \rightarrow \pi^*$ electronic transition is anticipated. In view of these potential complications in the spectrum of oxalyl chloride-fluoride, a great deal of use was made of repetitive patterns to establish the bands which belonged to the first $n \rightarrow \pi^*$ systems, and to

isolate bands which did not.

Balfour and King^(2,3,4) have noted that the $n \rightarrow \pi^*$ (S-S) and $n \rightarrow \pi^*$ (S-T) transitions have very similar vibrational structure for both oxalyl chloride and bromide. With a few exceptions, the same vibrational modes are active in both the S-S and S-T spectra. A similar behaviour is expected for oxalyl chloride-fluoride, and inspection of the frequencies of the strong bands near the $n \rightarrow \pi^*$ (S-S) origin (28724.5 cm^{-1}) and the $n \rightarrow \pi^*$ (S-T) origin (25828.7 cm^{-1}) (see Table 4.8) indicates that this is the case. In addition, it is found that at the S-T origin $+ (\nu_{\text{C=O}})_0^1$, $+ (\nu_{\text{C=O}})_0^2$, and $+ (\nu'_{\text{C=O}})_0^1$, bands appear strongly and act as sub-origins for band systems which also have the same band pattern (see Table 4.8). The region near the expected S-S origin $+ (\nu_{\text{C=O}})_0^1$, however, does not follow the pattern. To higher energy from the S-S origin, there is an increase of (absorption) intensity at $\sim +1285 \text{ cm}^{-1}$. Under high resolution, this absorption is seen to consist of two bands, at $+1279.2 \text{ cm}^{-1}$ and $+1294.1 \text{ cm}^{-1}$. In the band system associated with this region it is possible to assign a series of bands in combination with $+1294.1 \text{ cm}^{-1}$ (the weaker of the pair) which repeat the pattern established for the other origins and sub-origins; however, for the system of bands expected to appear in combination with $+1279.2 \text{ cm}^{-1}$, about half are missing (see the 30004 cm^{-1} band in Table 4.8).

Two explanations of the anomalous region near 0-0 (S-S) $+1285 \text{ cm}^{-1}$ are suggested here: (1) the existence of a new electronic transition with origin at $+1279.2 \text{ cm}^{-1}$, and (2) the existence of Fermi resonance between $(\nu_{\text{C=O}})_0^1$ and a combination band producing the observed doublet. If $+1279.2 \text{ cm}^{-1}$ (30004.0 cm^{-1}) is chosen as the origin of a new electronic transition, a system of short progressions and sequences may be assigned to the bands

TABLE 4.8

Principal Frequencies of the Vibrational Structure of COFCOCl as They Appear on the Various Origins and Sub-Origins of the First $n \rightarrow \pi^*$ Transition

Singlet-Triplet Origin		ST + 1 ν_{CO1}		ST + 2 ν_{CO1}		ST + 1 ν_{CO2}	
<u>25828.7</u>	0.0	<u>27120.8</u>	(1292.1)	<u>28375.6</u>	(1254.8)	<u>27520.2</u>	(1692.4)
25848.9	20.1	27140.6	19.8	Very weak		Not observed	
25914.3	85.6	27206.1	85.3	28459.9	84.3	27606.5	86.3
26010.6	181.9	27300.5	179.8	28556.7	181.1	27701.3	181.1
26111.5	282.8	27406.7	285.9	28654.9	279.3	27803.8	283.6*
26192.7	181.9	27480.8	179.8	Obscured by (COCl) ₂		27879.8	181.1
	+182.1		+180.3				178.5
26196.7	282.8	27491.5	285.9	28738.4	279.3	Not observed	
	+85.2		+84.8		+83.5		
26294.2	282.8	Obscured by (COCl) ₂		28836.4	279.3	27983.4	283.6
	+182.7				+181.4		179.6
Very weak	282.8	Not observed				Not observed	
	+283						
26120.8	1292.1	28375.6	1254.8			Obscured by SS	
27520.2	1692.4	Not observed				Obscured by SS	
				Not observed			
26246.0	417.3	27536.7	415.9			Region complex	
26531.0	702.2	Not observed				Region complex	
26901.9	1073.1	28182.4	1061.6			28578.9	1058.6
						*Abnormally weak.	

TABLE 4.8 (cont'd.)

Singlet-Singlet Origin		SS + 1 ν_{CO1}		SS + 2 ν_{CO1}		SS + 1 ν_{CO2}		30004.0	
28332.7	-391.7	29619.7	-399.1(FR)	30885	-391	Region		Not observed	
28507.4	-271.1(FR)	29799.9	-218.6	Very weak		Too Complex		Not observed	
<u>28724.5</u>	0.0	<u>30018.8</u>	(1294.1)	<u>31276</u>	(1257)	<u>30404.2</u>	(1679.7)	<u>30004.0</u>	(1279.2)
28747.5	23.0	30039.5	21.0	Too diffuse		Over-lapped		Over-lapped	
28809.0	84.6	30103.1	84.6	31358	83	30489.7	85.2	30089.1	85.1
28904.4	180.0	30199.1	180.6	~31450	~175	30582.8	177.8	Not observed	
29002.1	277.6	30298.1	277.7*	~31550	~275	30681.1	276.9	30283.0	279.0
29073.9	180.0	30367.0	180.6	↓ Lines become increasingly diffuse and inseparable from continuous background. ↓	30752.4	177.8	Not observed		
	+169.4		+167.9		30766.2	276.9	30380.0	279.0	
29086.0	277.6	30380.0	277.7		85.2		83.9		
	+83.9		+83.9		30861.4	276.9*	Very weak		
29183.1	277.6	Over-lapped by			180.3				
29278.1	277.6	SS + 1 ν_{CO}		30956.7	276.9*	30561.4	279.1		
	+276.0			275.6		278.3			
30018.5	1294.1	31276	1257	SS + 1 ν_{CO}		31276	1272		
30404.2	1679.7	31653	1634 [†]						
29143.4	418.9	Very weak		30821.6	417.4	Very weak			
29421.0	696.5	Obscured		Obscured		30700.3	696.3		
29635.1	910.6(FR)	Very weak		Lines become		30903	899		
29835.1	1110.6	31115.0	1097.2(FR)	diffuse		31114	1110		

*Intensity wrong
[†]Overlap by (COF)₂ makes this tentative.

*Intensity lower than the strong spectrum in this region.

not assigned to the $n \rightarrow \pi^*$ transition as combinations with $(\nu_{\text{C=O}})_0^1$ at $+1294.1 \text{ cm}^{-1}$ or $(\nu'_{\text{C=O}})_0^1$ at $+1679.7 \text{ cm}^{-1}$. Since the absorption system of COFCOCl becomes diffuse approximately 1000 cm^{-1} to the blue of 30004.0 cm^{-1} it is not possible to verify these assignments as has been done in Table 4.8 for the principal excited state frequencies appearing in the spectra of the first $n \rightarrow \pi^*$ transition. In addition, the isotope shift, which might be useful at this point, is obscured by a slight predissociation of the bands. The existence of a second electronic transition with origin at 30004 cm^{-1} remains a possibility which can neither be eliminated nor adequately confirmed.

The alternative explanation for the experimental results is that the pair of bands near $+1285 \text{ cm}^{-1}$ are a Fermi doublet. In the $n \rightarrow \pi^*$ systems of two similar molecules, acrolein ($\text{COCH}_2\text{-COH}$) and propynal ($\text{HC}\equiv\text{C-COH}$), the first member of the progression in excited state carbonyl stretch is found to be a Fermi doublet^(47,48,59). In the case of propynal, Brand Callomon and Watson⁽⁵⁹⁾ have developed a complex system of Fermi resonance involving three vibrational fundamentals. The doublet at $(\nu_{\text{CO}})_0^1$ is caused by resonance between $(\nu_{\text{C=O}})_0^1$ and a combination band involving two other excited state frequencies. In this case, the two bands of the Fermi doublet do not act as true sub-origins for additional quanta of the three modes involved. The detailed analysis of the $n \rightarrow \pi^*$ (S-S) system of oxalyl chloride-fluoride (discussed in Chapter 5) indicates that Fermi resonance is possible, in the excited state, between the fundamental band 0-0 (S-S) + ν_1 C=O stretch and the combination band 0-0 (S-S) + ν_3 (CF + CC stretch) + ν_9 (COX rock). On the basis of this postulate, a satisfactory analysis of the band system in the region near 0-0 (S-S) + 1285 cm^{-1} has been obtained. It is felt that

this explanation is preferable to the postulate of a new electronic transition originating at 30004 cm^{-1} .

The calculations of Section 3.10 and the detailed analysis (see 5.4) of the spectrum of COFCOC λ have identified the presence of a second $n \rightarrow \pi^*$ electronic transition to the blue of the first. This second transition appears weakly in COFCOC λ and is symmetry-forbidden for COFCOF; thus the analysis of COFCOC λ does not provide a solution to the problems remaining in the assignment of the oxalyl fluoride spectrum.

CHAPTER 5

THE VIBRATIONAL ANALYSIS OF THE $1,3A''(n_{1a'}, \pi_{1a}^*) \leftarrow \tilde{X}^1A'$ TRANSITIONS OF trans OXALYL CHLORIDE-FLUORIDE

5.1 Introduction

As was discussed in Chapter 4, the $n \rightarrow \pi^*$ transition has been well characterized for a number of compounds analogous to oxalyl chloride-fluoride. The pattern of activity of the fundamental vibrations is very similar among compounds of the series, and most of the assignments of frequencies to normal modes in the chloride-fluoride have relied heavily on this criterion. The vibrational spectrum of the ground state has been studied in the infra-red by Hencher and King⁽⁵²⁾ and in the infra-red and Raman by Adelhelm⁽⁸⁾. The assignment of ground state fundamentals in the ultraviolet has required some changes in the ground state analysis.

The rotational structure of the singlet-triplet transition is much more compact than that of the singlet-singlet. This results in a simpler appearance for the S-T spectrum, which is discussed first.

In the assignment of bands, the convention of Brand and Watson⁽⁶⁰⁾ has been adopted. The symbol $A_q^p B_s^n$ designates a transition which involves the vibrations numbered A and B in the ground state. The superscript p's and subscript q's refer to the number of quanta of these vibrations excited in the upper and lower electronic states respectively. Excited state vibrational modes have been labelled with the same numbers as the corresponding modes in the ground state.

5.2 The ${}^3A''(n_{1a'}, \pi_{1a''}^*) \leftarrow \tilde{X}^1A'$ Transition (Trans Isomer)

Table 5.1 gives a band-by-band assignment of the singlet-triplet $n \rightarrow \pi^*$ transition. A number of weak lines in the spectrum did not fit into the assignment as combination bands or hot bands and yet were not of sufficient intensity to be analyzed separately. These have been listed in Appendix IV. A photograph of a section of the spectrum near the origin is shown, with the corresponding microdensitometer trace, in Figure 5.1.

The ground state frequencies of oxalyl chloride-fluoride are summarized in Table 5.2. The excited state vibrational frequencies which appear as strong intervals of the spectrum have been described in Section 4.4. Additional weaker bands appear in the spectrum, and these have been attributed to vibrational frequencies of the same excited state. Comparison with the analyses of glyoxal⁽³²⁾, oxalyl bromide⁽⁴⁾, and oxalyl chloride^(2,3) produced the assignments shown in Table 5.3. These compounds all belong to the C_{2h} point group and have a higher degree of symmetry than the chloride-fluoride. Propenal and oxalyl chloride-fluoride belong to the C_s point group and both compounds have a larger number of totally symmetric normal modes than do the more symmetric compounds. (Propenal has a larger number of nuclei than the other compounds discussed, and comparisons with this molecule must be made with caution.) In both cases, a larger number of fundamentals appear in the spectra. Comparison with propenal produced the assignments shown in Table 5.4.

(a) Rotational Structure of the Bands

The bands of the S-T spectrum as photographed on the 20 foot McMaster Ebert spectrograph appeared in absorption as line-like features with no resolved structure. Some of the bands showed a slight degradation to lower frequency, but most of them appeared as lines less than 1 cm^{-1} wide. In many

cases the absorption bands of the spectrum appeared to be no wider than the atomic iron emission lines of the adjacent calibration spectrum.

(b) Isotope Effect

Chlorine has two stable isotopes, which have masses 35 (76% abundance) and 37 (24% abundance), and vibrations of the molecule which involve a motion of the chlorine atom differ slightly in frequency (usually by a few wavenumbers) for the two masses. The observed spectra consisted of a superposition of the two isotopic spectra with intensity ratios proportional to the natural abundances. This isotope effect was of great help in the assignment. Since the isotope shift was never more than a few wavenumbers, the weaker spectrum (due to the ^{37}Cl molecule) has not been listed separately. Table 5.1 lists the observed spectral frequencies for the isotope containing ^{35}Cl . The frequencies given refer to the peak positions of the absorption lines, or, where red degradation of a band was apparent, to the head at the blue edge of the band. The spectrum of the isotope of mass equal 37 has been included in Table 5.1 in terms of the isotope shift.

(c) The Origin Band

The origin at 3870 \AA (25828.7 cm^{-1}) is the most intense band of the weak spectrum, in agreement with the behaviour of the other oxalyl halides. The most concrete evidence in support of this assignment is, however, the observed isotope effect. Figure 5.2 shows how the observed isotopic shifts as a function of number of quanta excited extrapolate to zero at 25828.7 cm^{-1} . Balfour and King^(2,3) have found that the chlorine vibrational isotope shifts in the $n \rightarrow \pi^*$ (S-S) and $n \rightarrow \pi^*$ (S-T) transitions of oxalyl chloride are linear in quantum number and extrapolate to zero at the origin.

(d) Ground State Fundamentals

Even the best photographs obtained showed very little absorption to the red of the origin. The most prominent hot band occurs at ν_{00} -218.9 cm^{-1} with weaker bands at -257.2 cm^{-1} , -66.3 cm^{-1} and -132 cm^{-1} . The infra-red spectra reported by Hencher and King⁽⁵²⁾ and by Adelhelm⁽⁸⁾ differ in this region, with HK listing only a band at 278 cm^{-1} and A listing only a band at 230 cm^{-1} . A normal coordinate analysis carried out by Hencher⁽⁵⁾ using a Urey-Bradley force field transferred from oxalyl chloride and oxalyl fluoride calculates values of 222 cm^{-1} and 278 cm^{-1} for the low frequency in plane rocking modes which correlate with the antisymmetric and symmetric modes, respectively, in the molecules of C_{2h} symmetry. Since it is usually difficult experimentally to measure bands in this infra-red region accurately, the discrepancy between the infra-red and ultraviolet frequencies is not considered a serious difficulty. The interval between the origin and the strongest band at -218.9 is assigned as ν_9'' , the "antisymmetric" in plane rocking of the OCX groups. The normal coordinate analysis indicates significant motion of the chlorine atom in agreement with the observed isotope shift to 1.75 cm^{-1} . The band at ν_{00} -257.2 cm^{-1} is the strongest band to the red of ν_{00} -218.9 cm^{-1} . The band cannot be fitted as a sequence stacked on ν_{00} -218.9, and the interval 257.2 cm^{-1} is assigned to ν_8'' , the "symmetric" in plane rocking motion of the OCX groups. Again the normal coordinate analysis predicts a significant motion of the chlorine atom, in agreement with an observed isotope shift of 1.99 cm^{-1} .

By analogy with the spectra of glyoxal and propenal, the bands at ν_{00} -66.3 cm^{-1} and -132.0 cm^{-1} are assigned to the first and second quanta of the torsional vibration ν_{12}'' . HK list the infra-red frequency 129 cm^{-1} , observed

only in combinations, as ν_{12}'' , but since a value of 127 cm^{-1} is observed for glyoxal, the lower value seems more in keeping with the replacement of the hydrogen by a much more massive atom.

A problematic band at $\nu_{00} -178.3 \text{ cm}^{-1}$ is not assigned to a fundamental. No isotope effect is observed for the band (the nearest band of appropriate intensity is $+9.4 \text{ cm}^{-1}$ away) and the frequency interval is assigned as a sequence. An additional extremely weak band at $\nu_{00} -563.3 \text{ cm}^{-1}$ is tentatively assigned to 9_1^0 which is a combination of the in plane scissor motion with the C-Cl stretching motion. HK give a value of 570 cm^{-1} for this mode in the infra-red.

The singlet-singlet analysis shows the strongest hot band at $\nu_{00} -318.6 \text{ cm}^{-1}$. Although there is weak complex absorption in the region of -390 cm^{-1} from the singlet-triplet origin, the intensity is too weak to warrant listing these bands. This problem is discussed in more detail in Section 5.3.

(e) Excited State Fundamentals

The part of the spectrum which lies to the blue of the origin shows a much more complex vibrational structure than occurs for either oxalyl chloride or oxalyl bromide. This is attributed to the fact that an increased number of fundamentals are active in the transition. (There is a larger number of totally symmetric vibrational modes for the C_s molecule than for the C_{2h} molecules.) In addition, the region between $\nu_{00} +400 \text{ cm}^{-1}$ and $\nu_{00} +1000 \text{ cm}^{-1}$ contains a large number of weak bands. Since very few patterns are obvious among these weak bands, many have not been fitted into the assignment of the S-T system. Several of the bands in this region can be attributed to activity of excited state fundamentals, but these bands have intensities very little greater than the numerous weak bands. Because of this problem, assign-

ments have been divided into two categories depending upon the confidence with which they can be made.

Strong bands at $\nu_{00} + 145.9$, $+ 181.9$, $+ 237.3$, $+ 282.8$, $+ 1292.1$, and $+1692.4 \text{ cm}^{-1}$ have been assigned to 11_0^1 , 9_0^1 , 10_0^1 , 8_0^1 , 2_0^1 and 1_0^1 respectively. Both the ν_1 and the ν_2 modes involve stretching of the two carbonyl bonds, but ν_1 is more highly localized in the carbonyl bond adjacent to the chlorine atom. The ground and excited state values for the fundamentals are compared in Table 5.2. It is apparent that the frequency change between ground and excited is much larger for ν_2 than for ν_1 , and the CNDO calculations provide an explanation. The π_{1a}^* molecular orbital is antibonding along both carbonyl bonds with a slight localization at the end adjacent to the chlorine atom; the n_{1a}^- molecular orbital has some bonding character along the carbonyl bonds and with a significant localization at the end adjacent to the chlorine. The $n_{1a}^- \rightarrow \pi_{1a}^*$ promotion should produce a larger change in the strength of the C=O(Cl) bond and consequently in ν_2 relative to ν_1 .

Tables 5.3 and 5.4 summarize the vibrational modes active in $n \rightarrow \pi^*$ transitions of a series of related molecules. By analogy, the vibrational modes involving OCX rocking and scissors motion should be active in COFCOCl. The progression in OCX scissors motion will lie in the difficult region above $\nu_{00} + 400 \text{ cm}^{-1}$, but the strong bands at $\nu_{00} + 181.9 \text{ cm}^{-1}$ and $\nu_{00} + 282.8 \text{ cm}^{-1}$ are assigned to 9_0^1 and 8_0^1 respectively. ν_8 and ν_9 can be approximately described as the two COX rocking modes. Two well-characterized but less intense progressions in the frequency intervals $+ 145.9 \text{ cm}^{-1}$ and 237.3 cm^{-1} are assigned to 10_0^1 and 11_0^1 where ν_{10} and ν_{11} are the out-of-plane wagging modes.

The remainder of the assignments are made with a lower degree of confidence than those already described. The poorly characterized intervals

+1073.1, +722.2, and 417.3 cm^{-1} can be identified in the spectrum. The band $\nu_{00} + 1073.1 \text{ cm}^{-1}$ is overlapped by the band $9_1^0 2_0^1$ but an isotope shift of 2.04 cm^{-1} can be observed. The normal coordinate analysis of the ground state⁽⁵⁾ indicates that the chlorine atom does not move in ν_3 but does in ν_4 . The interval 1073.1 is assigned to $\nu_4(a')$. By comparison with the ground state frequencies, the frequency 722.2 cm^{-1} is probably $\nu_5(a')$. This mode is a complex combination of OCX rocking with bond stretching and involves considerable motion of the chlorine atom in agreement with an observed isotope shift of 2.56 cm^{-1} . A fundamental band with a somewhat diffuse profile appears at +417.3 cm^{-1} . The pattern of adjacent lines is such that the isotope shift for this band is either 0.0 cm^{-1} or 4.60 cm^{-1} . Although the latter value is surprisingly large, combination bands using the interval 417.3 cm^{-1} could be found which displayed the same isotope shifts. It may be noted in passing that if 417.3 cm^{-1} were attributed to pure ^{35}Cl motion, the ^{37}Cl band would occur at approximately $\sqrt{35/37} \times 417 = 405 \text{ cm}^{-1}$ which would represent a shift of 12 cm^{-1} . The fundamental ν_7 shows the largest motion of the chlorine atom of any of the modes and 417.3 cm^{-1} is accordingly assigned to $\nu_7(a')$, a combination of COCl scissors and C-Cl stretching motions.

Two in plane vibrations, ν_3 the C-F stretching mode, and ν_6 the COF scissors mode, remain unassigned. These have the values 1197 and 570 cm^{-1} in the ground state and are tentatively assigned in the excited state to the intervals 1147.7 and 603.6 cm^{-1} . Both appear to have small ($<0.5 \text{ cm}^{-1}$) isotope shifts.

The excited state assignments are summarized in Table 5.2. Only the torsional mode is not observed. The anticipated value of this mode is 151.9 cm^{-1} (66.3 + 85.6, see the next section) which places it in a region of strong

discrete absorption. The hot band 12_1^0 is very weak and it is believed that 12_0^1 is not prominent enough to identify.

(f) Sequences

The prominent interval $+ 85.6 \text{ cm}^{-1}$ is assigned to the sequence in the torsional mode ν_{12} in agreement with the observation of a strong torsional sequence in glyoxal ($+ 107.6 \text{ cm}^{-1}$)⁽⁴¹⁾, oxalyl fluoride (100.5 cm^{-1})⁽¹⁾, oxalyl chloride (78.3 cm^{-1})⁽²⁾ and oxalyl bromide (64.6 cm^{-1})⁽⁴⁾. Two additional members of the sequence are observed although the third is extremely weak.

There are in addition a large number of weaker bands near the origin which have been assigned as sequences or cross-sequences.[†] Cross-sequence bands in the $n \rightarrow \pi^*$ transition of propynal have been observed by Brand, Callomon and Watson⁽⁵⁹⁾.

Sequence bands have been assigned at $- 37.0 \text{ cm}^{-1}$ to ν_9 , the in plane COX rocking mode (the corresponding sequence in oxalyl chloride appears at $- 11 \text{ cm}^{-1}$), and, tentatively, at $- 178.3 \text{ cm}^{-1}$ to ν_{11} the out of plane wag. This last interval is large, but could not be assigned to a ground state fundamental.

Cross-sequences have been assigned at $- 73 \text{ cm}^{-1}$ to ν_9'' and ν_{11}' , the COX rocking and COX out of plane wagging modes, at $+ 63.8 \text{ cm}^{-1}$ to a cross-sequence between ν_9'' and ν_8' , the two in plane COX rocking modes, and at $+ 20.1 \text{ cm}^{-1}$ to ν_9'' and ν_{10}' , the other COX wagging mode. The singlet-singlet spectrum has a band at $+ 20 \text{ cm}^{-1}$ with a very atypical rotational profile.

[†]A cross-sequence is a transition between a lower state characterized by "n" quanta of excitation in one of the fundamental vibrations and an upper state characterized by "n" quanta in a different fundamental.

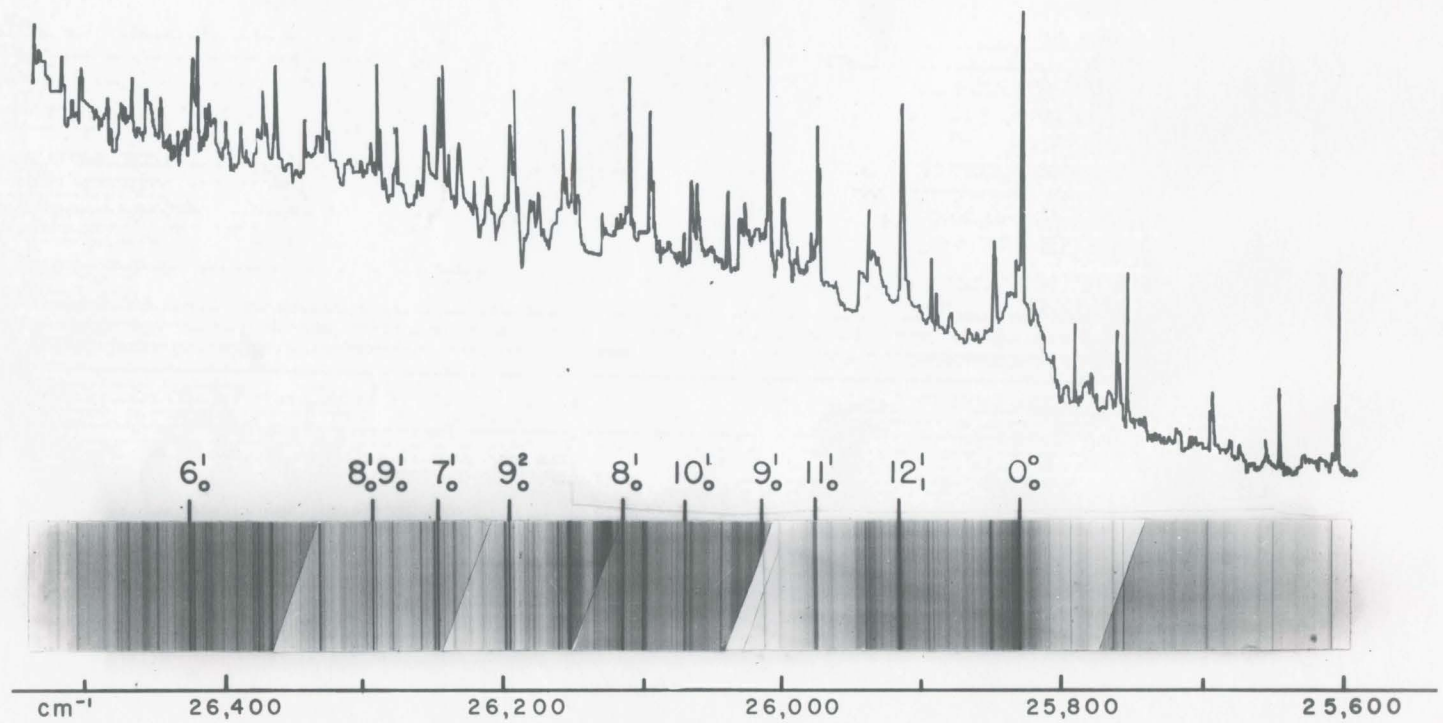


Figure 5.1 THE $\tilde{a}(^3A'') \leftarrow \tilde{X}(^1A')$ ABSORPTION SPECTRUM - COFCOCl

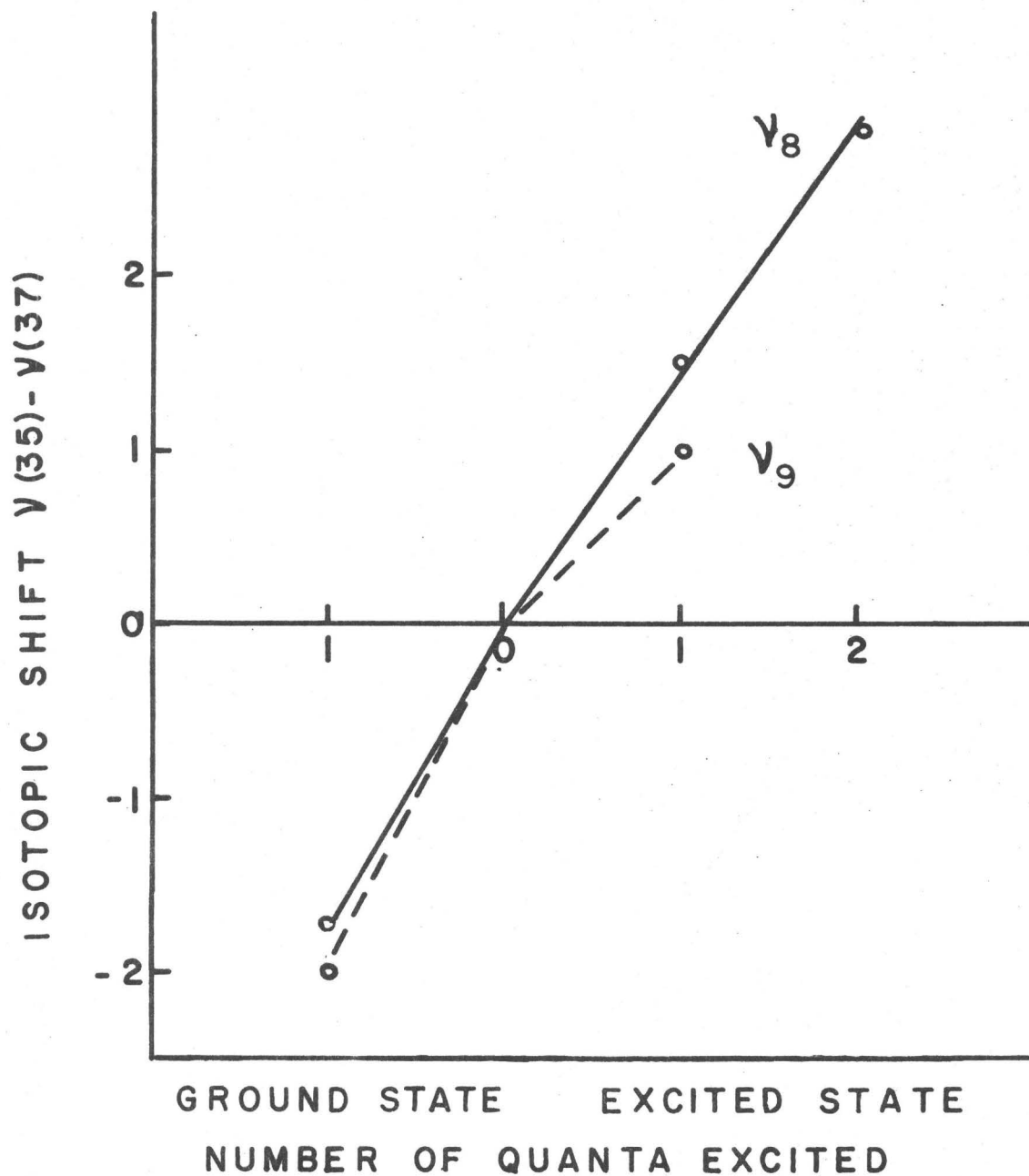


Figure 5.2 The Observed COFCO $^{35}\text{Cl}/^{37}\text{Cl}$ Isotopic Splittings in the $\tilde{a}(^3A'')$ and $\tilde{X}(^1A')$ States

TABLE 5.1

The Frequencies Observed in
 the $\tilde{a}^3(A'') \leftarrow \tilde{X}^1(A')$ Absorption Spectrum of COFCO³⁵Cℓ(trans)
 (with COFCO³⁷Cℓ-COFCOℓ³⁵ Isotopic Shift Included)

Energy (cm ⁻¹)	Int.	Assignment		Isotopic Shift	
25265.4	vvvw	6 ₁ ⁰	-563.3	-	
25571.5	vw	8 ₁ ⁰	-257.2	+1.99	
25609.9	w	9 ₁ ⁰	-218.9	+1.75	
25650.4	vw	11 ₁ ¹	-178.3	~0	
25696.7	vw	{ 9 ₁ ⁰ 12 ₁ ¹ 12 ₂ ⁰ ?	-218.9+86.8 -132	+1.35	1.55
25755.0	w	9 ₁ ⁰ 11 ₀ ¹	-218.9+145.2	0	0.3
25762.4	vw	12 ₁ ⁰	-66.3	+0.69	
25791.7	vw	9 ₁ ¹	-37.0	0	
25828.7	vs	0 ₀ ⁰	origin	0	
25848.9	w	(9 ₁ ⁰ 10 ₀ ¹)	+20.1	0	
25854.8	vvw	(8 ₁ ⁰ 9 ₀ ¹)	+25.9 = -257.2+283.3	-0.92	
25869.1	vvw	(9 ₂ ⁰ 10 ₀ ²)	+20.1+20.2	0	
25878.1	vw	9 ₁ ¹ 12 ₁ ¹	-37.0+86.4	0	
25892.5	vw	(9 ₁ ⁰ 8 ₀ ¹)	+63.8 = -218.9+282.6	+0.55	
25914.3	s	12 ₁ ¹	+85.6	0	
25935.6	vw	12 ₁ ¹ (9 ₁ ⁰ 10 ₀ ¹)	+85.6+21.3	0	
25974.6	m	11 ₀ ¹	+145.9	-1.38	
25978.5	vvw	(9 ₁ ⁰ 8 ₀ ¹)12 ₁ ¹	+63.8+86.0	0	
26000.0	w	12 ₂ ²	+85.6+85.7	0	
26010.6	s	9 ₀ ¹	+181.9	-1.48	
26031.5	vw	9 ₀ ¹ (9 ₁ ⁰ 10 ₀ ¹)	+181.9+20.9	-1.41	

26039.2	w	$11_0^1(9_1^0 8_0^1)$	+145.9+64.5	0
26061.7	w	$11_0^1(9_1^0 10_0^1)$	+145.9+87.1	-1.45
26066.1	w	10_0^1	+237.3	-0.96
26074.5	vw	$9_0^1(9_1^0 8_0^1)$	+181.9+64.7	-0.91
26085.4	vvvw	12_3^3	+85.6+85.7+85.4	0
26096.5	ms	$9_0^1 12_1^1$	+181.9+85.8	-1.94
26111.5	s	8_0^1	+282.8	-0.97
26117.7	vw	$9_0^1 12_1^1(9_1^0 10_0^1)$	+181.9+85.8+21.2	-
26120.6	vw	11_0^2	+145.9+145.9	-
26131.5	vw	$9_0^1(9_1^0 10_0^1)$	+282.8+20.0	-
26150.4	w	$10_0^1 12_1^1$	+237.3+84.3	-1.43
26157.8	w	$9_0^1 11_0^1$	+181.9+147.1	-2.39
26182.2	vw	$9_0^1 12_2^2$	+181.9+85.8+85.7	-
26192.7	m	9_0^2	+181.9+182.1	-2.84
26196.7	w	$8_0^1 12_1^1$	+282.9+85.2	-0.96
26212.4	vw	$11_0^1 10_0^1$	+237.3+146.3	-
26246.0	m	7_0^1	+417.3	-4.60
26248.4	w	$9_0^1 10_0^1$	+181.9+237.8	-
26258.4	vw	$8_0^1 11_0^1$	+282.8+146.9	-1.94
26279.3	vw	$9_0^2 12_1^1$	+181.9+182.1+86.6	-
26281.8	vw	$8_0^1 12_2^2$	+282.8+85.8+85.1	-
26294.2	ms	$8_0^1 9_0^1$	+282.8+182.7	-2.53
2633.7	m	$7_0^1 12_1^1$	+417.3+87.2	-4.39
26348.0	vw	$8_0^1 10_0^1$	+282.8+236.4	-1.99
26369.9	w	9_0^3	+181.9+182.1+177.2	-
26379.6	vw	$8_0^1 9_0^1 12_1^1$	+282.8+182.7+85.4	-2.71
26391.2	vvw	8_0^2	+282.8+279.6	-

26419.6	vw	$7 \begin{smallmatrix} 1 \\ 0 \end{smallmatrix} \begin{smallmatrix} 12 \\ 2 \end{smallmatrix} \begin{smallmatrix} 2 \\ 2 \end{smallmatrix}$	+417.3+87.2+85.9	-
26427.8	w	$7 \begin{smallmatrix} 1 \\ 0 \end{smallmatrix} \begin{smallmatrix} 9 \\ 0 \end{smallmatrix} \begin{smallmatrix} 1 \\ 0 \end{smallmatrix}$	+417.3+181.8	-6.25
26432.3	w	$6 \begin{smallmatrix} 1 \\ 0 \end{smallmatrix}$	+603.6	-
26455.1	vw	$9 \begin{smallmatrix} 3 \\ 0 \end{smallmatrix} \begin{smallmatrix} 12 \\ 1 \end{smallmatrix} \begin{smallmatrix} 1 \\ 1 \end{smallmatrix}$	+181.9+182.1+177.2+84.2	-
26464.6	vvw	$8 \begin{smallmatrix} 1 \\ 0 \end{smallmatrix} \begin{smallmatrix} 9 \\ 0 \end{smallmatrix} \begin{smallmatrix} 1 \\ 0 \end{smallmatrix} \begin{smallmatrix} 12 \\ 2 \end{smallmatrix} \begin{smallmatrix} 2 \\ 2 \end{smallmatrix}$	+282.8+182.7+85.4+84.9	-
26476.8	vw	$9 \begin{smallmatrix} 2 \\ 0 \end{smallmatrix} \begin{smallmatrix} 8 \\ 0 \end{smallmatrix} \begin{smallmatrix} 1 \\ 0 \end{smallmatrix}$	+181.9+182.1+284.2	-4.97
26517.2	vw	$6 \begin{smallmatrix} 1 \\ 0 \end{smallmatrix} \begin{smallmatrix} 12 \\ 1 \end{smallmatrix} \begin{smallmatrix} 1 \\ 1 \end{smallmatrix}$	+603.6+84.9	-
26531.0	vw	$7 \begin{smallmatrix} 1 \\ 0 \end{smallmatrix} \begin{smallmatrix} 8 \\ 0 \end{smallmatrix} \begin{smallmatrix} 1 \\ 0 \end{smallmatrix}$	+417.3+285.0	-5.26
26551.9	vw	$5 \begin{smallmatrix} 1 \\ 0 \end{smallmatrix}$	+723.2	-2.56
26615.9	vw	$7 \begin{smallmatrix} 1 \\ 0 \end{smallmatrix} \begin{smallmatrix} 8 \\ 0 \end{smallmatrix} \begin{smallmatrix} 1 \\ 0 \end{smallmatrix} \begin{smallmatrix} 12 \\ 1 \end{smallmatrix} \begin{smallmatrix} 1 \\ 1 \end{smallmatrix}$	+417.3+285.0+84.9	-
26713.4	vw	$7 \begin{smallmatrix} 1 \\ 0 \end{smallmatrix} \begin{smallmatrix} 8 \\ 0 \end{smallmatrix} \begin{smallmatrix} 1 \\ 0 \end{smallmatrix} \begin{smallmatrix} 9 \\ 0 \end{smallmatrix} \begin{smallmatrix} 1 \\ 0 \end{smallmatrix}$	+417.3+285.0+182.4	-
26901.9	m	$4 \begin{smallmatrix} 1 \\ 0 \end{smallmatrix}$	+1073.1	-2.04
		$9 \begin{smallmatrix} 0 \\ 1 \end{smallmatrix} \begin{smallmatrix} 2 \\ 0 \end{smallmatrix} \begin{smallmatrix} 1 \\ 0 \end{smallmatrix}$	-218.9+1292.0	
26943.5	w	$2 \begin{smallmatrix} 1 \\ 0 \end{smallmatrix} \begin{smallmatrix} 11 \\ 1 \end{smallmatrix} \begin{smallmatrix} 1 \\ 1 \end{smallmatrix}$	+1292.1-177.3	
26976.4		$3 \begin{smallmatrix} 1 \\ 0 \end{smallmatrix}$	+1147.7	
26987.7	vw	$9 \begin{smallmatrix} 0 \\ 1 \end{smallmatrix} \begin{smallmatrix} 2 \\ 0 \end{smallmatrix} \begin{smallmatrix} 1 \\ 0 \end{smallmatrix} \begin{smallmatrix} 12 \\ 1 \end{smallmatrix} \begin{smallmatrix} 1 \\ 1 \end{smallmatrix}$	-218.9+1292.0+85.8	
27054.7	vw	$12 \begin{smallmatrix} 0 \\ 1 \end{smallmatrix} \begin{smallmatrix} 2 \\ 1 \end{smallmatrix} \begin{smallmatrix} 1 \\ 0 \end{smallmatrix}$	-66.3+1292.3	
27081.6	w	$9 \begin{smallmatrix} 0 \\ 1 \end{smallmatrix} \begin{smallmatrix} 2 \\ 0 \end{smallmatrix} \begin{smallmatrix} 1 \\ 0 \end{smallmatrix} \begin{smallmatrix} 9 \\ 0 \end{smallmatrix} \begin{smallmatrix} 1 \\ 0 \end{smallmatrix}$	-218.9+1292.0+179.7	
27120.8	s	$2 \begin{smallmatrix} 1 \\ 0 \end{smallmatrix}$	+1292.1	
27140.6	m	$2 \begin{smallmatrix} 1 \\ 0 \end{smallmatrix} (9 \begin{smallmatrix} 0 \\ 1 \end{smallmatrix} \begin{smallmatrix} 10 \\ 0 \end{smallmatrix} \begin{smallmatrix} 1 \\ 0 \end{smallmatrix})$	+1292.1+19.8	
27206.1	ms	$2 \begin{smallmatrix} 1 \\ 0 \end{smallmatrix} \begin{smallmatrix} 12 \\ 1 \end{smallmatrix} \begin{smallmatrix} 1 \\ 1 \end{smallmatrix}$	+1292.1+85.3	
27262.1	w	$2 \begin{smallmatrix} 1 \\ 0 \end{smallmatrix} \begin{smallmatrix} 11 \\ 0 \end{smallmatrix} \begin{smallmatrix} 1 \\ 0 \end{smallmatrix}$	+1292.1+141.3	
27290.7	vw	$2 \begin{smallmatrix} 1 \\ 0 \end{smallmatrix} \begin{smallmatrix} 12 \\ 2 \end{smallmatrix} \begin{smallmatrix} 2 \\ 2 \end{smallmatrix}$	+1292.1+85.3+84.7	
27300.5	m	$2 \begin{smallmatrix} 1 \\ 0 \end{smallmatrix} \begin{smallmatrix} 9 \\ 0 \end{smallmatrix} \begin{smallmatrix} 1 \\ 0 \end{smallmatrix}$	+1292.1+179.8	
		$9 \begin{smallmatrix} 0 \\ 1 \end{smallmatrix} \begin{smallmatrix} 1 \\ 1 \end{smallmatrix} \begin{smallmatrix} 1 \\ 0 \end{smallmatrix}$	-218.9+1690.7	
27320.7	vw	$4 \begin{smallmatrix} 1 \\ 0 \end{smallmatrix} \begin{smallmatrix} 7 \\ 0 \end{smallmatrix} \begin{smallmatrix} 1 \\ 0 \end{smallmatrix}$	+1073.1+418.9	
27348.5	vw	$2 \begin{smallmatrix} 1 \\ 0 \end{smallmatrix} \begin{smallmatrix} 11 \\ 0 \end{smallmatrix} \begin{smallmatrix} 1 \\ 0 \end{smallmatrix} \begin{smallmatrix} 12 \\ 1 \end{smallmatrix} \begin{smallmatrix} 1 \\ 1 \end{smallmatrix}$	+1292.1+141.3+86.6	
27357.0	w	$2 \begin{smallmatrix} 1 \\ 0 \end{smallmatrix} \begin{smallmatrix} 10 \\ 0 \end{smallmatrix} \begin{smallmatrix} 1 \\ 0 \end{smallmatrix}$	+1292.1+236.2	

27386.2	w	$2_{00}^1 9^1 12^1_1$	+1292.1+179.8+84.5
27406.7	m	$2_{00}^1 8^1_0$	+1292.1+285.9
27441.6	w	$2_{00}^1 10^1 12^1_1$	+1292+236.2+84.7
27480.8	w	$2_{00}^1 9^2_0$	+1292.2+179.8+180.3
27482.8	w	$9_{10}^0 1^1 9^1_0$	-218.9+1690.7+182.2
27491.5	vw	$2_{00}^1 8^1 12^1_1$	+1292.1+285.9+84.8
27520.2	m	1^1_0	+1692.4
27536.7	w	$2_{00}^1 7^1_0$	+1292.1+415.9
27606.5	w	$1^1_{00} 12^1_1$	+1692.4+84.6
27622.3	vvw	$2_{00}^1 7^1 12^1_1$	+1292.1+415.9+85.6
27701.3	m	$1^1_{00} 9^1_0$	+1692.4+181.1
27713.8	vvw	$2_{00}^1 7^1 9^1_0$	+1292.1+415.9+171.1
27787.9	vw	$1^1_{00} 9^1 12^1_1$	+1692.4+181.1+83.9
27803.8	vw	$1^1_{00} 8^1_0$	+1692.4+283.6
27879.8	w	$1^1_{00} 9^2_0$	+1692.4+181.1+178.5
28182.4	vw	$2^1_{00} 4^1_0$	+1292.1+1061.6
28375.6	m	2^2_0	+1292.1+1254.8
28459.9	vw	$2^2_{00} 12^1_1$	+1292.1+1254.8+84.3
28518.1	w	$2^2_{00} 11^1_0$	+1292.1+1254.8+142.5
28556.7	m	$2^2_{00} 9^1_0$	+1292.1+1254.8+181.4
28578.9	w	$1^1_{00} 4^1_0$	+1692.4+1058.6
28605.5	vw	$2^2_{00} 10^1_0$	+1292.1+1254.8+229.9
28641.4	vw	$2^2_{00} 9^1 12^1_1$	+1292.1+1254.8+181.4+84.6
28654.9	w	$2^2_{00} 8^1_0$	+1292.1+1254.8+279.3
28738.4	vw	$2^2_{00} 8^1 12^1_1$	+1292.1+1254.8+279.3+83.5
28836.4	vw	$2^2_{00} 8^1 9^1_0$	+1292.1+1254.8+279.3+181.4

↓
Obscured by $\tilde{A}^1(A'')$ ← $\tilde{X}^1(A')$ System



TABLE 5.2

Ground and Excited State Frequencies for Oxalyl Chloride-Fluoride

Fundamental		$\tilde{\chi}^1(1A')$		$\tilde{a}^3(3A'')$	$\tilde{A}^1(1A'')$	
		HK ^a	Modified ^b			
a'	C=O(F) stretch	ν_1	1859		1692.4	1679.7
	C=O(Cl) stretch	ν_2	1790		1292.1	1282.8
	CF + CC stretch	ν_3	1197		(1147.7)	(1110.6)
	CCl + CC stretch	ν_4	932		(1073.1)	(976.0)
		ν_5	713		722.2	738.4
	COF scissors (asymmetric COX scissors)	ν_6	570	(563.3) ^c	(603.6)	594.5
	COC ℓ scissors (symmetric COX scissors)	ν_7	491 ^d		417.3	418.9
	COX rock (symm)	ν_8	278	257.2	282.8	277.6
	COX rock (asymm)	ν_9	222	218.9	181.9	180.0
a''	COX wag	ν_{10}	409	391.7	237.3	237.5
	COX wag	ν_{11}	360		145.9	143.9
	torsion	ν_{12}		(66.3)		

^aHencher and King⁽⁵¹⁾.

^bModified values indicated by the UV analysis.

^cAssignments which are considered tentative have been bracketed.

^dThis band has disappeared or undergone a large shift in the solid infrared spectrum⁽⁸⁾.

TABLE 5.3

Comparison of the Ground and Excited State Fundamentals Observed
in the Triplet $n \rightarrow \pi^*$ Spectra of Oxalyl Chloride-Fluoride
and a Series of Molecules

Fundamental	COFCOCl	COC $\&$ COCl	COBrCOBr	COHCOH ^c
<u>GROUND</u>				
CC stretch (a_g, a')				1207 ν_4
C-X stretch ^d (a_g, a')	X X X X	612 ^c ν_3 (vw)		
\angle OCX scissors ^a (a_g, a')		499 ^c ν_4 (w)	441 ν_4 (w)	
\angle OCX rock ^b (a_g, a')	257.2 ν_8 (vw)	280 ^c ν_5 (vw)	185 ν_5 (w)	553 ν_5
2X (Torsion) (a_u, a'')	132.0 $2\nu_{12}$ (vw)			254 $2\nu_7$
CX wag (b_g, a'')	391.7 ν_7 (w)			1048 ν_8
<u>EXCITED</u>				
\angle OCX rock ^b (a_g, a')	282.8 ν_8 (m)	281 ν_5 (m)	186 ν_5 (m)	509 ν_5 (m)
\angle OCX scissors ^a (a_g, a')	417.3 ν_7 (w)	401 ν_4 (s)	312 ν_4 (s)	ν_3
C-X stretch ^d (a_g, a')	xxxxx	635 ν_3 (m)	642 ν_3 (m)	ν_1
C-C stretch (a_g, a')	1073.1 ν_4 (w)	1028 ν_2 (w)	1002 ν_2 (s)	947 ν_4 (m)
C=O stretch (a_g, a')	1292.1 ν_2 (vs)	1508 ν_1 (vs)	1537 ν_1 (vs)	1391 ν_2 (s)
2X Torsion (a_u, a'')	?			464 $2\nu_7$ (w)
OCX wag (b_g, a'')	145.9 ν_{11} (w)	204 ν_8 (w)		737 ν_8 (ss)

^aIn glyoxal this mode is designated CH in plane rock.

^bIn glyoxal this mode is designated CCO bend.

^cFrom the $n \rightarrow \pi^*$ singlet spectrum (32).

^dThis mode is not really comparable in COFCOCl.

TABLE 5.4

Comparison of Ground and Excited State Fundamentals Observed
in the $n \rightarrow \pi^*$ Spectra of Oxalyl Chloride Fluoride and Propenal

Fundamental	COFCOC ℓ Singlet	COFCOC ℓ Triplet	Propenal Singlet
<u>GROUND STATE</u>			
\angle CCO bend (a')	218.7 (w)	218.9 ν_9 (w)	564.9 ν_{12}''
Torsion (a'')	66.0 (vw)	66.3 ν_{12} (vw)	156.2 ν_{18}''
<u>EXCITED STATE</u>			
Torsion (a')	?	?	251.8 ν_{18}'
\angle CCO bend (a')	180.0 (m)	181.9 ν_9 (m)	488.3 ν_{12}'
\angle OCX scissors ^a (a')	594.5 (vw)	603.6 ν_6 (vw)	1132.7 ν_8'
C=O stretch (a')	1279.2 (vs)	1292.1 ν_2 (vs)	1265.6
	1294.1 (m)		1294.7
Out of plane ^b wag (a'')	143.9 (w)	145.9 ν_{11} (w)	582.2 ν_{16}'
wag (a'')	237.5 (vw)	237.3 ν_{10} (vw)	644.0 ν_{15}'

^aIn propenal this mode is described as CH in plane rock.

^bThese are designated =CH₂ wag and -CH wag in propenal.

This assignment has been transferred from the singlet spectrum where the assignment is more restricted (see Section 5.3 (g)).

5.3 The ${}^1A''(n_{1a'}, \pi_{1a'}^*) \leftarrow \tilde{X}{}^1A'$ Transition (Trans Isomer)

Table 4.2 demonstrates the similarity between the singlet and triplet spectra. The most striking difference is the change in the rotational structure of the bands. The extensive rotational structure of each band in the S-S spectrum makes it impossible to observe the isotope shift in most cases, and weak bands are more difficult to identify. In many instances it has been necessary to refer to the singlet-triplet spectra for confirmation of assignments.

The band by band assignment of the singlet-singlet $n \rightarrow \pi^*$ spectrum is given in Table 5.6. A number of weak lines in the spectrum did not fit into the assignment of combination bands or hot bands, and have been included in Appendix IV. A photograph of a section of the spectrum near the origin is shown in Figure 5.3, together with the corresponding microdensitometer trace.

Again, the analyses of the spectra of oxalyl bromide, oxalyl chloride, glyoxal and propenal have been used extensively in assigning the spectrum. Table 5.7 compares the fundamentals active in the ground and excited state of the C_{2h} compounds and lists the assignments made in COFCOCl₂ on this basis. A comparison with propenal has been included in Table 5.4.

(a) Rotational Structure of the Bands

The origin band shows semi-regular fine structure. This structure, discussed in detail in Chapter 6, disappears for bands several hundred wave-numbers to the blue of the origin, but the band profile which is characterized by a blue degraded head remains sharp up to several thousand wave-numbers from the origin. According to the selection rules for electronic

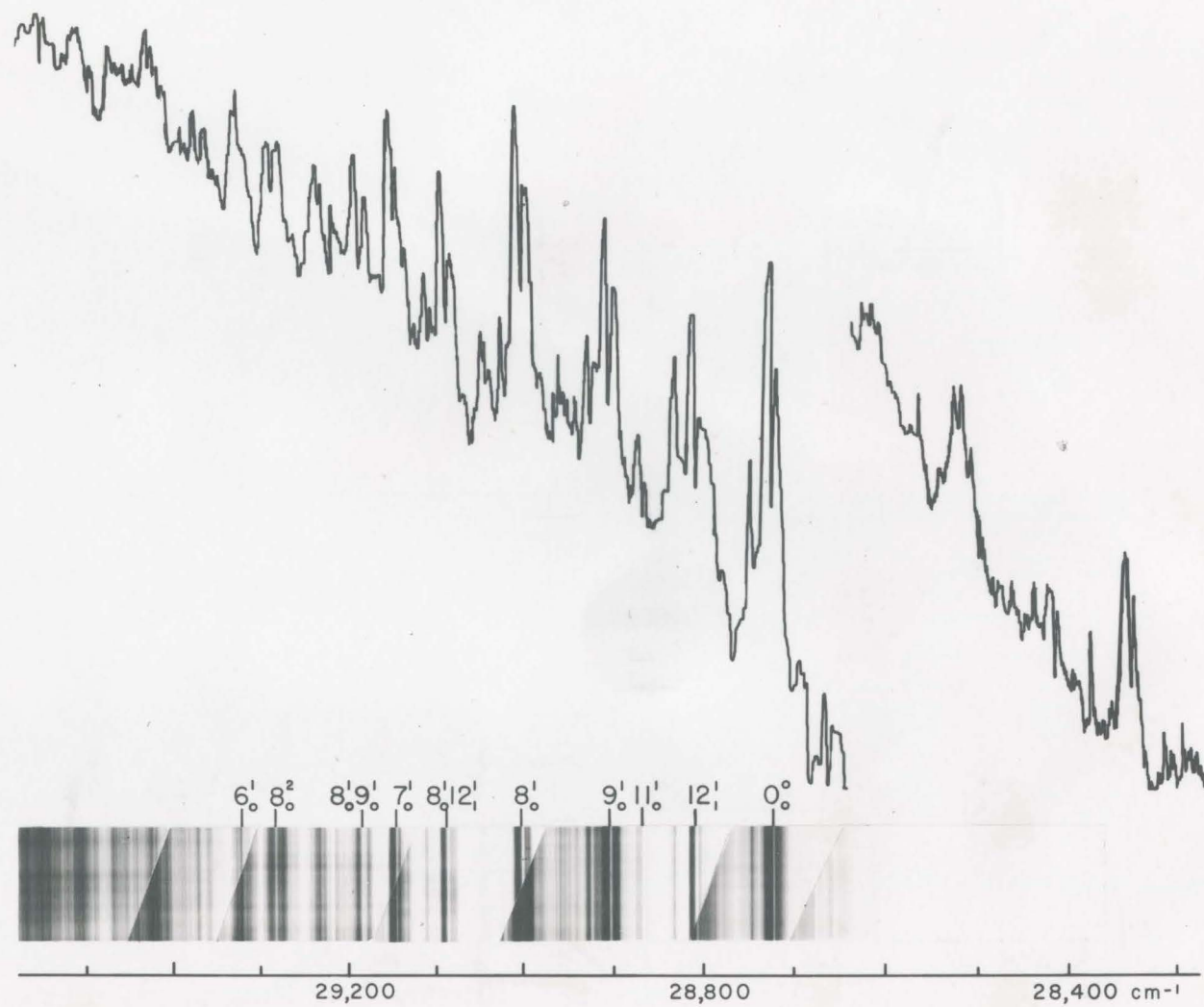


Figure 5.3 THE $\tilde{A}'(A') \leftarrow \tilde{X}'(A')$ ABSORPTION SPECTRUM - COFCOCL

transitions (see reference 6), the origin band and all totally symmetric fundamentals should appear as type C bands, while non-totally symmetric fundamentals should appear through vibronic mixing as type A-B hybrids. In the case of oxalyl chloride-fluoride, the distinction between type A-B and C bands is not dramatic (see Chapter 6). In addition, with eleven normal modes appearing, there is a large amount of overlap of adjacent bands, with the result that assignment of band type is often not possible. The profiles of most assigned bands appeared to be similar to that of the origin band. This distinguishes oxalyl chloride-fluoride from oxalyl chloride and oxalyl fluoride, where significant changes were observed in the type C band profiles.

(b) Perturbations

Perturbations are observed in two places in the S-S spectrum. As described in Section 4.4, there is a complex perturbation of the vibrational pattern in the region of the first member of the progression in C=O stretching motion. This complexity can be explained by Fermi resonance between three fundamentals. A second case is to be found in the region of the spectrum near the origin-A band which appears at $+ 20 \text{ cm}^{-1}$ has a rotational profile which is quite different from the origin band of oxalyl chloride-fluoride. The profile is sufficiently different to suggest the possibility of an impurity in the spectrum; however the interval $+ 20 \text{ cm}^{-1}$ appears throughout the spectrum with the same profile repeated. The conclusion is that the rotational structure is altered by rotational perturbation, perhaps Coriolis coupling, but an analysis of this rotational structure has not been attempted.

The Fermi-resonance at $+ 1300 \text{ cm}^{-1}$ is responsible for a large deviation from the anticipated vibrational structure in this region. Figure 5.4

compares the vibrational pattern at $+ 1300 \text{ cm}^{-1}$ with the pattern at the origin. The singlet-triplet spectrum showed a repetition of the vibrational pattern at the first member of the progression in ν_{CO} , but in the case of the S-S spectrum, a slight change in the frequencies of the fundamentals has produced the conditions for Fermi resonance. Table 5.5 summarizes the frequencies expected on the basis of simple combinations and illustrates how Fermi resonance can account for the observed structure. One of the most puzzling features of the $+ 1300 \text{ cm}^{-1}$ region of the spectrum was the inverting of the relative intensities of the bands $\nu_{00} + 1279.2 + 180 \text{ cm}^{-1}$ and $\nu_{00} + 1294.0 + 180 \text{ cm}^{-1}$ from the pattern observed for $\nu_{00} + 1279 \text{ cm}^{-1}$ and $\nu_{00} + 1294 \text{ cm}^{-1}$. It should be noted that this has been accounted by a very large negative anharmonicity in ν_9 (rocking). This anharmonicity was also observed at the origin in a situation where Fermi resonance does not appear to be the cause.

(c) Isotope Effect

As was the case in the triplet spectrum, the presence of two isotopes of chlorine was a valuable check on the vibrational assignments, although in this spectrum the extensive rotational structure created some difficulty in identifying the spectrum of COFCOCl^{37} . Again the spectrum of COFCOCl^{37} has been listed in terms of its separation from bands of the stronger spectrum of the 35 isotope.

(d) The Origin Band

The origin band has been assigned to the strongest band of the discrete spectrum at 3480 \AA (28724 cm^{-1}). This assignment is confirmed by the extremely small isotopic shift (0.2 cm^{-1}) observed for this band.

(e) The Ground State Fundamentals

Small sample quantity was not a problem in obtaining photographs of

Figure 5.4 Fermi Resonance Pattern at $\nu_{00} + 1300 \text{ cm}^{-1}$ Compared with the Normal Pattern at the Origin of the ${}^1A'' \leftarrow \tilde{X}{}^1A'$ Transition.

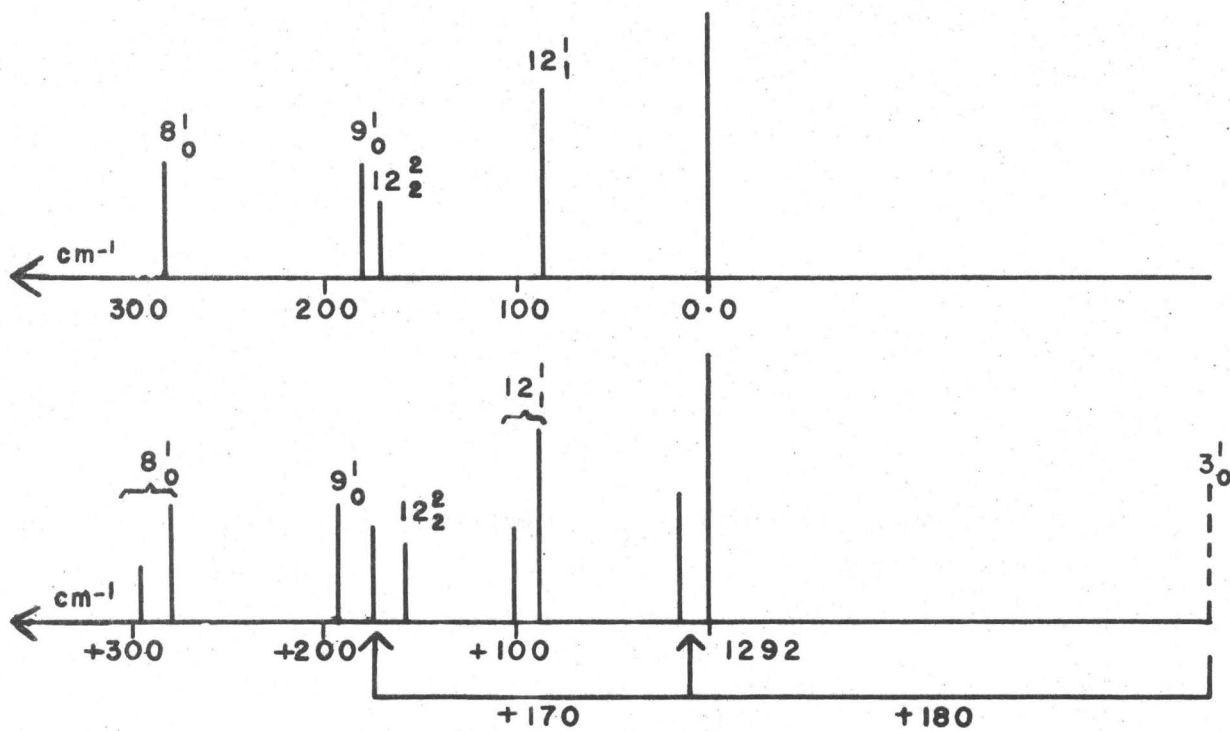


TABLE 5.5

Fermi Resonance Involving $\nu_1 - \nu_3 - \nu_9$ in COFCOCl $n \rightarrow \pi^*$ (Singlet-Singlet);

Unperturbed Values were Obtained from $G_0(\nu_1, \nu_3, \nu_9) = \sum_{i=1,3,9} w_i^0 \nu_i + \sum_{i,j=1,3,9} x_{ij} \nu_i \nu_j^a$

Assignment	Unperturbed Values	Observed Values	Δ
ν_3	180.0	180.0	
$2\nu_3$	349.4	349.4	
ν_1	1282.8	1279.2	-3.6
$\nu_9 + \nu_3$	1290.5	1294.1	+3.6
$\nu_1 + \nu_3$	1465.2	1474.6	+9.4
$\nu_9 + 2\nu_3$	1459.6	~1451	~ -9 (b)
$w_1^0 = 1295.2$	w_3^0 not obtainable	$w_9^0 = 185.3$	
$x_{11} = -12.4$	x_{33} not obtainable	$x_{99} = -5.3$	
$x_{19} = -2.5$	$x_{39} = -0.1$		

^aSee reference (7), page 21.

^bThis combination comes into Fermi resonance with $1^1_1 1^2_2$ (see Fig. 5.5).

the region lying to the red of the S-S origin, as was the case with the S-T spectrum. The increased intensity of the background continuum and overlap by the triplet spectrum, however, have reduced the amount of information which could be obtained from this region.

The most prominent band in the hot part of the spectrum falls at $\nu_{00} - 391.7 \text{ cm}^{-1}$. The profile of this band suggests an isotope shift compatible with an assignment as a hot band of the trans $n \rightarrow \pi^*$ (S-S) spectrum with origin at 28724 cm^{-1} . Comparison with similar compounds (Table 5.2) suggests assignment of the interval 391.7 cm^{-1} to ν_7 the COX scissors mode. This assignment, however, is difficult to reconcile with the absence of a similar strong band in the singlet-triplet spectrum. It is therefore preferable to assign 391.7 cm^{-1} to ν_{10}'' , the out of plane wag which can appear in the singlet-singlet spectrum through vibronic mixing without necessarily satisfying the condition of vibronic spin orbit perturbation required for singlet-triplet intensity. Unfortunately, the band 10_0^1 is not one of the strongest cold bands and it is necessary to invoke a large change in the normal mode on excitation, with corresponding change in intensity. The frequency of the mode drops from 392 to 237 cm^{-1} so this is possible. This assignment would suggest a reassignment of the corresponding band in oxalyl chloride and oxalyl bromide. Another possibility which cannot be eliminated is that the band belongs to the cis spectrum. The strong intensity of this band does not however seem compatible with the lower intensity of the cis origin.

The intervals - 256.7 and - 218.7 cm^{-1} have been assigned to the ground state vibrational modes ν_8'' and ν_9'' respectively, the COX rocking modes. A weak band at - 66.0 cm^{-1} is tentatively assigned to ν_{12} the tor-

sional mode. The weak band observed at -563.3 cm^{-1} in the singlet-triplet spectrum has not been observed here.

(f) The Excited State Fundamentals

Only the interval corresponding to the torsional mode is not observed in the excited state. The most prominent interval is 1282.8 (see Table 5.7) the carbonyl (chlorine) stretching mode. Two strong bands at $\nu_{00} + 277.6$ and $+180 \text{ cm}^{-1}$ are assigned to 8_0^1 and 9_0^1 where ν_8 and ν_9 are the in plane rocking modes. Weaker bands at $\nu_{00} + 235.5$ and $+143.9 \text{ cm}^{-1}$ are assigned to 10_0^1 and 11_0^1 where ν_{10} and ν_{11} are the out of plane wagging modes.

To the blue of $\nu_{00} + 400 \text{ cm}^{-1}$ the spectrum resembles the S-T spectrum with a large number of weak lines present. The progressions stand out less prominently and assignments between $\nu_{00} + 400 \text{ cm}^{-1}$ and $\nu_{00} + 1300 \text{ cm}^{-1}$ are made with a lower degree of certainty. Comparisons between the S-S and S-T spectrum have been used extensively in this region.

The two strongest bands of the region $\nu_{00} + 400 \text{ cm}^{-1}$ to $\nu_{00} + 1300 \text{ cm}^{-1}$ occur at $\nu_{00} + 1110.6$ and $+418.9 \text{ cm}^{-1}$ and have been assigned to 7_0^1 and 3_0^1 respectively; ν_7 is the COC \angle scissors motion and ν_3 is the CF stretching motion. The band at $\nu_{00} + 418.9 \text{ cm}^{-1}$ is one of the few bands of the spectrum which has a rotational contour different from that of the origin band, but in this case, the band could possibly be the superposition of two type C bands. A moderately strong band at $+1679.7 \text{ cm}^{-1}$ is assigned to 1_0^1 involving the carbonyl (F) stretching mode. The large frequency difference between the two excited state carbonyl stretching modes parallels the pattern observed in the S-T spectrum and supports the concept of localization of the first $n \rightarrow \pi^*$ transition on the carbonyl group nearest the chlorine atom.

Weaker bands at $\nu_{00} + 594.5 \text{ cm}^{-1}$ (isotope shift ~ 0), $+738.4 \text{ cm}^{-1}$

(isotope shift apparently $+ 3.8 \text{ cm}^{-1}$), and $+ 976.0 \text{ cm}^{-1}$ (isotope shift 1.6 cm^{-1}) have been assigned to 6_0^1 , 5_0^1 and 4_0^1 respectively. ν_6 is the COF scissors mode, while ν_5 and ν_4 are complex bending and stretching modes. The large isotope shift observed for ν_5^1 agrees with a similar large shift observed in the S-T spectrum and indicates that motion of the chlorine atom is involved heavily.

The region of the spectrum near $\nu_{00} + 900 \text{ cm}^{-1}$ presented a problem in the analysis. Strong (relative to nearby bands) absorption in this region appears to be the overlap of two bands at $\nu_{00} + 895.2$, and $+ 910.6 \text{ cm}^{-1}$. These two bands occur at -384 cm^{-1} from the strong bands at $\nu_{00} + 1279.2$ and $+ 1294.0 \text{ cm}^{-1}$. The most logical assignment appears to be in terms of this interval, but no strong band was observed at $\nu_{00} - 383 \text{ cm}^{-1}$, and no final assignment has been made.

(g) Sequences

The pattern of sequence bands in the S-S spectrum is similar to that in the S-T spectrum. The prominent interval $+ 84.6 \text{ cm}^{-1}$ is assigned to a sequence in ν_{12} , the torsional mode. In addition, a sequence band is assigned at -38.7 cm^{-1} to ν_9 . Cross-sequences have been assigned at 62.0 cm^{-1} to ν_9'' and ν_8' and at $+ 19.3 \text{ cm}^{-1}$ to ν_9'' and ν_{10}' .

The band at $\nu_{00} + 19.3 \text{ cm}^{-1}$ has proved to be a very puzzling feature of the spectrum, and no satisfactory explanation has been provided. This band has a rotational profile which is quite different from that of the origin and shows line structure for which the spacing is $\sim 0.35 \text{ cm}^{-1}$ (versus $\sim 0.1 \text{ cm}^{-1}$ for the origin). The origin (C-type) band has been matched by a computer synthesized contour, and the corresponding A and B-type bands do not resemble the band at $\nu_{00} + 19.3 \text{ cm}^{-1}$. The observation of the interval

$\sim +20 \text{ cm}^{-1}$ throughout the $\tilde{A}^1 \leftarrow \tilde{X}^1$ and $\tilde{a}^3 \leftarrow \tilde{X}^1$ spectra established definitely this interval as a sequence in the $n \rightarrow \pi^*$ transition, but the rotational contour remains unexplained.

The interval $\sim +20 \text{ cm}^{-1}$ appears in both the S-S and S-T spectra with an intensity equivalent to that of the second member of the torsional sequence, and the second member of the $+20 \text{ cm}^{-1}$ sequence also appears (weakly). This suggests that the ground state frequency involved is small, probably near 200 cm^{-1} . Only three vibrational modes have a ground state frequency which is low enough. The additional requirement that the sequence have nearly the same value in the S-S and S-T spectra leads to the assignment of $+19.3 \text{ cm}^{-1}$ to a cross-sequence in ν_9'' and ν_{10}' .

5.4 Additional $n \rightarrow \pi^*$ Transitions of COFCOCl (Trans)

In both the S-S and S-T spectra a small number of prominent lines occur which cannot be assigned in terms of the excited state fundamentals. These are attributed to a second electronic transition. Table 5.8 lists the bands attributed to $\tilde{B} \leftarrow \tilde{X}$ and Table 5.9 lists the bands attributed to $\tilde{b} \leftarrow \tilde{X}$. The CNDO calculations discussed in Chapter 3 indicate the possibility of additional low energy electronic transitions which exist for oxalyl chloride-fluoride because of its low symmetry. The transition observed here is probably the $A''(n_{1a'}, \pi_{2a'}^*) \leftarrow \tilde{X}^1 A'$ transition associated with the C=O(F) group. It is interesting to note that for the S-S (trans) $n \rightarrow \pi^*$ spectra, the origins of oxalyl chloride and oxalyl fluoride fall at 27189 cm^{-1} and 32815 cm^{-1} respectively whereas the two origins of oxalyl chloride-fluoride fall at 28724 cm^{-1} and 30815 cm^{-1} respectively. For the S-T spectra, the origins for oxalyl chloride and oxalyl fluoride fall at 24370 cm^{-1} and 29942 cm^{-1} whereas oxalyl chloride-fluoride has S-T origins at $+25829 \text{ cm}^{-1}$

and 28098 cm^{-1} . It would appear that the transition energies for oxalyl chloride fluoride cannot be predicted by simple averaging of the transition energies of oxalyl fluoride and oxalyl chloride; the association with the chromophoric groups has greater significance.

TABLE 5.6

The Frequencies Observed in
 the $\tilde{A}^1(A'') \leftarrow \tilde{X}^1(A')$ Absorption Spectrum of COFCO³⁵C₂ (trans)
 (with COFCO³⁷C₂ Included in Terms of the Observed Isotopic Shift)

Energy (cm ⁻¹)	Int.	Assignment	Isotopic Shift	
			Obs'd.	Calc.
28116.0	vvw	$10_1^0 9_1^0$	-391.7-216.8	-
28332.7	w	10_1^0	-391.7	+1.72
28414.3	vvw	$10_1^0 12_1^1$	-391.7+81.5	-
28435.2	vvw	$10_1^0 (9_1^0 10_0^1)$	-391.7+81.5+20.9	-
28466.1	vvw	8_1^0	-256.9	+1.35
28495.1	vvw	$10_1^0 12_2^2$	-391.7+81.5+80.9	-
28505.7	vw	9_1^0	-218.7	+1.22
28531.3	vvw	$10_1^0 9_0^1 (9_1^0 10_0^1)$	-391.7+181.3+17.3	-
28590.9	vw	$9_1^0 12_1^1$	-218.7+85.1	-
28609.5	vw	$10_1^0 8_0^1$	-391.7+276.7	-
28658.5	vw	12_1^0	-66.0	-
28685.7	vw	9_1^1	-38.7	-
28724.46	vs	0_0^0	origin	-0.20
28747.5	m	$(9_1^0 10_0^1)$	+23.0	-
28769.0	vw	$(9_2^0 10_0^2)$	+23.0+21.5	-
28783.3	vw	$9_1^0 8_0^1$	+58.9 = -218.7+277.6	0
28809.0	s	12_1^1	+84.6	-0.56
28832.0	w	$12_1^1 (9_1^0 10_0^1)$	+84.6+23.0	-
28854.3	vvw	$12_1^1 (9_2^0 10_0^2)$	+84.6+23.0+22.2	-
28868.3	w	11_0^1	+143.9	-2.01
28893.1	m	12_2^2	+84.6+84.0	-0.79
28904.4	s	9_0^1	+180.0	-1.47

28916.5	w	$12_2^2(9_1^0 10_0^1)$	+84.6+84.0+23.5	-
28927.0	w	$9_0^1(9_1^0 10_0^1)$	+180.0+22.6	-
28939.2	vw	$12_2^2(9_2^0 10_0^2)$	+84.6+84.1+23.5+22.7	-
28962.0	w	10_0^1	+237.5	-
28988.9	m	$9_0^1 12_1^1$	+180.0+84.5	-
29002.1	s	8_0^1	+277.6	-1.30
29024.5	w	$8_0^1(9_1^0 10_0^1)$	+277.6+22.4	-
29045.4	w	$9_0^1 11_0^1$	+180.0+141.0	-
29073.9	m	9_0^2	+180.0+169.4	-
29086.0	ms	$8_0^1 12_1^1$	+277.6+83.9	-
29108.8	w	$8_0^1 12_1^1(9_1^0 10_0^1)$	+277.6+83.9+22.8	-
29143.4	ms	7_0^1	+418.9	-
29157.7	vw	$9_0^2 12_1^1$	+180.0+169.4+83.9	-
29170.3	m	$8_0^1 12_2^2$	+277.6+83.9+84.2	-
29183.1	ms	$8_0^1 9_0^1$	+277.6+180.9	-
29228.7	m	$7_0^1 12_1^1$	+418.9+85.3	-
29266.9	w	$8_0^1 9_0^1 12_1^1$	+277.6+180.9+83.9	-
29281.9	m	8_0^2	+277.6+276.0	-
29302.7	vw	$8_0^2(9_1^0 10_0^1)$	+277.6+276.0+24.5	-
29318.9	m	6_0^1	+594.5	-
29323.6	w	$7_0^1 9_0^1$	+418.9+180.3	-
29351.3	w	$8_0^1 9_0^1 12_2^2$	+277.6+180.9+83.9+84.3	-
29366.2	w	$8_0^2 12_1^1$	+277.6+276.0+84.3	-
29421.0	m	$7_0^1 8_0^1$	+418.9+277.6	-
29438.9	vw	$7_0^1 8_0^1(9_1^0 10_0^1)$	+418.9+277.6+17.9	-
29462.9	w	5_0^1	+738.4	3.8
29506.1	w	$7_0^1 8_0^1 12_1^1$	+418.9+277.6+85.1	-

29548.5	vw	$5_0^1 12_1^1$	+738.4+85.6	
29601.8	vvw	$7_0^1 8_0^1 9_0^1$	+418.9+277.6+180.8	
29619.7	ms	$2_0^1 -384$	+1279.2-384.3	
29635.1	ms	$3_0^1 9_0^1 -384$	+1294.1-383.5	
29702.0	w	4_0^1	+976.0	1.6
29739.2	vvw	$5_0^1 8_0^1$	+738.4+276.3	
29799.9	m	$3_0^1 (9_1^0 9_0^1)$	+1110.6+183.4-218.6	~0
29835.1	ms	3_0^1	+1110.6	~0
29885.4	w	$3_0^1 (9_1^0 9_0^1) 12_1^1$	+1110.6+183.4-218.6+85.5	-
29919.3	w	$3_0^1 12_1^1$	+1110.6+84.2	
30004.0	vvs	2_0^1 Fermi	+1279.2	
30018.5	vs	$3_0^1 9_0^1$ Res.	+1110.6+183.4	
30039.5	w	$3_0^1 9_0^1 (9_1^0 10_0^1)$	+1110.6+183.4+21.0	
30049.1	vvw	$2_0^1 (9_2^0 10_0^2)$	+1279.2+45.1	
30089.1	ms	$2_0^1 12_1^1$	+1279.2+85.1	
30103.1	m	$3_0^1 9_0^1 12_1^1$	+1110.6+183.4+84.6	
30112.1	w	$3_0^1 8_0^1$	+1110.6+277.0	
30122.3	vw	$3_0^1 9_0^1 12_1^1 (9_1^0 10_0^1)$	+1110.6+183.4+84.6+19.2	
30133.3	vw	$3_0^1 8_0^1 (9_1^0 10_0^1)$	+1110.6+277.0+21.2	
30162.4	w	$2_0^1 12_2^2 ?$	+1279.2+85.1+73.3	
30177.1	m	$3_0^1 9_0^2$ Fermi	+1110.6+183.4+158.6	
30186.8	vw	$3_0^1 9_0^1 12_2^2$ Res.	+1110.6+183.4+84.6+83.7	
30199.1	ms	$2_0^1 9_0^1$	+1279.2+195.1	
30221.4	w	$2_0^1 9_0^1 (9_1^0 10_0^1)$	+1279.2+195.1+22.3	
30250.0	m	$3_0^1 7_0^1$	+1110.6+415.0	
30271.4	w	$3_0^1 7_0^1 (9_1^0 10_0^1)$	+1110.6+415.0+21.3	
30283.0	ms	$2_0^1 9_0^1 12_1^1$	+1279.2+195.1+84.0	

30296.2	w	$3\begin{smallmatrix} 1 & 1 & 1 \\ 0 & 0 & 0 \end{smallmatrix} \begin{smallmatrix} 8 \\ 8 \\ 0 \end{smallmatrix}$	+1110.6+183.4+277.7
30334.5	vw	$3\begin{smallmatrix} 1 & 1 & 1 \\ 0 & 0 & 1 \end{smallmatrix} \begin{smallmatrix} 7 \\ 12 \\ 1 \end{smallmatrix}$	+1110.6+415.0+84.5
30367.0	w	$2\begin{smallmatrix} 1 & 1 & 2 \\ 0 & 0 & 2 \end{smallmatrix} \begin{smallmatrix} 9 \\ 12 \\ 2 \end{smallmatrix}$	+1279.2+195.1+84.8+84.0
30380.0	vw	$3\begin{smallmatrix} 1 & 1 & 1 \\ 0 & 0 & 0 \end{smallmatrix} \begin{smallmatrix} 8 \\ 12 \\ 1 \end{smallmatrix} \begin{smallmatrix} 1 \\ 1 \\ 1 \end{smallmatrix}$	+1110.6+183.4+277.7+83.9
30404.2	m	$1\begin{smallmatrix} 1 \\ 0 \end{smallmatrix}$	+1679.7
30420.2	w	$2\begin{smallmatrix} 1 & 1 \\ 0 & 0 \end{smallmatrix}$	+1279.2+416.2
30477.4	w	$2\begin{smallmatrix} 1 & 1 & 1 \\ 0 & 0 & 0 \end{smallmatrix} \begin{smallmatrix} 9 \\ 8 \\ 0 \end{smallmatrix}$	+1279.2+195.1+278.3
30489.7	w	$1\begin{smallmatrix} 1 & 1 \\ 0 & 1 \end{smallmatrix} \begin{smallmatrix} 12 \\ 1 \end{smallmatrix}$	+1279.2+416.2+85.4
30541.3	vvw	$1\begin{smallmatrix} 1 & 1 \\ 0 & 0 \end{smallmatrix} \begin{smallmatrix} 11 \\ 0 \end{smallmatrix} ?$	+1679.7+139.1
30557.2	vvw	$2\begin{smallmatrix} 1 & 2 \\ 0 & 0 \end{smallmatrix} \begin{smallmatrix} 8 \\ 0 \end{smallmatrix}$	+1279.2+279.0+274.1
30561.4	vw	$2\begin{smallmatrix} 1 & 1 & 1 \\ 0 & 0 & 0 \end{smallmatrix} \begin{smallmatrix} 9 \\ 8 \\ 12 \end{smallmatrix} \begin{smallmatrix} 1 \\ 1 \\ 1 \end{smallmatrix}$	+1279.2+195.1+278.3+84.0
30573.9	vw	$1\begin{smallmatrix} 1 & 2 \\ 0 & 2 \end{smallmatrix} \begin{smallmatrix} 12 \\ 2 \end{smallmatrix}$	+1679.7+85.5+84.2
30582.8	w	$1\begin{smallmatrix} 1 & 1 \\ 0 & 0 \end{smallmatrix} \begin{smallmatrix} 9 \\ 0 \end{smallmatrix}$	+1679.7+177.8
30633.3	w	$1\begin{smallmatrix} 1 & 1 \\ 0 & 0 \end{smallmatrix} \begin{smallmatrix} 10 \\ 0 \end{smallmatrix} ?$	+1679.7+229.1
30668.0	m	$1\begin{smallmatrix} 1 & 1 & 1 \\ 0 & 0 & 1 \end{smallmatrix} \begin{smallmatrix} 9 \\ 12 \\ 1 \end{smallmatrix}$	+1679.7+177.8+85.3
30681.1	m	$1\begin{smallmatrix} 1 & 1 \\ 0 & 0 \end{smallmatrix} \begin{smallmatrix} 8 \\ 0 \end{smallmatrix}$	+1679.7+276.9
30700.3	vw	$2\begin{smallmatrix} 1 & 1 \\ 0 & 0 \end{smallmatrix} \begin{smallmatrix} 5 \\ 0 \end{smallmatrix}$	+1279.2+696.3
30750.3	vw	$1\begin{smallmatrix} 1 & 2 \\ 0 & 0 \end{smallmatrix} \begin{smallmatrix} 9 \\ 0 \end{smallmatrix}$	+1679.7+177.8+167.7
30766.2	vw	$1\begin{smallmatrix} 1 & 1 & 1 \\ 0 & 0 & 1 \end{smallmatrix} \begin{smallmatrix} 8 \\ 12 \\ 1 \end{smallmatrix}$	+1679.7+276.9+85.2
30821.6	w	$1\begin{smallmatrix} 1 & 1 \\ 0 & 0 \end{smallmatrix} \begin{smallmatrix} 7 \\ 0 \end{smallmatrix}$	+1679.7+417.4
30861.4	vw	$1\begin{smallmatrix} 1 & 1 & 1 \\ 0 & 0 & 0 \end{smallmatrix} \begin{smallmatrix} 8 \\ 9 \\ 0 \end{smallmatrix}$	+1679.1+276.9+180.4
30885.1	vw	$2\begin{smallmatrix} 2 & 0 \\ 0 & 1 \end{smallmatrix} \begin{smallmatrix} 10 \\ 1 \end{smallmatrix}$	+1279.2+1271.7-391
30903.2	m	$3\begin{smallmatrix} 2 \\ 0 \end{smallmatrix}$	+1110.6+1068.1
30956.7	m	$1\begin{smallmatrix} 1 & 2 \\ 0 & 0 \end{smallmatrix} \begin{smallmatrix} 8 \\ 0 \end{smallmatrix}$	+1679.7+276.9+275.6
31079.9	vw	$3\begin{smallmatrix} 2 & 1 \\ 0 & 0 \end{smallmatrix} \begin{smallmatrix} 8 \\ 0 \end{smallmatrix}$	+1110.6+1068.1+176.7
31092.2	w	$2\begin{smallmatrix} 1 & 1 \\ 0 & 0 \end{smallmatrix} \begin{smallmatrix} 3 \\ 0 \end{smallmatrix}$	+1279.2+1088.2
31162.5	vvw	$3\begin{smallmatrix} 2 & 1 & 1 \\ 0 & 0 & 1 \end{smallmatrix} \begin{smallmatrix} 9 \\ 12 \\ 1 \end{smallmatrix}$	+1110.6+1068.1+176.7+82.6
31176.4	w	$2\begin{smallmatrix} 1 & 1 & 1 \\ 0 & 0 & 1 \end{smallmatrix} \begin{smallmatrix} 3 \\ 12 \\ 1 \end{smallmatrix}$	+1279.2+1088.2+84.2

31275.7	ms	2_0^2	+1279.2+1271.7 (+1282.8+1268.1)
31358.1	m	$2_0^{212} \substack{1 \\ 1}$	+1279.2+1271.7+83.4
31450	w	$2_0^{291} \substack{1 \\ 0}$	+1279.2+1271.7+174
31550	vw	$2_0^{281} \substack{1 \\ 0}$	+1279.2+1271.7+274
32530	m	2_0^3	+1279.2+1271.7+1254 (+1282.8+1268.1+1254)

TABLE 5.7

Comparison of Ground and Excited State Fundamentals Observed in the
Singlet $n \rightarrow \pi^*$ Spectra of Oxalyl Chloride Fluoride and A Series
of Molecules

Fundamental	COFCOCl	COClCOCl	COBrCOBr	COHCOH
<u>GROUND STATE</u>				
C-C stretch (a_g, a')				1207 ν_4
C-X stretch ^c (a_g, a')	xxxx	612 $\nu_3(vvw)$		
\angle OCX scissors ^a (a_g, a')		499 $\nu_4(w)$	441 $\nu_4(vw)$	
\angle OCX rock ^b (a_g, a')	256.9	280 $\nu_5(vvw)$	186 $\nu_5(w)$	533 [†] ν_5
2X (torsion) (a_u, a'')	66.0			
CX wag (b_g, a'')	391.7			1048 ν_8
<u>EXCITED STATE</u>				
\angle OCX rock ^b (a_g, a')	277.6 $\nu_8(m)$	282 $\nu_5(s)$	186 $\nu_5(m)$	509 $\nu_5(m)$
\angle OCX scissors ^a (a_g, a')	418.9 $\nu_7(w)$	398 $\nu_4(s)$	312 $\nu_4(s)$	
C-X stretch ^c (a_g, a')	xxxx	619 $\nu_3(s)$	642 $\nu_3(w)$	
C-C stretch (a_g, a')	976.0 $\nu_4(vw)$	970 $\nu_2(w)$	1003 $\nu_2(m)$	947 $\nu_4(m)$
C=O stretch (a_g, a')	1282.8 $\nu_2(s)$	1460 $\nu_1(vs)$	1537 $\nu_1(vs)$	1391 $\nu_2(s)$
2X torsion (a_u, a'')	?			464 $2\nu_7(w)$
OCX wag (a_u, a'')	143.9 (w)	204 $\nu_8(w)$		737 $\nu_8(ss)$

TABLE 5.8

Lines Observed in the $\tilde{B} \leftarrow \tilde{X}$ Transition of $\text{COFCO}^{35}\text{Cl}$

Energy (cm^{-1})	Intensity	Displacement
30815	m	Possible origin (+2091 cm^{-1} from $0_0^0 \tilde{A}^1 \leftarrow \tilde{X}^1$)
30895	m	80
30965	vw	150
30980	vw	165
31050	vw	235
31115	m	300
31198	w	383
31490	w	675
31570	vw	755
31655	m	840
31735	m	920
31820	m	1005

TABLE 5.9

Lines Observed in the $\tilde{b} \leftarrow \tilde{X}$ Transition of COFCO³⁵Cℓ

Energy (cm ⁻¹)	Intensity	Displacement
28098.3	m	Possible origin (+2269.6 from $0_0^0 \tilde{a}^3 \leftarrow \tilde{X}^1$)
28162.0	vw	63.7
28200.1	vw	101.8
28240.9	vw	142.6
28278.6	m	180.3
28298.1	m	199.8
28519.7	m	421.4
28646.6	m	548.3
28795.4	m	697.1
29042.4	w	944.1
29125.0	w	1026.7

CHAPTER 6

ROTATIONAL STRUCTURE OF THE ORIGIN BAND OF THE ${}^1A''(n_{1a}^-, \pi_{1a}^{*}) \leftarrow \tilde{X}{}^1A'$ TRANSITION OF trans COFCOCl₂

6.1 Introduction

The 3481 Å band of trans oxalyl chloride-fluoride has been assigned as the origin of the absorption transition to the ${}^1A''(n_{1a}^-, \pi_{1a}^{*})$ excited electronic state on the basis of the vibrational structure associated with this transition. The ${}^1A'' \leftarrow \tilde{X}({}^1A')$ transition is polarized along the axis of the greatest moment of inertia and the origin band should be a C-type band.[†] The absorption in the region of 3481 Å has been photographed under very high resolution (in excess of 450,000), and a print of the origin band is shown in Figure 6.1 with the corresponding microdensitometer trace. The rotational profile contains a prominent blue degraded head, and closely spaced fine structure extending some 15 cm⁻¹ to higher and lower frequencies from the head. The fine structure to higher frequency is almost obscured by the strong absorption associated with the head, but the fine structure to lower frequency, consisting of a series of nearly regularly spaced line-like features, can easily be seen in Figure 6.1. Similar fine structure is observed for both oxalyl fluoride and oxalyl chloride.

Under medium resolution (i.e., spectra taken on the 20 ft. McMaster Ebert Spectrograph) the rotational contour, which is not reproduced here, has the same appearance as that shown in Figure 6.1, only the line-like features are not resolved.

[†]For a discussion of theory and terminology, see reference (6), Chapter 9, reference (7), Section II, 3, or reference (61).

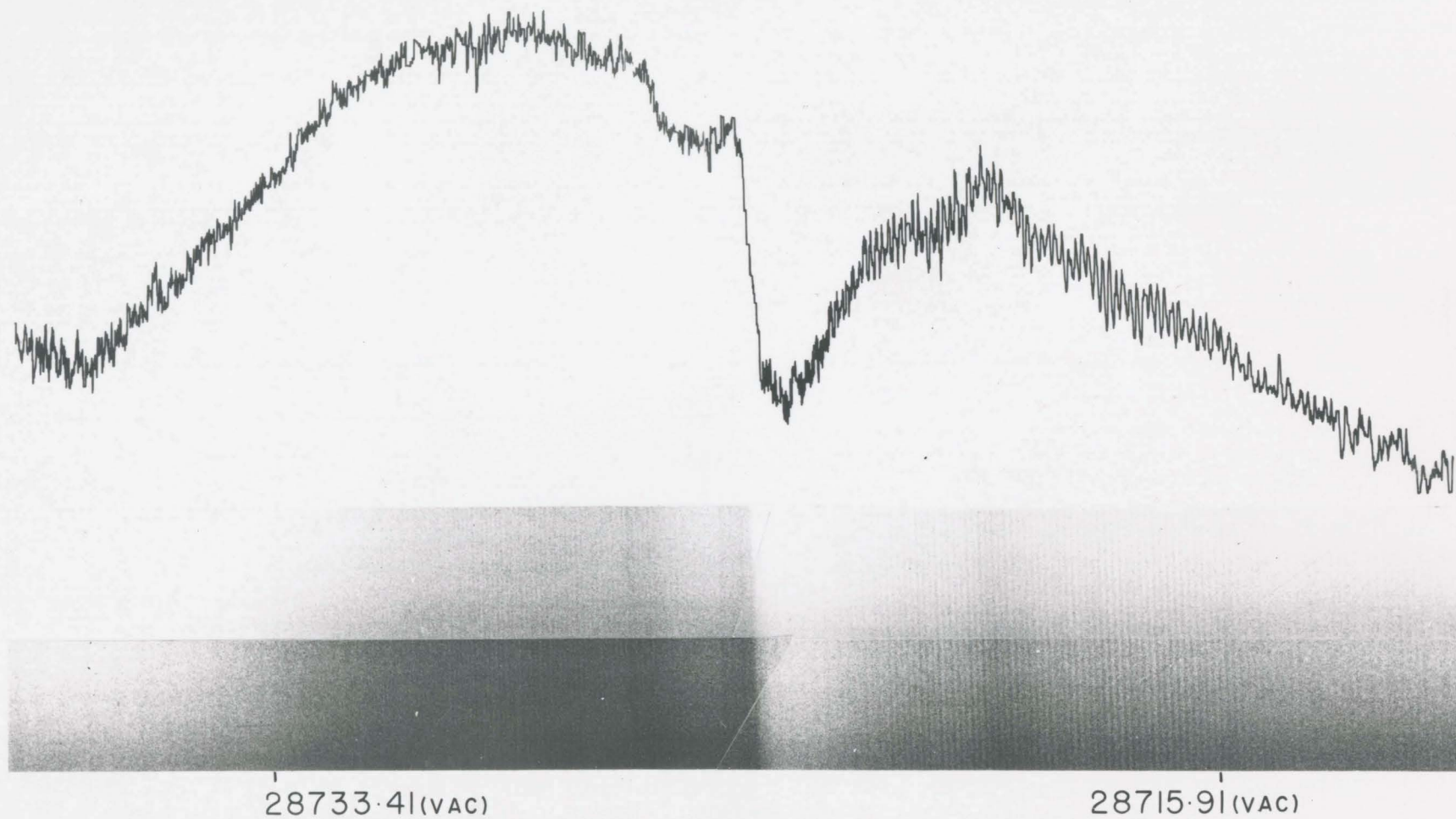


Figure 6.1 THE ORIGIN BAND OF $\tilde{A}('A'')$ \leftarrow $\tilde{X}('A')$
OXALYL CHLORIDE FLUORIDE

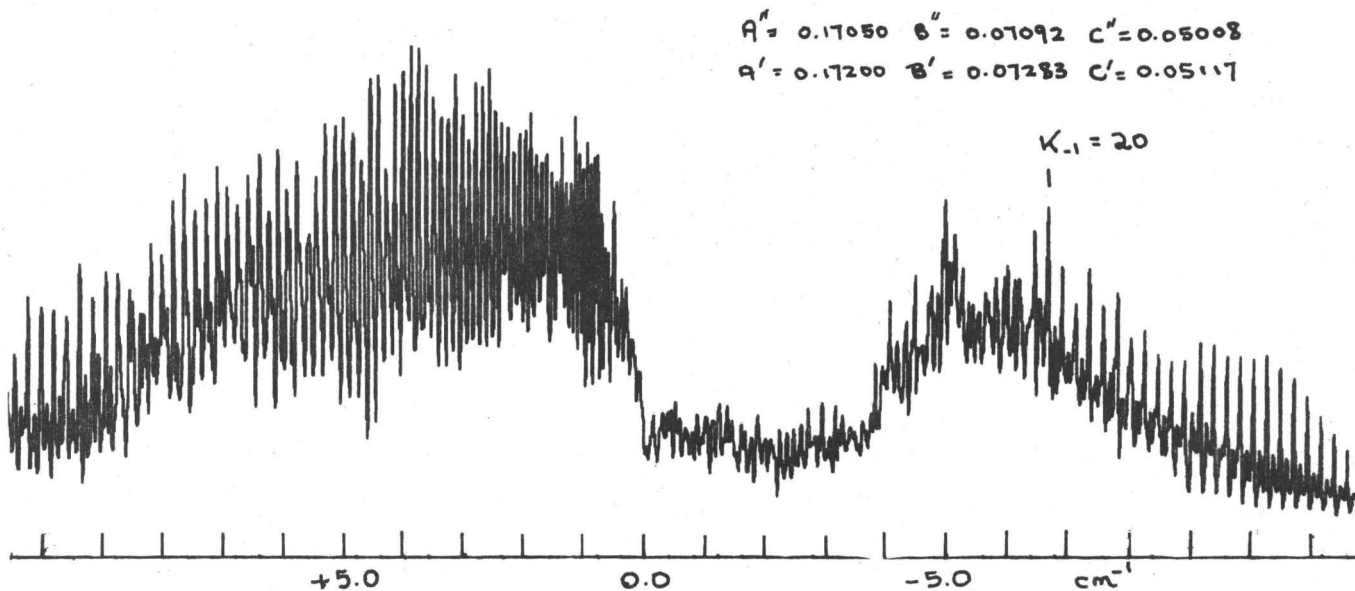


Figure 6.2. (a) Type C Contour Computed for the Origin of Oxalyl Chloride-Fluoride with Line Structure Produced by Head Formation in the K Subbands

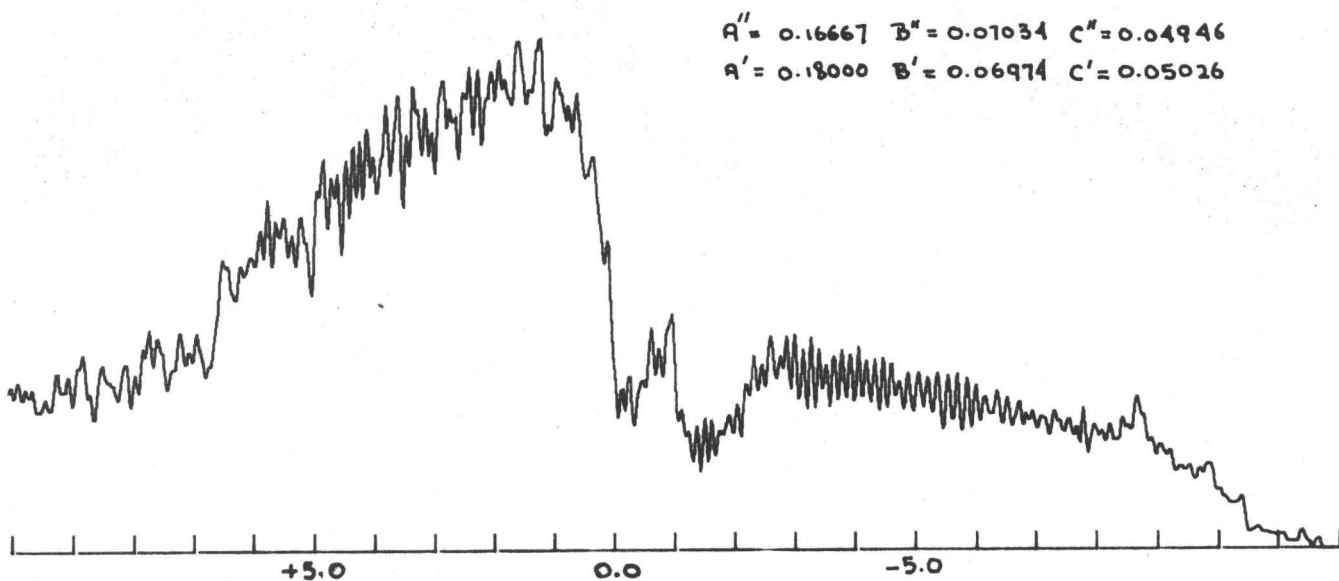


Figure 6.2 (b) Type C Contour Computed for the Origin of Oxalyl Chloride-Fluoride with Line Structure Produced by Multiple Coincidence of J Lines

$$A'' = 0.17050 \quad B'' = 0.07092 \quad C'' = 0.05008$$

$$A' = 0.17200 \quad B' = 0.07283 \quad C' = 0.05117$$

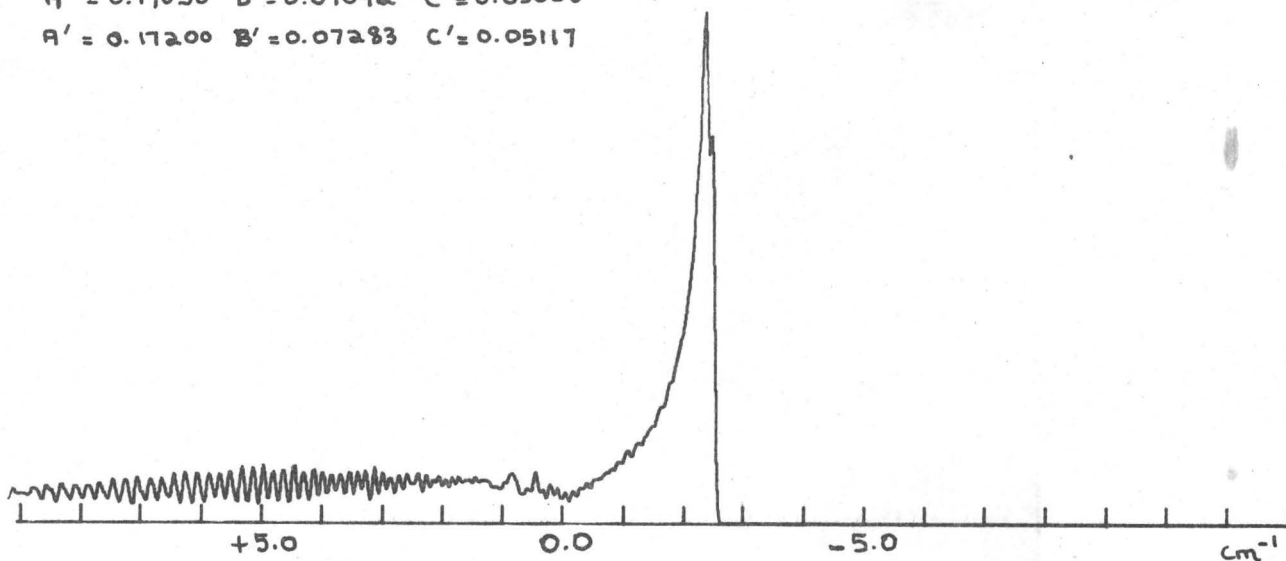


Figure 6.3. (a) Type A Contour Corresponding to the Type C Contour in Figure 6.2(a).

$$A'' = 0.17050 \quad B'' = 0.07092 \quad C'' = 0.05008$$

$$A' = 0.17200 \quad B' = 0.07283 \quad C' = 0.05117$$

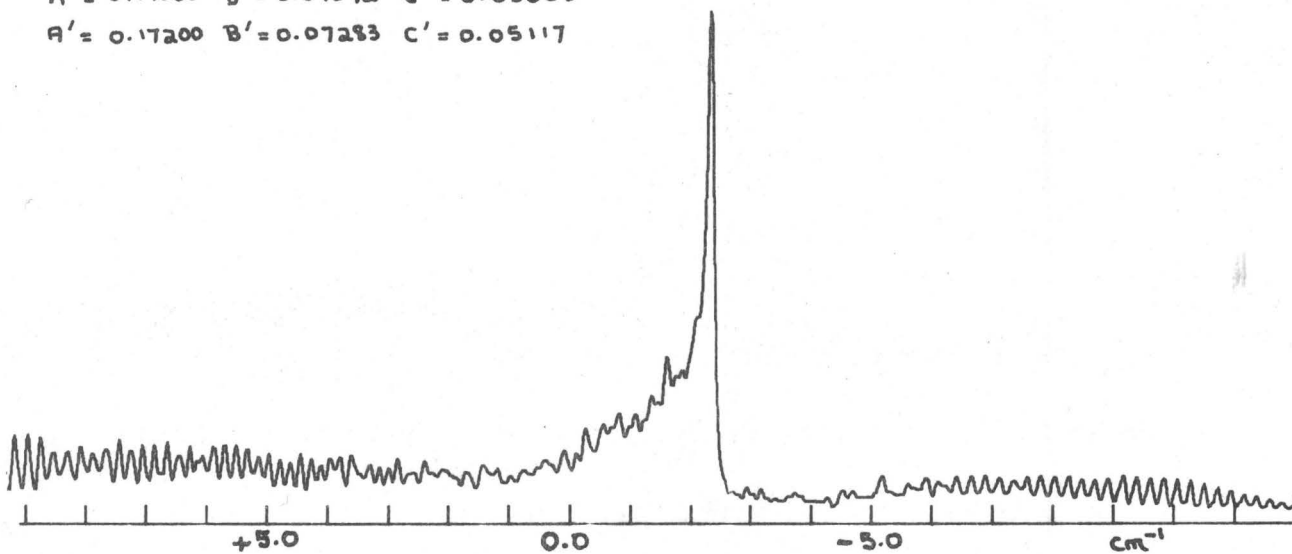


Figure 6.3. (b) Type B Contour Corresponding to the Type C Contour in Figure 6.2(a).

$$A'' = 0.16667 \quad B'' = 0.07034 \quad C'' = 0.04946$$

$$A' = 0.18000 \quad B' = 0.06974 \quad C' = 0.05026$$

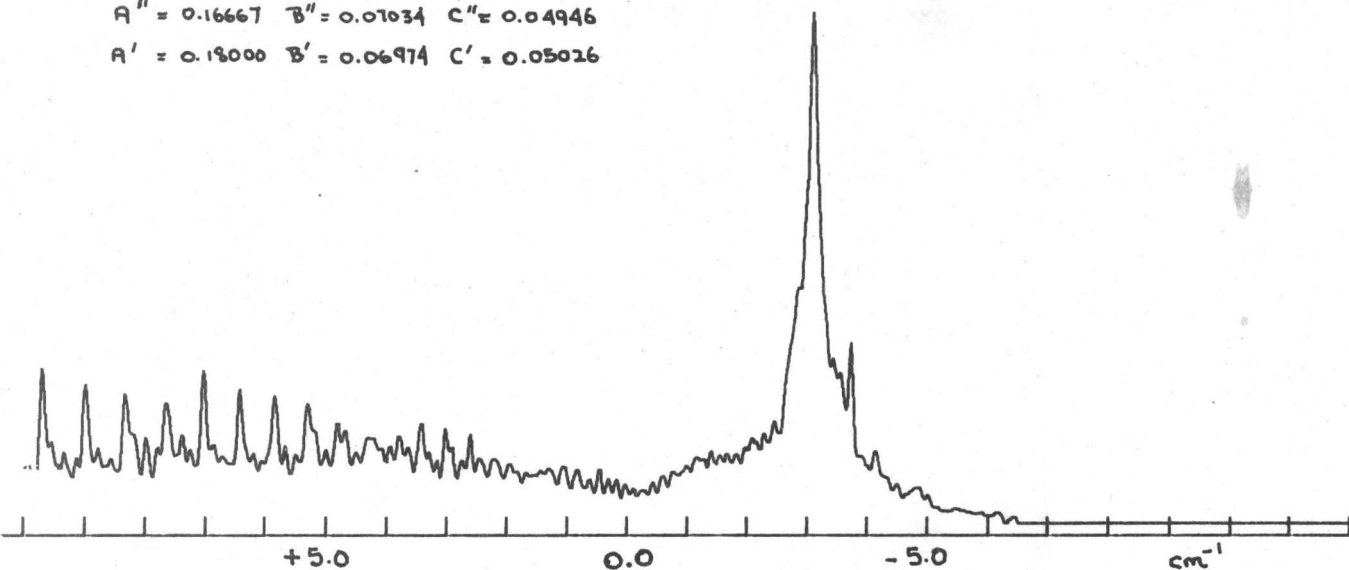


Figure 6.4. (a) Type A Contour Corresponding to the Type C Contour in Figure 6.2(b).

$$A'' = 0.16667 \quad B'' = 0.07034 \quad C'' = 0.04946$$

$$A' = 0.18000 \quad B' = 0.06974 \quad C' = 0.05026$$

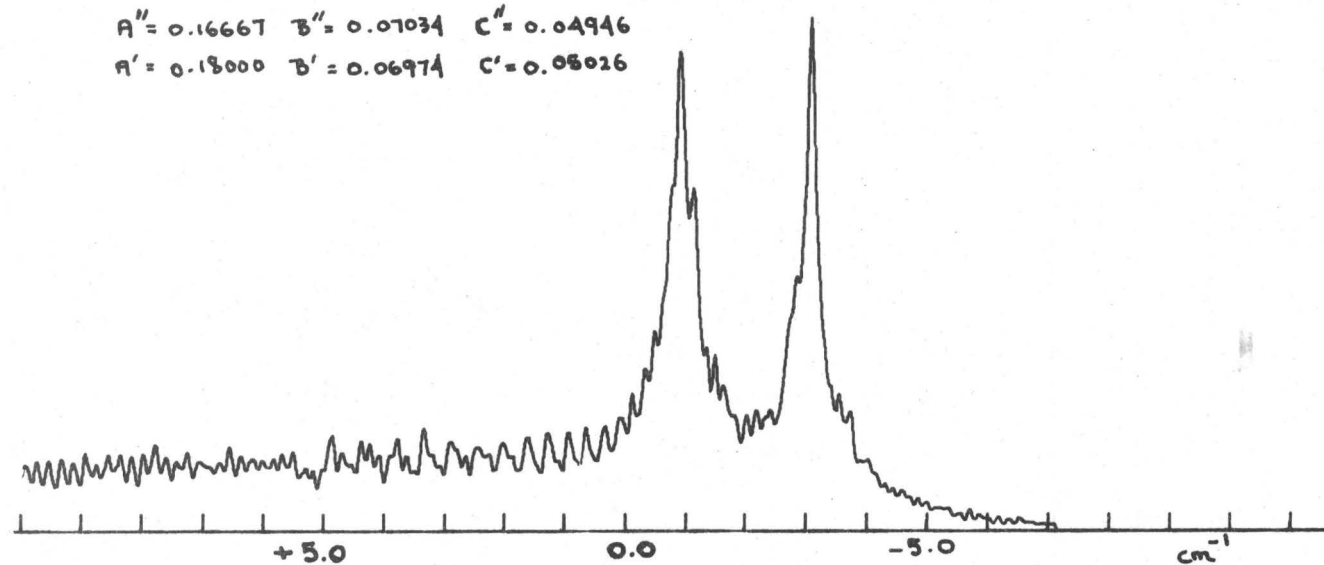


Figure 6.4. (b) Type B Contour Corresponding to the Type C Contour in Figure 6.2(b).

6.2 The Medium Resolution Contour

Theoretical rotational contours were generated by means of a computer program written by Parkin⁽⁶²⁾ but modified to calculate the asymmetric rotor eigenvalues for $J \leq 3$ exactly. In the program, eigenvalues for $3 < J < 85$ are obtained by an interpolation method in which eigenvalues are calculated exactly for 10 selected values of J . Only subbands with $K_{-1} < 30$ were calculated with the asymmetric rotor program; subbands with $30 < K_{-1} < 60$ were added to the contour by a symmetric rotor subroutine.

By means of the computed profiles, it was possible to show that the origin band contour under medium resolution could be satisfactorily identified as a C-type band of oxalyl chloride-fluoride. Since no information was available on the ground state rotational constants of COFCOCl₂, several sets of values were calculated from assumed ground state geometries. These values are listed in Table 6.1 and give an estimate of the magnitude and range of the rotational constants. Bond lengths and angles were selected by analogy with related molecules.

The profiles of the computed contours were sensitive to the values of ΔA ($A' - A''$), ΔB and ΔC , but not to the values of A'' , B'' , or C'' (within the range indicated by Table 6.1). An estimate of the value of ΔC was obtained by matching calculated heads with the observed head in Figure 6.1. The absorption in the region of this head can be attributed principally to the ${}^{r_q}Q$ and ${}^{p_q}Q^{\dagger}$ subbranches. In computed contours, these two subbranches appear as a central spike for $\Delta C \approx 0$, or as a blue or red degraded head for

[†]The first and second superscripts refer to ΔK_{+1} and ΔK_{-1} respectively.

TABLE 6.1

ROTATIONAL CONSTANTS FOR A SERIES OF ASSUMED GROUND STATE GEOMETRIES FOR OXALYL CHLORIDE FLUORIDE (trans)

r_{CC} Å	$r_{CO(F)}$ Å	$r_{CO(Cl)}$ Å	r_{CF} Å	r_{CCl} Å	$\angle CCO(F)$ deg.	$\angle CCO(Cl)$ deg.	$\angle COF$ deg.	$\angle COCl$ deg.	A cm^{-1}	B cm^{-1}	C cm^{-1}	κ
1.45	1.18	1.18	1.34	1.74	123	123	118	118	.0532	.0741	.1885	-.69
1.40	1.195	1.195	1.35	1.75	123	123	122	122	.0550	.0790	.1810	-.61
1.50	1.24	1.24	1.34	1.75	123	123	120	120	.0514	.0737	.1707	-.63
1.50	1.24	1.24	1.34	1.5	123	123	120	120	.0564	.0827	.1773	-.56
1.42	1.32	1.327	1.34	1.75	122	122	118	118	.0511	.0743	.1636	-.59
1.42	1.32	1.327	1.34	1.5	122	122	118	118	.0559	.0836	.1693	-.51
1.42	1.32	1.32	1.34	1.75	122	122	117	117	.0509	.0734	.1658	-.61
1.42	1.32	1.32	1.34	1.50	122	122	117	117	.0557	.0826	.1717	-.54
1.42	1.32	1.32	1.34	1.75	117	122	117	122	.0516	.0747	.1668	-.60

C positive or negative respectively. The same result is predicted by the empirical relation developed by McHugh et al⁽⁶³⁾ for "line" frequencies in the r_{qQ} and p_{qQ} subbranches of a C-type band.

$$\nu_Q = \nu_0 + \Delta C(n'' + 1)^2 - \Delta S \quad [6.1]$$

where $n = J + m$, $m = J - K_{-1}$ and $\Delta S = (2m^2 + 2m + 1)(\Delta A + \Delta B)/4$. The strongest rotational transitions in the Q subbranches occur for $J \approx K_{-1}$, where ΔS is small, and since n takes values from 0 upward, the degradation of the head depends principally on ΔC . It was found that $\Delta C \approx +0.0008 \text{ cm}^{-1}$ produced a reasonable match for the observed head.

The most intense subbranches of a C-type band of an asymmetric top are the p_{qP} , the p_{qQ} , the r_{qQ} and the r_{qR} subbranches.[†] The wing observed to high frequency from the head can be attributed principally to the r_{qR} subbranch while the low frequency wing can be attributed principally to the p_{qP} subbranch. It was found that values for $\Delta(A - \bar{B})^{\dagger\dagger}$ which lay outside the region -0.01 to $+0.01 \text{ cm}^{-1}$ produced a distinct head in the R or P wings respectively. Since the observed profile shows no head formation in either of the two wings, this established outside limits for $\Delta(A - \bar{B})$.

In a discussion of the calculation of absorption intensities associated with the band contour method Kidd and King⁽⁶⁴⁾ have pointed out the unsatisfactory nature of the simple approach used in current band contour programs. The medium resolution trace of the 3481 \AA band shows no distinctive sharp features, and it was felt that an attempt to obtain information from a simple matching of the intensity distributions in the experimental and calculated contours would be unwarranted.

[†]See reference (61), section 8g.

^{††} $\bar{B} = \frac{1}{2} (B + C)$ for a prolate top or $\bar{B} = \frac{1}{2} (A + B)$ for an oblate top.

6.3 The Fine Structure in the Very High Resolution Contour

The 3481 Å band photographed under very high resolution shows clearly a series of "lines" to the red of the strong head. Another series of "lines" can be seen less clearly to the blue of the head. The frequencies of these line-like features are listed in Table 6.2. (Frequency measurements of the very high resolution photographs were reproducible to within a hundredth of a wave number, and accuracy was better than $\pm 0.1 \text{ cm}^{-1}$.)

The rotational constants of a molecule as large as COFCOCl are so small that rotational line structure is not expected, even under very high resolution. The "lines" observed in the fine structure seen in Figure 6.1 do not arise from individual rotational transitions, but rather correspond to the coincidental superposition of several strong rotational lines. Rotational fine structure of this type has been observed for a considerable number of large molecules, most of them planar and aromatic, and this subject has been reviewed by Brown⁽⁶⁵⁾.

Fine structure can occur in the rotational contours of large molecules as a result of two types of pattern in the rotational lines: (a) head formation in the individual subbands characterized by given values of K''_{+1} and K''_{-1} , can produce successive "lines" due to the successive subbands, or (b) the spacing between neighbouring subbands, characterized by given K''_{+1} and K''_{-1} , can cause a phasing of the individual lines in the subbands with the result that many rotational lines superimpose to produce a fine structure "line". The spacing of the "lines" corresponds to the rotational constants in different ways for the two classes discussed above, and it is important to decide which class is applicable here. However, no completely satisfactory analysis of the fine structure has been obtained for oxalyl chloride-fluoride, and the two

TABLE 6.2

Line Frequencies of the Observed Fine Structure in the Origin Band
of COFCOCl

<u>BLUE SERIES</u>		<u>RED SERIES</u>	
Index [†]	Frequency (cm ⁻¹)	Index [†]	Frequency (cm ⁻¹)
47	28729.84	31	28722.03
46	.75	32	28721.93
45	.65	33	.81
44	.56	34	.69
43	.46	35	.58
42	.36	36	.47
41	.27	37	.36
40	.19	38	.25
39	28729.09	39	.12
38	28728.98	40	28721.01
37	.88	41	28720.88
36	.79	42	.77
35	.69	43	.65
34	.59	44	.51
33	.48	45	.43
32	.38	46	.31
31	.29	47	.19
30	.21	48	28720.07
29	.11	49	28719.96
28	28728.04	50	.84
27	28727.93	51	.71
26	.84	52	.58
25	.74	53	.45
24	.65	54	.34
23	.60	55	.22
22	.45	56	28719.10
21	.38	57	28718.97
20	.28	58	.84

BLUE SERIESRED SERIES

Index [†]	Frequency (cm ⁻¹)	Index [†]	Frequency (cm ⁻¹)
19	28727.20	59	28718.72
18	.09	60	.60
17	28727.01	61	.47
16	28726.91	62	.34
15	.84	63	.22
14	.76	64	28718.09
13	.66	65	28717.98
12	.57	66	.85
11	.47	67	.73
10	.37	68	.59
		69	.47
		70	.34
		71	.22
		72	.11
		73	28716.96
		74	.84
		75	.73
		76	.60
		77	.46
		78	.33
		79	.22
		80	28716.09
		81	28715.95
		82	.85
		83	.69
		84	.58
		85	.44
		86	.31
		87	.19
		88	28715.06
		89	28714.91
		90	.80

[†]This index has been assigned on the basis of extrapolating the series to an origin near 28725.5 cm⁻¹, the best estimate of the frequency of the band origin.

classes of fine structure are discussed in some detail in order to elaborate the difficulties encountered in applying to oxalyl chloride-fluoride the equations which have been developed to explain fine structure in other large molecules.

(a) Head Formation

Fine structure produced by head formation in the individual subbands has been reported for p-benzoquinone⁽⁶⁶⁾, phenol⁽⁶⁷⁾, and 2,1,3-benzothiadiazole⁽⁶⁸⁾. These molecules have been treated as nearly symmetric tops; symmetric top formulae were employed to make estimates of the rotational constants and these estimated values were refined by computer methods.

Within a subband (K''_{+1} , K''_{-1} fixed) head formation takes place in the P or R branch for ΔB positive or negative respectively. The head is formed at a J value approximately equal to $(\bar{B}' + \bar{B}'')/2\Delta\bar{B}$ for a P branch or $(3\bar{B}' - \bar{B}'')/2\Delta\bar{B}$ for an R branch. It is assumed that the separation of the heads in successive subbands is the same as the separation of successive subband origins. The positions of the subband origins are given by

$$v_0^{\text{sub}} \begin{matrix} \text{P} \\ \text{R} \end{matrix} = v_0 + (A' - \bar{B}') \pm 2(A' - \bar{B}')K'' + \Delta(A - \bar{B})K''^2 \quad \begin{matrix} K'' = 1, 2, 3, \dots \\ K'' = 0, 1, 2 \end{matrix} \quad [6.2]$$

$$v_0^{\text{sub}} \text{(Q)} = v_0 + \Delta(A - \bar{B})K''^2 \quad K'' = 0, 1, 2 \quad [6.3]$$

for the perpendicular ($\Delta K = \pm 1$) and parallel ($\Delta K = 0$) transitions of a prolate symmetric top respectively. (The corresponding expressions for the oblate limit are obtained by interchanging A and C.) If the heads are assigned a numerical index, then the head position as a function of the index has a linear coefficient which corresponds to a first approximation to $2(A' - \bar{B}')$ for perpendicular bands or to 0.0 for parallel bands. The quadratic dependence corresponds to $\Delta(A - \bar{B})$. The quadratic dependence is independent of the

choice of an indexing system, but the linear dependence is sensitive to this choice.

The fine structure produced by head formation depends upon the near symmetric top behaviour of rotational lines in the region of fine structure formation. The appearance of regular fine structure becomes more likely as $\chi = (2B - A - C)/(A - C)$ tends to the symmetric top limits ± 1 , and for given χ should appear for rotational transitions associated with high K and low J .

The well-defined fine structure which lies to the red of the strong head observed in Figure 6.1 almost certainly arises in the P^qP subbranch. The regularity of the fine structure "lines" increases with the value of K in agreement with the behaviour expected under (a) above. The frequencies of the red series were fitted by least squares to an equation of the form:

$$Y(I) = A_0 + A_1 I + A_2 I^2 \quad [6.4]$$

where I refers to an indexing system by which the observed "lines" are numbered. A value of $-0.0001308 \text{ cm}^{-1}$ is obtained for A_2 independent of the numbering of the bands, and a value near -0.1 cm^{-1} is obtained for A_1 for any choice of index which places the origin of the series near the head. This would suggest a value for $(A - \bar{B})$ of approximately 0.05 cm^{-1} . It can be seen by inspection of Table 6.1 that this value is almost half that expected on the basis of estimated geometries. This would appear to eliminate head formation as a mechanism for observing fine structure, but one further possibility exists.

For oxalyl chloride-fluoride there is the possibility that the observed fine structure consists of the staggered superposition of the spectra of the ^{35}Cl and ^{37}Cl isotopic molecules, each of which have fine structure spacing of $\sim 0.2 \text{ cm}^{-1}$. This proposal is supported by the observed

behaviour in oxalyl fluoride, where the line spacing of $\sim 0.3 \text{ cm}^{-1}$ agrees more closely with the trial molecular constants; however, a strong argument against it is that a regular 3:1 intensity alternation corresponding to the relative concentrations of the two isotopic molecules is not obvious in the spectrum.

The postulate of two superimposed spectra requires a re-indexing of the observed lines in which only alternate lines are numbered. Then in equation [6.4], the least squares fit gives values for A_2 of -0.00051 and -0.00059 for the two postulated series in the P wing while values for A_1 are near 0.2 cm^{-1} . The lines in the red series become obscured shortly after line 60 of the series (i.e., line ~ 30 of the staggered series). Since the restriction $J > K$ means that as K increases lines of successively increasing J are missing from the spectra, a point will be reached in successive subbands where there are no J lines to contribute to the subband head. If it is assumed that this occurs at $K \sim 50$, then a value of approximately $0.12/100$ or $+0.0012 \text{ cm}^{-1}$ is predicted for $\Delta\bar{B}$. We thus have the following relations predicted among the rotational constants: $A' - \bar{B}' \approx 0.1 \text{ cm}^{-1}$, $\Delta(A - \bar{B}) \approx -0.0005 \text{ cm}^{-1}$, $\Delta\bar{B} \approx +0.0012 \text{ cm}^{-1}$. If in addition, the inertial defect ($I_C - I_B - I_A$) is assumed to be zero, then all six rotational constants can be determined by choosing a value for one of them. A choice for A' of 0.1720 cm^{-1} in line with the values of Table 6.1, provides a set of ground and excited state rotational constants for which $\Delta C = +0.0011 \text{ cm}^{-1}$ in keeping with the requirements predicted by Section 6.2. A contour computed from these rotational constants had a suitable profile and showed the desired fine structure in the P wing. A composite contour was constructed by superimposing two contours (corresponding to the two isotopic molecules) with the

intensity ratio 3:1 and an assumed relative shift of 0.1 cm^{-1} to the blue for the COFCO³⁷Cℓ contour. (In the experimental contour, a possible isotope shift of $<0.2 \text{ cm}^{-1}$ to the blue was observed although a red shift can not be ruled out.) The composite contour, shown in Figure 6.2a, gives near agreement with the observed contour. The heads (lines) of the proposed COFCO³⁵Cℓ and COFCO³⁷Cℓ series have been identified in Figure 6.2a in terms of the K value of the subband in which the head occurred. Since head formation in each specific subband of the P^qP subbranch occurs to the red of the subband origins the series of lines produced in the computed contour extrapolate to an origin not at $\nu_0 - (A' - \bar{B}')$ (the frequency of the origin of the first K subband in the symmetric top limit), but to a point some 2.4 cm^{-1} to the red of this. The numbering of the K heads in Figure 6.2a then does not correspond to the empirical indexing system employed in Table 6.2.

The series of lines observed to the blue of the origin can be attributed to a system of heads in the R^oP subbranch. The poor definition of the blue series is in agreement with the relatively weak intensity of this subbranch. A least squares fit to equation [6.4] of the frequencies of alternate lines of the blue series gives a quadratic dependence which agrees with the quadratic coefficients for the two red series, but the linear coefficient determined for any reasonable indexing of the blue series is smaller (~ 0.17) than the corresponding term for the blue. This is unexplained except for the suggestion that it results from a deviation from symmetric top behaviour.

(b) Line Coincidences (Analytical)

The observation of fine structure in the rotational profiles of

large molecules has stimulated the development of simplified expressions for the energy levels of asymmetric top molecules which could be used in special cases to predict multiple coincidences among the rotational transitions, and line-like features in the rotational profile. This material has been reviewed by Brown⁽⁶⁵⁾. Although this approach has yielded a great deal of information for some other planar molecules, it has not been possible to apply any of the simplified expressions to the case of oxalyl chloride fluoride. Since the explanation given in Section 6.3(b) of the fine structure observed in the 3481 Å band of COFCOCl is not completely satisfactory, it was initially felt that this second type of behaviour might provide a better solution to the problem. A detailed discussion is given here to indicate that these derived expressions cannot be applied to oxalyl chloride-fluoride.

Simplified formulae for the energy levels of asymmetric top molecules can be obtained from a method developed by Gora [6.4]. The energy levels are given by

$$E(A,B,C) = CJ(J+1) + \frac{1}{2} (2J+1)m_1 [(B-C)(A-C)]^{1/2} - \frac{1}{4} m_2 (A+B-2C) \quad [6.5]$$

if correlation is made to the oblate top limit, or by

$$E(A,B,C) = AJ(J+1) - \frac{1}{2} (2J+1)m_1 [(A-B)(A-C)]^{1/2} + \frac{1}{4} m_2 (2A-B-C) \quad [6.6]$$

if correlation is made to the prolate limit.

$$m_n = (m+1)^n + m^n \quad [6.7]$$

$$m = J - K_{+1} \text{ (oblate) or } J - K_{-1} \text{ (prolate)}$$

These simplified expressions are valid in the region of high J and low K_{+1} for equation [6.5] or high J and low K_{-1} for equation [6.6] where the "K splitting" of the asymmetric top levels is absent. These conditions differ from the conditions for fine structure through head formation described in Section 6.3a.

In the case of planar molecules, equation [6.5] undergoes an additional simplification. Substitution of the relation for zero inertial defect

$$I_C = I_A + I_B \quad [6.8]$$

$$C^2 = (A-C)(B-C) \quad [6.9]$$

gives

$$E(A,B,C) = CJ(J+1) + \frac{1}{2} C(2J+1)m_1 - \frac{1}{4} m_2(A+B-2C) \quad [6.10]$$

or

$$E(A,B,C) = C(n+1)^2 - S \quad [6.11]$$

$$n = J + m$$

$$S = \frac{1}{4} m_2(A + B)$$

These expressions are based on the correlation to the oblate limit. No corresponding simplification of the prolate expression [6.6] is possible, and it has been customary to discuss all molecules - even near prolate tops ($K < 0$) - in terms of expression [6.11] and the selection rules for the oblate limit.

The rotational transitions of an asymmetric top (defined in terms of ΔJ , ΔK_{+1} and ΔK_{-1}) can be obtained from the above expressions for the energy levels. The intense transitions are those for which ΔK_{+1} , $\Delta K_{-1} = 0$, ± 1 , and the intense branches of the three bands have been summarized in Table 6.3. In cases where a simple expression for line frequencies in the branch can be obtained from equations [6.10] or [6.11] the expressions have

been included in Table 6.1. It can be seen that for an asymmetric top, on the basis of equations [6.5] and [6.10] fine structure can be expected in the P and R wings of the rotational contour of type A and B bands (perpendicular for the oblate top), and in the Q wing of the type C band (parallel for the oblate top).

Oxalyl chloride-fluoride displays fine structure in the P wing of a type C band. Since this was not predicted to occur by the expressions listed in Table 6.3, equations [6.5] and [6.6] have been examined in more detail to see if additional cases of line coincidence can be predicted. For the P^q_P branch, the m,n (oblate) selection rules are $\Delta m = -1$, $\Delta n = -2$, and equation [6.11] gives

$$\Delta E = -4nC' + (n+1)^2\Delta C + m(A+B) - \frac{1}{4} m_2(\Delta A + \Delta B) \quad [6.12]$$

Multiple coincidences in the high J low K_{+1} region occur only if (A+B) is some integral multiple of C. In that case where

$$\frac{A+B}{C} = \frac{AB}{C^2} = x \quad [6.13]$$

$$\Delta E = -(4n - mx)C' + (n+1)^2\Delta C - \frac{1}{4} m_2(\Delta A + \Delta B) \quad [6.14]$$

Thus for example if x is equal or near 3.0, multiple line coincidences may be expected between the transitions

$$P^q_P(J,K), P^q_P(J_{+1}, K_{+5}), P^q_P(J_{+2}, K_{+10}) \dots$$

while if x is 4.0 multiple line coincidences may be expected for

$$P^q_P(J,K), P^q_P(J, K_{+1}), P^q_P(J, K_{+2}) \dots$$

Again the values of ΔA , ΔB and ΔC must be small.

If, instead, the molecule is considered as a near prolate top, and

TABLE 6.3

Intense Branches for the A, B and C Type Bands of an Asymmetric Top Molecule with Simple Formula for the Line Energies of the Rotor as a Near Oblate Top where These Exist

Band Type	Intense Transitions	Reduced Expressions for Line Energy	Δm	Δn
A	qp _P	$\Delta E = \nu_0 + \Delta C n^2 - (2n+1)C'' - \Delta S$	0	-1
	qp _Q , qr _Q	Not Available.	+1	+1
	qr _R	$\Delta E = \nu_0 + \Delta C(n+1)^2 + (2n+3)C' - \Delta S$	0	+1
B	pp _P , rp _P	$\Delta E = \nu_0 + \Delta C n^2 - (2n+1)C'' - \Delta S$	0	-1
	pr _P	Not Available.	-2	-3
	pr _Q , rp _Q	Not Available.	+1	+1
	pr _R , rr _R	$\Delta E = \nu_0 + \Delta C(n+1)^2 + (2n+3)C' - \Delta S$	0	+1
	rp _R	Not Available.	+2	+3
C	pq _P	Not Available.	-1	-2
	rq _Q , pq _Q	$\Delta E = \nu_0 + \Delta C(n+1)^2 - \Delta S$	0	0
	rq _R	Not Available.	1	2

$$m = J - K_{+1}; n = J + m$$

$$S = \frac{1}{4} m_2(A+B)$$

$$m_2 = (m+1)^2 + m^2$$

$$\Delta E = E' - E''$$

equation [6.6] is employed, the selection rules become $\Delta J = -1$, $\Delta m = 0$, and the transition energies are given by

$$\begin{aligned} \Delta E = & -2A''J + (2J - 2K_{-1} + 1) [(A'' - B'')(A'' - C'')]^{1/2} \\ & + (J^2 - J)\Delta A + (2J^2 - 2JK + K - \frac{1}{2})\Delta [(A - B)(A - C)]^{1/2} + \frac{1}{4} m_2 (2\Delta A - \Delta B - \Delta C) \end{aligned} \quad [6.15]$$

The condition for multiple coincidences in this case is

$$\frac{2A''}{[(A'' - B'')(A'' - C'')]^{1/2}} = \text{Integer} = n \quad [6.16]$$

when
$$\begin{aligned} \Delta E = & -2A''[J + \frac{1}{n}(2J - 2K_{-1} + 1)] \\ & + \Delta A \text{ etc.} \end{aligned} \quad [6.17]$$

It should be noted that whereas the expressions of Table 6.3 predict fine structure in the high J , low K_{+1} region provided ΔA and ΔB are small, equations [6.14] and [6.17] require in addition a very specific relationship between A , B , and C . The fine structure predicted by equation [6.14] should have a spacing equal to C' while that predicted by equation [6.17] should have a fine spacing equal to $2A''$. It has been indicated in Table 6.1 that $C' \approx 0.05 \text{ cm}^{-1}$ while $A'' \approx 0.16 \text{ cm}^{-1}$. Since the observed spacing is approximately 0.1 cm^{-1} , equation [6.14] or [6.17] cannot explain the observed fine structure.

It has not been possible to extend the methods developed by McHugh et al⁽⁶³⁾ to the case of oxalyl chloride-fluoride.

(c) Line Coincidences (Empirical)

The equations discussed in the previous section do not include all types of superposition of the lines from different K subbands. If the molecule is treated as a near symmetric top, the spacing of the lines in a

K subband is determined approximately by the values of \bar{B} and $\Delta\bar{B}$, and the spacing between the K subband origins is determined approximately by $(A' - \bar{B}')$ and $\Delta(A - \bar{B}')$. An appropriate choice of rotational constants can produce the sought after multiple coincidences between the rotational lines of the K subbands for which the K_{-1} , K_{+1} values differ by 1, 2, 3, etc.

The Parkin program was used to print out individual line frequencies. Values for $\bar{B} \approx 0.06 \text{ cm}^{-1}$ and $\Delta\bar{B} \approx +0.0001 \text{ cm}^{-1}$ produced line spacings in agreement with observed fine structure (linear coefficient $\approx 0.1 \text{ cm}^{-1}$, quadratic coefficient -0.00013 cm^{-1}) in the K subbands with K greater than about 15. These two values together with $\Delta C = +0.0008 \text{ cm}^{-1}$ and an assumed value for A' are sufficient to determine the six rotational constants of the planar molecule (inertial defect assumed zero). It was initially assumed that $2(A' - \bar{B}')$ should be some integral multiple of the linear coefficient of the observed "line" structure, but when A' was chosen to give $2(A' - \bar{B}')$ the desired value, the resultant value of $\Delta(A - \bar{B})$ was of the order of $+0.01 \text{ cm}^{-1}$. Such a large value for $\Delta(A - \bar{B})$ resulted in a spacing of subband origins which was quadratically dependent on K and which did not create the multiple superpositions. It thus proved impossible to choose a value for A' analytically. Fine structure could be obtained in the computed contour by empirical adjustment of A' . A contour with $A' = 0.1800 \text{ cm}^{-1}$ is shown in Figure 6.2b. This value for A' is not unique and similar contours could be obtained for several other values.

It should be noted that in this section (6.3(c)), it has been assumed that the observed fine structure could be attributed solely to the more abundant $\text{COFCO}^{35}\text{Cl}$ isotopic molecule.

6.4 General Comments on the Rotational Structure

In this study of the rotational contour, an attempt was made to satisfy two objectives: (a) to show that the assigned origin at 3481 \AA could satisfactorily be classified as a type C band, and (b) to explain the cause of the regular fine structure observed in this band. It was fairly simple to establish requirements for the rotational constants which would satisfy criterion (a). Within these requirements it was shown that the fine structure could, potentially, be explained in two ways - through head formation in K subbands, or through constructive phasing of the J lines from neighbouring K subbands.

The contours shown in Figure 6.2 are preliminary contours which demonstrate that criterion (b) can be satisfied. The rotational constants which produce the fine structure shown in Figure 6.2(a) and 6.2(b) have not been optimized to produce the most satisfactory medium resolution contour. In view of the fact that the ground state rotational constants are not known, the results of such a procedure cannot have too much significance. It is felt that the next step in studying the oxalyl chloride-fluoride problem should be a consideration of the rotational structure of the corresponding bands of oxalyl chloride and oxalyl fluoride.

CHAPTER 7

CONCLUSIONS

The electronic absorption spectrum of oxalyl chloride-fluoride has been observed in the near ultraviolet. In keeping with the observed spectra of other oxalyl halides (oxalyl bromide, oxalyl chloride, oxalyl fluoride), the spectrum consists of discrete absorption in the region from 3000 Å to 4000 Å with intense continuous absorption to shorter wave lengths.

The discrete absorption of oxalyl chloride-fluoride (which belongs to the C_s point group) is of interest relative to the discrete spectra of the more symmetric oxalyl halides (which belong to the C_{2h} point group) because it represents a particularly simple example of the effect on an electronic spectrum of a reduction of molecular symmetry. Oxalyl chloride-fluoride differs from the chloride or the fluoride only by the replacement of a single atom at such a position in the molecule that the effect on the electronic and vibrational energy levels is small. COFCOCl₂ has been successfully treated as an approximate C_{2h} molecule; the $^1A''$ and $^3A''(n_{1a'}, \pi_{1a''}^*) \leftarrow \tilde{X}(^1A')$ transitions (which correlate with the 1A_u and $^3A_u(n_{og}^-, \pi_{au}^*) \leftarrow \tilde{X}(^1A_g)$ transitions of the C_{2h} oxalyl halides) have been observed with approximately the same energy and intensity as the corresponding allowed transition of oxalyl chloride or oxalyl fluoride, and the $^1A''$ and $^3A''(n_{1a'}, \pi_{2a''}^*) \leftarrow \tilde{X}(^1A')$ transitions (which correlate with the 1B_g and $^3B_g(n_{og}^-, \pi_{au}^*) \leftarrow \tilde{X}(^1A_g)$ transitions of the C_{2h} oxalyl halides) have been observed with an intensity that is much lower than the first $n \rightarrow \pi^*$ transition, while the corresponding transition of oxalyl chloride or oxalyl fluoride does not appear. The

first observation gives proof of the fact that molecular wave functions of the C_s molecule are very similar to those of the C_{2h} molecules while the second observation confirms the anticipated effect of asymmetric halogen substitution: transition moment integrals which were identically equal to zero (to a first order of approximation) for the C_{2h} oxalyl halides are small but non-zero for oxalyl chloride-fluoride by virtue of the decreased symmetry of the wave functions.

In addition, the vibrational analysis of the ${}^1A''$ and ${}^3A''(n_{1a'}, \pi_{1a}'')$ $\leftarrow \tilde{X}({}^1A')$ system of oxalyl chloride-fluoride reflects the decrease of symmetry. A larger number of fundamentals are active in the spectrum than were observed for the C_{2h} molecules for two reasons: (a) there are a larger number of totally symmetric fundamentals (which can have activity in the allowed $n \rightarrow \pi^*$ transition), and (b) a larger number of excited states can be effective in producing transition intensity for the non-totally symmetric mode through perturbations.

A general study of the electronic spectra of the oxalyl halides, and the related compounds glyoxal and biacetyl has produced new interpretations of the observed spectra, and simple CNDO calculations have proved to be very useful in the assignment of electronic transitions. A strong case has been advanced for the appearance, in the ultraviolet region, of the spectrum of the cis isomer of the oxalyl halides; the spectrum of the cis isomer occurs superimposed upon that of the trans. The results obtained are in general agreement with the spectra reported previously for cis acrolein and cis glyoxal. In addition, it has been shown that for glyoxal and biacetyl, the liquid and vapour phase ultraviolet spectrum is complicated by the presence of a third molecular species - a species formed through weak linkages between

two or more molecules. The spectra of these polymeric species are well isolated for glyoxal and biacetyl. Although no similarly well isolated system can be identified in the oxalyl halides, it is anticipated that polymeric species probably exist for the oxalyl halides and for a large number of other molecules. The presence of a polymeric species in the vapour phase is, perhaps, surprising and should be taken into consideration in experimental work related to the properties of such molecules.

BIBLIOGRAPHY

1. W. J. Balfour, Thesis (Ph.D.), McMaster University (1967).
2. W. J. Balfour and G. W. King, *J. Mol. Spect.*, 26, 384 (1968).
3. W. J. Balfour and G. W. King, *J. Mol. Spect.*, 27, 432 (1968).
4. W. J. Balfour and G. W. King, *J. Mol. Spect.*, 28, 497 (1968).
5. J. L. Hencher, Thesis (Ph.D.), McMaster University (1964).
6. G. W. King, "Spectroscopy and Molecular Structure", Holt, Rinehart, and Winston, Inc. (Toronto), 1964.
7. G. Herzberg, "Molecular Spectra and Molecular Structure, III, Electronic Spectra and Electronic Structure of Polyatomic Molecules", D. Van Nostrand Co. Inc. (Princeton, N.J.), 1966.
8. M. Adelhelm, Thesis (Dr. rer. nat.), Technischen Hochschule Stuttgart (1967).
9. G. W. King, *J. Sci. Instrumen.*, 35, 11 (1958).
10. D. C. Moule, P. D. Foo, A. Biernacki, *Journal of Physics*, E4, 449 (1971).
11. J. U. White, *J. Opt. Soc. Am.*, 32, 285 (1942).
12. H. J. Bernstein and G. Herzberg, *J. Chem. Phys.*, 16, 30 (1948).
13. J. A. Pople, D. P. Santry, G. A. Segal, *J. Chem. Phys.*, 43, S129 (1965).
14. J. A. Pople, G. A. Segal, *J. Chem. Phys.*, 43, S136 (1965).
15. J. A. Pople, G. A. Segal, *J. Chem. Phys.*, 44, 3289 (1966).
16. J. A. Pople and G. A. Segal, *J. Chem. Phys.*, 47, 158 (1967).
17. J. A. Pople, D. L. Beveridge, P. A. Dobosh, *J. Chem. Phys.*, 47, 2026 (1967).
18. M. J. S. Dewar, "Molecular Orbital Theory of Organic Chemistry", McGraw-Hill Book Company (New York), 1969, Chapters 2, 3.
19. H. L. McMurray, *J. Chem. Phys.*, 9, 231 (1941).
20. A. D. Walsh, *Trans. Far. Soc.*, 42, 66 (1946).
21. J. W. Sidman, *J. Chem. Phys.*, 27, 429 (1957).
22. K. Kuchitsu, T. Fukuyama, E. Morino, *J. Mol. Struct.*, 1, 463 (1968).
23. J. Paldus, D. A. Ramsay, *Can. J. Phys.*, 45, 1389 (1966).

24. R. Pariser, *J. Chem. Phys.*, 24, 250 (1956).
25. J. E. del Bené and H. H. Jaffé, *J. Chem. Phys.*, 48, 1807 (1968); 48, 4050 (1968); 49, 1221 (1968); 50, 1126 (1969).
26. S. P. McGlynn, T. Azumi, M. Kinoshita, "Molecular Spectroscopy of the Triplet State", New Jersey: Prentice-Hall (1969), Chapters 5, 6.
27. R. M. Hochstrasser, "Molecular Aspects of Symmetry", New York: W. A. Benjamin, Inc., Chapter 6.
28. D. S. McClure, *J. Chem. Phys.*, 20, 682 (1952);
29. M. Blume, R. E. Watson, *Proc. Roy. Soc.*, A271, 565 (1963).
30. G. Fleury, Thesis, "Analyse Vibrationnelle de Molecules du Type C_2O_2XY ", Université de Montpellier (Faculty des Sciences), July 4, 1970.
31. H. W. Thompson, *J. Chem. Phys.*, 7, 855 (1939); *Trans. Far. Soc.*, 36, 988 (1940).
32. J. C. D. Brand, *Trans. Far. Soc.*, 50, 431 (1955).
33. J. N. Murrell, "The Theory of Electronic Spectra of Organic Molecules", London: Methuen and Co. Ltd., p. 168 on.
34. G. W. King, *J. Chem. Soc.*, 1957, 5054.
35. F. W. Birss, J. M. Brown, A. R. H. Cole, A. Lofthus, S. L. N. G. Krishnamachari, G. A. Osborne, J. Paldus, D. A. Ramsay, L. Watmann, *Can. J. Phys.*, 48, 1230 (1970).
36. D. M. Agar, E. J. Bair, F. W. Birss, P. Borrell, P. C. Chen, G. N. Currie, A. J. McHugh, B. J. Orr, D. A. Ramsay, J-Y. Roncin, *Can. J. Phys.*, 49, 323 (1971).
37. J. W. Sidman, D. S. McClure, *J. Am. Chem. Soc.*, 77, 6461 (1955).
38. C. L. Carpenter, L. S. Forster, *J. Chem. Phys.*, 62, 874 (1958).
39. L. S. Forster, *J. Am. Chem. Soc.*, 77, 1417 (1955).
40. L. S. Forster, *J. Chem. Phys.*, 26, 1761 (1957).
41. W. Goetz, A. J. McHugh, D. A. Ramsay, *Can. J. Phys.*, 48, 1 (1970).
42. V. R. Ells, *J. Am. Chem. Soc.*, 60, 1864 (1938).
43. G. Lucazeau and C. Sandorfy, *J. Mol. Spect.*, 35, 214 (1970).
44. R. K. Harris, *Spectrochimica Acta*, 20, 1129 (1964).

45. W. Holzer and D. A. Ramsay, *Can. J. Phys.*, 48, 1759 (1970).
46. G. N. Currie and D. A. Ramsay, *Can. J. Phys.*, 49, 317 (1971).
47. J. C. D. Brand and D. G. Williamson, *Disc. Far. Soc.*, 35, 184 (1963).
48. J. M. Hollas, *Spectrochimica Acta*, 19, 1425 (1963).
49. A. C. P. Alves, J. Christoffersen, J. M. Hollas, *Mol. Phys.*, 20, 625 (1971); Erratum, 21, 384 (1971).
50. E. J. Bair, W. Goetz, D. A. Ramsay, *Can. J. Phys.*, 21, 2710 (1971).
51. J. L. Hencher and G. W. King, *J. Mol. Spect.*, 16, 158 (1965).
52. J. L. Hencher and G. W. King, *J. Mol. Spect.*, 16, 168 (1965).
53. K. G. Kidd and G. W. King, *J. Mol. Spect.*, 28, 411 (1968).
54. J. R. Durig and S. E. Hannum, F. G. Baglin, *J. Chem. Phys.*, 54, 2367 (1971).
55. J. R. Durig and S. E. Hannum, *J. Chem. Phys.*, 52, 6089 (1970).
56. J. R. Durig, S. C. Brown, S. E. Hannum, *J. Chem. Phys.*, 54, 4428 (1971).
57. B. D. Saksena and G. S. Jauhri, *J. Chem. Phys.*, 36, 2233 (1962).
58. J. W. Sidman, *J. Am. Chem. Soc.*, 78, 1527 (1956).
59. J. C. D. Brand, J. H. Callomon, J. K. G. Watson, *Disc. Far. Soc.*, 35, 175 (1963).
60. J. C. D. Brand, J. K. G. Watson, reported in *J. Mol. Spec.*, 10, 166 (1963).
61. H. C. Allen, Jr., P. C. Cross, "Molecular Vib-Rotors", John Wiley and Sons Inc. (New York), 1963.
62. J. E. Parkin, *J. Mol. Spect.*, 15, 483 (1965).
63. A. J. McHugh, D. A. Ramsay, I. G. Ross, *Aust. J. Chem.*, 21, 2835 (1968).
64. K. G. Kidd, G. W. King, *J. Mol. Spect.*, 40, 461 (1971).
65. J. M. Brown, *J. Mol. Spect.*, 31, 118 (1969).
66. J. M. Hollas, *Spectrochim. Acta*, 20, 1563 (1964).
67. J. Christoffersen, J. M. Hollas, G. H. Kirby, *Proc. Roy. Soc.*, A307, 97 (1968).
68. J. Christoffersen, J. M. Hollas, R. A. Wright, *Proc. Roy. Soc.*, A308, 537 (1969).

APPENDIX I

THE VAPOUR PHASE RAMAN SPECTRUM OF OXALYL CHLORIDE

The trans oxalyl halide molecules of the type $(COX)_2$ belong to the C_{2h} point group and have a center of symmetry. Since only the totally symmetric ground state fundamentals are active in the UV spectrum, it is necessary to compare vapour phase values for the ground state frequencies from the UV spectrum with liquid phase values from the Raman. In order to avoid the problem of vapour-liquid shifts in comparing the frequencies of the fundamental modes between Raman and UV, attempts were made to obtain the Raman spectra of the oxalyl halides in the vapour phase.

The first experiment which was attempted was to employ a multiple reflection collecting cell in order to increase the efficiency of collection from a "folded" (multiply reflected) laser beam. A 10 cm collecting cell was designed. The aperture of the cell was matched to the aperture of the spectrograph in the manner outlined by Callomon^(AI-1), and in addition the cell was so designed that the entire height of the entrance slit (approximately 5 cm) was illuminated.

For the experiment, a Spex, Czerny-Turner triple slit monochromator was used with a Spectra Physics model 140, 2-watt argon ion laser. The slits of the spectrograph are vertical, and the laser beam was multiply reflected within the cell in the plane parallel to the slits and the axis of the spectrometer by means of plane parallel mirrors above and below the cell. The laser beam was reflected about 10 times.

The laser spectrum of atmospheric nitrogen was run using the cell. It was found that no significant improvement was achieved over the normal

simpler configuration under which Raman spectra were usually run. An analysis of the two configurations was made.

(a) The Normal Configuration: In this configuration, the laser beam is passed twice through the line where the entrance slit is "back-focussed" by a condensing lens. The scattered light is collected once in the forward direction and once in the backward direction (after reflection from a concave mirror) through a solid angle equivalent to the aperture of the instrument.

(b) The Multiple-Reflection Collecting Cell: In this configuration a greater number of passes of the laser beam are employed, but none of them coincide with the position at which the entrance slit is "back-focussed". This means that only a negligible amount of light is collected in the spectrometer from a simple forward reflection. Although the scattered light from any point of the cell is collected through a solid angle equivalent to the aperture of the cell, much of it enters the spectrograph only after multiple reflections from the mirrors of the cell, with loss of intensity after each reflection. In addition, the laser beam does not illuminate all points of the cell.

It was concluded that for a condensed source such as the laser beam, which has dimensions that match the slit width of the spectrometer, it is not possible to use a multiple-reflection collecting cell to advantage. Such a cell has been used to obtain Raman spectra using a mercury arc light source (see reference AI-2). In this instance, the source illuminates every point in the cell, and the considerations employed in (a) and (b) above indicate that the multiple reflection collection cell provides a significant advantage in this case.

In order to settle a controversy in the UV analysis of the oxalyl

halides (see Section 4.3) an additional attempt was made to obtain the Raman spectrum of oxalyl chloride in the vapour phase. For this experiment, the spectrograph was set up in the usual configuration, and a cylindrical glass cell of ~ 3 mm diameter was used. A small amount of oxalyl chloride was sealed in the micro cell by use of a vacuum line. The cell was mounted in the cell holder of the spectrometer and heated to approximately 100°C by means of a hot air gun, thus vapourizing the sample. A spectrum was then run with spectrometer slits set at ~ 2 mm and without a filter in the laser beam (the latter to provide maximum power in the exciting frequency). A crude Raman spectrum overlapped by the plasma lines from the argon ion laser was obtained. It was possible to obtain some of the ground state frequencies in the vapour phase, and these frequencies have been listed in Table A1. No band can be observed in the region of 1217 cm^{-1} , the value proposed by Balfour and King^(AI-3) for the ground state frequency of the C-C stretching mode of oxalyl chloride in the vapour phase.

REFERENCES

- AI-1. J. H. Callomon, *Can. J. Phys.*, 34, 1048 (1956).
- AI-2. B.P. Stoicheff, *Can. J. Phys.*, 32, 330 (1954).
- AI-3. W. J. Balfour and G. W. King, *J. Mol. Spect.*, 25, 130 (1968).

TABLE A1

Ground State Vibrational Frequencies Observed by Raman Spectroscopy
for Oxalyl Chloride in the Vapour Phase

Frequency cm^{-1}	Intensity
231	w
262	w
285	w
311	w
386 sh	m
471	s
610	w
630	w
784	w
802	w
927	vW
1066	w
1350	w
1570	w
1800	m

APPENDIX II

THE SOLID STATE SPECTRUM OF OXALYL CHLORIDE

(a) Introduction

For the oxalyl halides (with the exception of oxalyl fluoride) it has proved to be impossible to observe temperature/intensity variations in the low temperature spectra of the molecules in the vapour phase because of their low vapour pressure and high freezing point (near 0°C). It was felt that the low temperature spectra in the solid phase might be of interest. Oxalyl chloride was chosen from the series because it is the most readily available and most easily handled.

(b) Experimental

Oxalyl chloride (obtained from Matheson Coleman and Bell) was used after single distillation. A Cary liquid helium cell was used to cool the sample for recording the spectra. This cell was modified to permit preparation of the sample by spraying the compound on a cold window at low pressure. No equipment was available to record or control sample temperature. Spectra were recorded photographically on the Hilger model E quartz prism spectrograph using I-O film (see Chapter 2), and spectrophotometrically on the Cary 14 spectrometer. When matrix isolation of oxalyl chloride was attempted, a vapour phase mixture of COCl_2 and SF_6 was deposited. The SF_6 was obtained from Matheson (of Canada). A crystalline quartz window was used in the cell as the cold window.

(c) The Spectra

All samples were prepared by depositing, slowly, the sample on the cold window while the window was maintained near liquid nitrogen temperature.

The spectrum of the ${}^1A_u(n\bar{1}a_g, \pi^*1a_u) \leftarrow \tilde{X}^1A_g$ transition was observed at liquid nitrogen temperature, and little difference was noted between the spectra of the COCℓCOCℓ/SF₆ solid solution and pure COCℓCOCℓ solid. The spectrum at 77°K has been reproduced in Figure A1; the intensity of the continuous background absorption is much lower in the low temperature spectrum than it is in the vapour spectrum, indicating that it is the "hot" part of an intense non-discrete transition to some higher energy excited state. The only structure observed in the spectrum at 77°K is a prominent progression having a frequency interval of approximately 1400 cm⁻¹ which has a maximum intensity at the third member (i.e., ν_0^2). It is assigned as a progression in the excited state carbonyl stretching mode. The frequencies of the observed peaks have been listed in Table A2. There is a change in the progression frequency after the fifth member at 2990Å. The CNDO calculations described in Section 3.10 indicate the possibility of a second $n \rightarrow \pi^*$ transition just to the blue of the first. The progression irregularity is considered to be evidence for the presence of a second electronic transition, the ${}^1A_u(n2a_g, \pi^*1a_u) \leftarrow \tilde{X}^1A_g$, for which the origin is near 35,000 cm⁻¹. This transition is not observed in the vapour phase because of the combined problems of the intense continuous background and predissociation of the first $n \rightarrow \pi^*$ transition.

The spectrum observed at 77°K sharpened up considerably when the cell was cooled with liquid helium. The best spectra were obtained for the COCℓCOCℓ/SF₆ solution, but the failure to observe the same quality of spectrum with pure COCℓCOCℓ was probably attributable to differences in sample preparation. The temperature was not measured, but it is believed that it was near the temperature of liquid helium. The spectra obtained are shown in Figure A2.

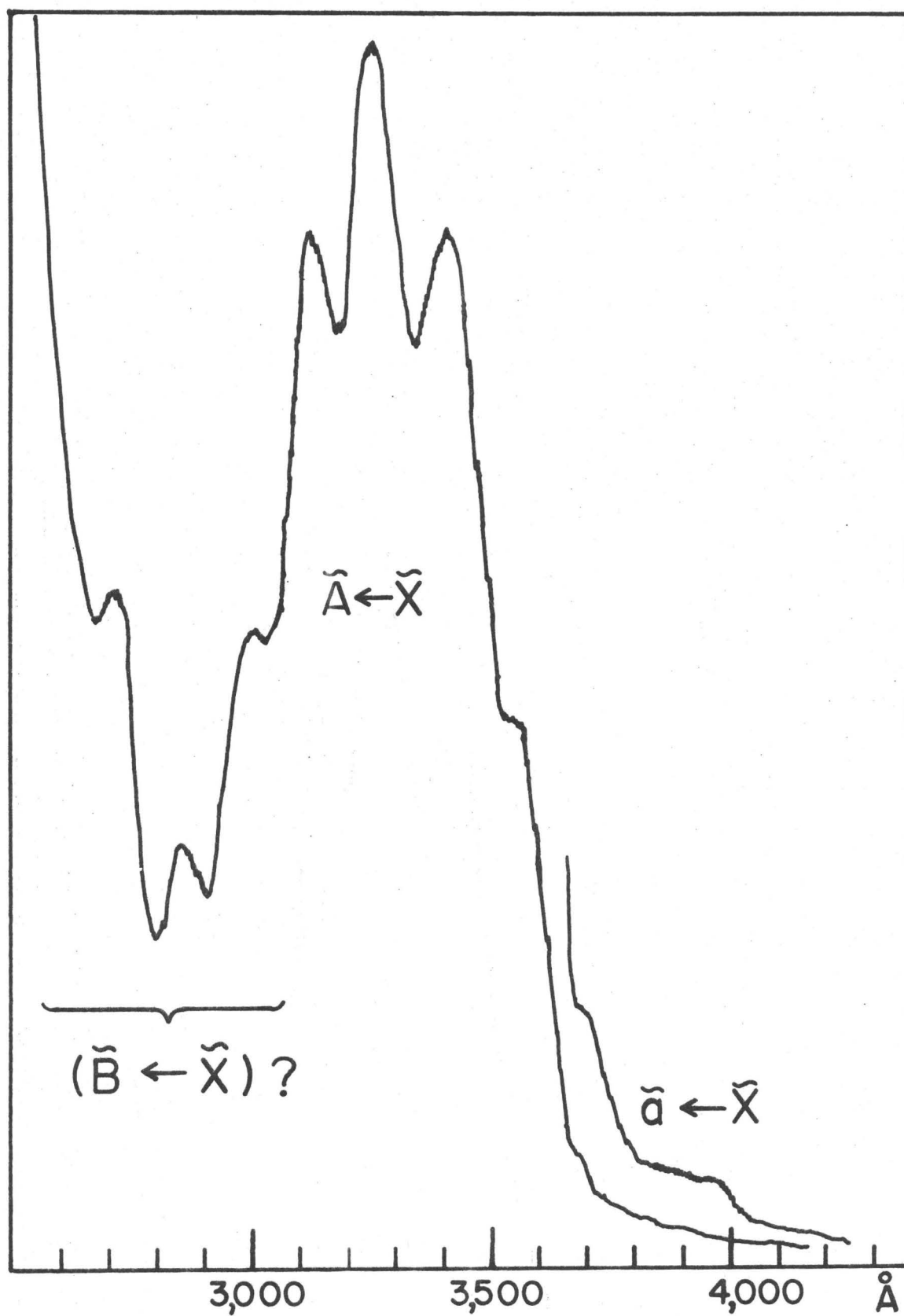


Figure A1 The Ultraviolet Absorption Spectrum of Oxalyl Chloride at 77°K.

TABLE A2

Bands Observed for Pure COC₂COCl₂ Solid at 77°K

Peak Positions [†] cm ⁻¹	Band Separations cm ⁻¹
25000 ††	(weak origin)
26400 sh ††	1400
27950 sh	(strong origin)
29350	1400
30750	1400
32050	1300
33450 sh	1400
35100	1650
36750	1650
38450 sh	1700

sh = shoulder

[†] measurement of peak at maximum peak height. Reliability of the numbers is approximately 50 cm⁻¹.

^{††} observed in the thick film only.

In the thick solid film, peaks were observed at 24940 cm^{-1} and 26390 cm^{-1} with total absorption to higher energy. These peaks are assigned to the 0_0^0 and 1_0^1 bands respectively of the ${}^3A_u(n\bar{1}a_g, \pi^*1a_u) \leftarrow \tilde{X}^1A_g$ electronic transition, indicating a value of $\sim 1450 \text{ cm}^{-1}$ for ν_1' the carbonyl stretching mode in the excited state. The ${}^3A_u(n\bar{1}a_g, \pi^*1a_u) \leftarrow \tilde{X}^1A_g$ transition was observed in emission from the crystal at 4.2°K by Shimada et al.^(AII-1). They list ν_{0-0} as 24780 cm^{-1} where their measurements were made on the leading (high energy) edge of the peak. Frequencies measured in this work were the frequencies at maximum peak height, which were used because of a lack of resolution. A measurement of the leading (low energy) edge of the 24940 cm^{-1} peak gives a value of 24780 cm^{-1} for ν_{00} in absorption for the $\text{COC}\ell\text{COC}\ell/\text{SF}_6$ solid solution, in agreement with the value observed in the emission spectrum. In the vapour phase, Balfour and King^(AII-2) report that the origin of the transition occurs at 24370 cm^{-1} . A small shift (410 cm^{-1}) to the blue exists between the vapour and solid phase values of ν_{0-0} .

In the thin solid film, the ${}^1A_u(n\bar{1}a_g, \pi^*1a_u) \leftarrow \tilde{X}^1A_g$ transition is observed. The frequencies of the observed peaks have been given in Table A3, and a tentative analysis of the spectrum is listed. Three frequency intervals, approximately 450 , 900 and 1500 cm^{-1} , figure prominently in the assignment. The band at $\nu_{00} + 470 \text{ cm}^{-1}$ has been assigned to the superposition of 4_0^1 and 5_0^1 because of its high intensity. The vibrational modes ν_4 and ν_5 are approximately described as the in plane $\angle\text{CCO}$ bending and the $(\text{COC}\ell)$ rocking modes respectively. The remaining intervals have been assigned to ν_2' and ν_1' respectively where ν_2 is described as the C-C stretching mode and ν_1 is described as the C=O stretching mode. By analogy with the $n \rightarrow \pi^*$ (S-T) transition, the origin of the S-S transition should occur at the leading edge

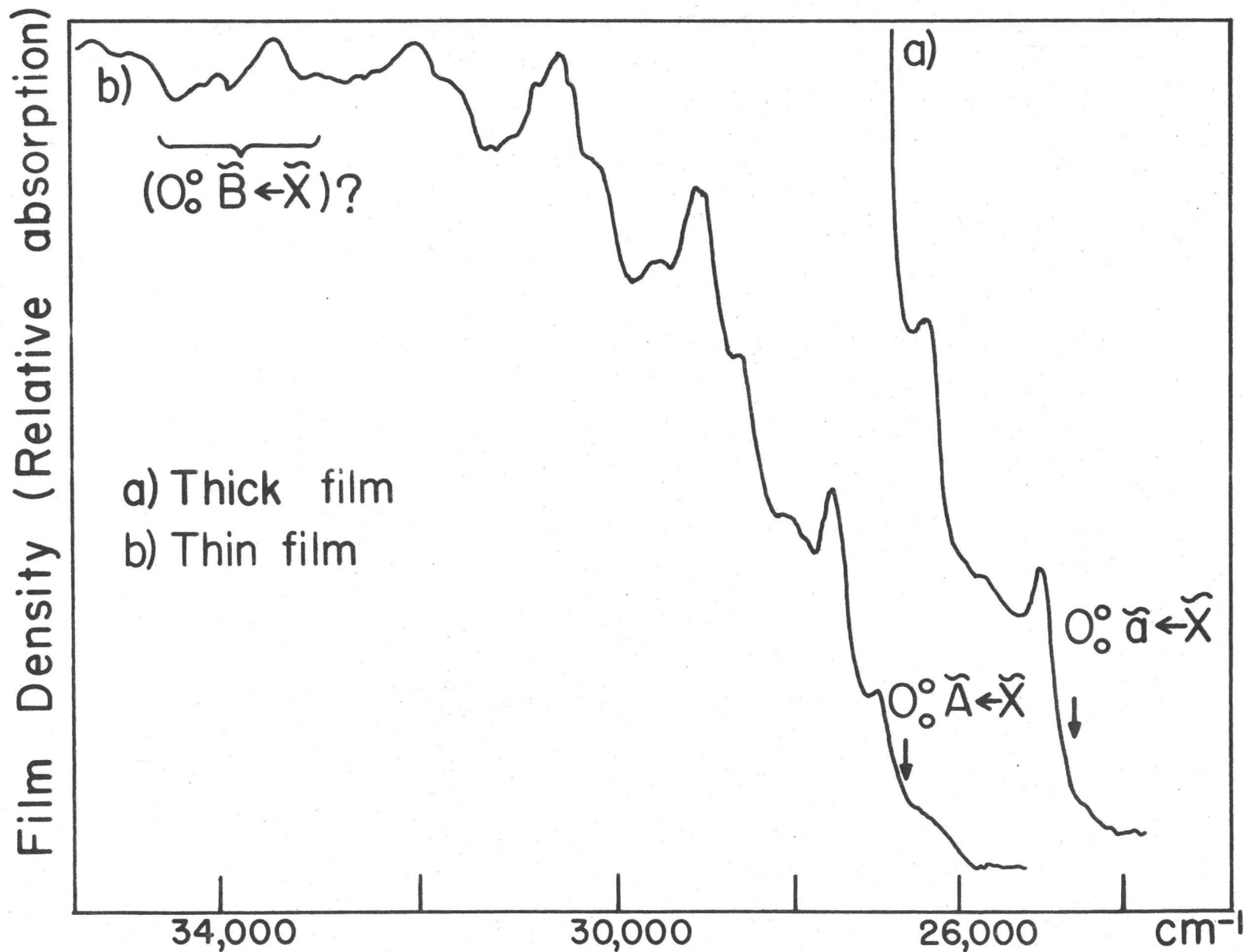


Figure A2. Microdensitometer Trace of the Absorption Spectrum of Oxalyl Chloride at Low Temperature (near 4°K).

TABLE A3

Observed Bands in the Liquid Helium Spectrum of Oxalyl Chloride
in an SF₆ Matrix

Frequencies cm ⁻¹	Intensity	Separation from the Origin	Assignment
27140 [†]	m	0.0	$\begin{matrix} 0 \\ 0 \end{matrix}$
27610	s	+470	$(4_0^1 + 5_0^1)$
28100	w	+960	$(2_0^1 + 4_0^2)$
28630	m	+1490	$\begin{matrix} 1 \\ 0 \end{matrix}$
28980	w(sh)	+960+880	$\begin{matrix} 2 \\ 0 \end{matrix}$
29060	s	+1490+430	$1_0^1(4_0^1 + 5_0^1)$
29490	w	+1490+860	$\begin{matrix} 1 & 1 \\ 0 & 2 \end{matrix}$
30080	m	+1490+1450	$\begin{matrix} 2 \\ 0 \end{matrix}$
30350	w(sh)	+1490+1450+270	$\begin{matrix} 2 & 5 \\ 0 & 0 \end{matrix}$
30480	s	+1490+1450+400	$\begin{matrix} 2 & 4 \\ 0 & 0 \end{matrix}$
30750	m(sh)	+1490+1450+670	$\begin{matrix} 2 & 3 \\ 0 & 0 \end{matrix}$?
30960	w	+1490+1450+880	$\begin{matrix} 2 & 2 \\ 0 & 0 \end{matrix}$
31560	m	+1490+1450+1480	$\begin{matrix} 3 \\ 0 \end{matrix}$
31970	s	+1490+1450+1480+410	$1_0^3(4_0^1 + 5_0^1)$
32290	w	+1490+1450+1480+730	$\begin{matrix} 3 & 2 \\ 0 & 0 \end{matrix}$
32510	w	+1490+1450+1480+950	$\begin{matrix} 3 & 3 \\ 0 & 0 \end{matrix}$
32820	w	+1490+1450+1480+1260	?
33290	m	32820 + 470	
33770	w	32820 + 950	
34270	vW		
34410	w		

TABLE A3 (cont'd.)

34840	m
35220	w

† The frequencies listed are the frequencies of the peaks at maximum absorption. The value for ν_{00} is 26850 cm^{-1} , the frequency of the leading (low energy) edge of this peak.

of the 27140 cm^{-1} peak. This gives a value of 26850 cm^{-1} for ν_{0-0} in the solid, a shift of 340 cm^{-1} to the red from the value of 27188.9 cm^{-1} reported for the vapour phase spectrum by Balfour and King^(AII-3). Again a break is observed in the pattern of the progressions beyond $\nu_{0-0} + 1_0^3$, providing additional evidence for a second electronic transition, the ${}^1A_u(n2a_g, \pi a_u^*) \leftarrow \tilde{X}{}^1A_g$, in this region.

The most puzzling feature of the low temperature spectrum of the solid is the marked difference in the intensity distribution as compared to that observed in the vapour phase spectrum. The overlap of two unresolved bands in the region of $\nu_{0-0} + 470 \text{ cm}^{-1}$ has been proposed as a partial answer, but in addition there must be a different Franck-Condon distribution of intensity in the solid state spectrum.

REFERENCES

- AII-1. Shimada, H, Shimada, R., Kanda, Y., Spect. Chim. Acta., 23A, 2821 (1967).
- AII-2. Balfour, W. J. and King, G. W., J. Mol. Spect., 27, 432 (1968).
- AII-3. Balfour, W. J. and King, G. W., J. Mol. Spect., 26, 384 (1968).

Acknowledgement: The work described in this Appendix was carried out as part of a joint project with D. Grangé.

APPENDIX III

THE EMISSION SPECTRUM OF OXALYL CHLORIDE

Introduction

As outlined in Chapter 4, and Appendix I, there has been considerable interest in obtaining the totally symmetric ground state vibrational frequencies of the C_{2h} oxalyl halides in the vapour phase. A series of experiments was conducted to observe the $n \rightarrow \pi^*$ transition in emission with a view to obtaining the ground state frequencies. Again oxalyl chloride was chosen because of its availability.

Experimental

The spectrograph, cell, and source of excitation used have been described by Lim and Moule^(AIII-1). Spectra were run on: 1) pure oxalyl chloride, 2) a 5/1 mixture of benzene/oxalyl chloride, with the samples flowed at low pressure.

Discussion of Results

When pure oxalyl chloride was investigated the strongest features observed in the emission spectrum were bands due to carbon monoxide. In addition a large number of weaker bands appeared which seemed (by virtue of their rotational profile) to arise from a transition of a polyatomic species. When the benzene/oxalyl chloride mixture was investigated, again the emission spectrum was a superposition of bands due to carbon monoxide and the polyatomic bands, but in this case the polyatomic bands had approximately the same intensity as the CO bands.

The presence of CO emission bands indicates the tendency for oxalyl chloride to dissociate in the rf discharge to yield carbon monoxide as one

of the products. In the CO emission both the Angstrom bands and the Herzberg bands are observed. These bands were used as calibration for measurement of the spectrum.

In the polyatomic emission, weak bands are observed at 3680 Å and 4100 Å which can be attributed to the origins of the ${}^1A_u(n,\pi^*) \leftarrow {}^1A_g$ and ${}^3A_u \leftarrow {}^1A_g$ transitions which have been observed in absorption for oxalyl chloride^(AIII-2,AIII-3). The strongest polyatomic emission, however, appears to have an origin near 4380 Å (22830 cm^{-1}). In the region to the red of 4380 Å a large number of weak bands occur, some of which arise from weak emission systems of CO and many of which appear to be polyatomic in origin. The absorption in the region of 4380 Å consists of a sharp spike associated with a less intense band some 40 cm^{-1} wide. A strong band with a similar profile occurs at $22830\text{ cm}^{-1} - 1095\text{ cm}^{-1}$. The 4380 Å band is proposed as the origin of ${}^1B_1 \rightarrow {}^1A_1$ transition of cis oxalyl chloride with the frequency interval 1095 cm^{-1} corresponding to the frequency of the C-C stretching mode in the ground state. (Durig et al^(AIII-4) give a value of 1059 cm^{-1} for cis C-C stretch. The discrepancies in the frequencies determined from the emission spectrum could be as large as this difference.) No strong band is identified in the region where the first member of the progression in the ground state carbonyl stretching mode is expected and the above proposal requires that the C-C stretching mode be more active than the CO stretching mode in the $n \rightarrow \pi^*$ system of the cis molecule.

REFERENCES

- AIII-1. C. T. Lim, D. C. Moule, *J. Mol. Spect.*, 37, 380 (1971).
 AIII-2. W. J. Balfour, G. W. King, *J. Mol. Spect.*, 27, 432 (1968).
 AIII-3. W. J. Balfour, G. W. King, *J. Mol. Spect.*, 26, 384 (1968).
 AIII-4. J. R. Durig, S. E. Hannum, *J. Chem. Phys.*, 52, 6089 (1970).

TABLE A4

Frequencies of Bands Observed in the Emission from a 5/1 Mixture of Benzene
and Oxalyl Chloride in under Radio Frequency Excitation

Frequency (cm ⁻¹)		
24370	m	
24245	m	
23910	w	
23650	vw	
23230	s	
23190	s	
23120	m	
22995	w	
22940	s	
22830	s (sharp spike)	Tentative origin ${}^1B_1 \rightarrow {}^1A_1$ cis oxalyl chloride
22745	m	
22304	vw	
4510.9 Å	s	CO
22085	w	
21820	w	
21735	s (sharp spike)	$\nu_{00} + 2_1^0$ (cis) ?
21500	m	
21375	m	
21290	m	
21760	m	
21110	m	
20955	m	
4835.3	vs	CO
20170	m (sharp spike)	
20110	m	

APPENDIX IV

FREQUENCIES OF OBSERVED BANDS IN THE ULTRAVIOLET SPECTRUM OF OXALYL CHLORIDE-FLUORIDE

A complete listing of all bands observed in the ultraviolet spectrum of oxalyl chloride-fluoride is given in Table A5. Several bands observed are believed to be due to oxalyl chloride. Such bands are marked with an asterisk.

TABLE A5

Frequencies of the Observed Band Heads in the Ultraviolet Spectrum
of Oxalyl Chloride Fluoride

Frequency (cm^{-1} vac)	Frequency (cm^{-1} vac)	Frequency (cm^{-1} vac)	Frequency (cm^{-1} vac)
24990.6	25526.9	25691.9	25830.7
996.5	528.6	696.7	832.0
25001.3	530.2	698.1	833.3
004.7	533.4	703.3	837.0
235.4	536.3	705.6	848.1
237.1	571.5	708.9	848.9
242.5	573.6	710.2	854.8
243.9	579.6	712.4	855.8
265.4	582.3	755.0	861.0
266.6	602.1	762.4	869.1
268.8	604.1	763.1	878.1
431.3	606.9	769.1	878.6
434.6	609.9	781.4	879.6
441.8	611.6	783.0	885.8
443.4	623.3	791.7	886.7
447.1	650.4	807.1	889.2
479.3	659.8	817.1	892.5
481.6	669.5	818.2	893.1
483.1	670.8	819.1	902.0
483.9	677.7	820.4	914.3
487.5	679.0	822.3	931.5
522.5	685.0	828.7	933.0

25935.6	26059.3	26171.8	26279.3
937.8	060.3	176.6	281.8
942.0	061.7	180.2	288.1
945.1	063.6	182.2	291.7
950.6	065.1	189.8	294.2
953.8	066.1	192.7	294.8
960.8	071.2	195.7	295.8
969.8	074.5	196.7	298.7
973.3	075.4	207.5	299.3
974.6	085.4	210.6	306.1
978.5	089.4	212.4	307.3
978.9	094.5	213.1	309.9
981.6	096.5	213.6	329.3
988.6	108.3	220.4	330.5
989.3	110.6	220.8	333.7
26000.0	111.5	221.7	338.2
003.9	114.1	234.4	339.4
009.1	116.5	237.2	340.8
010.6	117.7	237.9	341.3
012.6	120.6	241.4	346.0
022.1	129.0	246.0	348.0
024.7	131.5	248.4	369.9*
027.6	149.0	256.5	370.6
030.1	150.4	258.4	376.9
031.5	155.4	261.5	379.6
039.2	157.8	263.8	384.0
045.6	161.4	265.9	385.0

26391.2	26487.9	26567.2	26680.1*
393.0	493.1	569.9	684.9
396.5	495.3	575.6	686.3
419.6	496.1	578.3	690.4*
421.6	497.5	580.2	694.4
427.8	498.7	588.7*	696.1
432.3	502.8	592.7*	698.0
433.3	517.2	594.0*	699.7
437.0	523.2	597.0*	701.2
440.2	525.7	598.9*	702.7
443.2	527.3	602.9	704.2
445.4	528.5	606.3	710.9
448.2	529.0	610.0	713.4
454.5	531.0	611.7	714.5
455.1	533.9	615.9	723.0*
458.4	535.7	619.1	723.5*
459.6	537.4	621.5	767.4
463.2	544.5	634.7*	769.2
464.6	546.3	637.9	776.9*
466.8	548.4	645.5	778.3*
469.5	551.9	647.5	781.4
471.2	555.9	652.2	789.9
472.9	557.3	606.9	792.9
476.8	562.0	663.6	795.2
483.0	563.0	668.9	798.9
485.7	564.2	671.7	814.5
486.9	565.2	674.3	831.3

26835.1	27052.4	27142.4	27271.0*
837.9	054.7	165.7	272.0
845.5	069.9	168.2	287.4
848.0	077.7	171.9	289.3
851.5	081.6	177.1*	290.7
861.4	083.6	178.1*	298.6
899.8	085.2	182.2*	300.5
901.9	087.0	183.5*	316.1
903.2	089.5	185.2*	319.0
943.5	095.7	187.8*	320.7
949.3	096.6	189.0	325.1
966.2*	098.0	192.2	330.2
968.8*	100.1	206.1	335.1
970.0	102.0	207.1	344.2
972.5*	104.3*	209.0	348.5
976.4	118.4	210.2	355.2
982.6	120.8	218.6	357.0
987.7	123.6	220.1*	383.3
994.5	124.5	224.4*	385.1
996.7	126.6*	226.3	386.2
998.5	130.6	230.9	405.4
27007.5	131.5	234.4	406.7
011.6	133.3	260.6	407.6
015.7	134.5	262.1	417.3
048.3	135.7	265.8*	439.5
050.2	137.6	266.9*	441.6
051.6	140.6	268.3*	469.3

27470.9	27631.0	27737.5	27823.0
480.8	633.2	739.7	825.4
482.8	640.0	742.5	832.4*
491.5	657.5*	743.7	838.4
497.3	660.1*	750.2	840.3
499.2	663.7*	752.9	841.5
518.6	672.0*	755.1	843.6
520.2	675.7	756.5	845.9
534.8	678.2	759.0	856.5
536.7	680.9	760.9	863.7*
581.1	685.0	763.1	866.2
582.3	686.7	765.9	869.9
585.0*	690.0	768.3	871.2
587.6*	699.3	771.0	879.8
590.7*	701.3	774.9	881.8
593.4	702.5	776.6	882.6
594.6	704.4	780.7	887.2
599.3	707.4	785.1	889.8
604.8	711.2	787.9	894.2
606.5	713.8	789.3	904.2
611.5	717.5	802.3	922.8
614.5	720.5	803.8	926.7
617.2	724.7	805.4*	927.8
618.1	728.2	808.4*	931.2
622.3	732.3	812.0*	939.8
624.5	734.0	815.5*	942.6
628.6	735.6	818.3	944.0

27946.5	28063.1	28258.8	28479.80
949.2	067.1	260.9	495.13
957.5	069.2	277.0	505.73
959.7	070.9	278.6	507.37
961.4	072.1	289.2	510.87
962.3	074.4	291.2	513.99
964.2	076.8	298.1	515.21
966.5	078.4	332.7	518.12
969.9	089.0	334.5	519.67
973.0	098.3	349.5	531.32
976.1	107.5	353.1	556.73
978.9	111.7	355.0	578.88
983.4	116.0	362.8	590.85
996.2	128.9	366.6	605.49
28004.4	131.5	370.9	609.46
005.9	138.9	375.6	639.98
009.1	144.6	391.2	641.36
013.7	158.2	400.5	646.57
018.9	160.8	414.3	654.92
022.9	172.2	427.3	658.49
024.3	182.4	435.2	661.06
027.9	199.0	445.7	663.63
029.6	200.1	452.1	676.60
032.2	237.5	459.85	680.76
036.9	240.9	466.09	685.72
046.5	242.6	477.25	690.51
059.5	246.1	478.73	698.87

28724.46	28883.91	29108.8	29348.5
738.43	888.99	125.0	351.3
747.45	892.28	131.7	354.4
760.82	893.07	132.8	366.2
766.94	902.97	138.5	379.3
768.99	904.44	143.4	385.0
775.84	916.54	157.7	401.5
783.34	920.99	170.3	416.9
786.48	924.86	176.9	421.0
791.26	927.01	183.1	434.9
795.44	935.20	201.4	438.9
803.36	937.25	213.2	459.1
803.98	939.23	223.6	462.9
804.66	957.01	228.7	467.3
806.46	961.97	238.7	469.2
807.18	987.69	266.9	483.1
808.48	988.94	278.1	487.2
809.04	29000.76	281.9	499.6
832.06	002.06	294.5	506.1
836.36	017.87	302.7	514.2
852.41	024.5	308.3	519.7
854.25	042.4	313.4	527.3
855.09	045.4	318.9	538.9
856.15	073.9	323.6	548.5
866.31	086.0	328.7	562.1
868.32	100.3	340.0	582.3
878.35	105.8	344.1	584.3

29588.0	29792.0	30089.1	30367.0
594.1	793.8	103.1	380.0
597.2	799.9	112.1	381.4
601.8	810.9	122.3	404.2
619.7	813.3	133.3	413.5
621.8	815.4	151.9	420.2
629.3	822.2	155.2	440.6
633.3	824.8	162.4	450.2
635.1	835.1	163.8	459.0
652.9	836.7	172.9	465.3
660.1	850.3	177.1	473.4
662.4	857.4	186.8	477.4
674.0	863.9	191.8	488.7
675.9	885.4	199.1	489.7
677.2	898.7	221.4	498.6
700.4	919.3	238.4	505.7
702.0	940.2	250.0	510.8
717.7	952.5	260.7	520.1
725.4	960.4	271.4	528.9
735.9	30004.0	283.0	541.3
739.2	006.2	296.2	557.2
742.1	018.5	298.1	561.4
745.6	039.5	311.3	573.9
753.5	049.1	315.1	578.3
759.7	072.3	334.5	582.8
773.5	077.6	337.5	592.4
788.3	080.0	356.2	606.6

30610.8	30834.0	30079.9
615.4	839.2	092.2
633.3	845.5	108.7
639.6	851.4	114.7
643.7	855.5	138.1
646.8	861.4	159.3
655.7	865.6	162.5
658.8	871.2	176.4
668.0	885.1	182.8
681.1	893.7	186.9
700.3	895.4	195.2
711.7	903.2	198.4
723.7	916.9	208.0
734.1	920.0	212.0
750.3	925.8	261.0
752.4	934.0	275.7
759.0	956.7	315.5
760.7	965.9	338.2
763.8	975.2	341.8
766.2	983.2	358.1
779.2	993.0	380.5
794.9	31000.7	396.4
805.8	013.7	425.3
808.3	026.7	441.9
810.5	050.0	450
815.7	074.7	550
821.6	076.4	530

* These bands are attributed to oxalyl chloride.